

Advances

in Clinical and Experimental Medicine

MONTHLY ISSN 1899-5276 (PRINT) ISSN 2451-2680 (ONLINE)

www.advances.umed.wroc.pl

2020, Vol. 29, No. 6 (June)

Impact Factor (IF) – 1.227
Ministry of Science and Higher Education – 40 pts.
Index Copernicus (ICV) – 155.19 pts.



WROCLAW
MEDICAL UNIVERSITY

Advances
in Clinical and Experimental
Medicine



Advances in Clinical and Experimental Medicine

ISSN 1899-5276 (PRINT)

ISSN 2451-2680 (ONLINE)

www.advances.umed.wroc.pl

MONTHLY 2020
Vol. 29, No. 6
(June)

Advances in Clinical and Experimental Medicine is a peer-reviewed open access journal published by Wrocław Medical University. Its abbreviated title is Adv Clin Exp Med. Journal publishes original papers and reviews encompassing all aspects of medicine, including molecular biology, biochemistry, genetics, biotechnology, and other areas. It is published monthly, one volume per year.

Editorial Office

ul. Marcinkowskiego 2–6
50-368 Wrocław, Poland
Tel.: +48 71 784 11 36
E-mail: redakcja@umed.wroc.pl

Publisher

Wrocław Medical University
Wybrzeże L. Pasteura 1
50-367 Wrocław, Poland

© Copyright by Wrocław Medical University,
Wrocław 2020

Online edition is the original version of the journal

Editor-in-Chief

Maciej Bagłaj

Vice-Editor-in-Chief

Dorota Frydecka

Editorial Board

Piotr Dziągpiel
Marian Klinger
Halina Milnerowicz
Jerzy Mozrzymas

Thematic Editors

Marzenna Bartoszewicz (microbiology)
Marzena Dominiak (dentistry)
Paweł Domoślawski (surgery)
Maria Ejma (neurology)
Jacek Gajek (cardiology)
Mariusz Kuształ
(nephrology and transplantology)
Rafał Matkowski (oncology)
Ewa Milnerowicz-Nabzdyk (gynecology)
Katarzyna Neubauer (gastroenterology)
Marcin Ruciński (basic sciences)
Robert Śmigiel (pediatrics)
Paweł Tabakow (experimental medicine)
Anna Wiela-Hojeńska
(pharmaceutical sciences)
Dariusz Wołowicz (internal medicine)

International Advisory Board

Reinhard Berner (Germany)
Vladimir Bobek (Czech Republic)
Marcin Czyz (UK)
Buddhadeb Dawn (USA)
Kishore Kumar Jella (USA)

Secretary

Katarzyna Neubauer

Piotr Ponikowski
Marek Sąsiadek
Leszek Szenborn
Jacek Szepietowski

Statistical Editors

Dorota Diakowska
Leszek Noga
Lesław Rusiecki

Technical Editorship

Paulina Kunicka
Marek Misiak

English Language Copy Editors

Eric Hilton
Sherill Howard Pociecha
Jason Schock
Marcin Tereszewski

Pavel Kopel (Czech Republic)
Tomasz B. Owczarek (USA)
Ivan Rychlík (Czech Republic)
Anton Sculean (Switzerland)
Andriy B. Zimenkovsky (Ukraine)

Editorial Policy

Advances in Clinical and Experimental Medicine (Adv Clin Exp Med) is an independent multidisciplinary forum for exchange of scientific and clinical information, publishing original research and news encompassing all aspects of medicine, including molecular biology, biochemistry, genetics, biotechnology and other areas. During the review process, the Editorial Board conforms to the "Uniform Requirements for Manuscripts Submitted to Biomedical Journals: Writing and Editing for Biomedical Publication" approved by the International Committee of Medical Journal Editors (www.ICMJE.org/). The journal publishes (in English only) original papers and reviews. Short works considered original, novel and significant are given priority. Experimental studies must include a statement that the experimental protocol and informed consent procedure were in compliance with the Helsinki Convention and were approved by an ethics committee.

For all subscription-related queries please contact our Editorial Office:
redakcja@umed.wroc.pl

For more information visit the journal's website:
www.advances.umed.wroc.pl

Pursuant to the ordinance No. 134/XV R/2017 of the Rector of Wrocław Medical University (as of December 28, 2017) from January 1, 2018 authors are required to pay a fee amounting to 700 euros for each manuscript accepted for publication in the journal Advances in Clinical and Experimental Medicine.

„Podniesienie poziomu naukowego i poziomu umiędzynarodowienia wydawanych czasopism naukowych oraz upowszechniania informacji o wynikach badań naukowych lub prac rozwojowych – zadanie finansowane w ramach umowy 784/p-DUN/2017 ze środków Ministra Nauki i Szkolnictwa Wyższego przeznaczonych na działalność upowszechniającą naukę”.



Indexed in: MEDLINE, Science Citation Index Expanded, Journal Citation Reports/Science Edition, Scopus, EMBASE/Excerpta Medica, Ulrich's™ International Periodicals Directory, Index Copernicus

Typographic design: Monika Kołęda, Piotr Gil
DTP: Wydawnictwo UMW
Cover: Monika Kołęda
Printing and binding: EXDRUK

Contents

Original papers

- 639 Zheng Zhao, Siyuan Li, Hui Huang, Jing Fang, Huawei Wei, Yongming Xi
In vivo delivery of MMP3-shRNA and Sox9 lentivirus cocktail enhances matrix synthesis to prevent lumbar disc degeneration
- 649 Dingying Ma, Jun Qiao, Qiang Qu, Fei He, Wenhua Chen, Bo Yu
Weighted gene co-expression network analysis to investigate the key genes implicated in global brain ischemia/reperfusion injury in rats
- 661 Chun Jiang Yu, Dongying Ma, Ling Ling Song, Zhen Nan Zhai, Ye Tao, Ying Zhang, Ling Yu Cai, Ya Hui Hou, Hong Yuan Chen, Li Wang
The role of GLP-1/GIP receptor agonists in Alzheimer's disease
- 669 Abbas Alibakhshi, Mojgan Bandehpour, Zarin Sharifnia, Bahram Kazemi
The development and evaluation of a multi-epitope antigen as a serodiagnostic marker of *Toxoplasma gondii* infection
- 677 Nannan Li, Guoping Zhou
MicroRNA-548k upregulates a spliced variant of human CD2-associated protein by targeting its promoter
- 683 Wei Ma, Li-Sha Cheng, Wei Jiang, Sheng-Di Wu
The small heterodimer partner inhibits activation of hepatic stellate cells via autophagy
- 695 Jun Ge, Keyu Kong, Xiaoqiang Cheng, Tianyi Wu, Dingge Liu, Lingling Peng, Zhijia Shen, Guoyuan Lu, Yanping Shen
Isoflurane cerebral preconditioning in a spontaneous hypertension rat model is associated with sphingosine kinases
- 701 Lvlin Yang, Dongsheng Niu, Zhigang Bai, Jun Ma, Xichun Sun, Yuqi Liang, Jie Zhang
Application of 3D-FS-SPGR imaging combined synovial fluid GGCX detection in the evaluation of knee osteoarthritis
- 707 Magdalena Frej-Mądrzak, Agnieszka Jama-Kmieciak, Jolanta Sarowska, Dorota Teryks-Wołyniec, Anna Gryboś, Marian Gryboś, Irena Choroszy-Król
***Streptococcus agalactiae* and *Chlamydia trachomatis* detection in women without symptoms of infection**
- 715 Hiroyasu Matsuoka, Hirochika Matsubara, Aya Sugimura, Tsuyoshi Uchida, Tamo Kunimitsu, Tomofumi Ichihara, Yuichiro Oonuki, Yoshihiro Miyauchi, Tetsuo Kondo, Hiroyuki Nakajima
Detecting tumor-infiltrating Forkhead box P3-positive T cells in the prognosis of lung adenocarcinoma: Possible role of clustering tumor interleukin-12 subunit alpha and transforming growth factor beta 1 expression
- 727 Dong Sun Choi, Sang Do Shin, Young Sun Ro, Kyung Won Lee
Relationship between serum potassium level and survival outcome in out-of-hospital cardiac arrest using CAPTURES database of Korea: Does hypokalemia have good neurological outcomes in out-of-hospital cardiac arrest?
- 735 Monika Rutkowska, Sylwia Hnitecka, Marek Nahajowski, Marzena Dominiak, Hanna Gerber
Oral cancer: The first symptoms and reasons for delaying correct diagnosis and appropriate treatment

Multicenter study

- 745 Vojtech Dotlacil, Barbora Frybova, Natalie Polivka, Daniel Kardos, Peter Vajda, Krystian Toczewski, Rebeka Pechanová, Jozef Babala, Michal Rygl, Dariusz Patkowski
Current management of pediatric appendicitis: A Central European survey

Reviews

- 751 Krystyna Orendorz-Frączkowska, Hanna Temporal
Organ of hearing and balance in peri- and postmenopausal women. Effects of hormone replacement therapy on hearing and balance in peri- and post-menopausal women: The current state of knowledge
- 757 Piotr Frydrychowski, Marcin Michałek, Agnieszka Sławuta, Agnieszka Noszczyk-Nowak
Large animals as models of atrial fibrillation
- 769 Piotr K. Krajewski, Magdalena Krajewska, Jacek C. Szepietowski
Pruritus in renal transplant recipients: Current state of knowledge

In vivo delivery of MMP3-shRNA and Sox9 lentivirus cocktail enhances matrix synthesis to prevent lumbar disc degeneration

Zheng Zhao^{1,A–F}, Siyuan Li^{2,A–D,F}, Hui Huang^{1,A,B,F}, Jing Fang^{1,B,C,F}, Huawei Wei^{1,B,C,F}, Yongming Xi^{1,A–F}

¹ Department of Orthopedics, Affiliated Hospital of Qingdao University, China

² Department of Orthopedics, Shandong Provincial Third Hospital, Jinan, China

A – research concept and design; B – collection and/or assembly of data; C – data analysis and interpretation; D – writing the article; E – critical revision of the article; F – final approval of the article

Advances in Clinical and Experimental Medicine, ISSN 1899–5276 (print), ISSN 2451–2680 (online)

Adv Clin Exp Med. 2020;29(6):639–647

Address for correspondence

Yongming Xi

E-mail: yongming_xi@yahoo.com

Funding sources

The National Natural Science Foundation of China (NSFC, grant No. 81470104).

Conflict of interest

None declared

Received on September 22, 2019

Reviewed on March 31, 2020

Accepted on April 29, 2020

Published online on June 26, 2020

Abstract

Background. Intervertebral disc degeneration (IDD) is characterized by increased proteolytic degradation of the extracellular matrix (ECM), leading to a loss of collagen II and proteoglycan in the nucleus pulposus (NP). Although MMP3 has been reported to play a central role in disc degeneration, it is still unknown whether gene therapy targeting MMP3 can inhibit IDD.

Objectives. To investigate whether lentivirus-mediated MMP3 knockdown is capable of attenuating IDD. More importantly, we also explored whether combined gene therapy that simultaneously antagonizes MMP3 and overexpresses Sox9 can synergistically inhibit IDD and induce augmented matrix reconstitution in the degenerative NP.

Material and methods. We performed direct injection of lentiviral vectors LV-MMP3-shRNA and/or LV-Sox9 into rabbit lumbar discs. The animals were scanned using magnetic resonance imaging (MRI) at 8, 12 and 24 weeks after the operation. We also evaluated the gene expression and synthesis of NP matrix components, including collagen II, aggrecan and proteoglycan.

Results. The MRI scans showed remarkable needle-puncture-induced progressive IDD in animals injected with PBS or 10^7 viral particles (VP) of the control virus. In contrast, injection of 10^7 VP of LV-MMP3-shRNA or LV-Sox9 substantially inhibited IDD. MMP3 knockdown or Sox9 overexpression stimulated collagen II and aggrecan expression, as well as proteoglycan synthesis. Notably, the injection of a cocktail of LV-MMP3-shRNA and LV-Sox9 (5×10^6 VP each) greatly delayed the development of IDD and induced the highest levels of collagen II and proteoglycan production, indicating a synergistic effect in ECM induction.

Conclusions. Our results suggest that gene therapy targeting MMP3 is an efficient way to delay IDD. Combined gene therapy possesses a stronger capacity to induce matrix components in degenerative NP tissue than single-gene delivery.

Key words: gene therapy, disc degeneration, SOX9, MMP3

Cite as

Zhao Z, Li S, Huang H, Fang J, Wei H, Xi Y. In vivo delivery of MMP3-shRNA and Sox9 lentivirus cocktail enhances matrix synthesis to prevent lumbar disc degeneration. *Adv Clin Exp Med.* 2020;29(6):639–647. doi:10.17219/acem/121509

DOI

10.17219/acem/121509

Copyright

© 2020 by Wrocław Medical University

This is an article distributed under the terms of the Creative Commons Attribution 3.0 Unported (CC BY 3.0) (<https://creativecommons.org/licenses/by/3.0/>)

Introduction

Intervertebral disc degeneration (IDD) is a major cause of most musculoskeletal disorders of the spine that results in lower back pain, morbidity and physical disability.¹ Although the precise etiology and pathophysiology of disc degeneration has not been fully elucidated, IDD is generally believed to be a consequence of increased proteolytic degradation of extracellular matrix (ECM) macromolecules. During the disc degenerative process, the nucleus pulposus (NP) loses water and large amounts of aggregating proteoglycans and type II collagen (COL2A1), which leads to ECM breakdown and structural failure.²

A variety of studies have focused on the mechanisms underlying ECM degradation in IDD pathogenesis. An increasing amount of evidence has shown that matrix metalloproteinases (MMPs) play important roles in the degradation of matrix components during the disc degenerative process. Several MMP family members, such as MMP1, MMP2, MMP3, MMP7, MMP8, MMP9, MMP12, and MMP26, have been reported to be increasingly expressed in degenerated disc tissues, suggesting an association between MMP and IDD.^{3–6} Notably, Bachmeier et al. reported that among all MMPs tested (MMP1, MMP2, MMP3, MMP7, MMP8, MMP9, and MMP13), the expression of MMP3 was consistently and substantially upregulated in degenerated disc samples, and this process was accompanied with increased enzymatic activity of MMP3,⁷ implying that MMP3 plays a central role in disc degeneration. Besides elevated matrix-degrading MMPs, the loss of matrix-producing Sox9 also plays a role in ECM degradation in IDD. Being a key transcription factor in chondrogenic differentiation, Sox9 can directly stimulate gene expression of collagen type II and aggrecan,⁸ the major core protein in proteoglycan. Sive et al. detected a strong signal of Sox9 in normal NP tissues using in situ hybridization, which was accompanied by high-level expression of collagen II and aggrecan.⁹ However, the expression of Sox9 decreases with aging and disc degeneration.¹⁰ These studies suggest that MMP-induced excessive ECM degradation or loss of Sox9-reduced ECM synthesis is critically implicated in the pathogenesis of IDD. Hence, molecular therapy which targets MMP or restores Sox9 can be used to reconstitute matrix components in a degenerative NP.

Although spine disorders resulting from disc degeneration can be treated with surgery, including discectomy or spinal fusion, they are not curative and are associated with various complications. Non-surgical treatments – such as drugs, massage or physical therapy – however, can only relieve the clinical symptoms; they cannot delay or reverse the disc degenerative process. As a result, gene therapy has received considerable interest, as this approach can transfer the genes of therapeutic proteins to the disc cells, enabling them to manufacture the proteins endogenously, on a continuous or regular basis, allowing for long-term regulation of matrix synthesis with the potential

to prevent or delay IDD.¹¹ Nishida et al. conducted an initial study showing that direct injection of adenoviral TGF β 1 vectors into the rabbit lumbar discs led to a 100% increase in proteoglycan synthesis compared with intact control tissues.¹² Since then, gene therapy using several growth factors, including BMP2, GDF5, IGF1, and interleukin (IL)-1 receptor antagonist (IL-1Ra) for disc degeneration has been tested both in vitro and in vivo, as previously reported.^{11,13} Co-transduction of adeno-associated virus (AAV)-based Sox9 and OP1 vectors was reported to exhibit a stronger effect in the induction of proteoglycan and collagen II than AAV-Sox9 or AAV-OP1 alone.¹⁴

So far, gene therapy which targets an individual MMP molecule (particularly MMP3) against disc degeneration has not yet been reported. In our study, we performed direct injection of lentiviral vectors expressing MMP3-shRNA into NP tissues of lumbar discs in rabbits and evaluated the reconstitution of matrix components, specifically collagen type II and proteoglycan. We also investigated whether a cocktail of both MMP3-shRNA and Sox9 lentiviruses could trigger a synergistic effect to further augment matrix synthesis.

Material and methods

Lentiviral vectors

The lentiviral vectors harboring MMP3-shRNA (LV-MMP3-shRNA), Sox9 (LV-Sox9), or empty vectors were provided by Biowit Technologies (Shenzhen, China). All lentivirus vectors were stored at -80°C and diluted with phosphate-buffered saline (PBS) to a concentration of 5×10^5 viral particles (vp)/ μL right before use.

Animal study

This is an experimental study in a rabbit model. The protocol for the animal study was reviewed and approved by the Animal Care Committee of Qingdao University, China. A total of 25 New Zealand white rabbits were used in this study, with an average age of 4 months and an average body weight of 2.5 kg. Before surgery, the animals underwent magnetic resonance imaging (MRI) to exclude congenital spine deformity and disc disease.

For direct gene transfer, the animals were anesthetized with an intramuscular injection of 1.5% pentobarbital sodium at a dosage of 2 mL/kg. Following anesthesia, each animal was placed in a lateral position with all 4 limbs fixed. A vertical incision of about 3 cm was made from the iliac crest to the lower edge of the 12th rib via a right extraperitoneal approach. The peritoneum was bluntly dissected to expose the transverse processes from L3 to L7. A 24-gauge needle was used to pierce into the center of the exposed L3/4, L4/5, L5/6, and L6/7 lumbar discs (~5 mm) parallel to the upper and lower endplates. Then, a volume of 20 μL

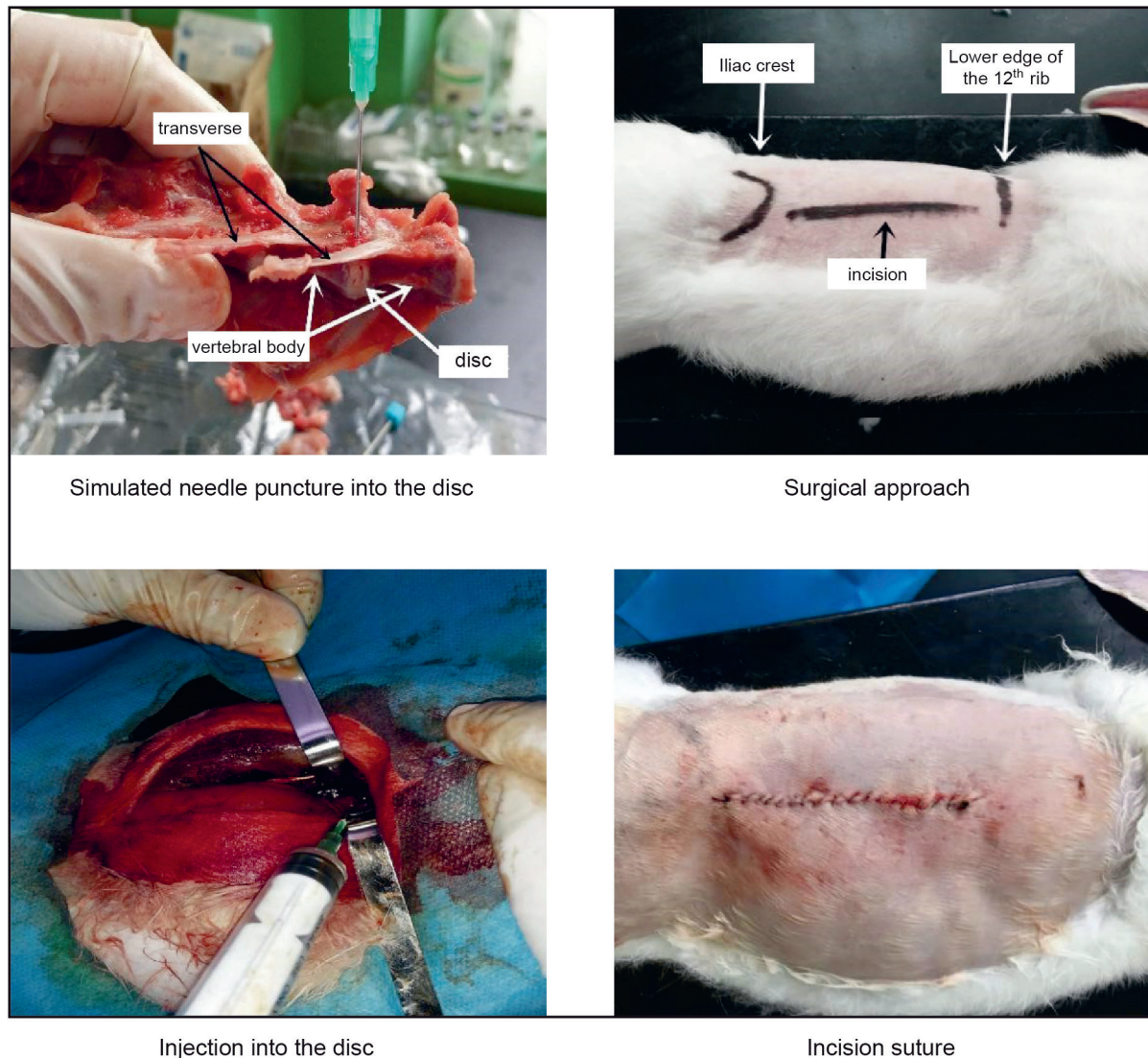


Fig. 1. In vivo gene delivery. Lentiviral vectors are directly injected into the rabbit lumbar discs (L3/4, L4/5, L5/6, and L6/7) through a surgical approach

containing PBS or 10^7 vp of lentivirus was injected directly into the NP tissue. All 25 rabbits were randomly divided into 5 groups and injected with a total volume of 20 μ L of PBS or lentivirus, as follows: group I – PBS; group II – 10^7 vp of empty virus (control); group III – 10^7 vp of LV-MMP3-shRNA; group IV – 10^7 vp of Lento-Sox9; and group V (cocktail) – 5×10^6 vp of LV-MMP3-shRNA + 5×10^6 vp of LV-Sox9. After injection, the opening was closed with sutures (Fig. 1). The rabbits were administered penicillin (800,000 units) intramuscularly before and after the operation. No incidences of infection or death were reported.

MRI assessment

The animals were examined with MRI at 8, 12 and 24 weeks after the operation. A Siemens Avanto 3.0T medical superconductive MRI scanner (Siemens AG, Munich, Germany) was used to scan the sagittal lumbar spine of the animals with a cervical coil. The parameters

of the scanner were as follows: T2-weighted sequence repetition time – 2,000–6,000 ms; echo time – 80–120 ms; bandwidth – 25 Hz; microwave – 16; matrix – 384×224 px; nex – 4; field of vision – 16×16 cm; thickness – 3 mm; and spacing – 0.2 mm. A degenerative disc mainly emitted a low signal, that is, the T2-weighted signal intensity decreased and the disc became thinner. Based on the changes in the T2-weighted signal, the improved Thompson classification method was used as the standard. The MRI data was blindly assessed by 2 independent senior radiologists.

Quantitative real-time polymerase chain reaction

At 24 weeks post-operation, the animals were sacrificed and the NP tissues were harvested. Total RNA was isolated using TRIzol reagent (Amresco, Solon, USA) and was reverse-transcribed to cDNA using qScript cDNA SuperMix (Quanta Biosciences, Woodbridge,

USA). Quantitative real-time polymerase chain reaction (qRT-PCR) was conducted with SYBR green master mix. The primers for rabbit genes were listed as follows: COL2A1, forward 5'-GGATAGA CCCCAACCAAGGC-3', reverse 5'-GCTGCTCCACCAGTTCTTCT-3'; MMP3, forward 5'-AGCCAATGGAAATGAAAACCTCTTC-3', reverse 5'-CCAGTGGATAGGCTGAGCAAA-3'; Sox9, 5'-GGTGCTCAAGGGCTACGACT-3', reverse 5'-GGGTG-GTCTTTCTTGCT G-3'; Actin, forward 5'-CTG-GAACGGTGAAGGTGACA-3', reverse 5'-CGGCCA-CATTGC AGAACT-3'. The PCR products were analyzed with an ABI PRISM 7900HT Sequence Detection System (Applied Biosystems, Foster City, USA). The cycling conditions were 50°C for 2 min and 95°C for 10 min, followed by 40 repetitions of 95°C for 15 s and 60°C for 1 min. One dissociation stage (95°C for 15 s, 60°C for 15 s and 95°C for 15 s) was added to produce the melting curve at the end of the cycling condition. Relative mRNA concentrations of the target genes were determined with ABI software (RQ Manager v. 1.2; Thermo Fisher Scientific, Waltham, USA), which normalizes the target gene threshold cycle to that of endogenous GAPDH transcripts ($\Delta\Delta C_t$), using the formula $2^{-\Delta\Delta C_t}$ to determine fold change.

Western blot

For western blot, cell lysates were isolated from NP tissues with RIPA lysis buffer (10 mM of Tris, pH 7.4, 100 mM of NaCl, 1 mM of EDTA, 1 mM of EGTA, 1 mM of NaF, 20 mM of $\text{Na}_4\text{P}_2\text{O}_7$, 2 mM of Na_3VO_4 , 1% Triton X-100, 10% glycerol, 0.1% sodium dodecylsulphate (SDS), and 0.5% deoxycholate). Protein concentrations were estimated using Bradford protein assay (Bio-Rad, Hercules, USA). An equal amount of protein (40 μg) was resolved using 10% SDS-PAGE and transferred to polyvinylidene difluoride (PVDF) membrane (Thermo Fisher Scientific). Non-specific binding sites were blocked with 5% nonfat dry milk (Roche, Basel, Switzerland) in Tris-buffered saline containing 0.1% Tween (TBST). The membrane was incubated with primary antibody against rabbit COL2A1 or aggrecan (Abcam, Cambridge, UK) in TBST at 4°C overnight on a shaker, and was then incubated with horseradish peroxidase (HRP)-conjugated secondary antibodies for 1 h at room temperature. The immunoblots were visualized using Western ECL Blotting Substrates (Bio-Rad). The protein bands were analyzed for densitometry using ImageJ software (National Institutes of Health, Bethesda, USA).

Proteoglycan assay

The amount of proteoglycan in the NP tissues was examined through determining soluble sulfated glycosaminoglycans (sGAG) using a Proteoglycan Detection Kit (Amsbio, Cambridge, USA) according to the manufacturer's protocol. Briefly, NP tissue was minced, homogenized and incubated with 1 mL of 20 mM sodium phosphate buffer

(pH 6.8) containing 1 mM of EDTA, 2 mM of dithiothreitol and 300 μg of papain at 60°C for 4 h until the tissue was soluble. Iodoacetic acid was added to a final concentration of 10 mM and was mixed well with 1 mL 50 mM Tris/HCl (pH 8.0). Both the samples and the sGAG standards were mixed with DMB dye. Absorbance was read in a microplate reader at an optical density (OD) of 520 nm.

Statistical analyses

The data was reported as means \pm standard deviation (SD) (or means \pm standard error of the mean (SEM); see figure legends) of at least 3 independent trials, and was analyzed with a two-tailed Student's t-test for 2 groups, or one-way analysis of variance (ANOVA) for multiple groups using GraphPad Prism software (GraphPad Software Inc, San Diego, USA). The variance is similar between the groups in the same trial. A p-value <0.05 was considered statistically significant.

Results

MRI reveals delayed disc degeneration by LV-MMP3-shRNA or LV-Sox9 vectors

Previous studies have reported that puncturing with a needle can induce progressive disc degeneration in rabbits.^{15–17} In our study, we performed direct injection of PBS, empty lentivirus, and lentivirus expressing MMP3-shRNA and/or Sox9 into rabbit lumbar discs, to explore whether gene therapy-mediated MMP3 knockdown or Sox9 overexpression could delay the development of IDD. The preoperative T2-weighted MRI scans revealed strong and uniform signals for each lumbar disc (Fig. 2A). However, at 8 weeks post-injection, the T2-weighted signal intensity decreased in the discs injected with PBS or empty virus, indicating an early degenerative process. Interestingly, discs injected with LV-MMP3-shRNA, LV-Sox9 or combined LV-MMP3-shRNA+LV-Sox9 vectors still appeared normal (Fig. 2B). At 12 weeks after the operation, MRI scans still displayed an intact structure in the PBS- or empty-virus-treated discs, although a more pronounced reduction of signal intensity was identified, indicating a progressively advanced NP degeneration. The MMP3-shRNA- or Sox9-lentivirus-injected discs also displayed a decrease in signal intensity, though to a much lesser extent. However, the cocktail injection of MMP3-shRNA and Sox9 lentivirus led to an only slightly reduced MRI signal (Fig. 2C). At 24 weeks after surgery, PBS or empty-virus-injected lumbar discs exhibited a strikingly less intense MRI signal with a loss of disc integrity, indicating severe disc degeneration. In contrast, the MMP3-shRNA- or Sox9-lentivirus-injected discs remained intact, even though the T2-weighted MRI scan showed reduced signal intensity. Notably, the discs injected with a cocktail of MMP3-shRNA and Sox9 lentiviruses not

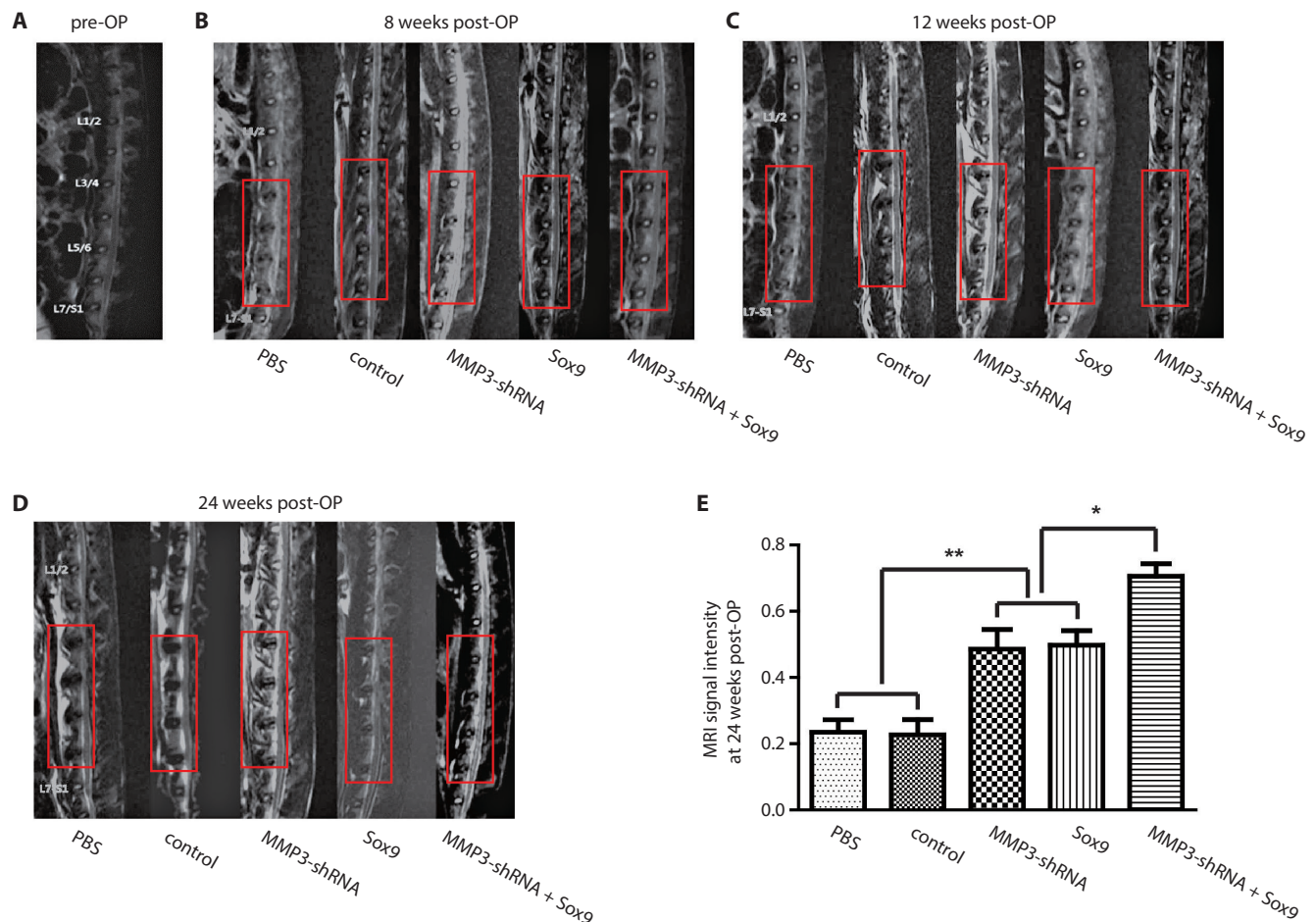


Fig. 2. MRI analysis. Lumbar discs are scanned using T2-weighted MRI at different time points: (A) before the operation (pre-OP), (B) 8 weeks after operation, (C) 12 weeks after the operation, and (D) 24 weeks after the operation. (E) MRI signal intensity at 24 weeks after the operation. Red boxes surround L3/4, L4/5, L5/6, and L6/7 intervertebral discs. Note that lentiviral delivery of MMP3-shRNA or Sox9 greatly delays needle-puncture-induced disc degeneration when compared to PBS or empty virus treatment, whereas combined gene delivery induces a synergistic effect in the attenuation of IDD

only appeared intact, but also displayed only a moderate decrease in MRI signal intensity (Fig. 2D,E; Table 1).

Based on the comparison of MRI signal intensity among different groups, lentivirus-mediated MMP3 knockdown or Sox9 overexpression efficiently delayed the progression of needle-puncture-induced disc degeneration. Importantly, injection of combined LV-MMP3-shRNA and LV-Sox9 vectors significantly exerted a greater capacity than MMP3-shRNA ($p = 0.026$) or Sox9 ($p = 0.017$) single transgene to delay the development of IDD, indicating a synergistic effect of cocktail gene delivery.

Lentiviral MMP3-shRNA or Sox9 gene transfer mediates long-term transgene expression

The animals were sacrificed at 24 weeks after the operation. The NP tissues were harvested from their lumbar discs for RNA and protein assays. We first evaluated transgene expression using qRT-PCR analysis and found that, compared to the control group, the *in vivo* transfer of LV-MMP3-shRNA vectors resulted in a 65% decrease

in MMP3 level. Interestingly, the injection of both lentiviruses decreased MMP3 mRNA to a level comparable to that of LV-MMP3-shRNA alone (Fig. 3A). On the other hand, LV-Sox9 viral vectors led to a 3.8-fold increase in Sox9 mRNA in comparison with the controls. Similarly, the cocktail of lentiviruses induced a 3.5-fold increase of Sox9 mRNA (Fig. 3B). These results not only suggest that lentiviral vectors can mediate long-term *in vivo* gene expression, but they also imply that combined transduction of 2 transgenes can stimulate higher gene expression than single-gene delivery.

Lentiviral MMP3-shRNA or Sox9 gene transfer increases collagen II expression

Given that the loss of collagen II and proteoglycan are the predominant pathological changes in IDD, we first examined whether *in vivo* gene delivery of lentivirus vectors could restore the expression of collagen II in NP tissues during a needle-puncture-induced degenerative process. Using qRT-PCR analysis, we found that injecting LV-MMP3-shRNA and LV-Sox9 induced a 1.82- and

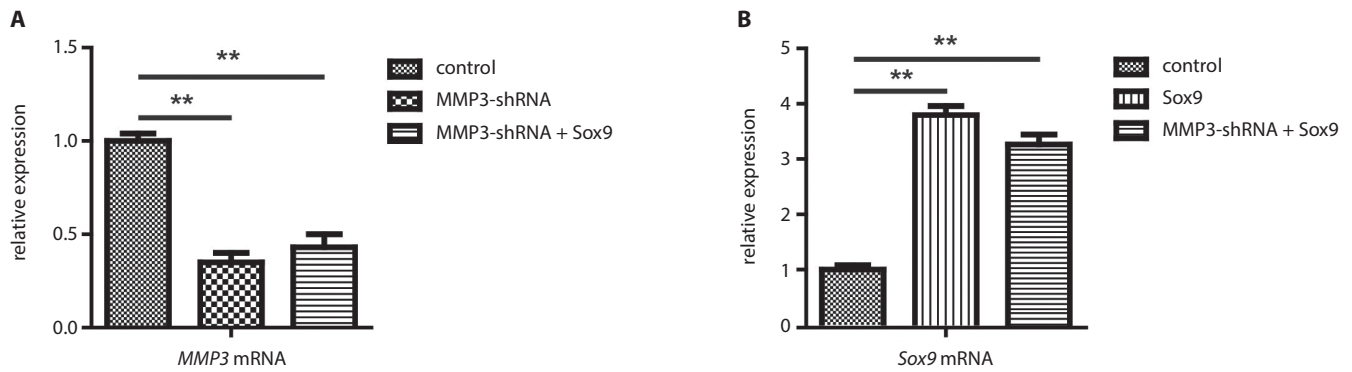


Fig. 3. Lentiviral gene delivery mediates long-term transgene expression. A. qRT-PCR analysis for MMP3 mRNA in NP tissue. B. qRT-PCR analysis for Sox9 mRNA in NP tissue. Data is presented as means \pm SEM. Note that cocktail gene delivery induces MMP3 or Sox9 mRNA to a comparable extent as the delivery of MMP3-shRNA or Sox9 lentivirus alone

** $p < 0.01$.

Table 1. MRI signal intensity (modified Thompson classification)

Group	Pre-OP	8 weeks	12 weeks	24 weeks*
PBS	1.000 \pm 0.051	0.677 \pm 0.097	0.367 \pm 0.081	0.235 \pm 0.037
Control	1.000 \pm 0.103	0.652 \pm 0.083	0.383 \pm 0.043	0.227 \pm 0.046
MMP3-shRNA	1.000 \pm 0.072	0.836 \pm 0.059	0.625 \pm 0.077	0.486 \pm 0.059
Sox9	1.000 \pm 0.067	0.845 \pm 0.064	0.655 \pm 0.062	0.498 \pm 0.044
MMP3-shRNA+Sox9	1.000 \pm 0.086	0.903 \pm 0.069	0.796 \pm 0.085	0.706 \pm 0.038

* Analysis between different groups as follows.

Groups	Fold change	p-value
MMP3-shRNA+Sox9 vs Sox9	1.42	<0.05
MMP3-shRNA+Sox9 vs MMP3-shRNA	1.45	<0.05
MMP3-shRNA+Sox9 vs control	3.11	<0.05
MMP3-shRNA+Sox9 vs PBS	3.00	<0.01
Sox9 vs MMP3-shRNA	1.02	>0.05
Sox9 vs controls	2.19	<0.05
Sox9 vs PBS	2.12	<0.05
MMP3-shRNA vs controls	2.14	<0.05
MMP3-shRNA vs PBS	2.07	<0.05
Controls vs PBS	0.09	>0.05

1.62-fold increase in Col2 α 1 mRNA, respectively, compared to the controls. Notably, the combined injection (LV-MMP3-shRNA+LV-Sox9) induced the highest level of COL2A1 mRNA among all 5 groups, which led to a 2.3-fold increase when compared with the controls, and a 1.26- or 1.41-fold increase compared to the LV-MMP3-shRNA- or LV-Sox9-treated group, respectively (Fig. 4A).

Using western blot analysis, we found that the transduction of LV-MMP3-shRNA or LV-Sox9 dramatically upregulated collagen II at the protein level: 3.11- and 3.33-fold compared to the controls. Similarly, injecting a MMP3-shRNA and Sox9 lentivirus cocktail led to the highest induction of COL2A1 among all groups tested, which was a 3.88-fold increase in comparison with the controls (Fig. 4B). These results suggest that direct *in vivo* gene therapy using lentiviral MMP3-shRNA or Sox9 vectors

promotes the expression of collagen II in degenerative NP tissues. Our findings also reveal that cocktail delivery of MMP3-shRNA and Sox9 lentiviruses can initiate a synergistic effect to augment collagen II expression.

Lentiviral MMP3-shRNA or Sox9 gene transfer increases proteoglycan synthesis

We then evaluated the production of proteoglycan, the primary ECM matrix in NP tissues, by assessing the expression of aggrecan (the major core protein in proteoglycan), as well as the synthesis of sGAG. Western blot analysis showed that lentivirus-mediated MMP3 knockdown increased aggrecan expression 2.3-fold compared to the controls. LV-Sox9, however, only slightly (but significantly – $p = 0.043$) stimulated aggrecan expression.

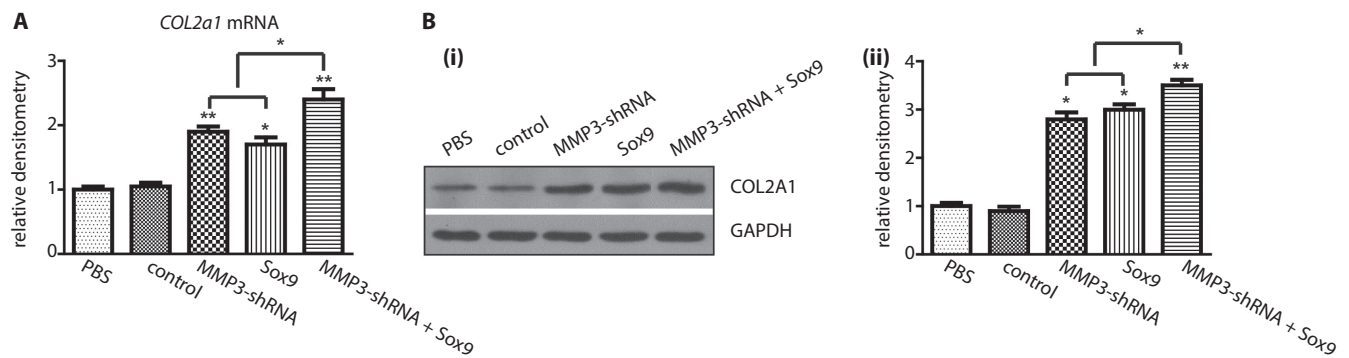


Fig. 4. MMP3 knockdown or Sox9 overexpression induces collagen II expression. A. qPCR analysis for COL2A1 mRNA. B. Western blot analysis for COL2A1 (i) and densitometry of protein bands normalized with GAPDH using ImageJ (ii). The p-values on top of the bars denote the comparison between each lentiviral transgene group and an empty lentivirus group. For (A), data is presented as means \pm SEM. For (B), data is presented as mean \pm SD

* $p < 0.05$; ** $p < 0.01$.

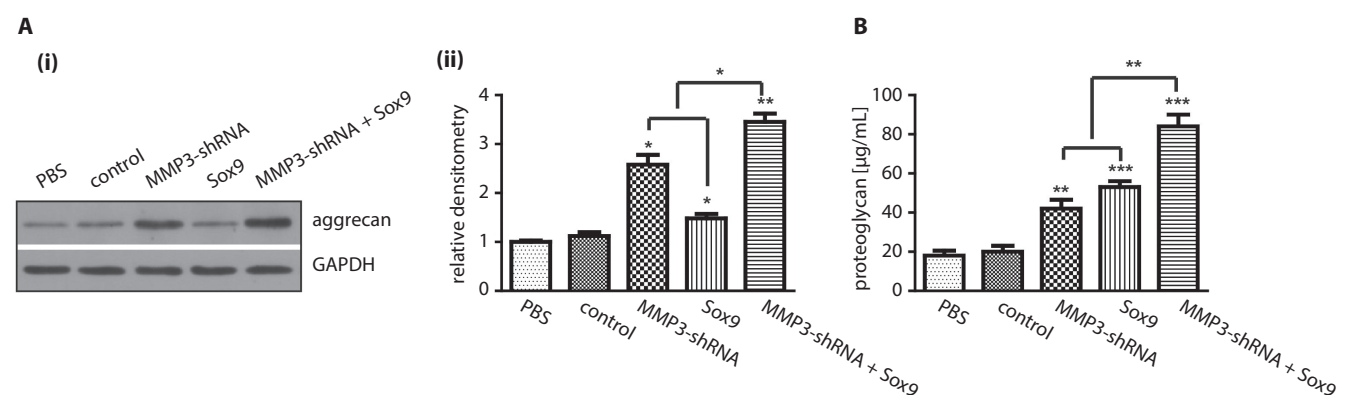


Fig. 5. MMP3 knockdown or Sox9 overexpression stimulates proteoglycan production. A. Western blot analysis for aggrecan (i) and densitometry of protein bands normalized with GAPDH using ImageJ (ii). B. Proteoglycan assay in NP tissue. The p-values on top of the bars denote the comparison between each lentiviral transgene group and an empty lentivirus group. For (A), data is presented as means \pm SD. For (B), data is presented as means \pm SEM

* $p < 0.05$; ** $p < 0.01$; *** $p < 0.001$.

In contrast, the injection of both lentiviruses resulted in the highest expression of aggrecan, which was a 3.08-fold increase in comparison with the controls (Fig. 5A).

Besides the upregulation of aggrecan by lentivirus, we found that the knockdown of MMP3 or overexpression of Sox9 resulted in a 2.1- and 2.65-fold higher synthesis of sGAG, respectively, compared to the controls. Strikingly, injecting both LV-MMP3-shRNA and LV-Sox9 vectors led to the strongest induction of sGAG: a 4.2-fold increase (Fig. 5B). These results suggest that lentivirus-mediated MMP3 knockdown or Sox9 overexpression increases proteoglycan production, and more importantly, indicates that the injection of a MMP3-shRNA/Sox9 lentivirus cocktail triggers a synergistic effect to enhance proteoglycan synthesis.

Discussion

As the major cause of lower back pain, IDD is characterized by excessive degradation of the ECM, particularly the type II collagen and aggrecan in NP tissues.¹⁸ Since

the matrix in NP mediates lumbar discs' resistance to compressive stresses,¹⁰ the reconstitution of matrix components using gene therapy is of great importance in the delay or attenuation of IDD. The family of MMPs is thought to constitute the major catabolic enzymes in the intervertebral disc.⁸ Increased MMP expression and/or activity have been implicated in the pathogenesis of IDD. Although gene therapy using viral or non-viral vectors to overexpress growth factors or cytokines has received considerable interest, a therapy that directly antagonizes MMP to prevent disc degeneration has not been studied, and this warrants investigation.

In our study, we established a needle-puncture-induced IDD model in rabbits, as reported previously.^{15–17} The MRI scans revealed that the lumbar discs injected with PBS or empty lentivirus underwent degenerative process as early as after 8 weeks, and the disc degeneration became extremely pronounced 24 weeks after injection. However, injecting lentivirus carrying MMP3-shRNA greatly delayed the progression of IDD on MRI, suggesting that the inhibition of MMP3 is effective in preventing disc degeneration. Biochemical assays further suggested

that lentivirus-mediated MMP3 knockdown increased the expression of collagen II at both the mRNA and protein levels. This finding is interesting because MMP3 mainly degrades collagen II and other types of collagen (e.g., III, IV, IX, and X), but it cannot degrade collagen I,¹⁹ which is the predominant type of collagen fibers in the later stages of disc degeneration. As a result, the knockdown of MMP3 using gene therapy not only avoids degradation of collagen II in the NP, but it does so without affecting the degradation of collagen I by other MMPs. Additionally, lentiviral delivery of MMP3-shRNA increased the production of proteoglycan, as evidenced by the upregulated expression of aggrecan and the synthesis of sGAG. These findings suggest that gene therapy targeting MMP3 represents an efficient approach against IDD.

As a master regulator for chondrogenic differentiation, Sox9 directly drives collagen II and aggrecan gene expression.⁸ A loss of Sox9 is closely associated with disc degeneration.¹⁰ In our study, direct in vivo gene delivery of the Sox9 lentivirus attenuated the progression of lumbar disc degeneration, as indicated by MRI scans. Overexpression of Sox9 also increased the production of collagen II and proteoglycan, suggesting that lentiviral Sox9 gene delivery can be used to alleviate IDD through its reconstitution of major matrix components. In support of our findings, Paul et al. previously reported that adenoviral vectors carrying the *Sox9* gene are able to increase the production of type II collagen in degenerated human disc cells.²⁰ Unfortunately, adenoviral vectors can only mediate transient gene expression, and their in vivo application is limited due to the virus-induced immune response. As such, lentiviral vectors carrying *Sox9*, which mediate long-term transgene expression without severe immunogenic activity, offer greater advantages over adenoviruses.

Notably, our study demonstrated that a cocktail delivery of MMP3-shRNA and Sox9 lentiviruses dramatically blocked lumbar disc degeneration in rabbits. Even 24 weeks after combined injection, a time point when extremely severe disc degeneration was observed in the animals injected with PBS or an empty virus, MRI scans still identified intact disc tissues, with the highest signal intensity among all lentivirus-treated groups. Interestingly, Moon et al. reported that combination therapy of TGF β 1, IGF1 and BMP2 adenoviral vectors is better than single-gene therapy because multiple gene transduction enables enhanced biological responses, such as proteoglycan synthesis.²¹ Likewise, in our study, the combined gene transfer of lentiviral MMP3-shRNA and Sox9 vectors displayed greater capacity than the injection of LV-MMP3-shRNA or LV-Sox9 alone in the induction of collagen II expression and proteoglycan production, suggesting that combined gene delivery triggers a synergistic effect in ECM synthesis. The mechanism underlying this synergy seems likely to be mediated through the simultaneous inhibition of matrix degradation (via MMP3 knockdown) and enhancement of matrix induction (via Sox9 overexpression),

thereby leading to maximized matrix production. Notably, we observed that delivery of the 2 lentiviruses reduced MMP3 – or increased Sox9 – mRNA to a level comparable to that of LV-MMP3-shRNA or LV-Sox9 gene delivery alone. We assume that there may be an interaction between the 2 transgenes to further impact their expression, resulting in augmented Sox9 or greatly reduced MMP3 expression. Our assumption is partially supported by a recent study, in which Sox9 was able to inhibit the enzymatic activities of MMP2 and MMP13 through its binding with the MMP gene promoter.²²

In general, our results demonstrate that lentivirus-mediated in vivo gene therapy targeting MMP3 or overexpressing Sox9 is efficient in delaying lumbar disc degeneration by restoring 2 major NP matrix components, collagen II and proteoglycan. Our results also suggest that gene therapy delivering MMP3-shRNA and Sox9 lentiviruses offers a promising approach for maximizing matrix reconstitution with a minimal dose of lentivirus mixture.

ORCID iDs

Zheng Zhao  <https://orcid.org/0000-0002-6523-3425>

Siyuan Li  <https://orcid.org/0000-0003-4220-4493>

Hui Huang  <https://orcid.org/0000-0002-7600-2331>

Jing Fang  <https://orcid.org/0000-0002-3372-8650>

Huawei Wei  <https://orcid.org/0000-0001-7483-0902>

Yongming Xi  <https://orcid.org/0000-0002-0861-6147>

References

- Hodgkinson T, Shen B, Diwan A, Hoyland JA, Richardson SM. Therapeutic potential of growth differentiation factors in the treatment of degenerative disc diseases. *JOR Spine*. 2019;2(1):e1045.
- Lyu FJ, Cheung KM, Zheng Z, Wang H, Sakai D, Leung VY. IVD progenitor cells: A new horizon for understanding disc homeostasis and repair. *Nat Rev Rheumatol*. 2019;15(2):102–112.
- Gruber HE, Hoelscher GL, Ingram JA, Hanley EN Jr. Matrix metalloproteinase-26, a novel MMP, is constitutively expressed in the human intervertebral disc in vivo and in vitro. *Exp Mol Pathol*. 2012;92(1):59–63.
- Eser B, Eser O, Yuksel Y, et al. Effects of MMP-1 and MMP-3 gene polymorphisms on gene expression and protein level in lumbar disc herniation. *Genet Mol Res*. 2016;15(3). doi:10.4238/gmr.15038669
- Lv FJ, Peng Y, Lim FL, et al. Matrix metalloproteinase 12 is an indicator of intervertebral disc degeneration co-expressed with fibrotic markers. *Osteoarthritis Cartilage*. 2016;24(10):1826–1836.
- Zigouris A, Alexiou GA, Batistatou A, Voulgaris S, Kyritsis AP. The role of matrix metalloproteinase 9 in intervertebral disc degeneration. *J Clin Neurosci*. 2011;18(10):1424–1425.
- Bachmeier BE, Nerlich A, Mittermaier N, et al. Matrix metalloproteinase expression levels suggest distinct enzyme roles during lumbar disc herniation and degeneration. *Eur Spine J*. 2009;18(11):1573–1586.
- Lefebvre V, Angelozzi M, Haseeb A. SOX9 in cartilage development and disease. *Curr Opin Cell Biol*. 2019;61:39–47.
- Sive JI, Baird P, Jeziorski M, Watkins A, Hoyland JA, Freemont AJ. Expression of chondrocyte markers by cells of normal and degenerate intervertebral discs. *Mol Pathol*. 2002;55(2):91–97.
- Gruber HE, Norton HJ, Ingram JA, Hanley EN Jr. The SOX9 transcription factor in the human disc: Decreased immunolocalization with age and disc degeneration. *Spine (Phila Pa 1976)*. 2005;30(6):625–630.
- Sobajima S, Kim JS, Gilbertson LG, Kang JD. Gene therapy for degenerative disc disease. *Gene Ther*. 2004;11(4):390–401.
- Nishida K, Kang JD, Gilbertson LG, et al. Modulation of the biologic activity of the rabbit intervertebral disc by gene therapy: An in vivo study of adenovirus-mediated transfer of the human transforming growth factor beta 1 encoding gene. *Spine (Phila Pa 1976)*. 1999;24(23):2419–2425.

13. Nishida K, Suzuki T, Kakutani K, et al. Gene therapy approach for disc degeneration and associated spinal disorders. *Eur Spine J*. 2008;17(Suppl 4):459–466.
14. Ren S, Liu Y, Ma J, et al. Treatment of rabbit intervertebral disc degeneration with co-transfection by adeno-associated virus-mediated SOX9 and osteogenic protein-1 double genes in vivo. *Int J Mol Med*. 2013;32(5):1063–1068.
15. Masuda K, Aota Y, Muehleman C, et al. A novel rabbit model of mild, reproducible disc degeneration by an annulus needle puncture: Correlation between the degree of disc injury and radiological and histological appearances of disc degeneration. *Spine (Phila Pa 1976)*. 2005;30(1):5–14.
16. Kwon YJ. A minimally invasive rabbit model of progressive and reproducible disc degeneration confirmed by radiology, gene expression, and histology. *J Korean Neurosurg Soc*. 2013;53(6):323–330.
17. Lei T, Zhang Y, Zhou Q, et al. A novel approach for the annulus needle puncture model of intervertebral disc degeneration in rabbits. *Am J Transl Res*. 2017;9(3):900–909.
18. Vo NV, Hartman RA, Yurube T, Jacobs LJ, Sowa GA, Kang JD. Expression and regulation of metalloproteinases and their inhibitors in intervertebral disc aging and degeneration. *Spine J*. 2013;13(3):331–341.
19. Newell N, Carpanen D, Evans JH, Pearcy MJ, Masouros SD. Mechanical function of the nucleus pulposus of the intervertebral disc under high rates of loading. *Spine (Phila Pa 1976)*. 2019;44(15):1035–1041.
20. Paul R, Haydon RC, Cheng H, et al. Potential use of Sox9 gene therapy for intervertebral degenerative disc disease. *Spine (Phila Pa 1976)*. 2003;28(8):755–763.
21. Moon SH, Nishida K, Gilbertson LG, et al. Biologic response of human intervertebral disc cells to gene therapy cocktail. *Spine (Phila Pa 1976)*. 2008;33(17):1850–1855.
22. Luo H, Wang C, Liu M, et al. Inhibition of SOX9 promotes inflammatory and immune responses of dental pulp. *J Endod*. 2018;44(5):792–799.

Weighted gene co-expression network analysis to investigate the key genes implicated in global brain ischemia/reperfusion injury in rats

Dingying Ma^{1,A,C}, Jun Qiao^{2,A,B}, Qiang Qu^{3,B,F}, Fei He^{4,A,D}, Wenhua Chen^{3,4,D–F}, Bo Yu^{4,C,D,F}

¹ Department of Rehabilitation Medicine, Ningbo No. 9 Hospital, China

² Department of Rehabilitation, Shanghai Second Rehabilitation Hospital, China

³ Department of Rehabilitation, School of International Medical Technology, Shanghai Sanda University, China

⁴ Department of Rehabilitation Medicine, Shanghai General Hospital, Shanghai Jiaotong University, China

A – research concept and design; B – collection and/or assembly of data; C – data analysis and interpretation; D – writing the article; E – critical revision of the article; F – final approval of the article

Advances in Clinical and Experimental Medicine, ISSN 1899–5276 (print), ISSN 2451–2680 (online)

Adv Clin Exp Med. 2020;29(6):649–659

Address for correspondence

Bo Yu

E-mail: Bobby_JTU@163.com

Funding sources

Shanghai Science and Technology Committee (grant No.16411955200) and Scientific Research and Innovation Team Funding Plan of Shanghai Sanda University, China.

Conflict of interest

None declared

Received on November 28, 2018

Reviewed on January 3, 2019

Accepted on May 1, 2020

Published online on June 19, 2020

Cite as

Ma D, Qiao J, Qu Q, He F, Chen W, Yu B. Weighted gene co-expression network analysis to investigate the key genes implicated in global brain ischemia/reperfusion injury in rats. *Adv Clin Exp Med.* 2020;29(6):649–659. doi:10.17219/acem/121918

DOI

10.17219/acem/121918

Copyright

© 2020 by Wrocław Medical University

This is an article distributed under the terms of the Creative Commons Attribution 3.0 Unported (CC BY 3.0) (<https://creativecommons.org/licenses/by/3.0/>)

Abstract

Background. Ischemia/reperfusion (I/R) refers to situations where blood is perfused into ischemic or hypoxic tissues, potentially resulting in an inflammatory response and oxidative injury.

Objectives. This study was conducted to explore the pathogenesis of I/R injury.

Material and methods. GSE82146 was extracted from the Gene Expression Omnibus, consisting of 15 complete global brain ischemia (CGBI) reperfusion hippocampus samples and 12 non-ischemic control (NIC) hippocampus samples. The differentially expressed genes (DEGs) between the CGBI and NIC samples were selected using LIMMA package, and were then analyzed with weighted gene co-expression network analysis (WGCNA). Using DAVID software, the DEGs in significant modules were run through enrichment analysis. The DEGs in significant modules were merged, and then a protein–protein interaction (PPI) network was built for them using Cytoscape software. After miRNAs and transcription factors (TFs) were predicted for the DEGs using the WebGestalt tool, a TF–miRNA–target regulatory network was built using Cytoscape software. Furthermore, quantitative real-time polymerase chain reaction (qRT-PCR) analysis was conducted to detect the levels of key genes.

Results. There were 390 DEGs in the CGBI samples. Based on WGCNA, brown and turquoise modules were screened as CGBI-associated modules. In the PPI network, key nodes *HSP90AA1* and *HSPA5* were able to interact with each other. In the regulatory network, *MYC*, *HSF1* and *miR-22* had higher degree values. Moreover, *HSPA5* was targeted by *MYC* in the regulatory network. In addition, upregulated *HSPB1* and *HMOX1*, as well as downregulated *NR4A2*, were confirmed with qRT-PCR analysis.

Conclusions. *HSPB1*, *HMOX1* and *NR4A2* were the key genes correlated with I/R injury. Additionally, *HSP90AA1*, *HSPA5*, *MYC*, *HSF1*, and *miR-22* might be related to the pathogenesis of I/R injury.

Key words: ischemia/reperfusion, differentially expressed genes, regulatory network, protein–protein interaction network, weighted gene co-expression network analysis

Introduction

Ischemia/reperfusion (I/R) refers to a situation where blood is perfused into tissues experiencing ischemia or hypoxia.¹ Although I/R promotes the repair of damage and the recovery of functioning in most cases, it can also lead to an inflammatory response and oxidative injury by inducing oxidative stress.² Ischemia/reperfusion is usually related to microvascular injury, and the imbalance of reactive oxygen species (ROS) and nitric oxide (NO) produced by activated endothelial cells is responsible for the subsequent inflammatory response.^{3,4} The development of I/R injury is influenced by ischemia time, aerobic degree, collateral circulation, and reperfusion conditions. The I/R injury has a powerful influence on the ischemic cascade of the brain, involving brain trauma and stroke.⁵ Hence, the molecular mechanisms of I/R injury need to be investigated to better alleviate its adverse effects in clinical practice.

By inhibiting nuclear factor- κ B (*NF- κ B*), ginkgolide B (*GB*) possesses anti-apoptotic and anti-inflammatory effects and has demonstrated neuroprotective roles in mice with ischemia-induced brain injury.^{6,7} The inhibition of P2X7 receptors (*P2X7Rs*) protects rats from cerebral I/R injury by decreasing inflammatory response and may serve as a novel therapeutic approach for transient global cerebral I/R injury. By increasing B-cell leukemia-2 (*Bcl-2*) expression and reducing Bcl-2-associated X protein (*Bax*) expression, propofol functions as a neuroprotective agent in I/R rats.⁸ Oxymatrine can protect the brain of stroke rats from focal I/R injury, and the activation of the nuclear factor erythroid 2-related factor 2 (*Nrf2*)/hemeoxygenase-1 (*HO-1*) pathway may promote the neuroprotective effects of oxymatrine in the focal brain I/R rat model.⁹ *MiR-124* mediates the expression of Ku autoantigen 70 (*Ku70*) and helps to reduce the neuronal death and brain dysfunction caused by I/R. *MiR-134* downregulation relieves cerebral ischemic injury through regulating the enhancing cyclic AMP (cAMP) response element-binding protein (*CREB*) and downstream genes, which provides a potential therapeutic target for the injury.¹⁰ Nevertheless, the genes and miRNAs affecting brain I/R injury have not been thoroughly explored.

In 2016, Wang et al. performed differential expression analysis on I/R in hippocampus CA1 and CA3, and found that CA3 is better at handling ischemic stress. However, the pathogenesis of I/R injury was not comprehensively researched by them.¹¹ To further identify the key genes and miRNAs involved in I/R injury, within this study, a series of bioinformatics analyses was carried out (such as differential expression analysis, weighted gene co-expression network analysis (WGCNA), enrichment analysis, and network analysis) on the expression profile data uploaded by Wang et al.¹¹ In addition, quantitative real-time polymerase chain reaction (qRT-PCR) analysis was conducted to confirm the key genes.

Material and methods

Data source

The microarray dataset GSE82146 (species: *Rattus norvegicus*) from the Gene Expression Omnibus database (GEO, <http://www.ncbi.nih.gov/geo>) was extracted, which was determined on the platform of GPL17117 (RaGene-2_0-st) Affymetrix Rat Gene 2.0 ST Array (transcript (gene) version). There were 15 complete global brain ischemia (CGBI) reperfusion hippocampus samples and 12 non-ischemic control (NIC) hippocampus samples in GSE82146. In Long Evans rats (male, 275–300 g), CGBI was induced with the two-vessel bilateral carotid artery occlusion and hypovolemic hypotension model,¹² as previously described.^{13–15} Our research was approved by the ethics committee of Ningbo No. 9 Hospital, China.

Differential expression analysis

The original data in CEL format was downloaded and preprocessed (including format conversion, filling in of the missing data, background correction (MicroArray Suite method), and data standardization (quartile method)) using the R oligo package (v. 1.36.1; <http://www.bioconductor.org/packages/release/bioc/html/oligo.html>).¹⁶ Next, the corresponding genes of the probes were annotated based on the annotation platform. For genes with multiple expression values (mapped to multiple probes), the average value was calculated as the unique expression value.

Using the R LIMMA package (v. 3.10.3; <http://www.bioconductor.org/packages/2.9/bioc/html/limma.html>),¹⁷ differential expression analysis between the CGBI and NIC samples was carried out. The differentially expressed genes (DEGs) were selected using the thresholds of adjusted p-value <0.05 and of logfold change (FC) >0.5.

WGCNA to identify disease-associated modules and genes

The WGCNA is a typical algorithm in system biology for constructing a gene co-expression network which can be used to identify modules of the relevant genes.¹⁸ To screen the CGBI-associated modules and genes, the expression values of the DEGs in each group were determined with WGCNA.¹⁸ The detailed processes of network building and module identification included consistency analysis between the datasets, the definition of gene co-expression-correlated matrix (the correlation coefficient between gene m and gene n was $S_{mn} = |\text{cor}_{(m,n)}|$), the definition of the adjacent function (the adjacent function was $a_{mn} = \text{power}_{(S_{mn}, \beta)}$), the determination of the parameters for the adjacent function (the weighting coefficient $\beta \geq 0.8$), the measurement of the degree of dissimilarity between the nodes, the identification of gene modules (the number of genes in the module ≥ 30), and the determination of the correlation between network module and disease state.

Enrichment analysis

Using DAVID software (v. 6.8; <https://david-d.ncifcrf.gov/>),¹⁹ Gene Ontology (GO)²⁰ and Kyoto Encyclopedia of Genes and Genomes (KEGG),²¹ enrichment analyses were conducted for the DEGs in significant modules. The thresholds for selecting significant terms were p -values <0.05 and counts of involved genes ≥ 2 .

Protein–protein interaction (PPI) network analysis

After the DEGs in significant modules were merged, they were input into the STRING database (v. 10.0; <http://www.string-db.org/>)²² to predict the PPIs among them. The species was rat and the parameter PPI score was set at 0.4. The PPI results were downloaded in TSV format and Cytoscape (v. 3.2.0; <http://www.cytoscape.org/>)²³ was used to construct the PPI network.

Transcription factor–miRNA–target regulatory network analysis

Using the WebGestalt tool (<http://www.webgestalt.org/>),²⁴ miRNAs and transcription factors (TFs) were predicted for the DEGs involved in the PPI network using Overrepresentation Enrichment Analysis (ORA). The species was rat and the reference background was the Affymetrix Rat Gene v. 2.0 ST platform. According to significance levels, the top 10 results of miRNA–target and TF–target were obtained and integrated. Then, a TF–miRNA–target regulatory network was built using Cytoscape software.²³

qRT-PCR analysis

The total RNA of 7 brain I/R tissues and 7 control tissues were isolated using a Trizol total RNA extraction kit (Invitrogen, Shanghai, China) following the manufacturer's instructions. The purity and integrity of RNA were evaluated separately by spectrophotometer (Merinton, Beijing, China) and 2% agarose gel electrophoresis. The primer sequences of key genes were designed for qRT-PCR experiments (Table 1), and were then produced by Sangon Biotech Co., Ltd. (Shanghai, China). The qRT-PCR experiments were carried out using SYBR Green master mix kit (Applied Biosystems, Foster City, USA). The 20- μ L PCR amplification system consisted of 10 μ L of SYBR Premix Ex Taq ($\times 2$), 8 μ L of cDNA template (keeping a consistent level after being diluted with ddH₂O), 1 μ L of forward primer (10 μ M), and 1 μ L of reverse primer (10 μ M). The reaction conditions were 40 cycles of 50°C for 3 min, 95°C for 3 min, 95°C for 10 s, and 60°C for 30 s. Afterwards, a melt curve was created. All experiments were repeated 3 times, and glyceraldehyde-3-phosphate dehydrogenase (*GAPDH*) was utilized as the reference gene.

Table 1. The primer sequences designed for qRT-PCR experiments

Primer names	Primer sequences (5'-3')
GAPDH-rF	AGACAGCCGCATCTTCTTGT
GAPDH-rR	CTTGCCGTGGGTAGAGTCAT
HSPB1-rF	GATCACTGGCAAGCACGAAG
HSPB1-rR	CCTGGAGGGAGCGTGATTT
HMOX1-rF	CGTGCTCGCATGAACACTCT
HMOX1-rR	GGCCTCTGGCGAAGAAACTC
NR4A2-rF	CTGTGAGCATTACGGTGTTCG
NR4A2-rR	ATCCTGTGGCTCTTCGGTT

Statistical analysis

The expression levels of the key genes were analyzed using the $2^{-\Delta\Delta C_t}$ method.²⁵ All data are presented as mean \pm standard error of the mean (SEM). SPSS v. 22.0 software (SPSS Inc., Chicago, USA) was used to perform statistical analysis, with $p < 0.05$ serving as the threshold of statistical significance.

Results

Differential expression analysis

There were 390 DEGs in the CGBI samples compared with the NIC samples, including 330 upregulated genes (such as heat shock protein B1 (*HSPB1*) and heme oxygenase (decycling) 1 (*HMOX1*)), and 60 downregulated genes (such as nuclear receptor subfamily 4 group A member 2 (*NR4A2*)). The clustering heatmap suggested that the samples could be obviously differentiated by the DEGs (Fig. 1).

WGCNA analysis and enrichment analysis

In order to meet the prerequisite of scale-free network distribution, the adjacency matrix weighting parameter “power” was explored. As a result, a “power” value of 19 was selected when the square of correlation coefficient first reached 0.8 (Fig. 2).

A co-expression network was constructed based on this “power” value. Firstly, the dissimilarity coefficients among the DEGs were calculated. Using the dissimilarity matrix, hierarchical clustering was performed to obtain a system clustering tree of the DEGs (Fig. 3A). According to the standards of a hybrid dynamic shear tree, the lowest gene number of each network module was set at 30. After network modules were identified using the dynamic shear method, the feature vector “eigengenes” was calculated for each module. Subsequently, the modules underwent clustering analysis, and the modules with close clustering relationships were merged into a new module. Finally,

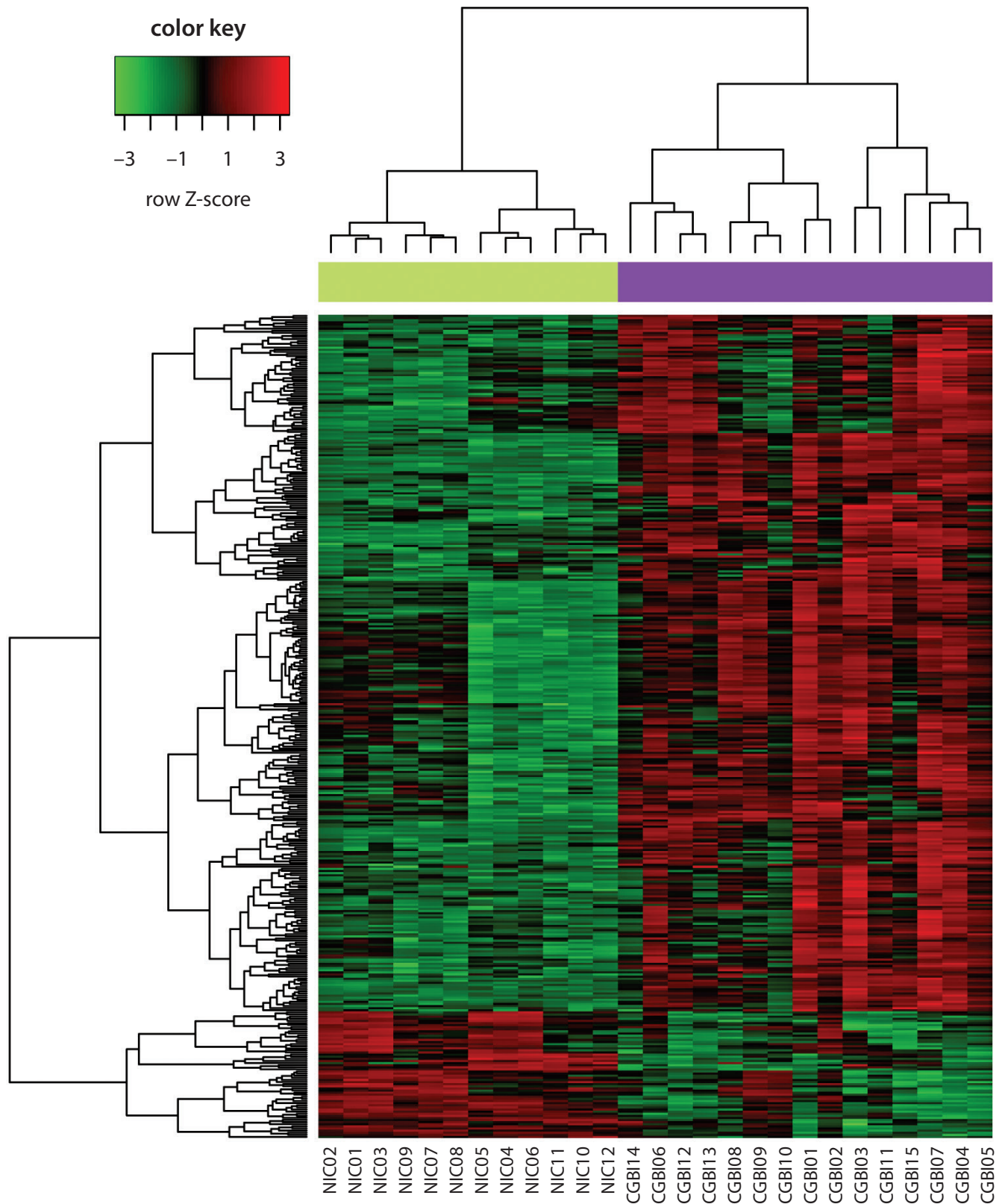


Fig. 1. Clustering heatmap for DEGs. Green and purple color in the sample strip separately represent the non-ischemic control (NIC) hippocampus samples and the complete global brain ischemia (CGBI) reperfusion hippocampus samples. The horizontal and vertical axes represent the clusters of samples and the clusters of genes, respectively

the DEGs were divided into 5 network modules (Fig. 3B), and the grey module was a set of the DEGs that could not be gathered into other modules.

To identify CGBI-associated modules, the feature vector of each module and CGBI was conducted with correlation analysis. The absolute values of correlation coefficients for

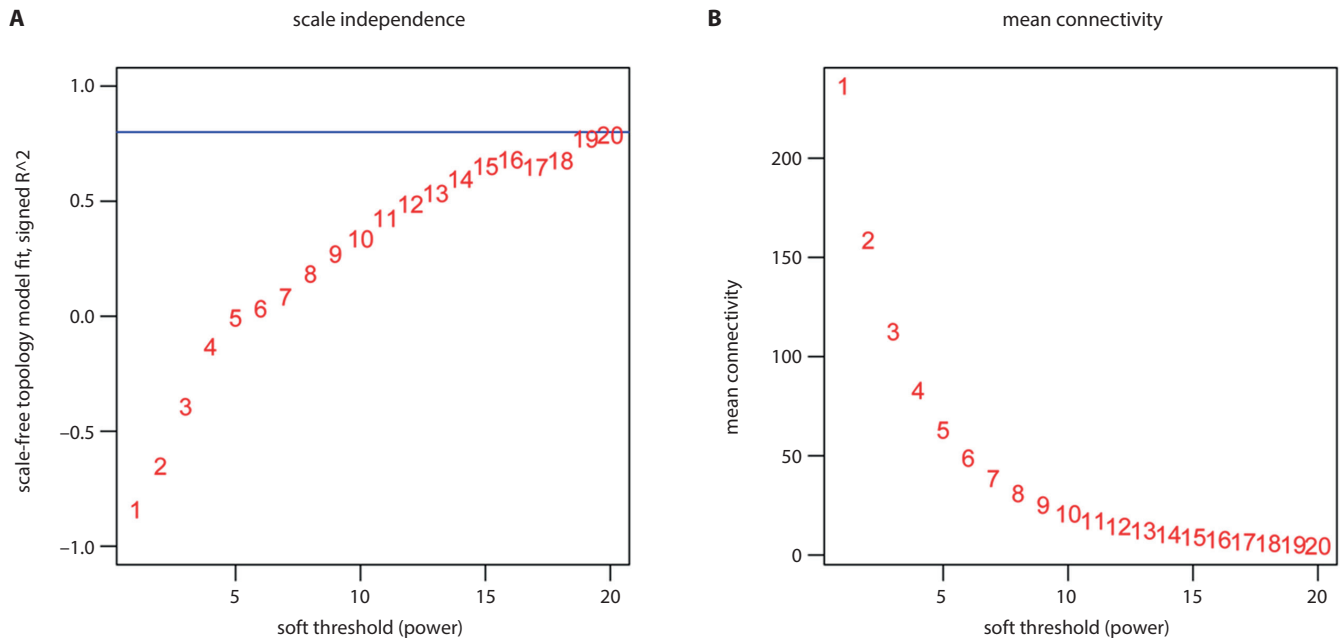


Fig. 2. The scale independence (A) and mean connectivity (B) for selecting the adjacency matrix weighting parameter “power”. The higher the square of correlation coefficient, the closer the network is to scale-free network distribution. The blue line represents the standard line when the square of the correlation coefficient reaches 0.8

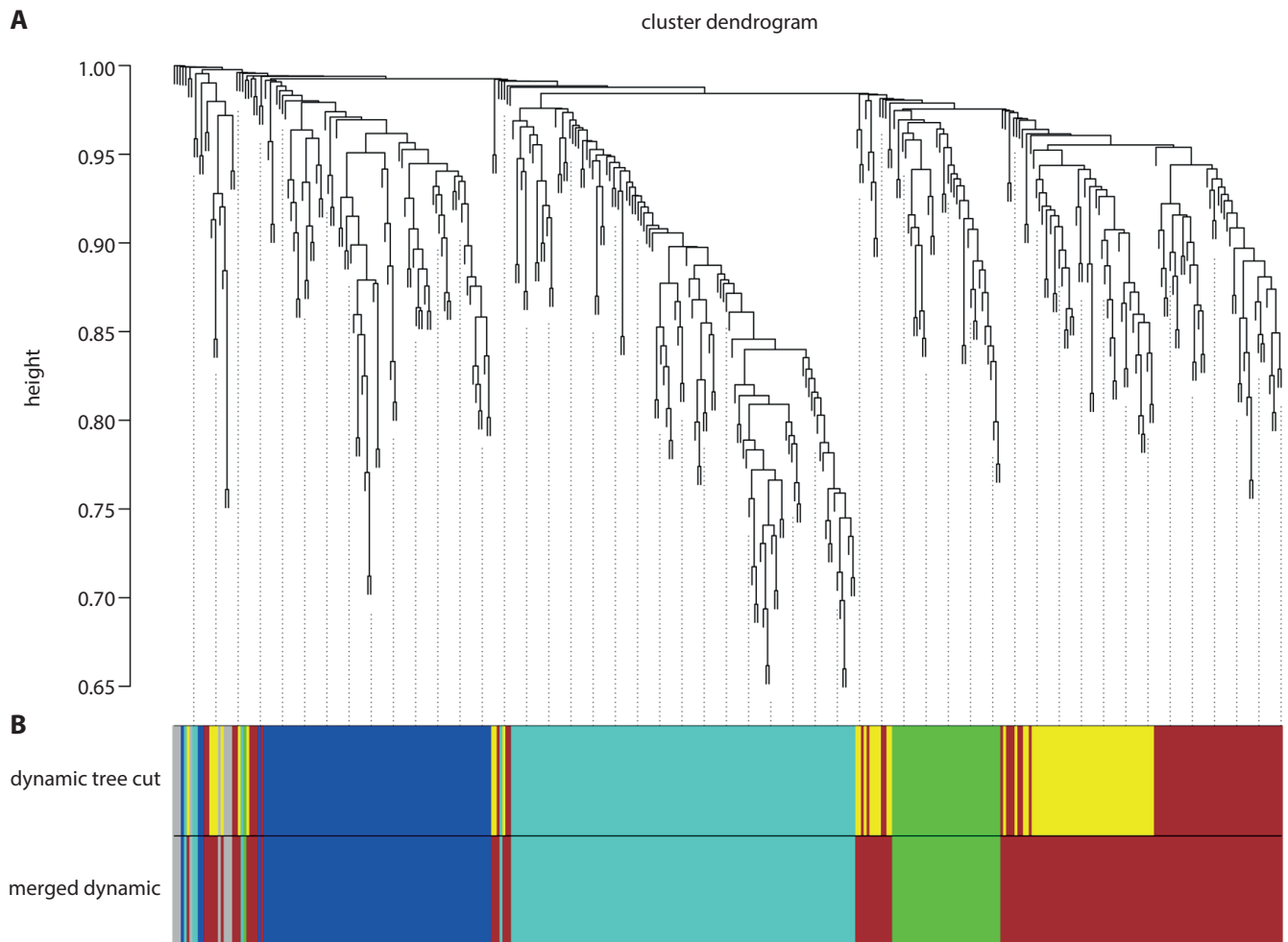


Fig. 3. The system clustering tree for the dissimilarity matrix (A), and the network modules before (dynamic tree cut) and after (merged dynamic) merging (B)

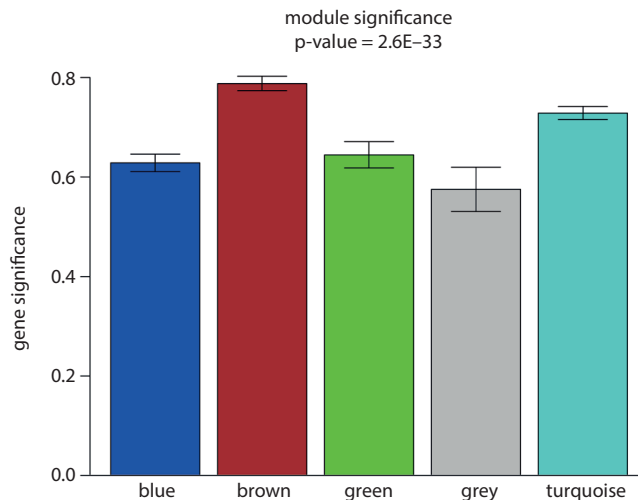


Fig. 4. The correlation graph of each module and complete global brain ischemia (CGBI). Horizontal axis and vertical axis separately represent module and gene significance

the modules were sorted, and it was found that the values for brown and turquoise modules were higher than 0.8 (Table 2). Meanwhile, the absolute values of gene significance for the modules were also calculated in order to screen CGBI-associated modules (Fig. 4). In addition, the heatmaps for the genes in the brown and turquoise modules are shown separately in Fig. 5A and 5B.

Functional and pathway enrichment analysis

The DEGs in the brown and turquoise modules were conducted with enrichment analysis. The DEGs in the brown module were mainly implicated in the positive regulation of gene expression (GO; p -value = $9.61E-09$) and protein processing in the endoplasmic reticulum (KEGG; p -value = $2.86E-07$). Also, the DEGs in the turquoise module were mainly involved in protein folding (GO; p -value = $3.33E-07$) and aminoacyl-tRNA biosynthesis (KEGG; p -value = $4.58E-07$) (Table 3).

PPI network analysis

The DEGs in the brown and turquoise modules were merged, and a total of 259 DEGs were obtained (including 115 upregulated genes in the brown module, 115 upregulated genes in the turquoise module, 18 downregulated genes in the brown module, and 11 downregulated genes in the turquoise module). Next, the PPI network was built; it had 164 nodes and 620 edges (Fig. 6A). According to the degree values of the network nodes, heat shock protein 90 alpha family class A member 1 (HSP90AA1; degree = 47) and heat shock protein 5 (HSPA5; degree = 25) were key nodes. Additionally, HSP90AA1 and HSPA5 interacted in the PPI network.

Table 2. The results of correlation analysis of each module and complete global brain ischemia

Module	Correlation coefficient	p-value
Brown	0.92	$1.74E-11$
Turquoise	0.83	$1.06E-07$
Blue	0.73	$1.64E-05$
Green	0.72	$2.57E-05$
Grey	-0.75	$5.85E-06$

TF-miRNA-target regulatory network analysis

A total of 228 TF-miRNA-target regulatory relationships were obtained, involving 6 TFs, 10 miRNAs, and 99 targets (including 46 upregulated genes in the brown module, 45 upregulated genes in the turquoise module, 5 downregulated genes in the brown module, and 3 downregulated genes in the turquoise module). The TF-miRNA-target regulatory network is shown in Fig. 6B. In the regulatory network, the myelocytomatosis oncogene (*MYC*; TF, degree = 38), heat shock transcription factor 1 (*HSF1*; TF, degree = 25), and *miR-22* (degree = 12) had higher degree values. Importantly, *MYC* could target *HSPA5* in the regulatory network.

qRT-PCR analysis

The levels of *HSPB1*, *HMOX1* and *NR4A2* in the brain I/R tissues and the control tissues were detected using qRT-PCR experiments. *HSPB1* ($p < 0.001$; Fig. 7A) and *HMOX1* ($p < 0.001$; Fig. 7B) were significantly upregulated in the brain I/R tissues compared with the control tissues, while *NR4A2* ($p < 0.001$; Fig. 7C) was significantly downregulated. These findings were consistent with the results of differential expression analysis.

Discussion

In this study, 390 DEGs (including upregulated *HSPB1* and *HMOX1*, as well as downregulated *NR4A2*) were identified in the CGBI samples. Through WGCNA analysis, the brown and turquoise modules were screened as CGBI-associated modules. After the DEGs in the brown and turquoise modules were merged, a PPI network was built for them. In the PPI network, HSP90AA1 and HSPA5 were the key nodes. Moreover, *MYC*, *HSF1* and *miR-22* had higher degree values in the TF-miRNA-target regulatory network. Additionally, the qRT-PCR experiments confirmed upregulated *HSPB1* and *HMOX1* and downregulated *NR4A2*.

Oxidative stress can induce the phosphorylation of *HSPB1* and *HSPB5*, which play neuroprotective roles

Table 3. The Gene Ontology (GO) terms (A) and pathways (B) enriched for DEGs in the brown and turquoise modules

(A)

Module	GO_ID	Biological process	Count	p-value	Genes
Brown	GO:0010628	positive regulation of gene expression	16	9.61E-09	<i>CCL3, RET, CAV1, SOX11, VIM, PARK2, HSPA1B, IL33, ATF4, ATF3, VEGFA, BCL11A, NFE2L2, MSN, FGF2, PPP1R15A</i>
	GO:0030968	endoplasmic reticulum unfolded protein response	8	1.29E-08	<i>HERPUD1, ATF3, STC2, YOD1, NFE2L2, PPP1R15A, EDEM1, DDIT3</i>
	GO:0034976	response to endoplasmic reticulum stress	9	4.18E-08	<i>ATF4, HERPUD1, STC2, TRIB3, HSPA5, PARK2, NFE2L2, PPP1R15A, DDIT3</i>
	GO:0006986	response to unfolded protein	5	1.62E-05	<i>HERPUD1, CHAC1, PARK2, HSPA1B, DDIT3</i>
	GO:0007568	aging	11	2.69E-05	<i>C1QB, GSTA3, CRYAB, VIM, VEGFA, HSPB1, NFE2L2, PPP1R15A, FGF2, DDIT3, TIMP1</i>
	GO:0045944	positive regulation of transcription from RNA polymerase II promoter	19	5.74E-05	<i>CCL3, CAMTA2, SOX11, PTBP1, ARID5A, NR4A2, TEAD1, PARK2, IL33, DDIT3, ATF4, ATF3, VEGFA, BCL11A, NFE2L2, USP16, NEUROD6, FGF2, FOSL1</i>
	GO:0043536	positive regulation of blood vessel endothelial cell migration	4	2.11E-04	<i>VEGFA, HSPB1, NFE2L2, FGF2</i>
	GO:0060548	negative regulation of cell death	6	2.20E-04	<i>SOX11, PARK2, HSPA1B, NFE2L2, PPP1R15A, FGF2</i>
	GO:0035690	cellular response to drug	6	3.46E-04	<i>MT2A, VEGFA, HSPA5, RNF149, NFE2L2, PPP1R15A</i>
	GO:0010629	negative regulation of gene expression	8	3.59E-04	<i>CCL3, CDKN1A, STC2, CRYAB, SOX11, VEGFA, BCL11A, PARK2</i>
Turquoise	GO:0006457	protein folding	9	3.33E-07	<i>ST13, TMX1, CCT5, HSP90AA1, CCT4, AARS, DNAJA1, DNAJB4, HSPA9</i>
	GO:0051085	chaperone-mediated protein folding requiring cofactor	3	2.60E-03	<i>HSPH1, CCT4, HSPD1</i>
	GO:0009409	response to cold	4	3.63E-03	<i>HSP90AA1, HSPA2, RBM3, HSPD1</i>
	GO:1902895	positive regulation of pri-miRNA transcription from RNA polymerase II promoter	3	5.58E-03	<i>JUN, STAT3, GNL3</i>
	GO:0006366	transcription from RNA polymerase II promoter	8	9.52E-03	<i>ARRB2, DBP, JUN, TARDBP, CEBPZ, DDX21, STAT3, GTF2H1</i>
	GO:0009408	response to heat	4	1.12E-02	<i>HSP90AA1, HSPA2, DNAJA1, HSPD1</i>
	GO:0043066	negative regulation of apoptotic process	9	1.18E-02	<i>CTH, JUN, NAA15, DNAJA1, MDM2, JAK2, HSPD1, NQO1, STAT3</i>
	GO:1902728	positive regulation of growth factor dependent skeletal muscle satellite cell proliferation	2	1.18E-02	<i>JAK2, STAT3</i>
	GO:1903748	negative regulation of establishment of protein localization to mitochondrion	2	1.18E-02	<i>HSPH1, DNAJA1</i>
	GO:0045944	positive regulation of transcription from RNA polymerase II promoter	13	1.81E-02	<i>CCNL1, STAT3, PRPF6, GTF2H1, HSPH1, DBP, TARDBP, JUN, GTF2F1, ETS2, CEBPZ, KDM3A, JAK2</i>

(B)

Module	Pathway_ID	Pathway name	Count	p-value	Genes
Brown	rno04141	protein processing in endoplasmic reticulum	12	2.86E-07	<i>ATF4, HERPUD1, CRYAB, HSPA5, PARK2, DNAJB1, YOD1, HSPA1B, NFE2L2, PPP1R15A, EDEM1, DDIT3</i>
	rno04010	MAPK signaling pathway	11	1.08E-04	<i>DUSP5, ATF4, DUSP2, MAP2K3, GADD45G, HSPB1, HSPA1B, FLNC, GADD45B, FGF2, DDIT3</i>
	rno05205	proteoglycans in cancer	6	3.61E-02	<i>CAV1, CDKN1A, VEGFA, MSN, FLNC, FGF2</i>
Turquoise	rno00970	aminoacyl-tRNA biosynthesis	8	4.58E-07	<i>TARS, YARS, CARS, NARS, RARS, AARS, LARS, EPRS</i>
	rno03040	spliceosome	7	3.67E-04	<i>SRSF3, SF3B1, HSPA2, CWC15, PRPF6, PRPF40A, RBM17</i>
	rno03008	ribosome biogenesis in eukaryotes	5	3.36E-03	<i>NOP58, WDR43, RIOK2, GNL3, NMD3</i>
	rno04915	estrogen signaling pathway	4	3.01E-02	<i>HSP90AA1, HSPA2, FKBP5, JUN</i>

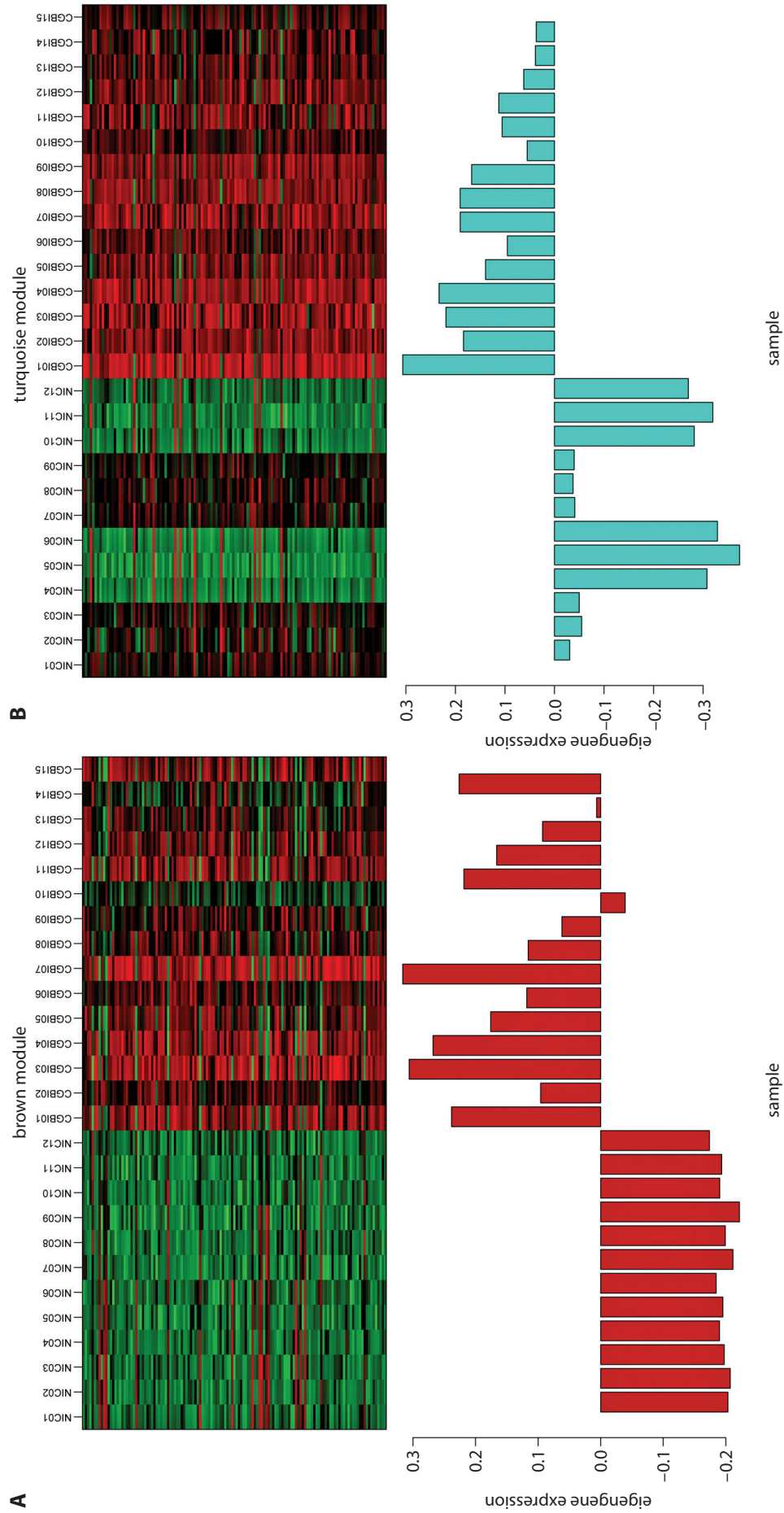


Fig. 5. The expression heatmaps for the genes in the brown (A) and turquoise (B) modules

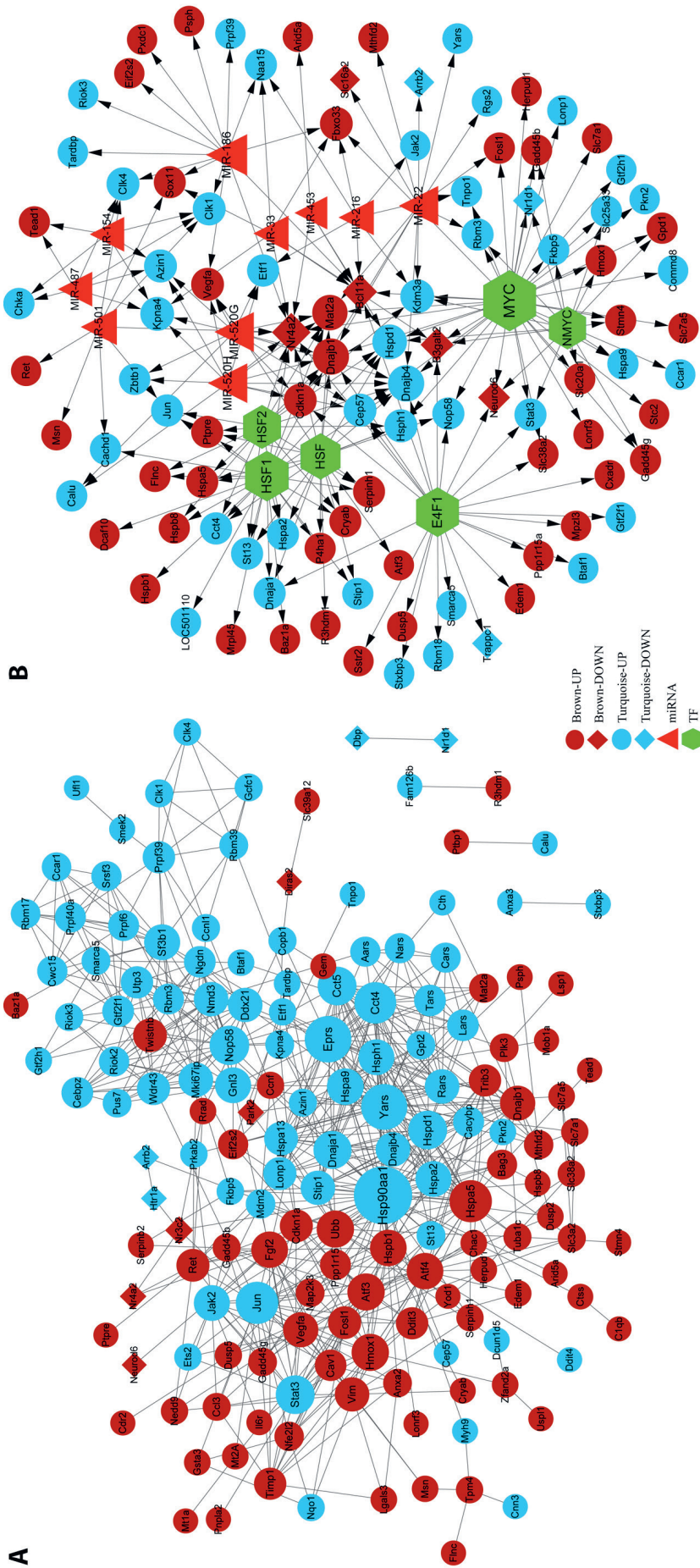


Fig. 6. The protein–protein interaction (PPI) network (A) and the transcription factor-miRNA-target regulatory network (B). Circles and prisms represent upregulated genes and downregulated genes, respectively. Red triangles and green hexagons represent miRNAs and TFs, respectively. Brown and blue represent genes in the brown and turquoise modules, respectively. The higher the degree value of a node, the larger the size of the node is. Arrows indicate the directions of regulation

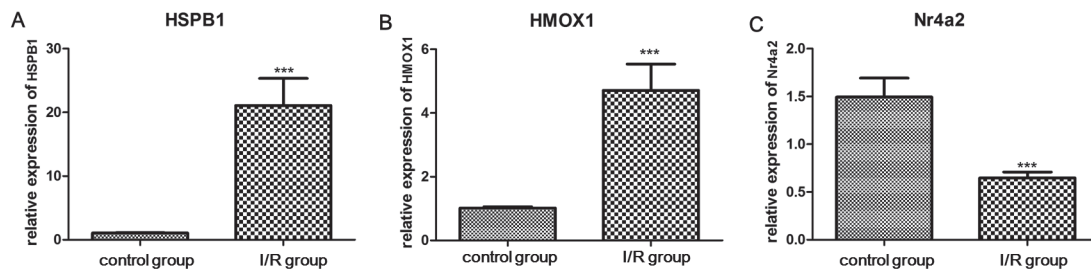


Fig. 7. The expression levels of *HSPB1* (A), *HMOX1* (B) and *NR4A2* (C) in brain I/R tissues and control tissues

*** $p < 0.001$.

in hippocampal neurons. Kupffer cells, which are the main expression sites of hepatic *HMOX1*, have anti-inflammatory effects and can resist the oxidative injury induced by I/R.²⁶ *NURR1* (also named *NR4A2*) contributes to intestinal regeneration following I/R injury by suppressing *p21* expression, which may provide new approaches for the therapy of intestinal I/R injury.²⁷ These findings support the thesis that *HSPB1*, *HMOX1* and *NR4A2* are related to the development and progression of I/R injury.

The mRNA expression of *HSP90AA1* is reduced following I/R and may be promoted by *miR-1* inhibition during myocardial I/R.^{28,29} A high protein expression of *HSPA5* can exert neuroprotective effects and stop neural ischemic injury by attenuating endoplasmic reticulum (ER) stress-induced apoptosis.³⁰ By negatively mediating ubiquitin carboxyl-terminal hydrolase isozyme L1 (*UCHL1*) and *HSPA5* protein levels, *miR-181b* downregulation protects mice from ischemic injury and provides a therapeutic strategy for ischemic stroke.³¹ *HSP90AA1* and *HSPA5* interacted in the PPI network, suggesting that *HSP90AA1* and *HSPA5* might play roles in I/R injury through interaction with each other.

The *MYC* expression is upregulated after acute I/R injury and may promote the low expression of the anti-apoptotic N-myc downstream-regulated gene 2 (*MDM2*), which may be associated with myocardial apoptosis in I/R rats.^{32,33} By weakening *NF-κB* activation and reducing *MYC* expression, copper/zinc-superoxide dismutase (*SOD1*) overexpression helps to decrease ischemic damage.³⁴ Granulocyte colony-stimulating factor (*G-CSF*) increases *HSF1* expression by promoting phosphorylation and the interaction of the signal transducer and activator of transcription-3 (*STAT3*) with *HSF1*, which possesses cardio-protective effects in I/R mice.³⁵ *HSF1* prevents the death of cardiomyocytes following I/R partly by activating *Akt* and inactivating caspase 3 and Jun N-terminal kinase.³⁶ These reports declared that *MYC* and *HSF1* might also be implicated in the mechanisms of I/R injury. *MYC* could target *HSPA5* in the regulatory network, indicating a role of *MYC* in I/R injury through mediation of *HSPA5*.

The *miR-22* plays a neuroprotective role by reducing inflammation and apoptosis, indicating that *miR-22* can be applied in the treatment of cerebral I/R injury.³⁷ It can suppress the apoptosis of cardiomyocytes by targeting

CREB binding protein (*CBP*); therefore, *miR-22* may serve as a novel target for preventing myocardial I/R injury.^{38,39} The *miR-22* inhibition helps to keep cardiac mitochondrial function, and thus has therapeutic potential for acute myocardial I/R injury.⁴⁰ *miR-22* decreases caveolin 3 (*Cav3*) expression and repairs endothelial nitric oxide synthase (eNOS) activity and NO production, inhibiting cardiac injury after I/R.⁴¹ Therefore, *miR-22* might be associated with the pathogenesis of I/R injury by regulating the DEGs.

Conclusions

In conclusion, 390 DEGs were identified between CGBI and NIC samples. Also, *HSPB1*, *HMOX1* and *NR4A2* were the key genes associated with I/R injury. Moreover, *HSP90AA1*, *HSPA5*, *MYC*, *HSF1*, and *miR-22* might be implicated in the pathogenesis of I/R injury. However, the experimental study was insufficient and our results must still be further confirmed in subsequent studies.

ORCID iDs

Dingying Ma <https://orcid.org/0000-0001-7196-290X>
 Jun Qiao <https://orcid.org/0000-0000-0000-0001>
 Qiang Qu <https://orcid.org/0000-0003-1786-887X>
 Fei He <https://orcid.org/0000-0002-4157-0099>
 Wenhua Chen <https://orcid.org/0000-0003-4596-1764>
 Bo Yu <https://orcid.org/0000-0002-6652-9201>

References

- Breton A. Ischemia and reperfusion injury: When cells almost die. *Vet Tech*. 2010;31: E1–E6.
- Dorweiler B, Pruefer D, Andradi TB, et al. Ischemia-reperfusion injury: Pathophysiology and clinical implications. *Eur J Trauma Emerg Surg*. 2007;33(6):600–612.
- Sirotković-Skerlev M, Pleština S, Bilić I, Kovac Z. Pathophysiology of ischaemia-reperfusion injury [in Croatian]. *Lijec Vjesn*. 2006;128(3–4):87–95.
- Kalogeris T, Baines CP, Krenz M, Korthuis RJ. Cell biology of ischemia/reperfusion injury. *Int Rev Cell Mol Biol*. 2012;298:229–317.
- de Groot H, Rauen U. Ischemia-reperfusion injury. Processes in pathogenetic networks: A review. *Transplant Proc*. 2007;39(2):481–484.
- Gu JH, Ge JB, Li M, Wu F, Zhang W, Qin ZH. Inhibition of NF-κB activation is associated with anti-inflammatory and anti-apoptotic effects of ginkgolide B in a mouse model of cerebral ischemia/reperfusion injury. *Eur J Pharm Sci*. 2012;47(4):652–660.
- Qin XF, Lu XJ, Ge JB, Xu HZ, Qin HD, Xu F. Ginkgolide B prevents cathepsin-mediated cell death following cerebral ischemia/reperfusion injury. *Neuroreport*. 2014;25(4):267–273.

8. Xi HJ, Zhang TH, Tao T, et al. Propofol improved neurobehavioral outcome of cerebral ischemia-reperfusion rats by regulating Bcl-2 and Bax expression. *Brain Res.* 2011;1410:24–32.
9. Li M, Zhang X, Cui L, et al. The neuroprotection of oxymatrine in cerebral ischemia/reperfusion is related to nuclear factor erythroid 2-related factor 2 (nrf2)-mediated antioxidant response: Role of nrf2 and heme-oxygenase-1 expression. *Biol Pharm Bull.* 2011;34(5):595–601.
10. Huang W, Liu X, Cao J, et al. miR-134 regulates ischemia/reperfusion injury-induced neuronal cell death by regulating CREB signaling. *J Mol Neurosci.* 2015;55(4):821–829.
11. Wang H, Tri AF, Chen X, Degracia DJ. Embryonic lethal abnormal vision proteins and adenine and uridine-rich element mRNAs after global cerebral ischemia and reperfusion in the rat. *J Cereb Blood Flow Metab.* 2016;37(4):1494–1507.
12. Smith ML, Bendek G, Dahlgren N, Rosén I, Wieloch T, Bo KS. Models for studying long-term recovery following forebrain ischemia in the rat. 2. A 2-vessel occlusion model. *Acta Neurol Scand.* 1984;69(6):385–401.
13. Jamison JT, Kayali F, Rudolph J, Marshall M, Kimball SR, Degracia DJ. Persistent redistribution of poly-adenylated mRNAs correlates with translation arrest and cell death following global brain ischemia and reperfusion. *Neuroscience.* 2008;154(2):504–520.
14. Jamison JT, Szymanski JJ, Degracia DJ. Organelles do not co-localize with mRNA granules in post-ischemic neurons. *Neuroscience.* 2011;199:394–400.
15. Szymanski JJ, Wang H, Jamison JT, Degracia DJ. HuR function and translational state analysis following global brain ischemia and reperfusion. *Transl Stroke Res.* 2013;4(6):589–603.
16. Carvalho BS, Irizarry RA. A framework for oligonucleotide microarray preprocessing. *Bioinformatics.* 2010;26(19):2363–2367.
17. Smyth GK. LIMMA: Linear models for microarray data. *Bioinformatics and Computational Biology Solutions Using R and Bioconductor.* 2011;2011:397–420.
18. Liu X, Hu AX, Zhao JL, Chen FL. Identification of key gene modules in human osteosarcoma by co-expression analysis weighted gene co-expression network analysis (WGCNA). *J Cell Biochem.* 2017;118(11):3953–3959.
19. Huang DW, Sherman BT, Lempicki RA. Systematic and integrative analysis of large gene lists using DAVID bioinformatics resources. *Nat Protoc.* 2009;4(1):44–57.
20. The Gene Ontology Consortium. Expansion of the gene ontology knowledgebase and resources. *Nucleic Acids Res.* 2017;45(Database issue):D331–D338.
21. Kanehisa M, Furumichi M, Tanabe M, Sato Y, Morishima K. KEGG: New perspectives on genomes, pathways, diseases and drugs. *Nucleic Acids Res.* 2017;45(D1):D353–D361.
22. Szklarczyk D, Morris JH, Cook H, et al. The STRING database in 2017: Quality-controlled protein–protein association networks, made broadly accessible. *Nucleic Acids Res.* 2017;45(Database issue):D362–D368.
23. Cline MS, Smoot M, Cerami E, et al. Integration of biological networks and gene expression data using Cytoscape. *Nat Protoc.* 2007;2(10):2366–2382.
24. Wang J, Vasaikar S, Shi Z, Greer M, Zhang B. WebGestalt 2017: A more comprehensive, powerful, flexible and interactive gene set enrichment analysis toolkit. *Nucleic Acids Res.* 2017;45(W1):W130–W137.
25. Livak KJ, Schmittgen TD. Analysis of relative gene expression data using real-time quantitative PCR and the 2(-delta delta C(T)) method. *Methods.* 2001;25:402–408.
26. Devey L, Ferenbach D, Mohr E, et al. Tissue-resident macrophages protect the liver from ischemia reperfusion injury via a heme oxygenase-1-dependent mechanism. *Mol Ther.* 2009;17(1):65–72.
27. Zu G, Yao J, Ji A, et al. Nurr1 promotes intestinal regeneration after ischemia/reperfusion injury by inhibiting the expression of p21 (Waf1/Cip1). *J Mol Med (Berl).* 2016;95:1–13.
28. Guo W, Shan Z. GW26-e0722 repression of miR-1 is required for recovery of Hsp90aa1 against cardiac ischemia/reperfusion injury in rats. *J Am Coll Cardiol.* 2015;66(16 Suppl):C21.
29. Zuehlke AD, Beebe K, Neckers L, Prince T. Regulation and function of the human HSP90AA1 gene. *Gene.* 2015;570(1):8–16.
30. Peng W, Nan Z, Jia L, Jiefei L, Song H, Junfa L. Micro-RNA-30a regulates ischemia-induced cell death by targeting heat shock protein HSPA5 in primary cultured cortical neurons and mouse brain after stroke. *J Neurosci Res.* 2015;93(11):1756–1768.
31. Peng Z, Li J, Li Y, Yang X, Feng S, Han S. Downregulation of miR-181b in mouse brain following ischemic stroke induces neuroprotection against ischemic injury through targeting heat shock protein A5 and ubiquitin carboxyl-terminal hydrolase isozyme L1. *J Neurosci Res.* 2013;91(10):1349–1362.
32. Sun Z, Shen L, Sun X, et al. Variation of NDRG2 and c-Myc expression in rat heart during the acute stage of ischemia/reperfusion injury. *Histochem Cell Biol.* 2011;135(1):27–35.
33. Ma YL, Zhang LX, Liu GL, Fan Y, Peng Y, Hou WG. N-Myc downstream-regulated gene 2 (*Ndr2*) is involved in ischemia-hypoxia-induced astrocyte apoptosis: A novel target for stroke therapy. *Mol Neurobiol.* 2017;54(5):3286–3299.
34. Huang CY, Fujimura M, Noshita N, Chang YY, Chan PH. SOD1 downregulates NF-kappaB and c-Myc expression in mice after transient focal cerebral ischemia. *J Cereb Blood Flow Metab.* 2001;21(2):163–173.
35. Ma H, Gong H, Chen Z, et al. Association of Stat3 with HSF1 plays a critical role in G-CSF-induced cardio-protection against ischemia/reperfusion injury. *J Mol Cell Cardiol.* 2012;52(6):1282–1290.
36. Zou Y, Zhu W, Sakamoto M, et al. Heat shock transcription factor 1 protects cardiomyocytes from ischemia/reperfusion injury. *Circulation.* 2003;108(24):3024–3030.
37. Yu H, Wu M, Zhao P, Huang Y, Wang W, Yin W. Neuroprotective effects of viral overexpression of microRNA-22 in rat and cell models of cerebral ischemia-reperfusion injury. *J Cell Biochem.* 2015;116(2):233–241.
38. Yang J, Chen L, Ding J, et al. MicroRNA-22 targeting CBP protects against myocardial ischemia-reperfusion injury through anti-apoptosis in rats. *Mol Biol Rep.* 2014;41(1):555–561.
39. Yang J, Yang J, Ding JW, Chen LH, Li S, Li XX. PM393 microRNA-22 protects against ischemia/reperfusion-induced myocardial injury via anti-apoptosis through its target gene *Cbp*. *Global Heart.* 2014;9:e141.
40. Du JK, Cong BH, Yu Q, et al. Upregulation of microRNA-22 contributes to myocardial ischemia-reperfusion injury by interfering with the mitochondrial function. *Free Radic Biol Med.* 2016;96:406–417.
41. Chen Z, Qi Y, Gao C. Cardiac myocyte-protective effect of microRNA-22 during ischemia and reperfusion through disrupting the caveolin-3/eNOS signaling. *Int J Clin Exp Pathol.* 2015;8(5):4614–4626.

The role of GLP-1/GIP receptor agonists in Alzheimer's disease

*Chun Jiang Yu^{1,A,B,F}, *Dongying Ma^{2,A,B,E}, Ling Ling Song^{3,B}, Zhen Nan Zhai^{1,B}, Ye Tao^{4,B,C}, Ying Zhang^{5,B,C}, Ling Yu Cai^{6,B,C}, Ya Hui Hou^{7,B,D}, Hong Yuan Chen^{1,B,E}, Li Wang^{8,A,C}

¹ Department of Neurology, Second Affiliated Hospital of the Harbin Medical University, China

² Department of Neurosurgery, Second Affiliated Hospital of the Harbin Medical University, China

³ Department of Neurology, Second Hospital of Chaoyang City, China

⁴ Department of Neurology, First Hospital of Suihua City, China

⁵ Department of Neurology, People's Hospital of Hulunbuir, China

⁶ Department of Neurology, 117 hospital of PLA, Hangzhou, China

⁷ Department of Neurology, People's Hospital of the West Coast New District of QingDao, China

⁸ Department of Geriatrics, Second Affiliated Hospital of the Harbin Medical University, China

A – research concept and design; B – collection and/or assembly of data; C – data analysis and interpretation; D – writing the article; E – critical revision of the article; F – final approval of the article

Advances in Clinical and Experimental Medicine, ISSN 1899–5276 (print), ISSN 2451–2680 (online)

Adv Clin Exp Med. 2020;29(6):661–668

Address for correspondence

Li Wang

E-mail: liwang741@126.com

Funding sources

The postdoctoral scientific research developmental fund of Heilongjiang Province (grant No. LBH-Q15100); postdoctoral scientific research developmental fund of Heilongjiang Province (grant No. LBH-Q18095); and National Natural Science Foundation of China (grant No. 61773134).

Conflict of interest

None declared

* These authors contributed equally to this work.

Received on May 9, 2019

Reviewed on May 30, 2019

Accepted on April 24, 2020

Cite as

Yu CJ, Ma D, Song LL, et al. The role of GLP-1/GIP receptor agonists in Alzheimer's disease. *Adv Clin Exp Med.* 2020;29(6):661–668. doi:10.17219/acem/121007

DOI

10.17219/acem/121007

Copyright

© 2020 by Wrocław Medical University

This is an article distributed under the terms of the Creative Commons Attribution 3.0 Unported (CC BY 3.0) (<https://creativecommons.org/licenses/by/3.0/>)

Abstract

Background. New glucagon-like peptide-1 (GLP-1) analogues developed in recent years have a long half-life and offer further prospects for clinical application. At present, the neuroprotection of GLP-1 analogues in Alzheimer's disease (AD) has just begun to be explored.

Objectives. To investigate how glucagon-like peptide-1 (liraglutide) plays a protective role in AD by regulating tau activation and BACE1 expression.

Material and methods. Human neuroblastoma cell line SH-SY5Y cells were cultured in vitro and pretreated with different concentrations of liraglutide, and then treated with different concentrations of okadaic acid (OA) in order to observe the apoptosis of the SH-SY5Y cells. After liraglutide treatment, the apoptosis of neurons in AD rats was detected using flow cytometry, and tau activation and β -site APP cleaving enzyme 1 (BACE1) expression were detected using western blot.

Results. Different concentrations of OA were able to induce apoptosis of SH-SY5Y cells in a dose-dependent manner. Different concentrations of liraglutide were used to pretreat SH-SY5Y cells, which were able to protect the SH-SY5Y cells from apoptosis induced by OA. Okadaic acid significantly increased tau activation and BACE1 expression in the SH-SY5Y cells, which was blocked with liraglutide pretreatment. The results of a water maze experiment showed that liraglutide had significant protective effects on memory and cognitive ability in AD rats induced with OA, inhibited apoptosis of neural cells in AD rats, and inhibited tau activation and BACE1 expression of neural cells in AD rats induced with OA.

Conclusions. Liraglutide has a protective effect on AD in vivo and in vitro, which may be mediated by preventing neuronal apoptosis and inhibiting the activation of tau and the expression of BACE1.

Key words: Alzheimer's disease, cognition, memory, nerve, glucagon-like peptide-1

Introduction

Alzheimer's disease (AD) is a primary degenerative disease of the central nervous system which seriously affects quality of life. At present, there is no effective treatment method.^{1–3} It is becoming more and more urgent to find an effective treatment for AD. In recent years, glucagon-like peptide-1 (GLP-1) has been found to have neurotrophic and protective effects.^{4,5} The GLP-1 receptor activation can be used to treat type 2 diabetes mellitus.⁶ Because AD and type 2 diabetes mellitus share a common pathogenesis, the use of GLP-1 receptor activation in the treatment of AD has attracted the attention of scholars around the world.⁷ However, GLP-1 has a very short half-life in vivo, so it cannot be used as a drug to treat related diseases. However, the new GLP-1 analogues developed in recent years have a long half-life and offer more prospects for clinical application. At present, the neuroprotection of GLP-1 analogues on AD has just begun to be explored. There are few reports on the mechanism of GLP-1 analogues on AD protection.

Neuronal apoptosis is thought to be one of the major causes of neuronal loss in AD. Neurocyte apoptosis was first reported by Su et al. in 1994. It was found that there were fragments of DNA in the brain neurons of AD patients. Thus, the concept of neurocyte apoptosis was introduced into the neuropathology of AD.⁸ Tau proteins are microtubule-associated proteins with small molecular weight. The tau protein in the brain of AD patients is highly phosphorylated,⁹ and the phosphorylation of tau is regulated by protein kinase and protein phosphatase, the most important of which are protein phosphatase PP2A and protein kinase GSK-3 β .^{10,11} Protein kinase and protein phosphatase are in a dynamic balance in normal individuals, but the activity of PP2A in the brain of AD patients is significantly lower than that of normal adults. Tau in neurons is over-phosphorylated and can aggregate into a double helix and further forming neurofibrillary tangles.¹² β -site amyloid precursor protein (APP) cleaving enzyme 1 (BACE1) is a transmembrane aspartate protease that can cleave β -site APP to produce neurotoxic amyloid- β (A β).¹³ The deposition of A β in the brain is closely related to the development of AD.^{14,15}

In this study, we explored the therapeutic effect of liraglutide on AD in vitro and in vivo by constructing an AD model, and we explored whether liraglutide played a role by regulating the process closely related to AD. This study found that liraglutide had a protective effect on AD, which may be through the prevention of neuronal apoptosis, as well as inhibition of tau activation and BACE1 expression in nerve cells.

Material and methods

Reagents

SH-SY5Y cells were purchased from the Institute of Basic Medical Sciences, Chinese Academy of Medical

Sciences (Beijing, China). An annexin V/7AAD apoptosis staining kit was purchased from Biolegend company (San Diego, USA). Okadaic acid (OA) was purchased from Sigma-Aldrich (St. Louis, USA). Supersignal West Femto/Pico HRP sensitive chemiluminescent substrate was purchased from Simmerfeld Technology Co., Ltd. (Beijing, China). Mouse anti-human pS396 tau antibody, mouse anti-human pS199/202 tau antibody and mouse anti-human BACE1 antibody were purchased from CST (New York, USA). C57BL/6 female rats were purchased from Beijing Weitonglihua Laboratory Animal Technology Co., Ltd. (Beijing, China; certificate No. CELAIC).

SH-SY5Y cell culture

The cells were cultured in Dulbecco's modified Eagle's medium (DMEM) (Thermo Fisher Scientific, Waltham, USA) containing 10% fetal bovine serum (FBS; Hyclone, Logan, USA). The medium was replaced every 2–3 days. The cells were pretreated with 0.1 μ M, 1 μ M and 10 μ M liraglutide for 72 h, and then they were treated with 0 nM, 10 nM and 20 nM of OA for 48 h.

Flow cytometry

The cells were collected at 1,000 g for 5 min and washed once with 1% phosphate-buffered saline (PBS). The cells were suspended with 100 μ L of binding buffer, and 5 μ L of annexin V dye and 5 μ L of 7-AAD dye were added. After incubating at room temperature for 15 min, the cells detected using flow cytometry.

Western blot

The total protein of the cells was homogenized in cold radioimmunoprecipitation assay (RIPA) buffer (Beyotime, Shanghai, China). The total protein was centrifuged at 13,000 \times g for 20 min at 4°C. The supernatants were collected, and protein concentration was measured using a modified bicinchoninic acid (BCA) protein concentration assay kit (Beyotime) in accordance with the manufacturer's protocol. The extracted protein was separated using 8% SDS-PAGE (Bio-Rad, Hercules, USA) and 5% concentrated gel (Bio-Rad) and transferred to nitrocellulose membrane (Simmerfelder Technology). The membrane was blocked with 5% bovine serum albumin (BSA) for 2 h and incubated with primary antibodies, including anti-pS396 tau, anti-pS199/202 tau and anti-BACE1, at 4°C overnight. On the 2nd day, the membrane was washed with 0.1% tris-buffered saline-Tween (TBST) 3 times, 5 min each time. Then, the membrane was incubated with the corresponding horseradish peroxidase (HRP)-conjugated secondary antibodies at room temperature for 1 h. After being washed 3 times with 0.1% TBST, the signals were visualized using Supersignal West Femto HRP. Actin was used as an internal control.

Establishment of AD rat model

The rats were randomly divided into a sham operation control group, a test group (OA group) and a liraglutide treatment group, with 10 rats in each group. The rats in the control group did not undergo any treatment. The rats in test and liraglutide treatment groups were injected with 0.5 μ L of OA dissolved in 10% dimethyl sulfoxide (DMSO) into the hippocampus. The concentration was 0.8 mmol/L, and the injection was slowly performed at 0.1 μ L/min. The needle was kept in place for 10 min, and then pulled out slowly. On the 16th day after OA injection, the rats in the treatment group were subcutaneously injected with 300 μ g/kg of liraglutide, and the rats in the control and test groups were injected with the same amount of saline solution for 30 days.

Y-maze and Morris water maze

The Y-maze consists of 3 equal-length arms (50 \times 18 \times 35 cm) with an angle of 120° between each arm. Each arm has a movable partition in the center. The inner arm and bottom of the maze are painted black. Visual cues are placed on the walls of the 3 arms. After each test, the arm of the labyrinth was sprayed with alcohol to eliminate olfactory stimulation. When the spontaneous round examination was tested, the rats were placed at the end of one arm and allowed to explore for 8 min freely. The video camera system recorded the behavioral changes of the animals for 8 min. The following parameters were recorded: 1) the total number of entries – the number of times that the animals entered the maze arm (with the 4 feet of a rat entering the arm counting as 1 time); 2) alternations – successively entering all 3 arms once; and 3) the number of maximum alternations – the total arm number was 2. The percentage of the auto cycles is the total number of cycles/*100%.

The Morris water navigation test was performed according to the following procedure. The rats headed toward the wall of the pond, and randomly took 1 of the 4 starting positions – east, west, south, or north – into the water. The time the rats took to find an underwater platform(s) was recorded. In preceded training, if this time exceeded 60 s, the rats were guided to the platform. Then, they were allowed to stay on the platform for 10 s. The rats were removed and dried. When necessary, they were placed under an 150 W incandescent lamp for 5 min and then put back into the cage. Each rat was trained 4 times a day, the interval between 2 training sessions was 15–20 min, and the training lasted for 5 days. 3. On the 2nd day after the final training, the platform was removed and the 60 s training was initiated. The rats were placed into the water from the opposite side of the original platform quadrant. The time spent in the target quadrant (the quadrant where the platform was originally placed) was recorded, as well as the number of entries

into the quadrant as a spatial memory index. After the 2nd day of training, 4 days of counterpoint training began. The platform was placed in the quadrant of the original platform, and the method was the same as the acquired training. The rats were trained 4 times a day. The time and distance of swimming and the swimming speed were recorded each time.

Statistical analysis

SPSS v. 16.0 software (IBM Corp., Armonk, USA) was used to analyze the data, and the measurement data was described as means \pm standard deviation (SD). A t-test was used to compare the measurement data between the 2 groups. Comparisons of experimental groups were evaluated with one-way analysis of variance (ANOVA) followed by Bonferroni analysis. A p-value \leq 0.05 was considered statistically significant.

Results

The protective effect of liraglutide on OA-induced apoptosis in SH-SY5Y cells

The apoptotic rates of the SH-SY5Y cells treated with different concentrations of OA (0 mM, 10 nM and 20 nM) were 1.31 \pm 1.22, 13.4 \pm 2.78 and 21.47 \pm 4.21, respectively ($p < 0.05$; Fig. 1). According to these results, 10 nM of OA is able to significantly induce apoptosis, so this concentration was used to induce apoptosis in SH-SY5Y cells in subsequent experiments. In addition, apoptosis of SH-SY5Y cells was detected after treatment with different concentrations of liraglutide (0.1 μ M, 1 μ M and 10 μ M). The apoptosis rates of SH-SY5Y cells were 12.93 \pm 3.12, 7.34 \pm 2.98 and 5.84 \pm 1.91, respectively ($p < 0.05$; Fig. 1). Because the protective effects of 1 μ M and 10 M of liraglutide on the apoptosis of SH-SY5Y cells were not statistically significantly different, 1 μ M was selected as the intervention dose in subsequent experiments.

The effect of liraglutide pretreatment on OA-mediated activation of tau and BACE1 in SH-SY5Y cells

As shown in Fig. 2A, the activation of tau phosphorylation in the SH-SY5Y cells was significantly upregulated by OA treatment, while the activation of tau phosphorylation induced by OA was significantly decreased by pretreatment with liraglutide ($p < 0.01$). The expression level of BACE1 in the SH-SY5Y cells treated with OA was significantly upregulated by tau phosphorylation ($p < 0.01$; Fig. 2B). However, after pretreatment with liraglutide, the increased expression level of BACE1 induced by OA was significantly lower ($p < 0.01$; Fig. 2B).

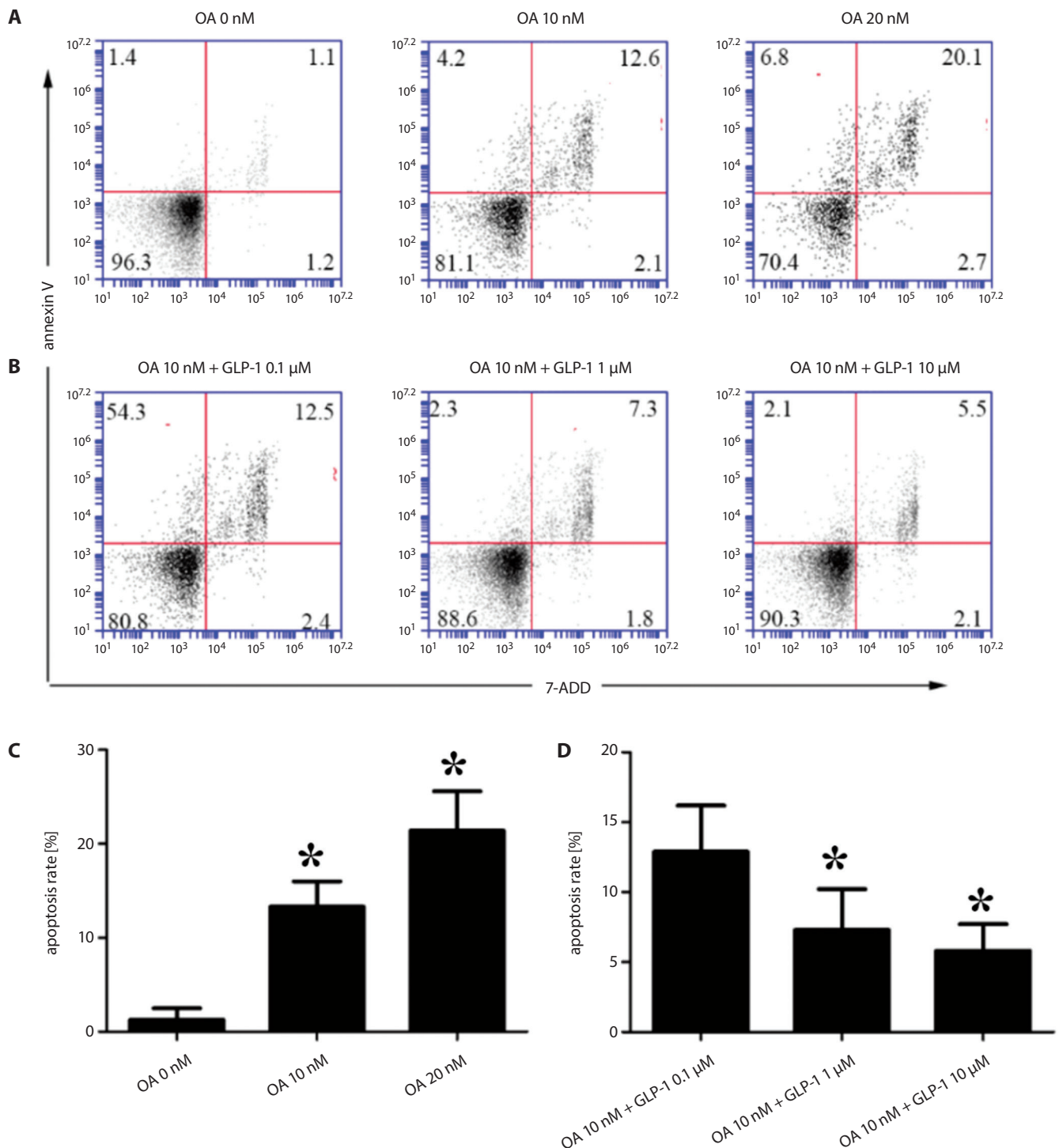


Fig. 1. Apoptosis of SH-SY5Y cells induced by OA and/or liraglutide was detected with apoptosis staining. **A.** The results of apoptosis staining induced with OA. **B.** The results of apoptosis staining induced with OA and liraglutide. **C.** The apoptosis rate of SH-SY5Y cells induced with OA. **D.** The apoptosis rate of SH-SY5Y cells induced with OA and liraglutide. Data are expressed as means \pm SD ($n = 3$)

* $p < 0.05$ vs the OA 0 nM group or the OA 10 nM+GLP-1 0.1 mM group.

The learning and memory function of rats before and after treatment with liraglutide

In order to detect the protective effect of liraglutide on OA-induced memory impairment, a Y-maze was used to test the ability of rats to recognize and remember a new

environment. As shown in Fig. 3A, OA significantly affected the spontaneous behavior of rats compared with the control group, and this damage was significantly restored after treatment with liraglutide ($p < 0.01$; Fig. 3A). However, there were no protective effects of liraglutide on OA-induced spatial recognition ($p > 0.01$; Fig. 3B).

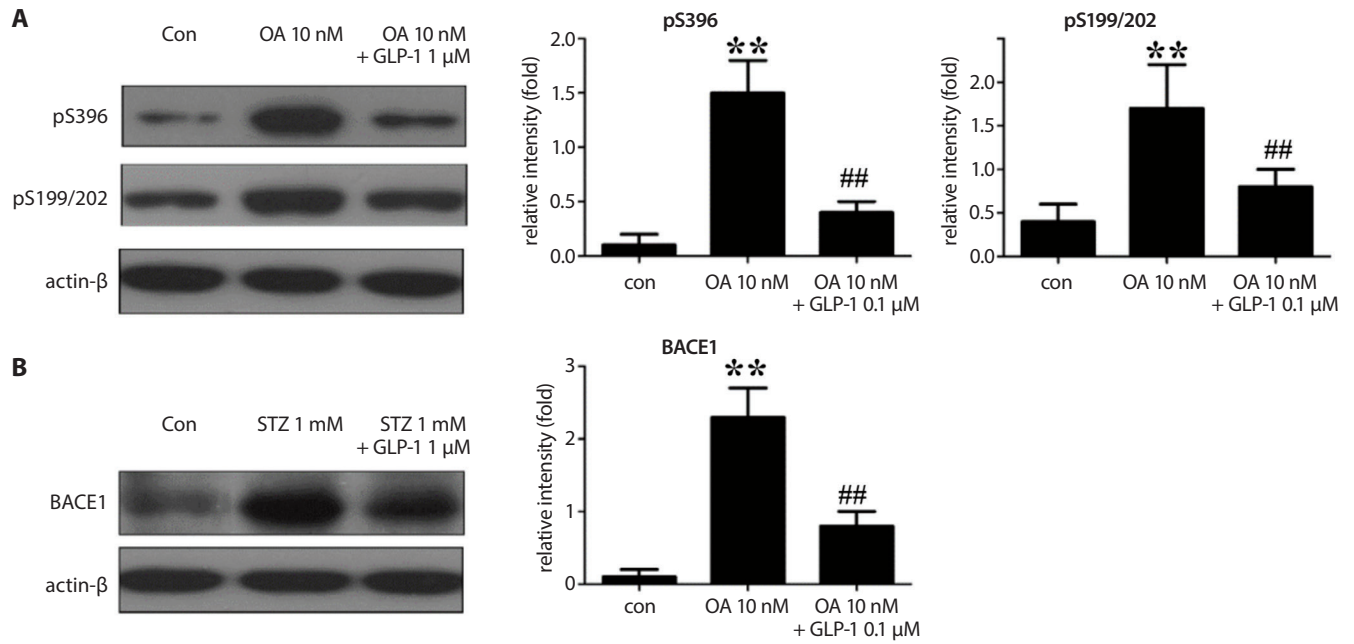


Fig. 2. The effects of liraglutide pretreatment on OA-mediated activation of tau and BACE1 in SH-SY5Y cells. A. Tau phosphorylation level. B. BACE1 expression level. Band intensities are normalized to actin-β intensity and are expressed as relative values. Data are expressed as means ±SD (n = 3)

**p < 0.01 vs the control group; ##p < 0.01 vs the OA 10 nM group.

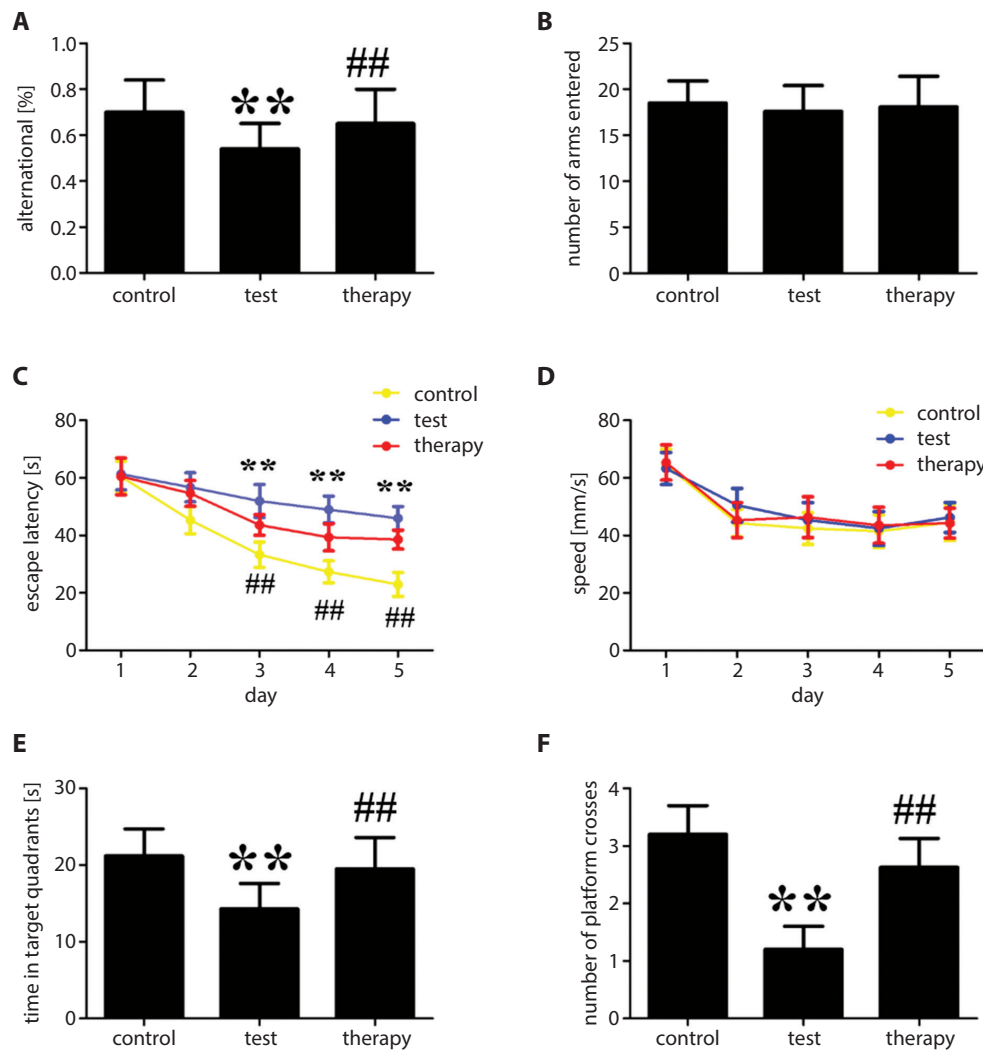


Fig. 3. Water maze test detection of learning and memory function in rats before and after treatment. A. Spontaneous Alternating Response Ability. B. Spatial Recognition Ability. C. Average Avoidance Latency of Hidden Platform. D. Swimming Speed. E. Residence Time in Target Quadrant. F. Platform Crossing Number. Data is expressed as means ±SD

**p < 0.01 vs the control group; ##p < 0.01 vs the test group (OA group).

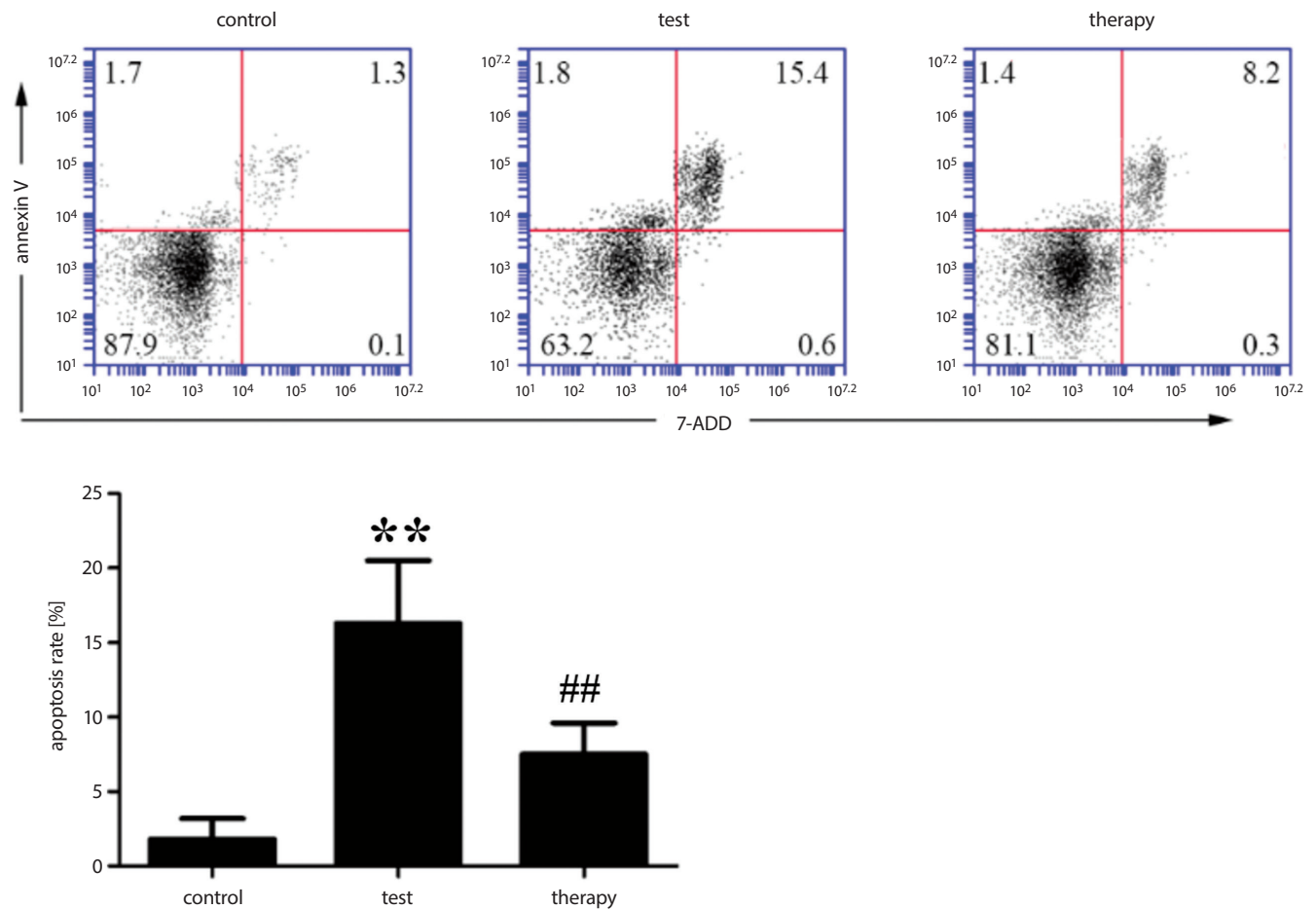


Fig. 4. The effects of liraglutide pretreatment on neuronal apoptosis in rats with AD. Data are expressed as means \pm SD

** $p < 0.01$ vs the control group, ## $p < 0.01$ vs the test group (OA group).

A Morris water maze was used to detect the protective effect of liraglutide on OA-induced cognitive impairment. As shown in Fig. 3C, the average escape latency of the hidden platforms in the OA group was significantly higher, while it was significantly lowered when the treatment with liraglutide was employed ($p < 0.01$). However, there was no significant difference in swimming speed between the OA and the OA+liraglutide groups ($p > 0.01$; Fig. 3D). As shown in Fig. 3E and 3F, liraglutide shortened the residence time and decreased the number of platform crossings in the target quadrant of rats induced by OA ($p < 0.01$). These results suggest that liraglutide has a significant protective effect on learning and memory impairment of AD rats induced with OA.

Effect of liraglutide on neuronal apoptosis in AD rats

As shown in Fig. 4, the level of neuronal apoptosis in the test group was significantly higher than that of the control group (1.84 ± 1.41 vs 16.36 ± 2.14 ; $p < 0.01$). In addition, the level of neuronal apoptosis in the liraglutide treatment group was markedly lower when compared to the test group (7.53 ± 2.18 vs 16.36 ± 2.14 ; $p < 0.01$). These

results indicate that liraglutide treatment can significantly reduce the level of neuronal apoptosis induced using OA in AD model rats.

Effect of liraglutide on tau activation and BACE1 expression in neurons of AD rats

As shown in Fig. 5A, the activation of tau phosphorylation induced by OA in the neurons of AD in a rat model was significantly higher, and when treated by liraglutide it was significantly inhibited ($p < 0.01$). The change in BACE1 expression level was consistent with the activation of tau phosphorylation. The expression level of the BACE1 protein in the neurons of OA-induced AD rats was significantly higher, while this increase in BACE1 expression induced by OA was significantly inhibited after pretreatment with liraglutide ($p < 0.01$; Fig 5B).

Discussion

Alzheimer's disease, which accounts for 60–70% of dementia cases, is characterized by progressive loss of memory and cognitive abilities, as well as behavioral changes that

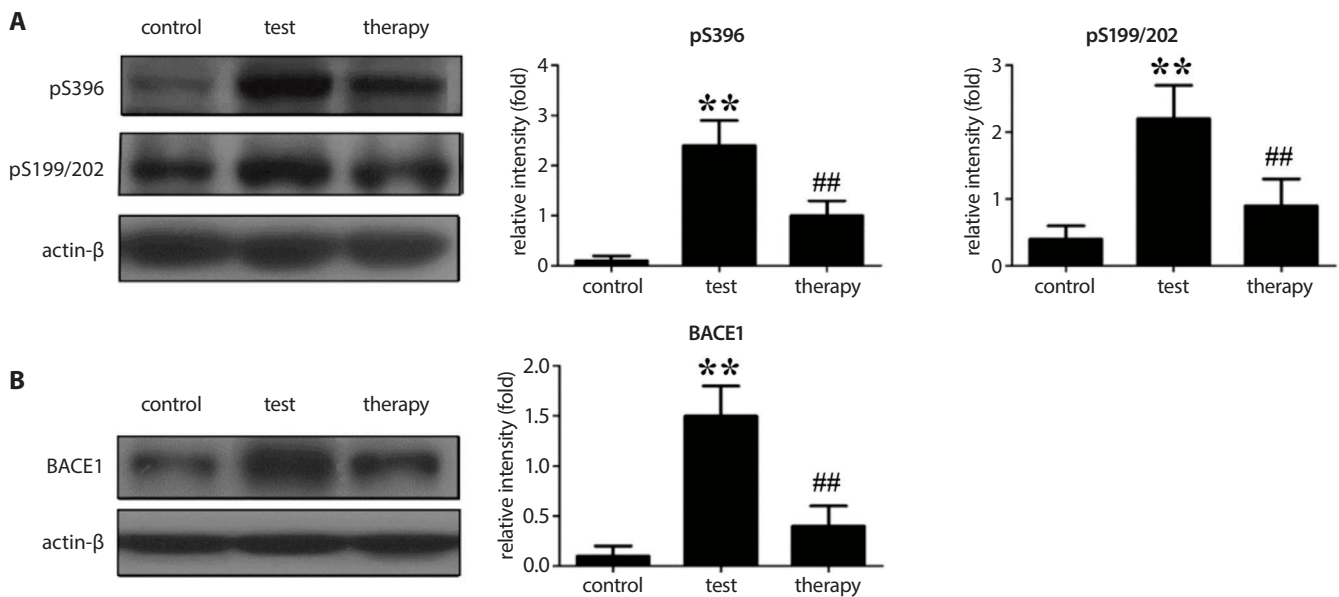


Fig. 5. The effects of liraglutide pretreatment on tau activation and BACE1 expression in the neural cells of rats with AD. A. Tau phosphorylation activation level. B. BACE1 protein expression level. Band intensities were normalized to actin- β intensity and are expressed as relative values. Data is expressed as means \pm SD (n = 3)

**p < 0.01 vs the control group; ##p < 0.01 vs the test group (OA group).

ultimately lead to disability and dependence.^{16,17} At present, the treatment of AD can only alleviate the symptoms of patients, but cannot fundamentally change the pathogenesis of AD. Therefore, it is very important to study the mechanism of AD. We carried out a preliminary study on the mechanism of liraglutide in the treatment of AD. The results showed that apoptosis of nerve cells was associated with AD, which was mainly manifested in increased levels of apoptosis of the nerve cells in a rat model of AD in comparison with the control group. In vitro experiments showed that OA, which is able to induce apoptosis of SH-SY5Y cells, can also induce apoptosis in AD rats in a dose-dependent manner. At the same time, the experimental results confirmed that the occurrence of AD will be accompanied by an increase in tau phosphorylation activation levels and BACE1 protein expression levels. Furthermore, liraglutide had a certain therapeutic effect on AD. In the water navigation task, the memory and cognitive function of rats treated with liraglutide were improved to a certain extent; this effect may come about through the prevention of neuronal apoptosis, the inhibition of the activation of tau and the expression of BACE1.

Okadaic acid, a protein phosphatase-2A (PP2A) inhibitor, has the effect of inducing tau protein hyperphosphorylation activation and inducing neuronal apoptosis.^{18,19} In vivo, OA stimulates the deposition of amyloid- β (A β) and subsequently leads to neurodegeneration, synaptic loss and memory impairment, all of which are similar to those of AD.²⁰ Okadaic acid has been shown to induce AD in rats. One of the key roles of OA in an AD model is that OA can induce tau protein hyperphosphorylation.²¹ This study confirmed that OA can induce tau protein hyperphosphorylation











in SH-SY5Y cells in vitro, and in vivo experiments also confirmed that the phosphorylation and activation level of tau protein in rat neural cells was significantly higher in AD rats. We concluded that the phosphorylation activation of tau is closely related to the occurrence and development of AD. These results are consistent with the results of a previous study.²² We continued to observe the role of tau activation in the treatment of AD with liraglutide. It was found that liraglutide pretreatment significantly decreased the level of tau phosphorylation activation in SH-SY5Y cells induced by OA. As shown by in vivo experiments, liraglutide treatment can also inhibit the activation of tau phosphorylation, indicating that there was a certain correlation between the inhibition of tau activation and the therapeutic effect of liraglutide.

BACE1 was first discovered by Vassar in 1999 and has been proven to play an important role in the pathogenesis of AD.²³ It can produce neurotoxic A β by splitting the β -site APP. The deposition of A β in the brain is closely related to the development of AD.^{14,15} Therefore, it can theoretically inhibit the production of A β by inhibiting BACE1 to treat AD. In recent years, there have been many clinical studies on the use of BACE1 inhibitors in AD. Some of these studies have failed, while others are still observing efficacy.²⁴ In addition to blocking the expression of BACE1 directly, other drugs can also inhibit the expression of BACE1 and have a certain therapeutic effect on AD. The results in vitro showed that liraglutide pretreatment could block the increase of BACE1 expression induced by OA. In vivo experiments have demonstrated that the level of BACE1 expression in the nerve cells of AD rats was lower in the treatment group. It is preliminarily suggested that another

mechanism of liraglutide in treating AD may be through inhibiting the expression of BACE1 protein.

Both in vivo and in vitro studies have demonstrated that liraglutide has a protective effect on AD, possibly by preventing neuronal apoptosis and inhibiting tau activation and BACE1 expression. The results provide a scientific basis for future research on AD therapy and its mechanism.

ORCID iDs

Chun Jiang Yu  <https://orcid.org/0000-0003-4031-8657>
 Dongying Ma  <https://orcid.org/0000-0003-3723-8170>
 Ling Ling Song  <https://orcid.org/0000-0002-0555-1712>
 Zhen Nan Zhai  <https://orcid.org/0000-0003-2585-8989>
 Ye Tao  <https://orcid.org/0000-0002-8809-1626>
 Ying Zhang  <https://orcid.org/0000-0002-9441-4591>
 Ling Yu Cai  <https://orcid.org/0000-0003-4375-5801>
 Ya Hui Hou  <https://orcid.org/0000-0002-6582-2529>
 Hong Yuan Chen  <https://orcid.org/0000-0002-5941-3403>
 Li Wang  <https://orcid.org/0000-0001-7248-7434>

References

- Auti ST, Kulkarni YA. A systematic review on the role of natural products in modulating the pathways in Alzheimer's disease. *Int J Vitam Nutr Res.* 2017;87(1–2):99–116.
- Alasmari F, Ashby CR Jr, Hall FS, Sari Y, Tiwari AK. Modulation of the ATP-binding cassette B1 transporter by neuro-inflammatory cytokines: Role in the pathogenesis of Alzheimer's disease. *Front Pharmacol.* 2018;9:658.
- Voss T, Li J, Cummings J, et al. Randomized, controlled, proof-of-concept trial of MK-7622 in Alzheimer's disease. *Alzheimers Dement (NY).* 2018;4:173–181.
- Knezovic A, Osmanovic Barilar J, Babic A, et al. Glucagon-like peptide-1 mediates effects of oral galactose in streptozotocin-induced rat model of sporadic Alzheimer's disease. *Neuropharmacology.* 2018;135:48–62.
- Li L. The molecular mechanism of glucagon-like peptide-1 therapy in Alzheimer's disease, based on a mechanistic target of rapamycin pathway. *CNS Drugs.* 2017;31(7):535–549.
- Weisnagel SJ. The role of glucagon-like peptide-1 receptor agonists in cardiovascular disease prevention in type 2 diabetes mellitus: Evidence from the most recent clinical trials. *Ann Transl Med.* 2018;6(10):194.
- Athauda D, Foltynie T. The glucagon-like peptide 1 (GLP) receptor as a therapeutic target in Parkinson's disease: Mechanisms of action. *Drug Discov Today.* 2016;21(5):802–818.
- Su JH, Anderson AJ, Cummings BJ, Cotman CW. Immunohistochemical evidence for apoptosis in Alzheimer's disease. *Neuroreport.* 1994;5(18):2529–2533.
- Mandelkow EM, Mandelkow E. Biochemistry and cell biology of tau protein in neurofibrillary degeneration. *Cold Spring Harb Perspect Med.* 2012;2(7):a006247.
- Watkins GR, Wang N, Mazalouskas MD, et al. Monoubiquitination promotes calpain cleavage of the protein phosphatase 2A (PP2A) regulatory subunit $\alpha 4$, altering PP2A stability and microtubule-associated protein phosphorylation. *J Biol Chem.* 2012;287(29):24207–24215.
- Lee J, Hong H, Im J, Byun H, Kim D. The formation of PHF-1 and SMI-31 positive dystrophic neurites in rat hippocampus following acute injection of okadaic acid. *Neurosci Lett.* 2000;282(1–2):49–52.
- Goedert M, Jakes R, Qi Z, Wang JH, Cohen P. Protein phosphatase 2A is the major enzyme in brain that dephosphorylates tau protein phosphorylated by proline-directed protein kinases or cyclic AMP-dependent protein kinase. *J Neurochem.* 1995;65(6):2804–2807.
- Coimbra JRM, Marques DFF, Baptista SJ, et al. Highlights in BACE1 inhibitors for Alzheimer's disease treatment. *Front Chem.* 2018;6:178.
- Wang P, Zheng X, Guo Q, et al. Systemic delivery of BACE1 siRNA through neuron-targeted nanocomplexes for treatment of Alzheimer's disease. *J Control Release.* 2018;279:220–233.
- Andrew RJ, Fernandez CG, Stanley M, et al. Lack of BACE1 S-palmitoylation reduces amyloid burden and mitigates memory deficits in transgenic mouse models of Alzheimer's disease. *Proc Natl Acad Sci U S A.* 2017;114(45):E9665–E9674.
- Masters CL, Bateman R, Blennow K, Rowe CC, Sperling RA, Cummings JL. Alzheimer's disease. *Nat Rev Dis Primers.* 2015;1:15056.
- De-Paula VJ, Radanovic M, Diniz BS, Forlenza OV. Alzheimer's disease. *Subcell Biochem.* 2012;65:329–352.
- Kim D, Su J, Cotman CW. Sequence of neurodegeneration and accumulation of phosphorylated tau in cultured neurons after okadaic acid treatment. *Brain Res.* 1999;839(2):253–262.
- Yoon S, Choi J, Yoon J, Huh JW, Kim D. Okadaic acid induces JNK activation, bim overexpression and mitochondrial dysfunction in cultured rat cortical neurons. *Neurosci Lett.* 2006;394(3):190–195.
- Cho MH, Kim DH, Choi JE, Chang EJ, Seung-Yongyoon. Increased phosphorylation of dynamin-related protein 1 and mitochondrial fission in okadaic acid-treated neurons. *Brain Res.* 2012;1454:100–110.
- Foidl BM, Humpel C. Differential hyperphosphorylation of tau-S199, -T231 and -S396 in organotypic brain slices of Alzheimer mice. A model to study early tau hyperphosphorylation using okadaic acid. *Front Aging Neurosci.* 2018;10:113.
- Vergallo A, Bun RS, Toschi N, et al. Association of cerebrospinal fluid α -synuclein with total and phospho-tau181 protein concentrations and brain amyloid load in cognitively normal subjective memory complainers stratified by Alzheimer's disease biomarkers. *Alzheimers Dement.* 2018;14(12):1623–1631.
- Vassar R, Bennett BD, Babu-Khan S, et al. Beta-secretase cleavage of Alzheimer's amyloid precursor protein by the transmembrane aspartic protease BACE. *Science.* 1999;286(5440):735–741.
- Coimbra JRM, Marques DFF, Baptista SJ, et al. Highlights in BACE1 inhibitors for Alzheimer's disease treatment. *Front Chem.* 2018;6:178.

The development and evaluation of a multi-epitope antigen as a serodiagnostic marker of *Toxoplasma gondii* infection

Abbas Alibakhshi^{A,B,D}, Mojgan Bandehpour^{C,F}, Zarin Sharifnia^{C,E}, Bahram Kazemi^{A,F}

Cellular and Molecular Biology Research Center, Shahid Beheshti University of Medical Sciences, Tehran, Iran

A – research concept and design; B – collection and/or assembly of data; C – data analysis and interpretation; D – writing the article; E – critical revision of the article; F – final approval of the article

Advances in Clinical and Experimental Medicine, ISSN 1899–5276 (print), ISSN 2451–2680 (online)

Adv Clin Exp Med. 2020;29(6):669–675

Address for correspondence

Mojgan Bandehpour
E-mail: bandehpour@gmail.com

Funding sources

None declared

Conflict of interest

The present study was conducted in the Cellular & Molecular Biology Research Center of Shahid Beheshti University of Medical Sciences, Tehran, Iran. This article was extracted from Abbas Alibakhshi's Ph.D. thesis. The project was funded by the Deputy of Shahid Beheshti University of Medical Sciences (grant No. 4971) and the experiments were carried out in concordance with ethics code SBMU.REC.1393.749.

Received on July 17, 2017

Reviewed on March 1, 2018

Accepted on February 18, 2019

Published online on June 23, 2020

Abstract

Background. *Toxoplasma gondii* (*T. gondii*) is a ubiquitous protozoan parasite which causes a serious disease called toxoplasmosis. The high prevalence of *T. gondii* infection has attracted a great deal of interest in its diagnosis and treatment. The use of pure antigens shows high sensitivity and specificity, but challenges such as cross-reactivity remain diagnostic difficulties.

Objectives. The aim of this study was to use 3 surface antigens (SAGs) of *T. gondii* to design gene-encoding a multi-epitope and immunogenic protein as a serodiagnostic marker.

Material and methods. The multi-epitope antigen was expressed using *Escherichia coli* BL21 (DE3) cells and purified using affinity chromatography. To evaluate acute toxoplasmosis, 95 human sera with anti-*T. gondii* IgG, 25 human sera without anti-*T. gondii* IgG and 6 serum samples with nosocomial infections were collected and submitted to an enzyme-linked immunosorbent assay (ELISA) analysis. The potential of purified protein as a diagnostic marker of *T. gondii* infection was also investigated using ELISA analysis.

Results. The western blot analysis for both protein expression and purification confirmed that the protein was expressed and purified successfully. The results of validation showed a sensitivity of 72.6% and a specificity of 90.3% for recombinant ELISA.

Conclusions. Although this protein showed potential for detecting *T. gondii*, the sensitivity and specificity were lower than in tests that use the whole body of the parasite.

Key words: diagnosis, *Toxoplasma gondii*, multi-epitope antigen, surface antigens

Cite as

Alibakhshi A, Bandehpour M, Sharifnia Z, Kazemi B.
The development and evaluation of a multi-epitope antigen as a serodiagnostic marker of *Toxoplasma gondii* infection.
Adv Clin Exp Med. 2020;29(6):669–675.
doi:10.17219/acem/104554

DOI

10.17219/acem/104554

Copyright

© 2020 by Wrocław Medical University
This is an article distributed under the terms of the
Creative Commons Attribution 3.0 Unported (CC BY 3.0)
(<https://creativecommons.org/licenses/by/3.0/>)

Introduction

Toxoplasma gondii, a ubiquitous protozoan parasite, is one of the most successful pathogens that can infect almost all warm-blooded animals, including humans. The primary infection is mostly asymptomatic in humans, but it can cause severe damage, especially in pregnant women and immunocompromised hosts with T-cell defects. For example, transmission from an infected mother to a fetus may lead to spontaneous abortion or stillbirth.¹ Recently, it has been found that *T. gondii* infection can correlate with neuropsychiatric disorders, including depression and suicidal behavior.²

Toxoplasma gondii infection in humans occurs in 3 stages, including tachyzoite, bradyzoite and oocyst environmental stages. People can be infected through ingestion of oocytes. Tissue cysts containing bradyzoites appear in all warm-blooded animals, including humans. Rapidly replicating tachyzoites, which are responsible for acute toxoplasmosis, divide inside specialized vacuoles of the host cells.³ The complicated virulence is dependent on factors involved in the interaction between the parasite and the host in cell invasion and intracellular development, as well as factors involved in the host immune response. Resident surface proteins are among the virulence factors affecting the gliding, attachment and invasion of the parasite. In initial studies on *T. gondii*, P30 (surface antigen SAG1), which causes strong antibody responses, was identified as a glycosylphosphatidylinositol (GPI)-anchored surface protein.⁴ Later investigations led to the detection of more surface antigens in *T. gondii*. These antigens have different roles in pathogenesis, including attachment and invasion of the parasite to the host cells and immune modulation. Surface antigens 2, 3, 4, 5, and SAG1-related sequences (SRS) are other proteins on the surface of *T. gondii* tachyzoites and bradyzoites.⁵

Molecular factors involved in infection diseases are generally used as serodiagnostic markers. At the same time, serological tests that measure antibodies raised against infection are the primary methods for diagnosing *T. gondii* infection. These tests usually measure immunoglobulin M (IgM, as an indication of recent infection) or immunoglobulin G (IgG) (as a demonstration of the immune status against a particular pathogen) antibody titers using laboratory methods. A panel of serological tests has been used to demonstrate specific antibodies against *T. gondii*.⁶ Although conventional antibody screening against *T. gondii* (and also many other pathogens) is an optimal strategy to prevent and decrease mainly congenital type toxoplasmosis, the low accuracy of the crude native antigens makes them unsuitable for use in diagnostic methods. Furthermore, there are difficulties in standardizing diagnostic kits that employ native antigens. Therefore, assuming it may be fruitful to replace these antigens with alternative proteins and peptides, investigations have been inclined significantly towards alternative and standard methods

with the help of suitable reagents with high diagnostic sensitivity. Recently, peptide-based antigens and poly-epitope antigens have been considered by some researchers as increasing the sensitivity and specificity of diagnostic tests for some pathogens.⁷ In this method, only a highly immunogenic region of an antigen in the form of a peptide or a poly-epitope protein is employed to diagnose the presence or absence of specific antibodies in human serum.

In the present study, we constructed a synthetic gene encoding epitopes and highly immunogenic regions of 3 surface genes of *T. gondii*, namely SAG1 (P30), SAG2 (P22) and SAG3 (P43), for the production of a poly-epitope protein as a novel reagent to detect infection caused by *T. gondii*.

Material and methods

Sequence retrieval, in silico analysis and design of a poly-epitope protein

Nucleotide sequences for 3 surface antigens (SAG1, SAG2 and SAG3) of the extremely virulent RH strain of *T. gondii* were obtained from the National Center for Biotechnology Information (NCBI; Bethesda, USA) Nucleotide Database. After translation into amino acid sequences, all 3 proteins were aligned with proteins from different virulent strains using the Clustal algorithm. The secondary and tertiary structures of the proteins were considered for further evaluation. Amino acid distribution was analyzed using the LRRfinder server (<http://www.lrrfinder.com>), and the transmembrane topology of the proteins was studied with methods available on the TMHMM server (<http://www.cbs.dtu.dk/services/TMHMM-2.0/>) for investigating the location of immunogenic regions. The IEDB,⁸ ABCpred,⁹ Bcepred,¹⁰ and Bepipred¹¹ web servers were used to predict B-cell epitopes; the epitopes were selected mainly on the basis of the Kolaskar and Tongaonkar antigenicity method.¹² Finally, 3 immunogenic regions were chosen from the surface antigens and then connected to each other with linker peptides. A 405-nucleotide sequence containing epitopes was synthesized into the multiple cloning sites (MCS) of the pQE30 expression vector.

Expression and purification of the poly-epitope protein

The recombinant pQE30 vector was analyzed using polymerase chain reaction (PCR) for confirmation of the synthesized sequence. After the transformation of the recombinant vector into *Escherichia coli* BL21 (DE3) cells, protein expression was induced by placing 1 mM of the final isopropyl-D-thiogalactopyranoside (IPTG) concentration in a Luria broth (LB) medium. Aliquots of the medium were removed 2 h and 3 h after the induction of protein expression. The cells were lysed in lysis

buffer (50 mM Tris-HCl, 10% glycerol, 0.1% Triton X-100, and 1 mM phenylmethylsulfonyl fluoride (PMSF)). To verify and assess the protein expression, western blot analysis was carried out on protein extracts. First, 2X SDS-loading buffer (100 mM Tris-HCl pH 6.8, 20% glycerol, 4% SDS, 0.005% bromophenol blue, and 200 mM DTT) was added to the proteins, and then the samples were heated at 85°C for 5 min. The proteins of the cell extracts were separated on a 12% polyacrylamide gel and run in 1X Tris-Glycine SDS buffer (TGS). The proteins were transferred to a nitrocellulose membrane sheet and blocked with 3% skimmed milk powder in phosphate buffer saline (PBS) for 1 h. The membrane layer was washed 3 times in PBS with 0.1% Tween (PBST). Anti-polyhistidine-alkaline phosphatase (ALP) antibody in a 1:10,000 dilution was then used to incubate the membrane layer with 40 rpm shaking for 2 h. The washing step was repeated and finally bromo-color-indolyl-phosphate (BCIP) and nitro blue tetrazolium (NBT) were applied to detect the target protein on the membrane sheet.

After confirmation of protein expression, the aliquots taken 3 h after induction were used for the protein purification process. Using the pQE30 vector, a His6 tag was conjugated to the target protein. In this process, the lysis of the cells was carried out in equilibrium buffer (2 M urea, 20 mM Tris-HCl, 500 NaCl, 50 mM imidazole, 0.5% Triton X-100, and PMSF, pH 8) and the samples were sonicated on ice for 1 h. The lysate was centrifuged at 5,000 rpm for 20 min, and the supernatant was poured into an Ni(II)-based immobilized metal ion affinity chromatography column. The column was shaken for 1 h and then washed 3 times with washing buffer (0.4 M urea, 20 mM Tris-HCl, 500 NaCl, 50 mM imidazole, 0.5% Triton X-100, and PMSF, pH 8) and finally eluted with elution buffer (0.4 M urea, 20 mM Tris-HCl, 500 NaCl, and 500 mM imidazole, pH 8). The purification process was confirmed with western blot analysis and dot-blot analysis. The western blot was carried out as described above for the confirmation of protein expression, but instead of using the anti-polyhistidine ALP antibody, we used the anti-polyhistidine antibody conjugated to horseradish peroxidase (HRP) and its chromogenic substrate, 3,3'-diaminobenzidine (DAB), along with hydrogen peroxide (H₂O₂). For dot-blot, a drop of liquid from the purification process and a drop of flow-through were placed directly on a nitrocellulose membrane sheet; the membrane was then blocked with skimmed milk, washed, incubated with anti-polyhistidine HRP antibody and detected with DAB, as in the process described for western blot analysis.

Serum samples and indirect IgG ELISA

The potential of purified protein as a diagnostic marker of *T. gondii* infection was investigated using enzyme-linked immunosorbent assay (ELISA) analysis. To evaluate acute toxoplasmosis, 95 human sera with anti-*T. gondii* IgG and

25 human sera without anti-*T. gondii* IgG were collected from Nilou Medical Laboratory in Tehran, Iran, as well as 6 serum samples with nosocomial infections (infections other than toxoplasmosis). All of the serum samples were first analyzed using a commercial IgG ELISA kit (Euroimmun AG, Lübeck, Germany). To set up the assay, different concentrations of purified protein in 1 × PBS were prepared and used to coat a polystyrene 96-well microtiter plate, which was incubated overnight at room temperature. Afterward, the plate was washed 3 times with PBST (1 × PBS and 0.05% Tween 20) and then blocked with 300 µL of 1% bovine serum albumin (BSA) in 1 × PBS for 1.5 h. The plate was washed 3 times and 100 µL of a series of 2 anti-*T. gondii* IgG-positive and 2 anti-*T. gondii* IgG-negative serum samples that had already been prepared using 1 × PBS were added to each well. The plate was left at room temperature for 2.5 h. The plate was again washed 3 times; 100 µL of HRP-conjugated rabbit anti-human IgG (1:10,000 dilution in 1 × PBS) was added to each well; and the plate was left at room temperature for 1 h. After re-washing the plate, 100 µL of 3,3',5,5'-tetramethylbenzidine (TMB) substrate was added, and after 15 min at room temperature, the reaction was stopped with 50 µL of 2N H₂SO₄. The optical density (OD) of each well was measured with an ELISA reader at wavelength 450 nm with a reference wavelength of 630 nm. The assay was repeated for all of the serum samples at a 1:200 dilution and with 1 µg/mL of purified protein. The mean ± standard deviation (SD) of all 25 anti-*Toxoplasma* IgG-negative serum samples was considered the cut-off value.

Statistical analysis

The sensitivity and specificity were calculated using the VassarStats website (<http://vassarstats.net/>) with the following formulae: sensitivity = $TP/(TP+FN) \times 100$ and specificity = $TN/(TN+FP) \times 100$ (TP – true positive, FN – false negative, TN – true negative, FP – false positive). The sensitivity and specificity were calculated with receiver operating characteristic (ROC) curve using Prism graphing and statistics software (GraphPad Software, San Diego, USA).

Results

Design of the poly-epitope protein

The alignment of amino acid sequences of 3 surface antigens obtained from the RH strain showed high similarity with other pathogenic strains of *T. gondii*. The selection of immunological regions was based on the distribution of amino acids and transmembrane topology. The analysis of the predictions obtained from the TMHMM server showed that all 3 proteins were embedded on the cell surface and therefore available to the immune system

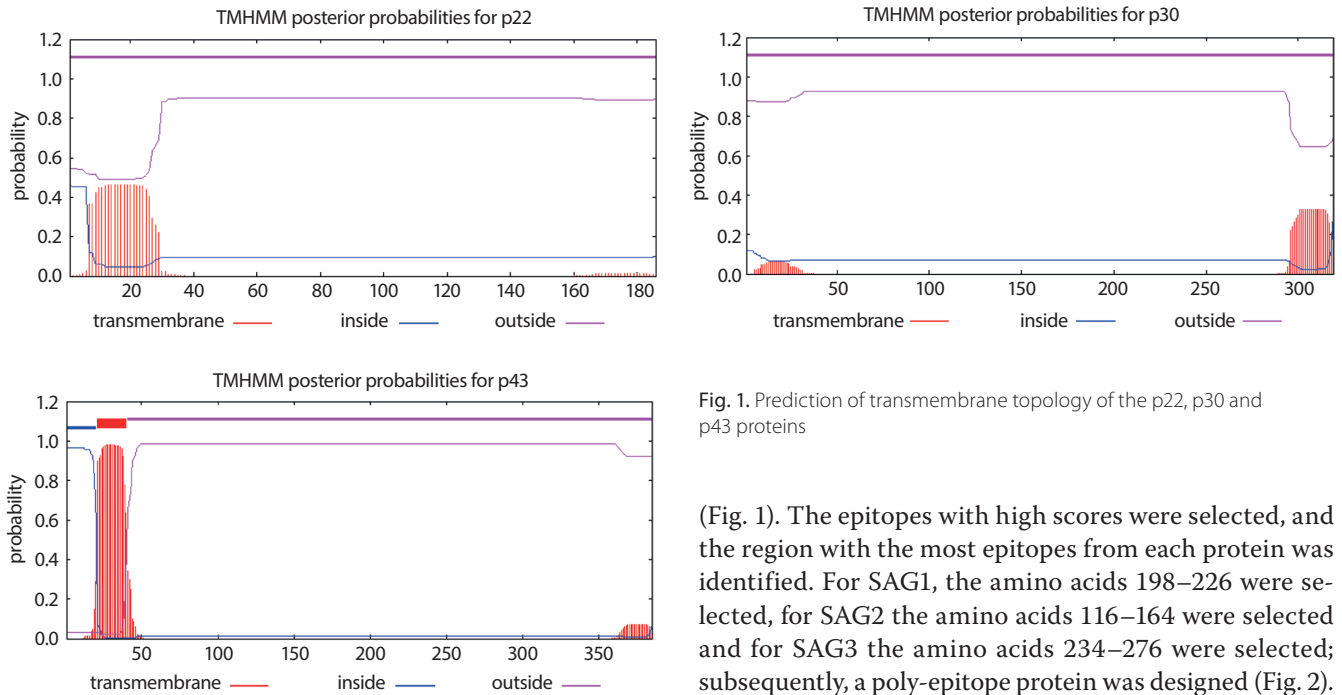


Fig. 1. Prediction of transmembrane topology of the p22, p30 and p43 proteins

(Fig. 1). The epitopes with high scores were selected, and the region with the most epitopes from each protein was identified. For SAG1, the amino acids 198–226 were selected, for SAG2 the amino acids 116–164 were selected and for SAG3 the amino acids 234–276 were selected; subsequently, a poly-epitope protein was designed (Fig. 2).

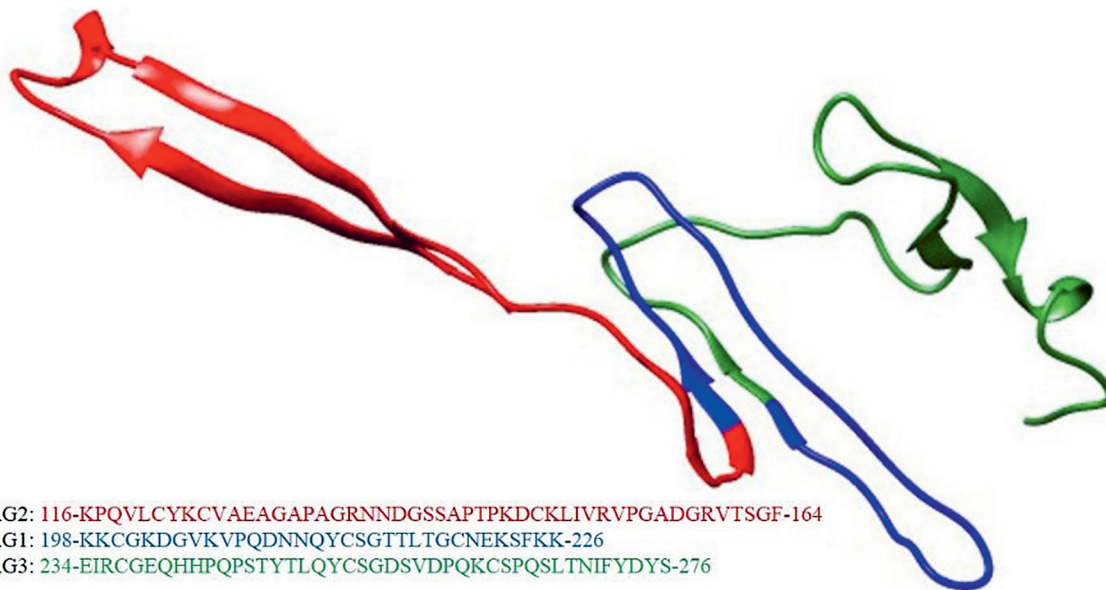


Fig. 2. Predicted tertiary structure of the multi-epitope protein by the Phyre2 protein fold recognition server

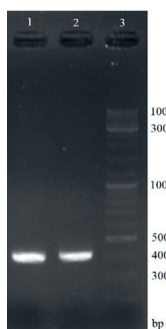


Fig. 3. PCR results of the multi-epitope gene fragment: lanes 1 and 2 – PCR product; lane 3 – DNA ladder

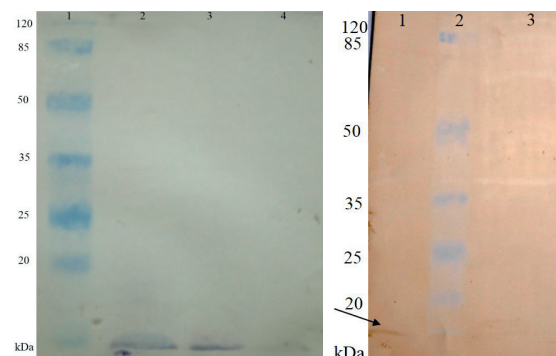


Fig. 4. Western blot analysis of expressed (left) and purified (right) proteins: lane 1 – protein molecular size marker; lanes 2 and 3 – lysate of induced cells 2 h and 3 h after induction; lane 4 – lysate of cells without the vector as a control. Right: lane 1 – lysate of induced cells after purification; lane 2 – protein molecular size marker; lane 3 – lysate of cells without the vector as a control

The size of the multi-epitope gene (405 bp) was confirmed with PCR (Fig. 3). The calculation of molecular weight showed a protein with a molecular weight of about 12 kDa.

Analysis of the purified protein

The western blot analysis of protein expression revealed that protein is expressed at both 2 h and 3 h after induction. The expressed protein was purified using affinity chromatography, after which western blot and dot-blot analysis confirmed that the protein was purified successfully but not completely (Fig. 4).

IgG ELISA analysis

The cut-off value was 1.65. From 95 serum samples with anti-*T. gondii* IgG, 69 cases were positive by poly-epitope protein. Two cases from the negative serum samples and 1 case from the nosocomial infections were also positive (Fig. 5). The comparison of the results of the commercial and recombinant ELISA assays indicated a sensitivity of 72.6% and a specificity of 90.3% for the recombinant ELISA (Table 1). Moreover, the result of the ROC curve analysis using GraphPad Prism software showed the area under the curve as 0.93 (0.88 to 0.97) with a 95% confidence interval (95% CI) (Fig. 6).

Table 1. Sensitivity and specificity of multi-epitope IgG ELISA for diagnosis of toxoplasmosis

Sensitivity [%]	Specificity [%]	Positive predictive value [%]	Negative predictive value [%]	Agreement [%]
72.6	90.3	95.8	51.8	76.9

Agreement: $(TP+TN)/(TP+TN+FP+FN) \times 100$.

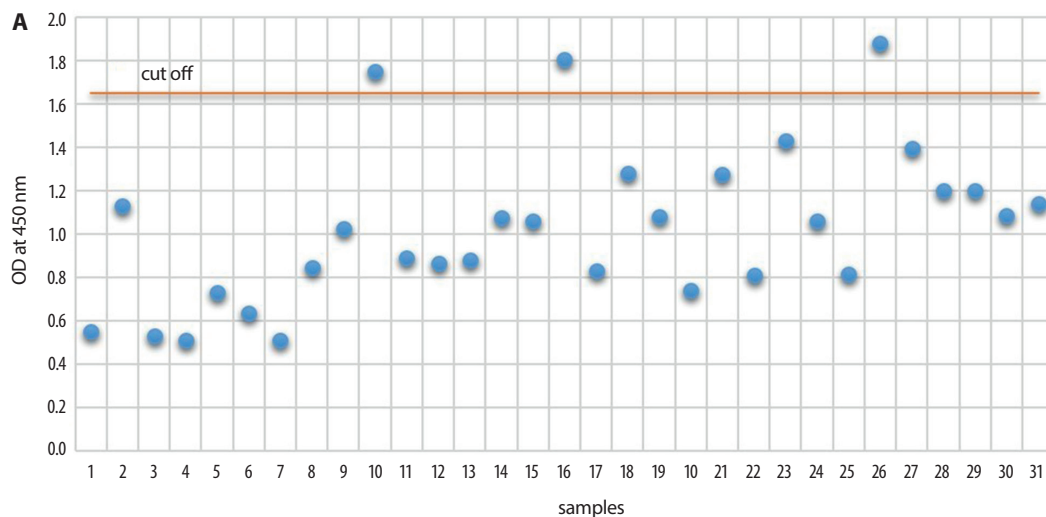
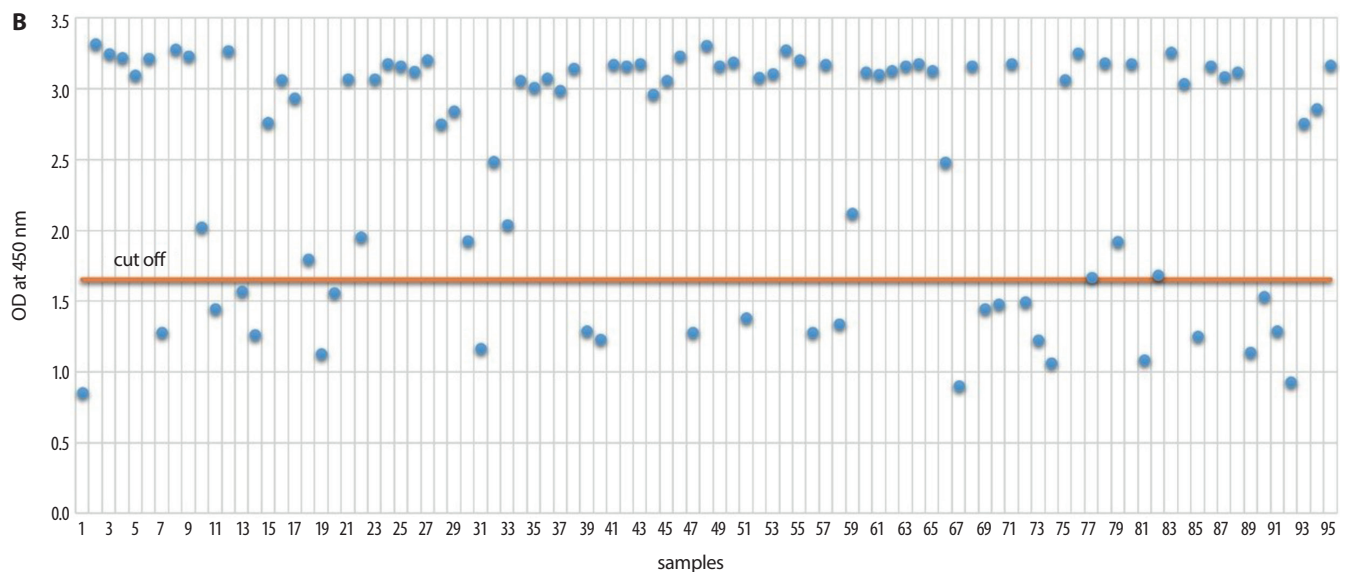


Fig. 5. Results of IgG ELISA

A – negative samples;
B – positive samples.



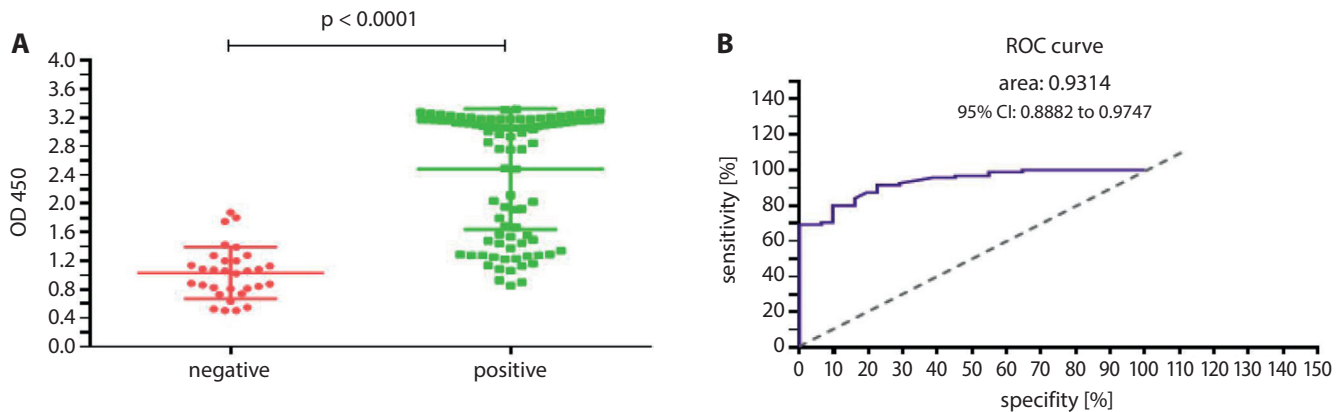


Fig. 6. Results of ROC analysis in the assessment of diagnostic marker utility. A – optical density values of 2 anti-*T. gondii* IgG-positive and 2 anti-*T. gondii* IgG-negative serum samples; B – ROC curve; graphical plot of sensitivity vs specificity

Discussion

The current study evaluated the potential of a poly-epitope protein comprising 3 immunological regions obtained from surface antigens of *T. gondii* as a diagnostic tool. The selection of epitopes was based on various factors, mainly regions with high immunogenicity. For example, the nature of a given polarity of amino acids and also the number of hydrophilic residues in the protein and thus the solubility of the protein have a remarkable effect on the immunogenicity of antigens. Moreover, the cellular location of antigens and their accessibility to the immune system may be an important factor in designing diagnostic proteins. The *in silico* analysis exhibited that all 3 surface antigens in this study possess more hydrophilic amino acids. They also have significant elements accessible to the immune system.¹³ Studies have also shown that these proteins can be considered in controlling strategies against toxoplasmosis, including diagnosis and vaccine design.¹⁴ Most of the diagnostic studies have been based on whole antigens.

Native antigens have shown promising results in detecting pathogenic microorganisms, including *T. gondii*, but their use entails problems like high price, low sensitivity and low specificity. This may be due to different reasons, such as cross-reactivity. A new alternative method is the use of a multi-epitope-based antigen with the help of *in silico* prediction tools in which only highly immunogenic regions or only regions which do not show cross-reactivity with other microorganism antigens are selected. This study showed that although a multi-epitope protein comprising epitopes from SAG1, SAG2 and SAG3 can detect some of the individuals suffering from toxoplasmosis, we need further investigation to improve the diagnosis of this infection by modified epitopes, by selecting other epitopes and even by involving other antigens of *T. gondii*. The current multi-epitope protein showed that such proteins could be a potential candidate for use in diagnostic work; however, more studies

as well as other methods are needed to increase the sensitivity and specificity of multi-epitope antigens to use as target tools in diagnostic kits. Hajissa et al. produced a synthetic protein consisting of epitopes obtained from 3 *T. gondii* antigens for use as a diagnostic marker and vaccine candidate.⁷ In their study, 9 epitopes from 3 antigens (SAG1, GRA2 and GRA7) were used for the construction of a multi-epitope protein. GRAs are dense granule antigens in *T. gondii* which cause high induction of antibody response in humans. The ability of this designed protein to detect anti-*Toxoplasma* antibodies was analyzed with western blot and ELISA, which have shown that the protein can detect acute *T. gondii* infection with high sensitivity and specificity.

The most important thing in designing these proteins is choosing appropriate antigens with high immunogenicity, and then selecting epitopes with the highest score using web servers with high predictive potential. Therefore, *in silico* analysis and software-based prediction techniques are vital steps toward a promising multi-epitope protein for use in diagnostic kits. Studies have shown that for *T. gondii*, surface antigens are ideal candidates for diagnosis as well as for vaccine design; each of these antigens alone has been studied as a potential diagnostic marker. Khanaliha et al. evaluated 3 surface antigens (SAGs 1, 2 and 3) separately for their diagnostic usefulness and efficacy. Recombinant SAG1, SAG2 and SAG3 produced in *E. coli* showed suitable antigens to detect anti-*Toxoplasma* IgG with 93.6%, 95.4% and 100% sensitivity, and specificity of 92.9%, 89.4% and 91.2%, respectively.¹⁴ The relatively low values in our study could indicate that better designing and further investigation in the selection of epitopes is required.

The differences between the current study and those mentioned above could be due to various reasons. Protein conformation and protein folding are influenced by the reaction conditions, such as pH and temperature during experiments in artificially differentiated conditions as opposed to the natural synthesis of the protein. Therefore,

a test that uses the whole body of the parasite has greater sensitivity and specificity than the tests using selected epitopes in this study, and may achieve better results by adding other antigen-determinant epitopes.

References

- Opsteegh M, Kortbeek TM, Havelaar AH, van der Giessen JW. Intervention strategies to reduce human *Toxoplasma gondii* disease burden. *Clin Infect Dis*. 2015;60(1):101–107.
- Hsu PC, Groer M, Beckie T. New findings: Depression, suicide, and *Toxoplasma gondii* infection. *J Am Assoc Nurse Pract*. 2014;26(11):629–637.
- Blader IJ, Coleman BI, Chen CT, Gubbels MJ. Lytic cycle of *Toxoplasma gondii*: 15 years later. *Annu Rev Microbiol*. 2015;69:463–485.
- Dubremetz JF, Lebrun M. Virulence factors of *Toxoplasma gondii*. *Microbes Infect*. 2012;14(15):1403–1410.
- Lekutis C, Ferguson DJ, Grigg ME, Camps M, Boothroyd JC. Surface antigens of *Toxoplasma gondii*: Variations on a theme. *Int J Parasitol*. 2001;31(12):1285–1292.
- Montoya JG. Laboratory diagnosis of *Toxoplasma gondii* infection and toxoplasmosis. *J Infect Dis*. 2002;185(Suppl 1):S73–S82.
- Hajissa K, Zakaria R, Suppian R, Mohamed Z. Design and evaluation of a recombinant multi-epitope antigen for serodiagnosis of *Toxoplasma gondii* infection in humans. *Parasit Vectors*. 2015;8:315.
- Vita R, Overton JA, Greenbaum JA, et al. The immune epitope database (IEDB) 3.0. *Nucleic Acids Res*. 2015;43(Database issue):D405–D412.
- Saha S, Raghava GP. Prediction of continuous B-cell epitopes in an antigen using recurrent neural network. *Proteins*. 2006;65(1):40–48.
- Saha S, Raghava GPS. BcePred: Prediction of continuous B-cell epitopes in antigenic sequences using physico-chemical properties. In: Nicosia G, Cutello V, Bentley PJ, Timmis J, eds. *Artificial Immune Systems: Third International Conference, ICARIS 2004, Catania, Sicily, Italy, September 13–16, 2004 Proceedings*. Berlin-Heidelberg; Springer 2004:197–204.
- Larsen JE, Lund O, Nielsen M. Improved method for predicting linear B-cell epitopes. *Immunome Res*. 2006;2:2.
- Kolaskar AS, Tongaonkar PC. A semi-empirical method for prediction of antigenic determinants on protein antigens. *FEBS Lett*. 1990;276(1–2):172–174.
- Tomavo S, Schwarz RT, Dubremetz JF. Evidence for glycosyl-phosphatidylinositol anchoring of *Toxoplasma gondii* major surface antigens. *Mol Cell Biol*. 1989;9(10):4576–4580.
- Khanaliha K, Motazedian MH, Kazemi B, Shahriari B, Bandehpour M, Sharifniya Z. Evaluation of recombinant SAG1, SAG2, and SAG3 antigens for serodiagnosis of toxoplasmosis. *Korean J Parasitol*. 2014;52(2):137–142.

MicroRNA-548k upregulates a spliced variant of human CD2-associated protein by targeting its promoter

Nannan Li^{B,F}, Guoping Zhou^A

Department of Pediatrics, First Affiliated Hospital, Nanjing Medical University, China

A – research concept and design; B – collection and/or assembly of data; C – data analysis and interpretation; D – writing the article; E – critical revision of the article; F – final approval of the article

Advances in Clinical and Experimental Medicine, ISSN 1899–5276 (print), ISSN 2451–2680 (online)

Adv Clin Exp Med. 2020;29(6):677–682

Address for correspondence

Guo-Ping Zhou
E-mail: zhouguoping@jssph.org.cn

Funding sources

This work was funded by the National Natural Science Foundation of China (grants: No. 81170661, No. 31640048 to GPZ, No. 81300023 to RJ, and No. 81500013 to LLZ), the Provincial Natural Science Foundation of Jiangsu (grant No. BK20131020 to RJ), and the Nanjing Science and Technology Plan Project (grant No. 201503003 to GPZ).

Conflict of interest

None declared

Received on November 1, 2017

Reviewed on January 11, 2018

Accepted on May 7, 2020

Published online on July 1, 2020

Abstract

Background. MicroRNAs (miRNAs) regulate gene expression by repressing the translation or directing the degradation of mRNA in the cytoplasm. However, recent studies have shown that miRNAs act to regulate transcription at target gene promoters.

Objectives. To investigate whether miR-548k regulates CD2AP002 expression at the transcriptional level.

Material and methods. The CD2AP002 promoter region was cloned and its promoter activity was examined in HEK293 cells using luciferase assay. The CD2AP002 promoter region was characterized bioinformatically. The HEK293 cells were treated with a miR-548k mimic or inhibitor and the luciferase activity of the CD2AP002 promoter and the mRNA expression of CD2AP002 were assayed. A chromatin immunoprecipitation assay was performed with antibody against RNA polymerase II at the CD2AP002 promoter region in HEK293 cells.

Results. The CD2AP002 promoter region contained 2 putative miR-548k binding sites, and mutational analysis revealed that both of those sites contributed to transcriptional activity. The miR-548k mimics increased CD2AP002 promoter activity and mRNA expression. In contrast, the miR-548k inhibitor significantly reduced CD2AP002 promoter activity and mRNA expression. Finally, the chromatin immunoprecipitation assay showed that the enrichment of RNA polymerase II at the CD2AP002 promoter region was enhanced in the HEK293 cells treated with the miR-548k mimic.

Conclusions. This is the first study to demonstrate that miR-548k upregulates CD2AP002 expression by targeting its promoter.

Key words: transcriptional regulation, gene promoters, CD2-associated protein, microRNA-548k, spliced variant

Cite as

Li N, Zhou G. MicroRNA-548k upregulates a spliced variant of human CD2-associated protein by targeting its promoter. *Adv Clin Exp Med.* 2020;29(6):677–682. doi:10.17219/acem/122168

DOI

10.17219/acem/122168

Copyright

© 2020 by Wrocław Medical University
This is an article distributed under the terms of the Creative Commons Attribution 3.0 Unported (CC BY 3.0) (<https://creativecommons.org/licenses/by/3.0/>)

Introduction

Primary focal segmental glomerulosclerosis (FSGS) is a destructive type of nephrotic syndrome and the main cause of primary nephropathy.¹ Several gene mutations have been found in patients with primary FSGS, including the CD2-associated protein (CD2AP). The human CD2AP is an 80-kDa protein that was originally cloned as a protein involved in T cell activation.² In T cells, CD2AP binds the adhesion molecule CD2 and modulates the cytoskeletal polarity. CD2AP knockout mice exhibit high proteinuria at a young age followed by glomerulosclerosis, and they die from renal failure. The histological characteristics of the kidney lesions of CD2AP-deficient mice are similar to human FSGS.³

Alternative pre-messenger RNA (pre-mRNA) splicing plays an important role in the disease and its development. At least 74% of human multi-exon genes are alternatively spliced.⁴ Alternative splicing is a general mechanism for regulating gene expression and is associated with numerous diseases, such as thalassemia syndromes and dementia.^{5,6} CD2AP includes 5 spliced variants which may regulate the wild-type CD2AP. However, the mechanism underlying the regulation of the spliced variant of CD2AP remains unknown.

MicroRNAs (miRNAs) are a class of small non-coding RNAs that regulate gene expression by repressing translation or directing sequence-specific degradation of complementary mRNA in the cytoplasm.⁷ However, recent studies have shown that miRNAs act to regulate the stability of nuclear transcripts, silencing or activating transcription at the target gene promoters.^{8–12} miR-548 is a large and poorly conserved primate-specific miRNA gene family. There are 69 human miR-548 genes, located in almost all human chromosomes; this widespread distribution pattern indicates an evolutionary origin from transposable elements.¹³ However, the role of miR-548k remains elusive. In this study, we aimed to investigate whether miR-548k may regulate CD2AP002 expression at the transcriptional level. Because CD2AP function is implicated in renal diseases such as FSGS, we selected the human embryonic kidney cell line HEK293 as the experimental model and employed different approaches to characterize the regulation of CD2AP002 transcription by miR-548k.

Material and methods

Cell culture and transfection

Human embryonic kidney HEK293 cells were purchased from the American Type Culture Collection (Manassas, USA), and maintained in Dulbecco's modified Eagle's medium (DMEM) supplemented with 10% heat-inactivated fetal bovine serum (FBS), 100 U/mL of penicillin and 100 µg/mL of streptomycin in a humidified atmosphere of 5% CO₂ at 37°C. Transfections were carried out

in HEK293 cells using Lipofectamine 3000 (Invitrogen, Carlsbad, USA) according to the manufacturer's protocol.

Plasmids

A 2,827 bp of the 5'-flanking region of the human CD2AP002 gene was cloned using human genomic DNA extracted from the HEK293 cells as the template and primers synthesized by Invitrogen (the sequences were **CGGGGTACCGAGATAACAAAAACAGATACCGAAG** and **GGAAGATCTTCTTTACCATTAAAGTTCGCCCTC**, respectively, with the Kpn I and Bgl II restriction sites in bold and underlined). The polymerase chain reaction (PCR) was carried out using high-fidelity DNA polymerase. The PCR protocol was 30 cycles at 98°C for 10 s, 60°C for 15 s and 68°C for 3 min. The PCR product was digested with Kpn I and Bgl II and ligated into a pGL3-basic vector to generate pGL3-CD2AP002 (named pGL3-2827). The clones were verified with sequencing. pGL3-2827 was scanned for sites complementary to known human miRNAs, using online RegRNA software (<http://regrna.mbc.nctu.edu.tw/html/prediction.html>).

A deletion mutant of the plasmid containing the 5'-flanking region of CD2AP002 was generated with PCR using pGL3-2827 as the template and primers synthesized by Invitrogen (the sequences were **CGGGGTACCTCTAAGTCCTGAAAACCTTGGCACG** and **GGAAGATCTTCTTTACCATTAAAGTTCGCCCTC**, respectively, with Kpn I and Bgl II restriction sites in bold and underlined). The plasmid was named pGL3-2200.

Site-directed mutagenesis of the putative miR-548k binding sites in the promoter region of CD2AP002 was performed with a Fast Mutagenesis System (Invitrogen). The sequence containing the 1st miR-548k binding site was mutated from TACGGTATTGACTATAAGTATTTTA to the miR-548k mutation TACGGTATTGACTATAAATATTTTA, and the sequence containing the 2nd miR-548k binding site was mutated from TTGTTCTTTTTTAAGTACTTTT to the mutation TTGTTCTTTTTTAAGTAGTTT (mutations shown in bold). The mutations were confirmed with sequencing.

Double-stranded miRNA and inhibitor

The miR-548k mimic, the miR-548k inhibitor, the mismatched derivatives miR-548k-5MM, and the corresponding nonspecific control dsRNA (negative control) were synthesized with RiboBio (Guangzhou, China).

Luciferase assay

HEK293 cells were cultured for 24 h and then transfected with reporters and controls. The luciferase assay was performed 24 h after transfection using the dual-luciferase reporter gene assay kit (Promega; Madison, USA) according to the manufacturer's instructions.

Real-time PCR

Total RNA, including miRNA, was extracted using Trizol reagent (Invitrogen). A total of 1 µg of RNA was reverse-transcribed into cDNA with a PrimeScript RT Master Mix Perfect kit (Takara, Dalian, China). Real-time PCR (RT-PCR) was performed using SYBR Premix Ex Taq™ (Takara, Dalian, China) and an ABI PRISM 7700 sequence detection system (PE Applied Biosystems, Wellesley, USA). The primers were synthesized by Invitrogen with sequences as follows: CD2AP002-F CTCCAAAGCCTGAAGTATGATAGC, CD2AP002-R AAATGAACTACTCCCTCCAGA and GAPDH-F TGGTATCGTGGAAGGACTCATGAC, and GAPDH-R TGC-CAGTGAGCTTCCCGTTCAGC. The reaction conditions were 95°C for 10 min (1 cycle), followed by 40 cycles of 95°C for 15 s, 60°C for 15 s and 70°C for 1 min. GAPDH was used as the internal reference.

To detect the level of miR-548k, the miRNA was converted into cDNA with reverse transcription using a TaqMan MicroRNA reverse transcription kit (Applied Biosystems). To quantify miR-548k expression, RT-PCR was performed with the use of a TaqMan miRNA assay kit for hsa-miR-548k (Applied Biosystems). The primers were synthesized by Invitrogen with the following sequences: miR-548k Forward TCGGCGGAAAAGTACTTGCGGAT, Reverse ATCCAGTGCAGGGTCCGAGG and U6 Forward GGTCGGGAGGAAAGAGGGC, Reverse GCTAATCTTCTGTATCGTTCC. The PCR protocol was 95°C for 5 min (1 cycle), followed by 40 cycles of 90°C for 15 s, 60°C for 15 s and 72°C for 1 min. U6 served as an endogenous control to normalize miR-548k expression. The relative expression levels were calculated using the equation: $Folds = 2^{-\Delta\Delta Ct}$. Each sample was analyzed 3 times.

Chromatin immunoprecipitation assay

The HEK293 cells were transfected with miR-548k mimics or negative control miRNA with a scramble sequence (miR-NC). The cells were cross-linked with 1% formaldehyde for 10 min at room temperature before being stopped with glycine. Using a Magna/EZ-Magna chromatin immunoprecipitation assay (ChIP) Kit (Upstate Biotechnology, Lake Placid, USA), the cells were washed with cold PBS and harvested in lysis buffer supplemented with Protease Inhibitor Cocktail II (Upstate Biotechnology). Sonication of cross-linked chromatin was performed to obtain 200–1,000-bp chromatin fragments. Immunoprecipitation was performed using 5 µg each of Anti-Acetyl Histone H3 (Upstate 06-599B; Upstate Biotechnology), Anti-IgG (Upstate PP64B; Upstate Biotechnology) and 10 µg of Anti-RNA polymerase II (Santa Cruz sc-899X; Santa Cruz Biotechnology, Santa Cruz, USA) overnight at 4°C with rotation. In order to recover the antibody/antigen/DNA complexes, 20 µL of Protein

A beads (Upstate Biotechnology) were added, and the mixture was washed 4 times. The eluted samples were treated with Proteinase K (Upstate Biotechnology) and incubated for 2 h at 62°C and 10 min at 95°C to reverse the cross-links. DNA purification was performed using spin columns (Upstate Biotechnology). The purified DNA was amplified by promoter specific primers as follows: ChIP-F1 ATGTATCTCCTTGTAGTTGAATCTG and ChIP-R1 ACTTATTTAGCCTCTATCTTGTGTA (targeting the 1st putative miR-548k binding sites on CD2AP002 promoter); ChIP-F2 GCACGTAATAAGTGCTCAG and ChIP-R2 AATAGAATGAGGTGGAAGA (targeting the 2nd putative miR-548k binding sites on the CD2AP002 promoter). The input of each sample was used as an internal control. The PCR products were visualized with gel electrophoresis on 2% agarose gel, and confirmed with sequencing.

Statistical analysis

The data is presented as means ± standard deviation (SD) of 3 or more independent results. Statistical significance was assessed using a two-tailed, unpaired Student's t-test. A p-value <0.05 was selected as the level denoting significant differences.

Results

miR-548k upregulates CD2AP002 expression by binding to its promoter in HEK293 cells

Scanning analysis of the CD2AP002 promoter showed that 2 sequences located at positions -2537 and -2041 relative to the transcription start site were highly complementary to miR-548k (Fig. 1A–C). To confirm that miR-548k upregulates CD2AP002 expression, we overexpressed miR-548k in HEK293 cells (Fig. 1D). Luciferase assay showed that the CD2AP002 promoter (pGL3-2827), which had 2 putative miR-548k binding sites, exhibited significantly higher luciferase activity in the HEK293 cells with an overexpression of miR-548K compared to the control cells (Fig. 1E). Furthermore, RT-PCR showed that CD2AP002 mRNA level was significantly higher in the HEK293 cells with an overexpression of miR-548K compared to the control cells (Fig. 1F).

To determine whether the induction of CD2AP002 promoter activity was specific to the sequence of miR-548k, we performed deletion mutation and point mutation of 2 putative miR-548k binding sites. The luciferase assay revealed that both basic and miR-548k-stimulated luciferase activities were significantly reduced in miR-548k site-directed deletion mutation and two-point mutations in the CD2AP002 promoter compared to the wild-type promoter (Fig. 2A). Furthermore, we synthesized a miR-548k mutant to create a mismatch with

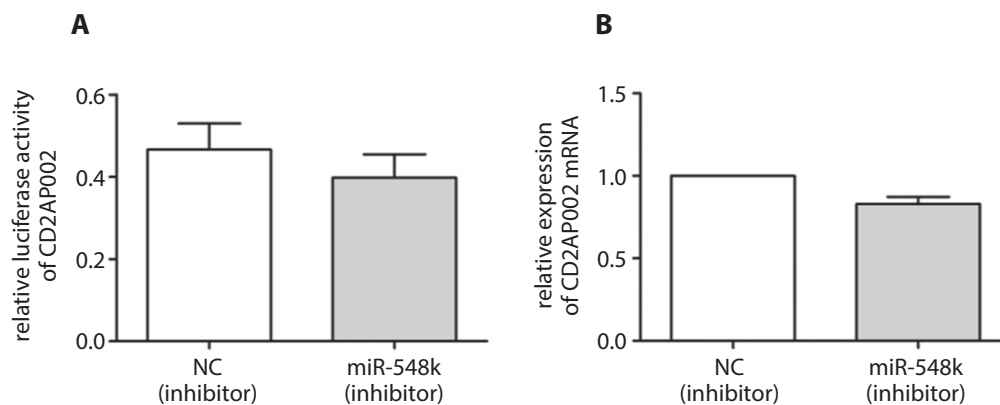


Fig. 3. miR-548k inhibitor represses the expression of CD2AP002. A – HEK293 cells were transfected with 200 nM of miR-548k inhibitor or miR-NC (negative control) and reporter constructs. Dual-luciferase reporter assay was performed 24 h later. B – relative expression of CD2AP002 was determined with RT-PCR and normalized to GAPDH in HEK293 cells transfected with 200 nM of miR-548k inhibitor or miR-NC (negative control). All data is presented as mean ±SD from 3 independent trials

the target sites; the luciferase assay showed that this mutant miR-548k-5MM could not induce CD2AP002 promoter activity (Fig. 2B). Taken together, these findings indicate that miR-548k upregulates CD2AP002 expression by binding to 2 putative recognition sites in the promoter region of CD2AP002 in HEK293 cells.

miR-548k inhibitor downregulates CD2AP002 expression in HEK293 cells

To test whether the miR-548k inhibitor downregulated CD2AP002 expression, we transfected the HEK293 cells with a miR-548k inhibitor, which was designed specifically to bind to and sequester a mature miR-548k sequence, and its miR-NC as the control. Luciferase assay demonstrated that the miR-548k inhibitor reduced basic luciferase activity driven by the CD2AP002 promoter (Fig. 3A). Moreover, RT-PCR showed that the miR-548k inhibitor reduced the expression of CD2AP002 mRNA in HEK293 cells (Fig. 3B).

Enrichment of miR-548k at the CD2AP002 promoter

To confirm that miR-548k binds to the CD2AP002 promoter directly, we performed a ChIP assay. RNA polymerase II (pol II) holoenzyme is known to be recruited

to the promoters of protein-coding genes in living cells. Thus, we used an antibody specific to pol II for ChIP and mapped 2 regions corresponding to the transcription start sites of CD2AP002. The PCR and sequencing results revealed that miR-548k was associated with the CD2AP002 promoter at an endogenous level in HEK293 cells. In the cells transfected with the miR-548k mimic, we found increased recruitment of miR-548k at CD2AP002 transcription start sites (Fig. 4). These results suggest that miR-548k is recruited to the CD2AP002 promoter to activate the transcription of CD2AP002.

Discussion

Alternative splicing is a key mechanism for expanding transcript and protein diversity of mammalian genes. CD2AP is a multi-domain scaffolding protein that has a critical role in renal function. Our previous studies have shown that the CD2AP promoter in human renal tubular cells could be regulated by CREB, Sp1 and E2F1.¹⁴ However, little is known about the regulation of alternative splicing of CD2AP. In this study, we focused on a splicing variant CD2AP002 and characterized its promoter in HEK293 cells.

Recent studies have indicated the role of non-coding RNAs in diseases.¹⁵ For instance, transgenic expression of miR-193a in mice rapidly induced FSGS with extensive podocyte foot process effacement.¹⁶ The concentrations of serum miR-30a-5p, miR-151-3p, miR-150, miR-191, and miR-19b were significantly higher in nephritic syndrome (NS) children than in controls.¹⁷ In addition, the expression of miR-141, miR-205 and miR-192 was correlated with disease severity and progression in patients with IgA nephropathy.¹⁸

Interestingly, miRNA-induced transcriptional regulation has been reported in mammalian systems. miR-373 could upregulate E-cadherin and CSDC2, both of which contained complementary sequences to miR-373 in their promoters.¹⁹ miR-320 could recruit AGO1 and other factors to silence POLR3D expression.²⁰ Moreover, Younger et al. found that miRNAs could inhibit the expression

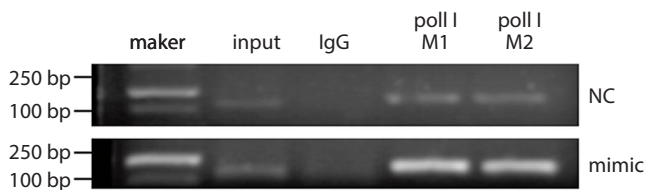


Fig. 4. Enrichment of pol II at CD2AP002 promoter by miR-548k. HEK293 cells were transfected with miR-NC (negative control) or the miR-548k mimic. At 24 h post-transfection, the cells were harvested and subjected to ChIP assay using a pol II-specific antibody or normal rabbit IgG (negative control) to immunoprecipitate transcriptionally active regions of DNA. Purified DNA was analyzed with RT-PCR using primers targeting 2 putative miR-548k binding sites on the CD2AP002 promoter. DNA pulled down in the absence of antibody (No Ab) served to identify background amplification. The input DNA was amplified as a loading control. Representative results from 3 independent trials with similar results are shown

of progesterone receptor (PR) by targeting its promoter.²¹ Recently, our group reported that miR-939 downregulated CD2AP expression by targeting its promoter in HEK-293T cells.²² However, in this study, we found that miR-548k could activate CD2AP002 expression at the transcriptional level and we identified 2 putative binding sites for miR-548k in the promoter region of CD2AP002. The sequence specificity was confirmed using deletion and point mutation assay. A ChIP assay further demonstrated that miR-548k activated transcription by direct binding to the promoter of CD2AP002.

However, the detailed mechanism by which miRNAs modulate transcriptional regulation by targeting promoters remains unclear. In the cytoplasm, the function of miRNAs is well known to direct an Argonaute-containing complex to target and repress or degrade mRNAs. More recently, a regulatory role for miRNAs and Argonaute has been reported in the nucleus, where miRNAs guide Argonaute to target gene promoters and directly regulate transcription. We assume that miR-548k could recruit Argonaute to a CD2AP002 promoter, overlapping the binding sites of some transcription factors, which therefore come into contact with transcription factors and RNA polymerase II in a positive manner. Further studies are required to test this possibility.

Conclusions

Our findings demonstrate for the first time that miR-548k upregulates CD2AP002 expression by targeting specific sites in its promoter region. Our study may provide new insight into the role of miRNAs in gene expression regulation and disease progression.

References

1. Dragovic D, Rosenstock JL, Wahl SJ, Panagopoulos G, DeVita MV, Michelis MF. Increasing incidence of focal segmental glomerulosclerosis and an examination of demographic patterns. *Clin Nephrol*. 2005;63(1):1–7.
2. Wolf G, Stahl RA. CD2-associated protein and glomerular disease. *Lancet*. 2003;362(9397):1746–1748.
3. Shih NY, Li J, Karpitskii V, et al. Congenital nephrotic syndrome in mice lacking CD2-associated protein. *Science*. 1999;286(5438):312–315.
4. Johnson JM, Castle J, Garrett-Engele P, et al. Genome-wide survey of human alternative pre-mRNA splicing with exon junction microarrays. *Science*. 2003;302(5653):2141–2144.
5. Radmilovic M, Zukic B, Stankovic B, et al. Thalassemia syndromes in Serbia: An update. *Hemoglobin*. 2010;34(5):477–485.
6. Andreadis A. Tau gene alternative splicing: Expression patterns, regulation and modulation of function in normal brain and neurodegenerative diseases. *Biochim Biophys Acta*. 2005;1739(2–3):91–103.
7. Bartel DP. MicroRNAs: Genomics, biogenesis, mechanism, and function. *Cell*. 2004;116(2):281–297.
8. Kalantari R, Chiang CM, Corey DR. Regulation of mammalian transcription and splicing by nuclear RNAi. *Nucleic Acids Res*. 2016;44(2):524–537.
9. Paugh SW, Coss DR, Bao J, et al. MicroRNAs form triplexes with double stranded DNA at sequence-specific binding sites: An eukaryotic mechanism via which microRNAs could directly alter gene expression. *PLoS Comput Biol*. 2016;12(2):e1004744.
10. Suzuki K, Ahlenstiel C, Marks K, Kelleher AD. Promoter targeting RNAs: Unexpected contributors to the control of HIV-1 transcription. *Mol Ther Nucleic Acids*. 2015;4(1):e222.
11. Cho S, Park JS, Kang YK. AGO2 and SETDB1 cooperate in promoter-targeted transcriptional silencing of the androgen receptor gene. *Nucleic Acids Res*. 2014;42(22):13545–13556.
12. Benhamed M, Herbig U, Ye T, Dejean A, Bischof O. Senescence is an endogenous trigger for microRNA-directed transcriptional gene silencing in human cells. *Nat Cell Biol*. 2012;14(3):266–275.
13. Liang T, Guo L, Liu C. Genome-wide analysis of mir-548 gene family reveals evolutionary and functional implications. *J Biomed Biotechnol*. 2012;2012:679563.
14. Zou L, Xu HG, Ren W, Jin R, Wang Y, Zhou GP. Transcriptional activation of the human CD2AP promoter by E2F1. *PLoS One*. 2012;7(8):e42774.
15. Ni X, Liao Y, Li L, Zhang X, Wu Z. Therapeutic role of long non-coding RNA TCONS_00019174 in depressive disorders is dependent on Wnt/ β -catenin signaling pathway. *J Integr Neurosci*. 2018;17(2):125–132. doi:10.3233/JIN-170052
16. Gebeshuber CA, Kornauth C, Dong L, et al. Focal segmental glomerulosclerosis is induced by microRNA-193a and its downregulation of WT1. *Nat Med*. 2013;19(4):481–487.
17. Luo Y, Wang C, Chen X, et al. Increased serum and urinary microRNAs in children with idiopathic nephrotic syndrome. *Clin Chem*. 2013;59(4):658–666.
18. Wang G, Kwan BC, Lai FM, et al. Intrarenal expression of microRNAs in patients with IgA nephropathy. *Lab Invest*. 2010;90(1):98–103.
19. Place RF, Li LC, Pookot D, Noonan EJ, Dahiya R. MicroRNA-373 induces expression of genes with complementary promoter sequences. *Proc Natl Acad Sci U S A*. 2008;105(5):1608–1613.
20. Kim DH, Saetrom P, Snøve O Jr, Rossi JJ. MicroRNA-directed transcriptional gene silencing in mammalian cells. *Proc Natl Acad Sci U S A*. 2008;105(42):16230–16235.
21. Younger ST, Corey DR. Transcriptional gene silencing in mammalian cells by miRNA mimics that target gene promoters. *Nucleic Acids Res*. 2011;39(13):5682–5691.
22. Huang YP, Qiu LZ, Zhou GP. MicroRNA-939 downregulates CD2-associated protein by targeting promoter in HEK-293T cells. *Ren Fail*. 2016;38(4):508–513.

The small heterodimer partner inhibits activation of hepatic stellate cells via autophagy

Wei Ma^{A–D}, Li-Sha Cheng^{B,E}, Wei Jiang^E, Sheng-Di Wu^F

Department of Gastroenterology and Hepatology, Zhongshan Hospital, Fudan University, Shanghai Institute of Liver Diseases, China

A – research concept and design; B – collection and/or assembly of data; C – data analysis and interpretation; D – writing the article; E – critical revision of the article; F – final approval of the article

Advances in Clinical and Experimental Medicine, ISSN 1899–5276 (print), ISSN 2451–2680 (online)

Adv Clin Exp Med. 2020;29(6):683–693

Address for correspondence

Wei Jiang
E-mail: jiang.wei@zs-hospital.sh.cn

Funding sources

None declared

Conflict of interest

None declared

Received on January 18, 2020
Reviewed on February 29, 2020
Accepted on May 8, 2020

Published online on June 29, 2020

Cite as

Ma W, Cheng L-S, Jiang W, Di-Wu S. The small heterodimer partner inhibits activation of hepatic stellate cells via autophagy. *Adv Clin Exp Med.* 2020;29(6):683–693. doi:10.17219/acem/122175

DOI

10.17219/acem/122175

Copyright

© 2020 by Wrocław Medical University
This is an article distributed under the terms of the Creative Commons Attribution 3.0 Unported (CC BY 3.0) (<https://creativecommons.org/licenses/by/3.0/>)

Abstract

Background. Hepatic fibrosis is a health concern worldwide, and it is of great importance to develop effective therapeutic targets. The small heterodimer partner (SHP) is a regulator of lipid and bile acid metabolism in the liver.

Objectives. The objective of this study was to investigate the contribution of SHP to hepatic fibrosis and the underlying mechanism.

Material and methods. An in vivo rat model of hepatic fibrosis was created through treatment with carbon tetrachloride. We used arginine-glycine-aspartic acid-poly (ethylene glycol)-polyethyleneimine (RGD-PEG-PEI) for the specific transfer of SHP into hepatic stellate cells (HSC). The level of gene expression was detected using quantitative real-time polymerase chain reaction (qRT-PCR). The LX2 cell line was selected for the in vitro assay. Artificial activation of LX2 in vitro was conducted through treatment with platelet-derived growth factor-BB (PDGF-BB), and autophagy was activated using rapamycin. Gain and loss of function assays were performed using a SHP-expressing plasmid or siRNA-SHP. Both qRT-PCR and western blotting were utilized to detect the level of gene expression.

Results. RGD-PEG-PEI-mediated the specific transduction of SHP into HSC in the liver and effectively increased the expression of SHP in the rat liver. After treatment with RGD-PEG-PEI-SHP, downregulation of liver fibrosis-associated genes was observed. The results of the in vitro assay indicated that SHP attenuated the stimulating effect of PDGF-BB on the activation of LX2 cells. Overexpression of SHP leads to significant downregulation of HSC activation-associated molecular factors, including α -smooth muscle actin, tissue inhibitor of metalloproteinase-1, and type I collagen. Conversely, increased expression of these molecules could be observed following knockdown of SHP. Furthermore, SHP affected fibrosis by inhibiting autophagy activated through treatment with rapamycin in LX2 cells. Overexpression of SHP may prevent liver fibrogenesis through inhibition of autophagy in HSC.

Conclusions. The SHP may prevent liver fibrogenesis through inhibition of autophagy in HSC. A SHP-targeting therapy-based anti-fibrosis strategy possesses potential for application to the treatment of liver fibrosis.

Key words: hepatic stellate cells, autophagy, liver fibrosis, small heterodimer partner

Introduction

Liver cirrhosis is a severe chronic disease, mainly caused by chronic hepatitis B virus and hepatitis C virus infections, alcohol abuse, and non-alcoholic steatohepatitis.¹ It affects 1–2% of the population worldwide. Currently, there are no effective clinical therapies for liver cirrhosis, except for the management of the primary cause or liver transplantation.²

Hepatic fibrosis is the pre-pathological stage of cirrhosis, which may last for nearly 10 years prior to progressing into cirrhosis. Nevertheless, it is a reversible process and can be attenuated or reversed through the use of effective therapies.³ Hepatocytes possess marked regenerative capability, and the replication of hepatocytes can easily replace the necrotic hepatocytes. However, chronic and sustained damage may impair the regenerative capability of hepatocytes, activating hepatic stellate cells (HSC) to induce liver fibrogenesis through secretion of α -smooth muscle actin (α -SMA), tissue inhibitors of metalloproteinase 1 (TIMP1) and type I collagen. Activation of HSC is a pivotal step in the development of hepatic fibrosis.⁴ Recent studies have suggested the reversibility of hepatic fibrosis,⁵ and several HSC-targeting therapies have been proposed as attractive strategies for the treatment of liver fibrosis, such as inhibition of HSC activation, promotion of HSC phenotypic conversion, promotion of HSC apoptosis, and induction of HSC senescence.⁶ It was reported that the Yes-associated protein and hedgehog inhibitors can suppress myofibroblastic activity by reducing aerobic glycolysis in HSC.⁷ Yang et al. confirmed the protective role of heme oxygenase-1 in inhibiting fibrosis by enhancing nuclear transcription factor kappa B signaling pathway-mediated apoptosis of HSC.⁸ Senescence of activated HSC may be achieved through the upregulation of p53 and p21 by interleukin 10 (IL-10).⁹ Collectively, this evidence indicated that suppression of HSC activation may be a feasible therapeutic target against hepatic fibrosis.

Autophagy, a process of degradation of “old” or “broken” organelles, is utilized by cells to maintain homeostasis and survival during stress.¹⁰ Loss of HSC lipid droplet (LDs), a typical feature of the activation of liver stellate cells, was observed during the process of HSC activation; it is accompanied by an increased level of autophagy.¹¹ Selective reduction of autophagy activity (e.g., treatment with autophagy inhibitor 3-methyladenine or inhibition of the autophagy-related gene autophagy related-5 (Atg5)) can lead to a significant increase in the number and size of LDs in HSC, causing LDs to accumulate and impairs HSC activation.^{12,13} These results suggest that autophagy may act as energy supplier for the activation of HSC by breaking down and reutilizing LDs.¹⁴ Thoen et al. also confirmed the essential contribution of autophagy to liver cirrhosis by inducing the activation of HSC.¹⁵

As a unique member of the nuclear receptor (NR) superfamily, small heterodimer partner (SHP) does not contain

a conserved DNA binding domain. However, its dimerization and ligand-binding domain confers critical ability for directly binding to multiple NRs and exert its function as a transcriptional inhibitor of gene expression.¹⁶ Several mechanisms may be utilized by SHP to repress the transcription of NR target genes. Interaction between SHP and the activation function-2 domain of NRs, mediated by functional LXXXLL-related motifs, can lead to direct competition with coactivator binding.¹⁷ It was also reported that the SHP-RNAs complex of the DNA promoter region may be dissociated, as a result of the interaction between SHP and NRs.¹⁸ In addition, SHP may exert a direct inhibitory effect on transcription by recruiting a conventional corepressor to its C terminus, which contains a strong transcriptional repression domain. The *SHP* gene is expressed in a variety of tissues, with the liver being the most SHP-rich organ.¹⁹ Aberrant expression of SHP is associated with numerous diseases, such as obesity and diabetes,²⁰ lipodystrophy syndromes,²¹ and cancer.²² However, the relationships between SHP, autophagy and liver fibrosis remain to be elucidated.

Binding to the type VI collagen receptor on the HSC surface confers circular polypeptide C*GRGDSPC* the ability to specifically target HSC.²³ Our research team previously synthesized the novel cyclic peptide C*GAGASPK* with a more stable spatial conformation. This peptide contains an arginine-glycine-aspartic acid (RGD) sequence and can bind to activated HSC.²⁴ Polyethyleneimine (PEI) can be ingested by cells through phagocytosis, endocytosis and pinocytosis, and combined with DNA molecules through electrostatic interaction. Modification of the transfection complex using poly(ethylene glycol) (PEG) can transform it into a sterically stable nanoparticle, shielding change to reduce the interaction with plasma components.²⁵ For the elucidation of the regulatory effect of SHP on liver fibrosis in vivo, we utilized RGD-PEG-PEI as a polymer carrier to transport a plasmid overexpressing the *SHP* gene into HSC in the liver of rats. An in vitro assay was also utilized to confirm the regulatory effects of SHP on the activation of HSC, and further analyze the mechanism involved in this process.

Material and methods

Chemicals and antibodies

Rabbit anti-SHP (1/200 dilution; Novus, St. Charles, USA) was used for immunohistochemistry. The following antibodies were used for western immunoblotting: β -actin and α -SMA (A5316 and A5228, respectively) (Sigma-Aldrich, St. Louis, USA), type I collagen, P62, Atg12, and LC3-I/II (Cell Signaling Technology Inc, Danvers, USA). Polyvinylidene difluoride membranes, 4–15% Tris hydrochloride gels (BioRad, Richmond, USA), enhanced chemiluminescence reagents (Denville Scientific Inc, Metuchen,

USA), and a protease inhibitor cocktail (Shengyi, Shanghai, China) were used. Human recombinant platelet-derived growth factor-BB (PDGF-BB) and rapamycin (Beyotime Biotechnology, Shanghai, China) were used to study the effect of activation and autophagy in LX2 cells. For quantitative real-time polymerase chain reaction (qRT-PCR), the RNAeasy Kit (Qiagen, Valencia, USA) and High Complementary DNA (cDNA) Reverse Transcription kit (Applied Biosystems, Foster City, USA) were utilized.

Animals

All experimental protocols were approved by the Committee of Ethics of Animal Experiments at Zhongshan Hospital, Shanghai, China (approval No. 20188223). Male, specific pathogen-free Norway rats (age: 6 weeks) were provided by the Experimental Animal Center of Shanghai Medical College of Fudan University (China). The animals were housed in groups at 20 ±5°C (55% ±5% humidity) with free access to standard chow and water. A total number of 20 rats were used in this study (animal No. 20180006013073). The study protocol potentially caused slight suffering to the animals; however, animals that lost >30% of the initial body weight were euthanized after being deeply anesthetized with pentobarbital at a dose of 40 mg/kg.

Animal models

Liver fibrosis was induced in rats through the administration of carbon tetrachloride (CCl₄).²⁶ RGD-PEG-PEI-SHP was synthesized as previously described.²⁷ Animals were randomly divided into the following 3 groups: sham (n = 6), CCl₄ (n = 7) and CCl₄+RGD-PEG-PEI-SHP (n = 7). Animals in the control group were treated with 0.9% saline twice weekly for 8 weeks. In the CCl₄ group, rats received intraperitoneally CCl₄ (700 µL/kg of body weight) dissolved in olive oil twice weekly for 2 weeks. In the RGD-PEG-PEI-SHP group, the rats received intraperitoneally CCl₄ (700 µL/kg of body weight) dissolved in olive oil twice weekly for 2 weeks. After 1 week, rats received RGD-PEG-PEI-SHP (concentration: 50 µg/mL; dosage: 0.5 mL/100 g) at weeks 4 and 6. All animals were sacrificed at week 8. The content of liver hydroxyproline and serum hyaluronic acid was measured through routine clinical biochemistry. Additionally, samples obtained from each liver were stored in a –80°C refrigerator for qRT-PCR analysis.

Isolation of total mRNA and assessment of gene expression through qRT-PCR

The TRIzol reagent (Takara Biochemicals, Kyoto, Japan) was utilized to extract total mRNA from cells or rat tissue according to the instruction provided by the manufacturer. Following the removal of genomic DNA from the extracted RNA, the PrimeScript Reverse Transcription Reagent Kit

Table 1. The primer sequences of qRT-PCR

Gene	Primer sequence (5'-3')
<i>α-SMA</i>	Forward: CTCTGGACGCACAACCTGGCATC Reverse: CACGCTCAGCAGTAGTAACGAAGG
<i>SHP</i>	Forward: GTGCCAGCATACTCAAGAAG Reverse: TGGGGTCTGTCTGGCAGTT
<i>ATG3</i>	Forward: ACATGGCAATGGGCTACAGG Reverse: CTGTTTGACCCGCTTATAGCA
<i>ATG9</i>	Forward: AGCGTGAGCTGACAGAGTGAC Reverse: AGCGTGAGCTGACAGAGTT
<i>ATG12</i>	Forward: CTGCTGGCGACACCAAGAAA Reverse: CGTGTTCGCTCTACTGCC
<i>ATG14</i>	Forward: TTCAGAGGCATAATCGCAAAC Reverse: CCAGACGCTCATAATGACTTCTT
<i>PDGF-β</i>	Forward: CTCGATCCGCTCCTTTGATGA Reverse: CGTTGGTGCCTCTATGAG
<i>Col1A1</i>	Forward: GTCCGATGACGTGATCTGTGA Reverse: CCGTGGTTTCTTGGTCCGT
<i>TIMP1</i>	Forward: ACCACCTTATACCAGCGTTATGA Reverse: GGTGTAGACGAACCCGATGTC
<i>MMP2</i>	Forward: CCCACTGCGGTTTTCTCGAAT Reverse: CAAAGGGGTATCCATCGCCAT
<i>Fibronectin</i>	Forward: TGGAACTTCTACCAGTGCGAC Reverse: TGT CTT CCC ATC ATC GTA ACA C
<i>TGF-β1</i>	Forward: AGCTGCGCTTGACAGATTA Reverse: AGCCCTGTATTCCGTCTCT
<i>MMP2</i>	Forward: ACAAGTGGTCCCGTAAAGT Reverse: GTAAACAAGGCTTCATGGGGG
<i>β-actin</i>	Forward: CACTGTCGAGTCGCTCC Reverse: TCATCCATGGCGAACTGGTG

qRT-PCR – quantitative real-time polymerase chain reaction.

with gDNA Eraser (Takara Biochemicals) was used to reverse-transcribe the extracted RNA into single-stranded cDNA. Quantitative RT-PCR was performed to measure the levels of cDNA using the ABI PRISM 7500 PCR Sequence Detection System (Applied Biosystems) according to the instructions provided by the manufacturer of the Prime Script RT-PCR Kit (Takara Biochemicals). After denaturation for 30 s at 95°C, the samples were subjected to 40 cycles of treatment, consisting of 5 s at 94°C and 32 s at 60°C. A melting curve was generated to test the specificity of primers. Glyceraldehyde-3-phosphate dehydrogenase (GADPH) was used as an internal reference. The primers used are listed in Table 1.

Western blotting

Tissue was dissolved in 1 mL of radioimmunoprecipitation assay (RIPA) buffer (Beyotime Biotechnology), and the total amount of protein was quantified using the Bradford Protein Assay (Beyotime Biotechnology). Protein homogenates were boiled for 15 min at 100°C. For western blotting, proteins (50 µg) were loaded on sodium dodecyl sulfate-polyacrylamide gel electrophoresis (SDS-PAGE) gels, and transferred onto polyvinylidene fluoride (PVDF)

membranes at 100 V for 70 min. Membranes were blocked with 5% bovine serum albumin (BSA) solution for 1 h prior to incubation with SHP (1:2,000; Santa Cruz Biotechnology, Santa Cruz, USA), α -SMA (1:1,000; Santa Cruz Biotechnology) and β -actin (1:1,000; Santa Cruz Biotechnology) antibodies overnight at 4°C. Membranes were washed using Tris-buffered saline with Tween 20 (TBST 20) and probed with appropriate secondary antibodies (labeled with alkaline phosphatase) for 1 h. The ImageJ software (National Institutes of Health, Bethesda, USA) was used to determine the intensity of protein bands.

siRNA-mediated downregulation of SHP

LX2 cells, an immortalized human HSC line,²⁸ were cultured at 37°C in an atmosphere of 5% CO₂ in Dulbecco's Essential Medium (Gibco BRL Life Technologies, Waltham, USA) containing 10% fetal bovine serum (FBS), antibiotics (penicillin/streptomycin) and 2 mM L-glutamine. SHP knockdown was performed according to the approved guidelines. LX2 cells were transfected with targeted or control siRNA; the sense sequence for siRNA-SHP was 5-UAGAAAGCAAGCCAGGAAGAUGACC-3 (Jima Company, Shanghai China). After trypsinization, LX2 cells were seeded into six-well plates at a density of 2×10^5 per well and cultured overnight. Cells were transfected with Lipofectamine 3000 Transfection Reagent (L3000; Invitrogen, Waltham, USA) for 48 h according to the protocol provided by the manufacturer. Transfected cells were cultured for at least 24 h and 48 h for RNA and western blotting analysis, respectively.

Overexpression of SHP in LX2 cells

The overexpression plasmid of SHP (NM-021969, rTA3 and ORF-200bp) was constructed by GeneChem Co. Ltd (Shanghai, China). LX2 cells were seeded into six-well plates. After 24–48 h of incubation, the transfection mixture was removed and replaced with fresh medium. The SHP cDNA was obtained through PCR amplification, subcloned into a vector, and transfected with a SHP-expressing plasmid or negative control using Lipofectamine 3000 (Invitrogen), according to the instructions provided by the manufacturer.

Activation and autophagy in LX2 cells

LX2 HSC were seeded into six-well plates (3×10^5 cells per plate) in Dulbecco's modified Eagle's medium (DMEM) supplemented with 10% FBS. After 24 h, the cells were starved in serum-free medium for 12 h, followed by incubation with PDGF-BB (20 ng/mL) for 48 h. Rapamycin, a macrolide antibiotic, is widely used for inducing autophagy in a variety of cell types. In this study, we used rapamycin (0.5 ng in 0.5 μ L 0.1% dimethyl sulfoxide; Alexis Biochemicals, San Diego, USA) to activate autophagy in LX2 HSC. Briefly,

LX2 cells were initially starved in serum-free medium for 12 h, and subsequently incubated with rapamycin for 24 h. The expression of related genes was analyzed through western blotting and qRT-PCR.

Statistical analysis

All animal data represent at least 6 independent replicates and is expressed as mean \pm standard deviation (SD). Data for LX2 cells represent the average of 3–6 replicates and is expressed as mean \pm SD. Analysis of variance (ANOVA) or Student's t-test were used for statistical comparisons. Statistical tests were performed using the INSTAT statistical software (GraphPad Software, San Diego, USA). In all cases, $p < 0.05$ denoted statistical significance.

Results

RGD-PEG-PEI-SHP complex prevents the development of liver fibrosis in the CCl₄-treated model

The RGD-PEG-PEI carrier specifically transported the plasmid overexpressing SHP into HSC in the liver. Treatment with CCl₄ was an established model for liver fibrosis, characterized by inflammation and necrosis.²⁹ Liver immunohistochemistry and western blotting showed that the expression of SHP in the RGD-PEG-PEI-SHP group was significantly increased than that observed in the sham group. In comparison with the sham group and RGD-PEG-PEI-SHP group, the CCl₄ group showed significantly higher levels of hydroxyproline in the liver and hyaluronic acid in the serum (Fig. 1A and B). The western blotting of liver showed that the expression of SHP in the RGD-PEG-PEI-SHP group was significantly increased than that observed in the sham group. In contrast, this expression was decreased in the model group (Fig. 1C and D). These findings indicated that the SHP-targeting drug-loaded complex effectively increased the expression of SHP in liver tissue.

Quantitative RT-PCR analysis of the mRNA levels of SHP, α -SMA, TIMP1, collagen α 1(I), transforming growth factor- β 1 (TGF- β 1), and matrix metalloproteinase 2 (MMP2) (Fig. 1E–J) in whole liver homogenates showed that the expression of some profibrogenic markers (TGF- β 1 and α -SMA) in the RGD-PEG-PEI-SHP group was significantly reduced ($p < 0.005$ vs CCl₄ group). Moreover, in the RGD-PEG-PEI-SHP group, the expression of the *SHP* gene increased by 1.7-fold ($p < 0.005$ vs the sham group), consistent with previous histological results. The expression of the TIMP1 and collagen α 1(I) genes in the RGD-PEG-PEI-SHP group was significantly induced ($p < 0.05$ vs CCl₄ group). However, there was no statistically significant difference in the expression of the *MMP2* gene observed in the RGD-PEG-PEI-SHP group ($p > 0.05$ vs CCl₄ group). These results suggest that the RGD-PEG-PEI-SHP

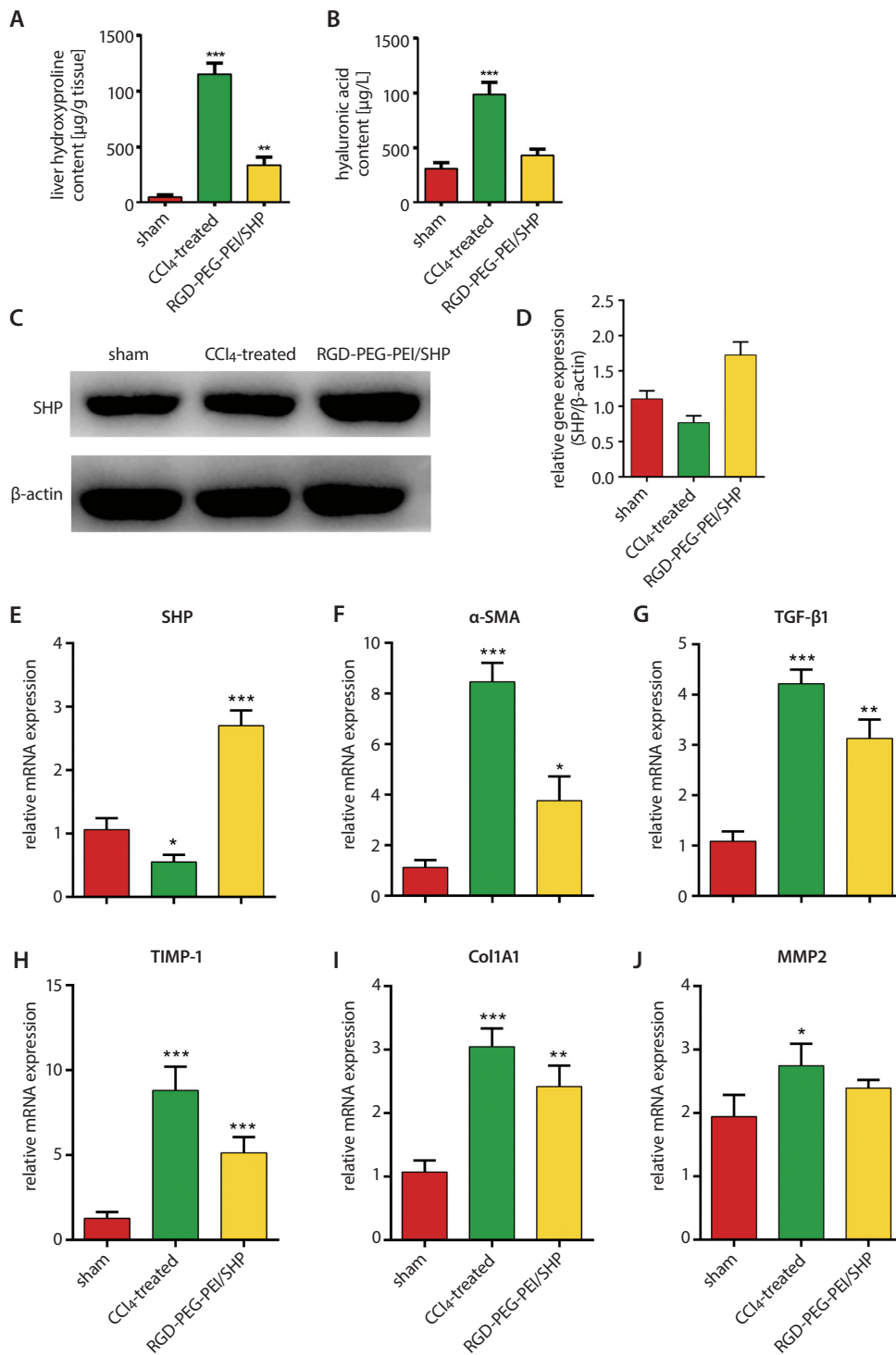


Fig. 1. RGD-PEG-PEI-SHP complex prevents the development of liver fibrosis in the CCl₄ treatment model. A and B. Liver hydroxyproline content and serum hyaluronic acid content in rats. C. Protein expression of SHP in the liver was determined with western blotting and shown as a histogram. E–J. Relative gene expression of SHP, α -SMA, TGF- β 1, TIMP1, Col1a1, and MMP2 was measured with qRT-PCR. Data is presented as the mean \pm SD; n = 6; *p < 0.05; **p < 0.01; ***p < 0.001 vs the sham group

complex can significantly improve the degree of liver fibrosis in the rat model induced by CCl₄, and is not associated with significant hepatotoxicity.

SHP regulates the expression of fibrosis-related genes in HSC

In vivo studies have indicated that SHP prevents the development of liver fibrosis. Therefore, we sought to confirm whether SHP prevents fibrosis mainly by inhibiting

the activation of HSC. For this purpose, we initially silenced the expression of SHP in LX2 cells using an anti-SHP siRNA, and subsequently stably overexpressed the *SHP* gene through the transfection of the plasmid. Quantitative RT-PCR and western blotting demonstrated that the 3 siRNAs of SHP successfully downregulated the expression of SHP in LX2 cells (Fig. 2A,B). It is worth noting that si-SHP-3 exhibited the highest inhibition efficiency, reaching 87% (n = 6; p < 0.0001 vs sham group). We also overexpressed the SHP using transfected with the plasmid (Fig. 2C,D). The α -SMA,

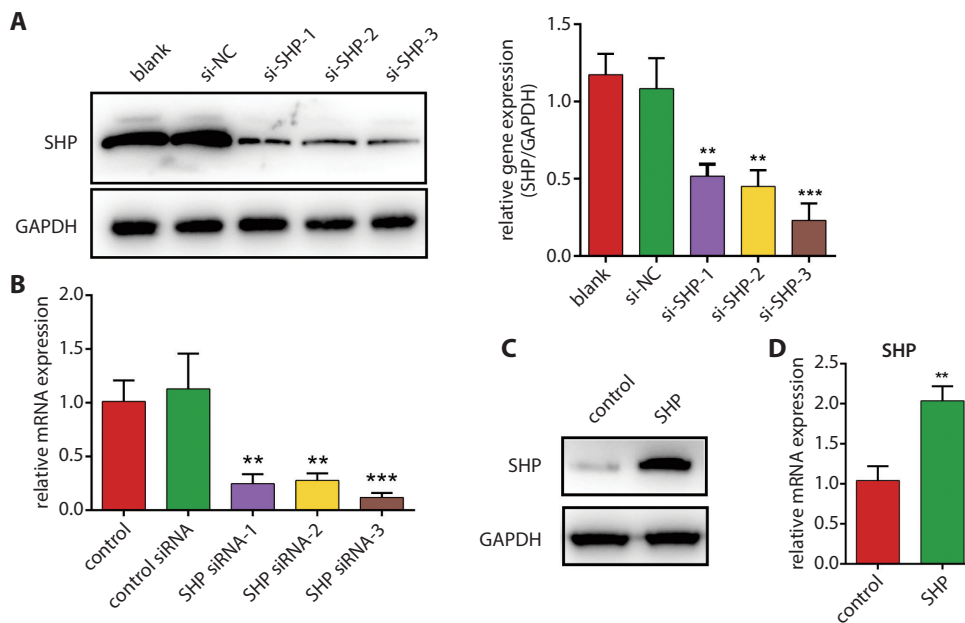


Fig. 2. The SHP silencing and overexpression in LX2 cells. Anti-SHP siRNA was used as described in the Material and methods section. A. Western blotting analysis of SHP obtained from LX2 cells treated with different sequences of siRNA and shown as a histogram. B. mRNA expression of SHP was measured using qRT-PCR. C. Western blotting analysis of SHP obtained from LX2 cells treated with the plasmid. D. mRNA expression of SHP was measured with qRT-PCR. Data is presented as the mean \pm SD; $n = 6$; ** $p < 0.01$; *** $p < 0.001$ vs the control group

collagen $\alpha 1(I)$ and fibronectin are 3 key markers of HSC activation and liver fibrosis. In addition, TGF- β , PDGF, etc., could change the phenotype of HSC and induce their activation. The results of the western blotting analysis showed that knockdown of the *SHP* gene increased the expression of type I collagen and α -SMA (Fig. 3A). We found that the gene expression of collagen $\alpha 1(I)$ and *TIMP1* also increased, following treatment with si-RNA LX2 (Fig. 3B).

Similarly, qRT-PCR analysis of collagen $\alpha 1(I)$, TGF- $\beta 1$, PDGF- β , and α -SMA in si-SHP LX2 cells showed different degrees of increase in mRNA levels compared with control (Fig. 3C).

In contrast, the gene expression of MMP2 decreased by approx. 50% (Fig. 3B; $p < 0.005$ vs sham group). We overexpressed the *SHP* gene to further investigate the role of SHP in regulating the expression of hepatic fibrosis-related genes. Western blotting analysis demonstrated that the relative expression of SHP protein in total lysates obtained from LX2 cells transfected with the plasmid was significantly enhanced compared to that measured in LX2 cells transfected with an empty plasmid vector. These findings were consistent with the results of the qRT-PCR analysis (Fig. 2C,D). Following overexpression of the *SHP* gene, the expression of both fibrosis-related and HSC activation-related genes was decreased, which is contrary to the results observed after silencing the *SHP* gene (Fig. 3D–F). It is particularly noteworthy that the increased expression of SHP could significantly promote a two-fold change in the expression of the *MMP2* gene (Fig. 3E, $n = 3$, $p < 0.01$ vs sham group). Thus, the results clarified that the *SHP* gene exerts a regulatory effect on fibrosis-related genes.

SHP inhibits the PDGF-BB-induced activation of LX2 cells

A large number of studies have confirmed that PDGF-BB can be used to induce the activation of HSC in vitro.^{26,28}

We treated LX2 cells with PDGF-BB (20 ng/mL) for 48 h to induce HSC activation. The 3 groups were the following: normal LX2 cells (control group), LX2 cells of the PDGF-BB intervention group and LX2 cells overexpressing the *SHP* gene from the PDGF-BB intervention group. The western blotting analysis showed that, after treatment of LX2 cells with PDGF-BB (20 ng/mL), the levels of type I collagen and α -SMA were significantly increased compared with those reported in the control group, indicating that PDGF-BB promotes the activation of LX2 cells (Fig. 4A). Although the expression of SHP decreased, the difference was not statistically significant. In the LX2-overexpressing SHP group, the levels of type I collagen and α -SMA were also decreased in SHP-overexpressing LX2 cells compared with those observed in cells subjected to treatment with PDGF-BB alone ($p < 0.05$ vs the PDGF-BB group).

The HSC activation is often accompanied by the increased expression of TGF- $\beta 1$, PDGF- β and fibronectin, which is closely related to liver fibrosis. Quantitative RT-PCR results showed that the levels of α -SMA, TGF- $\beta 1$, PDGF- β , and fibronectin were significantly increased in LX2 cells treated with PDGF-BB, compared with those noted in the control group (Fig. 4B–E). This treatment was also performed in the SHP overexpression group. The gene expression of α -SMA, TGF- $\beta 1$, PDGF- β , and fibronectin exhibited different degrees of recovery compared with those recorded in the sham group. These results indicate that SHP inhibits the activation of LX2 cells treated with PDGF-BB.

SHP inhibits the activation of LX2 cells via autophagy

Recent studies have shown that liver fibrosis is closely related to the enhancement of autophagy.^{30–32} Previous results showed that overexpression of SHP increased the expression of genes involved in the inhibition of fibrosis and

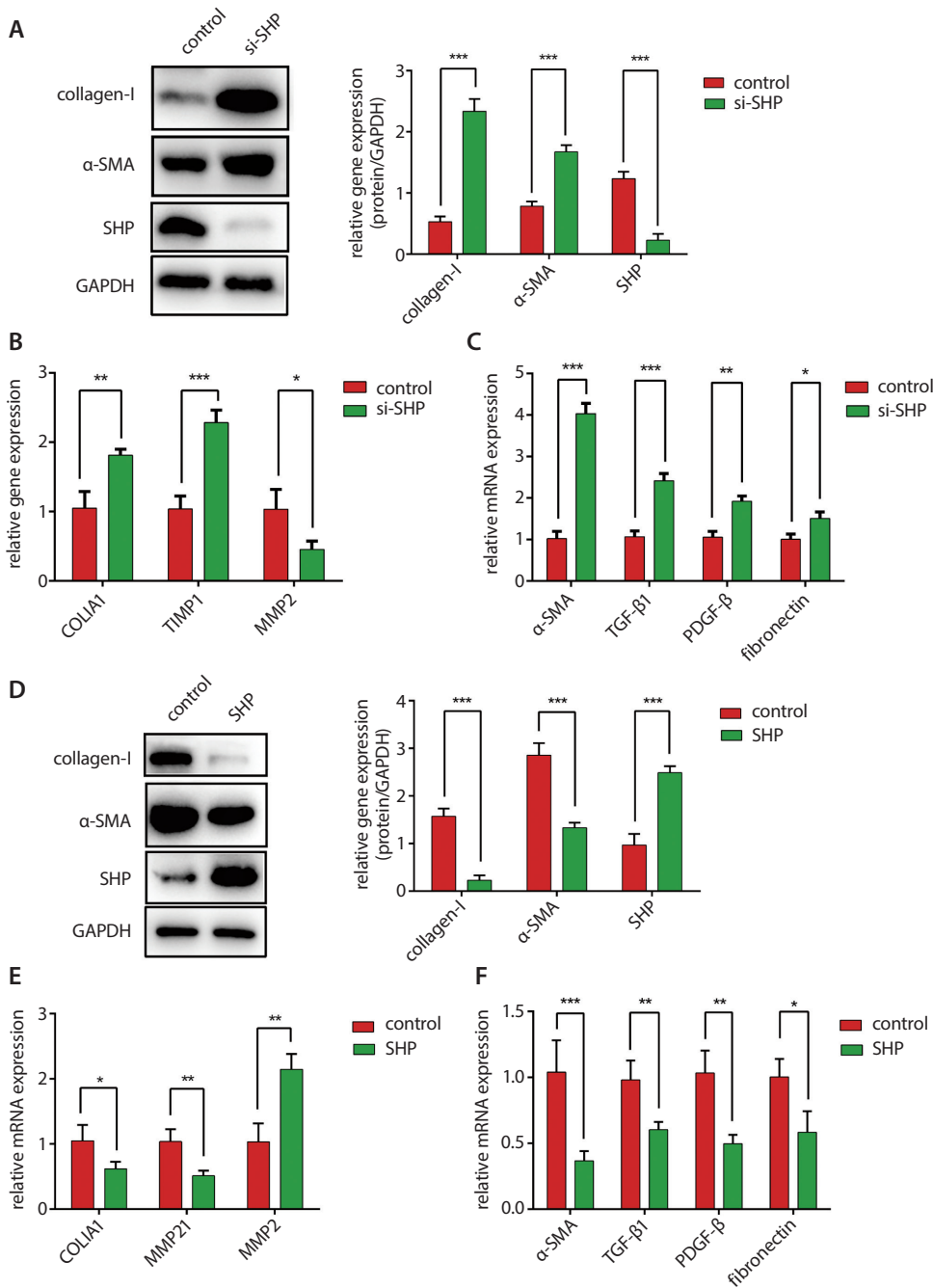


Fig. 3. The SHP regulates the expression of fibrosis-related genes in HSC. Anti-SHP siRNA was used as described in the Materials and methods section. A. LX2 cells were incubated with SHP siRNA, and the protein expression of SHP and α-SMA were determined with western blotting and shown as a histogram. B and C. Relative gene expression of ColA1, MMP1, MMP2, α-SMA, TGF-β1, PDGF-β1, and fibronectin was measured using qRT-PCR. The SHP overexpression was sufficient to downregulate the expression of type I collagen and upregulate α-SMA in LX2 cells. D. Protein expression of SHP and α-SMA was determined through western blotting and shown as a histogram. E and F. Relative gene expression of ColA1, MMP1, MMP2, α-SMA, TGF-β1, PDGF-β1, and fibronectin was measured with qRT-PCR. Data are presented as the mean ±SD; n = 6; *p < 0.05; **p < 0.01; ***p < 0.001 vs the control group

activation of HSC. Therefore, we inferred that SHP can act as an anti-fibrosis factor by inhibiting autophagy. To test this hypothesis, we compared the expression of autophagy-related genes in LX2 cells overexpressing SHP. The western blotting analysis showed that the expression of α-SMA was decreased in the SHP group compared with the control group. Furthermore, the expression of autophagy-related genes *Atg12* and *LC3-I/II* was downregulated, whereas that of *P62* was significantly increased (Fig. 5A). Quantitative RT-PCR results showed that the mRNA levels of *Atg3*, *Atg9*, *Atg12*, and *Atg14* in the SHP-overexpressing group were higher than those measured in the control group (Fig. 5B).

To further confirm whether SHP inhibits the activation of LX2 cells through autophagy, we treated wild-type LX2

cells and LX2 cells overexpressing SHP with rapamycin as previously described. After treatment with rapamycin (24 h), western blotting showed that the levels of *Atg12*, and *LC3-I/II* were significantly increased, whereas those of *p62* were decreased compared with the control group. These findings indicated that autophagy in LX2 cells was enhanced in response to treatment with rapamycin. However, in the LX2 cells overexpressing SHP, autophagy was significantly inhibited after treatment with rapamycin compared with the autophagy observed in the rapamycin-alone group (Fig. 5C). Quantitative RT-PCR results were consistent with those of western blotting (Fig. 5D,E). Therefore, this evidence shows that SHP mainly affects fibrosis by inhibiting autophagy in LX2 cells.

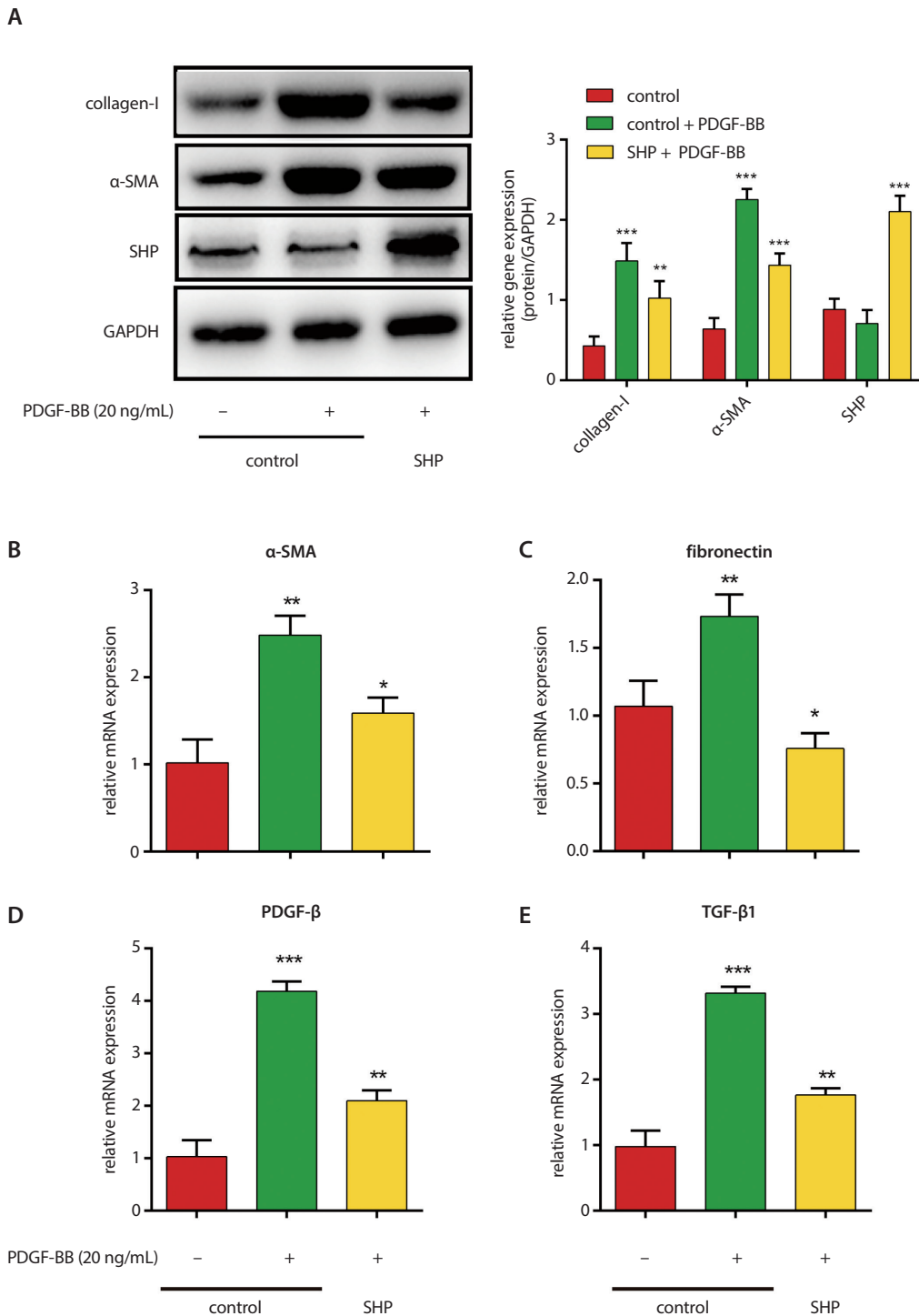


Fig. 4. The SHP inhibits PDGF-BB-induced activation of LX2 cells. LX2 cells were treated with PDGF-BB (20 ng/mL) as mentioned in the Materials and methods section. A. Protein expression of SHP, type I collagen, and α-SMA was determined with western blotting and shown as a histogram. B–E. Relative gene expression of ColA1, fibronectin, PDGF-β1, and TGF-β1 was measured with qRT-PCR. Data is presented as mean ±SD; n = 6; *p < 0.05; **p < 0.01; ***p < 0.001 vs the blank control group

Discussion

Liver fibrosis is a common process of liver self-repair in response to chronic liver injury, characterized by the typical manifestation of deposition of extracellular matrix (ECM).³³ Currently, effective treatments for clinical application are not available, thereby posing a great threat to human health. Several types of cell impairment can also be observed in the fibrotic liver, such as hepatocyte apoptosis and necrosis, recruitment of inflammatory cells,

remodeling of liver sinusoid endothelial cells, and activation of HSC.^{34,35} Activated HSCs are regarded as the main source of ECM in the fibrotic liver. Activated HSC can produce collagen and ECM to replace parenchymal tissue caused by scarring. Moreover, inhibition of HSC activation plays a critical role in the prevention and treatment of fibrosis. Extensive efforts were conducted to explore the mechanism involved in the activation of HSC, proposing the concept that liver fibrosis may be a reversible process. Specifically targeting molecules required for HSC

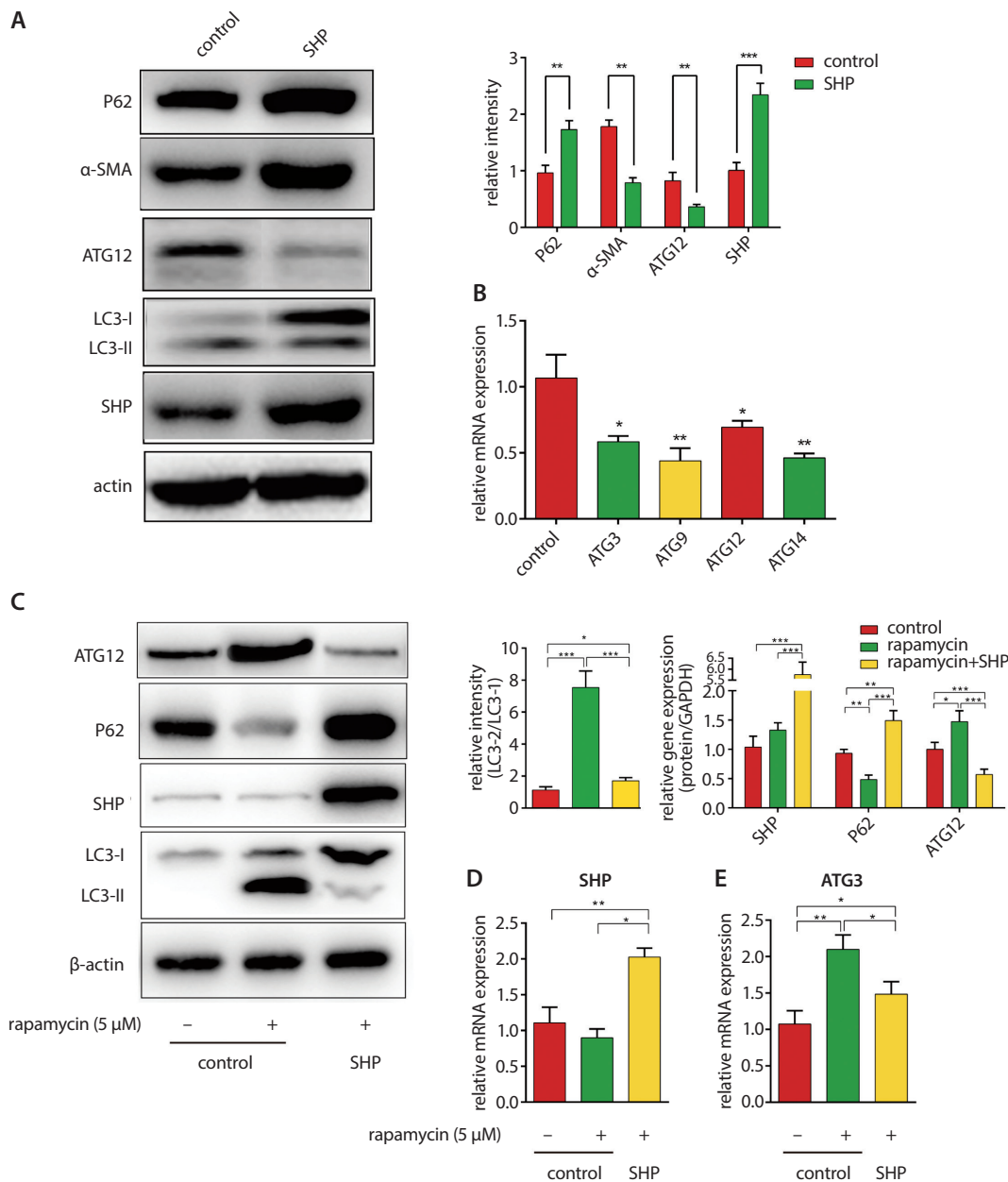


Fig. 5. The SHP inhibits the activation of LX2 cells through autophagy. Overexpression of SHP was achieved through transfection of a plasmid. A. Protein expression of P62, α-SMA, Atg12, LC3-I/II, and SHP was determined with western blotting and shown as a histogram. B. Relative gene expression of Atg3, Atg9, Atg12, and Atg14 was measured with qRT-PCR. LX2 cells were treated with rapamycin (5 μM) as mentioned in the Material and methods section. C. Protein expression of Atg12, P62, SHP, and LC3-I/II was determined with western blotting and shown as a histogram. B–E. Relative gene expression of SHP and Atg3 was measured using qRT-PCR. Data is presented as mean ±SD; n = 6; *p < 0.05; **p < 0.01; ***p < 0.001 vs the blank control group

activation may be a feasible therapeutic strategy against liver fibrosis.

In the present study, we explored the regulatory effect of SHP in the activation of HSC both in vivo and in vitro, and further analyzed the underlying mechanism. A rat liver fibrosis model induced using CCl₄ was applied to further determine the biological effect of SHP in liver fibrosis in vivo. An RGD-PEG-PEI-mediated specific transduction of SHP into rat liver HSC effectively increased the expression of SHP. After treatment with RGD-PEG-PEI-SHP, downregulation of liver fibrosis-associated genes was observed. These results confirmed that SHP inhibits the activation of HSC, further reversing the progress of liver fibrosis in vivo.

The human LX2 cell line was selected as an in vitro model to further evaluate the inhibitory effect of SHP

on the activation of HSC, as well as the underlying mechanisms. The SHP mimics were transduced into LX2 cells to increase its expression, whereas siRNA-SHP was used to inhibit the expression of SHP. We found that overexpression of SHP leads to significant downregulation of the mRNA and protein levels of HSC activation-associated molecular factors, such as α-SMA, TIMP1 and type I collagen. In contrast, increased expression of these molecules can be observed after knockdown of SHP, suggesting that SHP can inhibit the activation of HSC. The PDGF-BB is the strongest mitogenic cytokine of HSC, commonly utilized as a stimulator of HSC activation in the liver fibrosis model.³⁶ Our study evaluated the effect of SHP on HSC activation induced by PDGF-BB, suggesting that it attenuates the stimulatory effect of PDGF-BB on HSC activation. This finding further elucidated the inhibitory role of SHP

in the activation of HSC. Additionally, the Cell Counting Kit-8 assay also confirmed that SHP could notably suppress growth in LX2 cells. Matrix metalloproteinases are a group of proteolytic enzymes that degrade the ECM. The activities of these enzymes are closely related to the expression of their specific inhibitors (TIMPs). The MMP2 is the main enzyme that reduces extracellular matrix collagen, while TIMP1 inhibits most MMPs. These results suggested that SHP ameliorates liver fibrosis by inhibiting HSC activation and suppressing HSC proliferation to reduce the number of these cells.

Autophagy is a complex metabolic process utilized by cells to degrade their misfolding proteins and damaged organelles, contributing to the maintenance of cellular homeostasis during the destruction of intracellular pathogens and nutrient deprivation.³⁷ Activation of autophagy in HSC contributed to the transformation of the fat-rich phenotype into an activated myofibroblast phenotype. Autophagy promotes the digestion of LDs in resting HSC, which is the activation and fibrosis of HSC. In recent years, the regulatory role of autophagy in the activation of HSC attracted considerable attention owing to the observation that autophagy could break down LDs – an established feature of HSC activation. However, there is a contradictory effect of autophagy on liver fibrosis. Autophagy can act as an inhibitor of HSC activation, attenuating liver fibrosis.³⁸ Several studies have suggested the role of autophagy as an inducer of HSC activation. Accumulating evidence suggests that autophagy plays an energy-providing role in the activation of HSC, and inhibition of autophagy in HSC can attenuate the development of liver fibrosis.³⁹ Hernandez-Gea et al. also reported the role of autophagy in aggravating liver fibrosis by degrading LDs to provide energy for HSC.¹³ Furthermore, the enhancement of autophagy in HSC promoted cell proliferation and the production of type I collagen through hypoxia-inducible factors and the TGF- β /Smad signaling pathway.⁴⁰ These results suggest that autophagy may be a double-edged sword in liver fibrosis. In the present study, we explored the relationship between SHP, autophagy and liver fibrosis. In vitro testing demonstrated that SHP can inhibit autophagy in HSC, as shown by the decreased expression of autophagy marker proteins (e.g., LC3-II or Atg12) and increased expression of P62 (which is negatively correlated with autophagy).⁴¹ These results indicate that SHP may partially inhibit the activation of HSC by attenuating autophagy in these cells.

Conclusions

The results of our study suggest that overexpression of SHP may prevent liver fibrogenesis through inhibition of autophagy in HSC. A SHP-targeting therapy-based anti-fibrosis strategy possesses potential for application to the treatment of liver fibrosis.

ORCID iDs

Wei Ma  <https://orcid.org/0000-0001-5195-1541>
 Li-Sha Cheng  <https://orcid.org/0000-0003-2099-7517>
 Wei Jiang  <https://orcid.org/0000-0003-0904-3990>
 Sheng-Di Wu  <https://orcid.org/0000-0002-5979-869X>

References

1. Ge PS, Runyon BA. Treatment of patients with cirrhosis. *N Engl J Med*. 2016;375(8):767–777.
2. Forouzanfar MH, Alexander L, Anderson HR, et al. Global, regional, and national comparative risk assessment of 79 behavioural, environmental and occupational, and metabolic risks or clusters of risks in 188 countries, 1990–2013: A systematic analysis for the Global Burden of Disease Study 2013. *Lancet*. 2015;386(10010):2287–2323.
3. Albanis E, Friedman SL. Antifibrotic agents for liver disease. *Am J Transplant*. 2006;6(1):12–19.
4. Seki E, Schwabe RF. Hepatic inflammation and fibrosis: Functional links and key pathways. *Hepatology*. 2015;61(3):1066–1079.
5. Bedossa P, Paradis V. Approaches for treatment of liver fibrosis in chronic hepatitis C. *Clin Liver Dis*. 2003;7(1):195–210.
6. Park EJ, Zhao YZ, Lian L, Kim YC, Sohn DH. Skullcapflavone I from *Scutellaria baicalensis* induces apoptosis in activated rat hepatic stellate cells. *Planta Med*. 2005;71(9):885–887.
7. Xu W, Lu C, Zhang F, Shao J, Zheng S. Dihydroartemisinin restricts hepatic stellate cell contraction via an FXR-S1PR2-dependent mechanism. *IUBMB Life*. 2016;68(5):376–387.
8. Yang H, Chen B, Zhao Z, et al. Heme oxygenase-1 exerts pro-apoptotic effects on hepatic stellate cells in vitro through regulation of nuclear factor-kappaB. *Exp Ther Med*. 2018;16(1):291–299.
9. Huang YH, Chen MH, Guo QL, et al. Interleukin10 promotes primary rat hepatic stellate cell senescence by upregulating the expression levels of p53 and p21. *Mol Med Rep*. 2018;17(4):5700–5707.
10. Levine B, Klionsky DJ. Development by self-digestion: Molecular mechanisms and biological functions of autophagy. *Dev Cell*. 2004;6(4):463–477.
11. Yamaguchi K, Yang L, McCall S, et al. Diacylglycerol acyltransferase 1 anti-sense oligonucleotides reduce hepatic fibrosis in mice with non-alcoholic steatohepatitis. *Hepatology*. 2008;47(2):625–635.
12. Blommaert EF, Krause U, Schellens JP, Vreeling-Sindelarova H, Meijer AJ. The phosphatidylinositol 3-kinase inhibitors wortmannin and LY294002 inhibit autophagy in isolated rat hepatocytes. *Eur J Biochem*. 1997;243(1–2):240–246.
13. Hernandez-Gea V, Ghiassi-Nejad Z, Rozenfeld R, et al. Autophagy releases lipid that promotes fibrogenesis by activated hepatic stellate cells in mice and in human tissues. *Gastroenterology*. 2012;142(4):938–946.
14. Singh R, Kaushik S, Wang Y, et al. Autophagy regulates lipid metabolism. *Nature*. 2009;458(7242):1131–1135.
15. Thoen LF, Guimaraes EL, Grunsven LA. Autophagy: A new player in hepatic stellate cell activation. *Autophagy*. 2012;8(1):126–128.
16. Zhang Y, Hagedorn CH, Wang L. Role of nuclear receptor SHP in metabolism and cancer. *Biochim Biophys Acta*. 2011;1812(8):893–908.
17. Johansson L, Bavner A, Thomsen JS, Farnegardh M, Gustafsson JA, Treuter E. The orphan nuclear receptor SHP utilizes conserved LXXLL-related motifs for interactions with ligand-activated estrogen receptors. *Mol Cell Biol*. 2000;20(4):1124–1133.
18. Ourlin JC, Lasserre F, Pineau T, et al. The small heterodimer partner interacts with the pregnane X receptor and represses its transcriptional activity. *Mol Endocrinol*. 2003;17(9):1693–1703.
19. Lee HK, Lee YK, Park SH, et al. Structure and expression of the orphan nuclear receptor SHP gene. *J Biol Chem*. 1998;273(23):14398–14402.
20. Nishigori H, Tomura H, Tonooka N, et al. Mutations in the small heterodimer partner gene are associated with mild obesity in Japanese subjects. *Proc Natl Acad Sci U S A*. 2001;98(2):575–580.
21. Cao H, Hegele RA. Identification of polymorphisms in the human SHP1 gene. *J Hum Genet*. 2002;47(8):445–447.
22. Park YY, Choi HS, Lee JS. Systems-level analysis of gene expression data revealed NROB2/SHP as potential tumor suppressor in human liver cancer. *Mol Cells*. 2010;30(5):485–491.
23. Marcelino J, McDevitt CA. Attachment of articular cartilage chondrocytes to the tissue form of type VI collagen. *Biochim Biophys Acta*. 1995;1249(2):180–188.

24. Li F, Song Z, Li Q, Wu J, et al. Molecular imaging of hepatic stellate cell activity by visualization of hepatic integrin alphavbeta3 expression with SPECT in rat. *Hepatology*. 2011;54(3):1020–1030.
25. Schiffelers RM, Ansari A, Xu J, et al. Cancer siRNA therapy by tumor selective delivery with ligand-targeted sterically stabilized nanoparticle. *Nucleic Acids Res*. 2004;32(19):e149.
26. Fiorucci S, Antonelli E, Rizzo G, et al. The nuclear receptor SHP mediates inhibition of hepatic stellate cells by FXR and protects against liver fibrosis. *Gastroenterology*. 2004;127(5):1497–1512.
27. Zhan C, Wei X, Qian J, Feng L, Zhu J, Lu W. Co-delivery of *TRAIL* gene enhances the anti-glioblastoma effect of paclitaxel in vitro and in vivo. *J Control Release*. 2012;160(3):630–636.
28. Renga B, Mencarelli A, Migliorati M, et al. SHP-dependent and -independent induction of peroxisome proliferator-activated receptor-gamma by the bile acid sensor farnesoid X receptor counter-regulates the pro-inflammatory phenotype of liver myofibroblasts. *Inflamm Res*. 2011;60(6):577–587.
29. Scholten D, Trebicka J, Liedtke C, Weiskirchen R. The carbon tetrachloride model in mice. *Lab Anim*. 2015;49(1 Suppl):4–11.
30. Tsuchida T, Friedman SL. Mechanisms of hepatic stellate cell activation. *Nat Rev Gastroenterol Hepatol*. 2017;14(7):397–411.
31. Liu K, Lee J, Kim JY, et al. Mitophagy controls the activities of tumor suppressor p53 to regulate hepatic cancer stem cells. *Mol Cell*. 2017; 68(2):281–292.e5.
32. Yu L, Chen Y, Tooze SA. Autophagy pathway: Cellular and molecular mechanisms. *Autophagy*. 2018;14(2):207–215.
33. Schuppan D, Popov Y. Hepatic fibrosis: From bench to bedside. *J Gastroenterol Hepatol*. 2002;17(Suppl 3):S300–S305.
34. Tomita K, Teratani T, Suzuki T, et al. Free cholesterol accumulation in hepatic stellate cells: Mechanism of liver fibrosis aggravation in nonalcoholic steatohepatitis in mice. *Hepatology*. 2014;59(1):154–169.
35. Du P, Ma Q, Zhu ZD, et al. Mechanism of corilagin interference with IL-13/STAT6 signaling pathways in hepatic alternative activation macrophages in schistosomiasis-induced liver fibrosis in mouse model. *Eur J Pharmacol*. 2016;793:119–126.
36. Bonner JC. Regulation of PDGF and its receptors in fibrotic diseases. *Cytokine Growth Factor Rev*. 2004;15(4):255–273.
37. Yu L, Chen Y, Tooze SA. Autophagy pathway: Cellular and molecular mechanisms. *Autophagy*. 2018;14(2):207–215.
38. Ni HM, Williams JA, Yang H, Shi YH, Fan J, Ding WX. Targeting autophagy for the treatment of liver diseases. *Pharmacol Res*. 2012;66(6): 463–474.
39. Thoen LF, Guimaraes EL, Dolle L, et al. A role for autophagy during hepatic stellate cell activation. *J Hepatol*. 2011;55(6):1353–1360.
40. Thomes PG, Trambly CS, Thiele GM, et al. Proteasome activity and autophagosome content in liver are reciprocally regulated by ethanol treatment. *Biochem Biophys Res Commun*. 2012;417(1):262–267.
41. Yang R, Song Z, Wu S, Wei Z, Xu Y, Shen X. Toll-like receptor 4 contributes to a myofibroblast phenotype in cardiac fibroblasts and is associated with autophagy after myocardial infarction in a mouse model. *Atherosclerosis*. 2018;279:23–31.

Isoflurane cerebral preconditioning in a spontaneous hypertension rat model is associated with sphingosine kinases

*Jun Ge^{1,2,B–F}, *Keyu Kong^{1,2,B–F}, Xiaoqiang Cheng^{1,2,B,C,E,F}, Tianyi Wu^{2,B,D,F}, Dingge Liu^{2,B,D,F},
Lingling Peng^{2,B,D,F}, Zhijia Shen^{2,B,D,F}, Guoyuan Lu^{3,A,F}, Yanping Shen^{3,A,C,E,F}

¹ Department of Surgery, First Affiliated Hospital of Soochow University, Suzhou, China

² Medical College, Soochow University, Suzhou, China

³ Department of Nephrology, First Affiliated Hospital of Soochow University, Suzhou, China

A – research concept and design; B – collection and/or assembly of data; C – data analysis and interpretation;
D – writing the article; E – critical revision of the article; F – final approval of the article

Advances in Clinical and Experimental Medicine, ISSN 1899–5276 (print), ISSN 2451–2680 (online)

Adv Clin Exp Med. 2020;29(6):695–700

Address for correspondence

Yanping Shen
E-mail: shenyanping@suda.edu.cn

Funding sources

None declared

Conflict of interest

None declared

* These authors contributed equally to this work.

Received on June 16, 2019

Reviewed on January 23, 2020

Accepted on May 1, 2020

Published online on June 29, 2020

Abstract

Background. Isoflurane preconditioning could reduce different kinds of brain injury via sphingosine kinase (SPK). Both sphingosine kinase 1 and sphingosine kinase 2 play important roles in brain protection. However, the effects of isoflurane preconditioning on SPK expression in hypertension have not been investigated before.

Objectives. To verify whether the neuroprotective effects of the anesthetic isoflurane after an ischemic injury are altered in hypertension and to identify its possible mechanisms involving SPK.

Material and methods. Wistar rats (control) and spontaneous hypertension rats (SHR) were exposed to isoflurane preconditioning before transient middle cerebral artery occlusion. The infarct volumes of cortical and subcortical brain areas were measured. The expression levels of SPK1 and SPK2 were measured before and after isoflurane preconditioning.

Results. In the SHR group, isoflurane preconditioning significantly reduced only the infarct volumes of the subcortical brain ($p < 0.05$), not of the cortical brain. After 3 h of isoflurane exposure and preconditioning, SPK2 levels in the SHR group increased in the cortical brain ($p < 0.05$), but not in the subcortical brain area. Unlike in the control group, isoflurane exposure and preconditioning could significantly increase SPK2 levels in both cortical and subcortical brain area.

Conclusions. The brain protection effects induced by isoflurane preconditioning after an ischemic injury are mainly mediated by the SPK2 isoform and are somewhat impaired in hypertension. Attention should be paid to ischemic injury patients with hypertension.

Key words: cerebral preconditioning, isoflurane, hypertension, brain ischemic injury

Cite as

Ge J, Kong K, Cheng X, et al. Isoflurane cerebral preconditioning in a spontaneous hypertension rat model is associated with sphingosine kinases. *Adv Clin Exp Med.* 2020;29(6):695–700. doi:10.17219/acem/121944

DOI

10.17219/acem/121944

Copyright

© 2020 by Wrocław Medical University

This is an article distributed under the terms of the Creative Commons Attribution 3.0 Unported (CC BY 3.0) (<https://creativecommons.org/licenses/by/3.0/>)

Introduction

Cerebral preconditioning is a procedure by which a noxious stimulus below the threshold of damage, such as hypoxia, isoflurane and pro-inflammatory cytokines, is applied to the brain in order to induce tolerance to it or to a different noxious stimulus.^{1,2} Isoflurane, one of the anesthetics which is typically inhaled, is widely used in various surgical procedures. Pre-exposure to isoflurane increases tolerance to hypoxic ischemic cerebral damage, including that incurred during a stroke.³ The sphingosine-1-phosphate (S1P) receptor is widely distributed throughout the nervous system. It mediates multiple cellular processes, including proliferation, apoptosis and migration, and is regulated by the expression of sphingosine kinase (SPK).⁴ Studies have found that isoflurane could reduce different kinds of brain injury, including both hypoxic ischemia and hemorrhage, in rats through S1P-related pathway.^{5,6} Moreover, a recent study has indicated that fingolimod (FTY720), a novel protective agent for ischemic brain injury, can be phosphorylated by SPK and that it can then activate the S1P receptor, suggesting that SPK may be an important effector in neuroprotective mechanisms.^{7,8} Altray et al.⁶ illustrated that in hemorrhage damage, isoflurane could attenuate neuronal cell death in the cortex, associated with an increase in SPK1. In hypoxic ischemic cerebral damage, Lai et al. found a similar result – that isoflurane preconditioning could elevate tolerance levels, mediated by the overexpression of SPK2.⁹ Both SPK1 and SPK2 play important roles in brain protection.

Currently, with the aging of society, hypertension is becoming increasingly common worldwide. It is well known that hypertension is a risk factor for hypoxic ischemic cerebral damage such as stroke. However, the effects of isoflurane preconditioning on SPK expression during hypertension have not been investigated before. With a spontaneous hypertension rat (SHR) model, we evaluated the protective effects of isoflurane preconditioning on hypoxic ischemic cerebral damage, as well as the biological roles of SPK.

Material and methods

Reagents and instruments

Isoflurane, Tween 20, and 2,3,5-trihenylterzolium chloride (TTC) were purchased from Sigma-Aldrich (St. Louis, USA). Coated monofilament was purchased from Doccol Corporation (Sharon, USA). Chloral hydrate was purchased from Sinopharm Chemical Reagent Co. (Shanghai, China). Protein marker was purchased from Fermentas (Waltham, USA). Polyvinylidene difluoride (PVDF) membrane was purchased from Merck Millipore (Burlington, USA). Primary antibodies of SPK1 (sc-22702) and SPK2 (sc-22704) were purchased from Santa Cruz Biotechnology (Santa Cruz, USA). β -actin and IgG secondary antibody

were purchased from Multi Sciences (Hangzhou, China). EZ-ECL kit was purchased from Biological Industries (Beit HaEmek, Israel); PH Indicator was purchased from Leici Device Works (Shanghai, China). A 5417R High-speed Freezing Centrifuge was purchased from Eppendorf (Hamburg, Germany). A 752 Ultraviolet Spectrophotometer was purchased from Puxi General Instruments (Beijing, China). A DYY-4C electrophoresis system was purchased from Tanon Science & Technology (Shanghai, China). A UVP BioSpectrum Imaging System was purchased from UVP (Upland, USA).

Model establishment

Wistar and SHR rats (male, 300–350 g), provided by the Animal Experiment Center of Soochow University, were housed with a 12-hour light–dark cycle with food and water provided ad libitum. All experimental procedures were carried out in strict accordance with National Institutes of Health (NIH) guidelines for the care and use of laboratory animals (NIH Publication No. 8023, revised 1978) and Laboratory Animal Guidelines for ethical review of animal welfare (GB/T 35892-2018, China). The experimental procedures have been approved by the Ethics Committee of the First Affiliated Hospital of Soochow University, Suzhou, China.

Cerebral preconditioning with isoflurane

For the experimental group, the Wistar and SHR rats were exposed to 1% isoflurane for 3 h in a chamber ($N_2:O_2 = 7:3$). They recovered in an incubator at 28°C for 30 min, and were then returned to their cages for 24 h. The control rats were placed in a chamber without isoflurane. Three hours after isoflurane pre-treatment, samples were collected for detection of SPK expression.

Middle cerebral artery assay

The rats were anesthetized with 2% isoflurane, and sustained with 1.5% isoflurane ($N_2:O_2 = 7:3$). The rectal temperature was measured and maintained within the normal physiological range during the surgical procedure. The left middle cerebral artery (MCA) was carefully isolated and occluded with a coated monofilament for 60 min, following the surgical approach described by Izumi et al.¹⁰ The rats were allowed to recover and awaken back in the chambers following the operation.

Measurement of cerebral infarct volume

Twenty-four hours after the operation, the rats were anesthetized with chloral hydrate (1 g/kg). Infarct volume was marked with TTC staining. The rats were perfused with 2% TTC in ddH₂O for 10 min using a catheter placed into the ascending aorta via the apex of the left

ventricle. The brain was carefully removed 45 min later and frozen in isopentane for cryomicrotome. The brain tissues were sliced into 1-mm-thick sections. The volume of MCA occlusion was measured with an image analysis system (ImageJ; National Institutes of Health, Bethesda, USA), as described by O'Donnell et al.¹¹

Western blot

The cerebral cortex and subcortex were homogenized in lysis buffer, and the supernatants were extracted after 30 min of centrifugation at 14,000 rpm. Protein concentrations were determined with a spectrophotometer at 595 nm. A total of 70 µg of proteins was subjected to SDS-PAGE and then transferred onto a PVDF membrane. Thereafter, non-specific binding was blocked with 5% bovine serum albumin for 2 h at room temperature. The membranes were then incubated overnight at 4°C with antibodies against SPK1 (sc-22702) and SPK2 (sc-22704). After rinsing in phosphate-buffered saline-Tween (PBST; 0.1% Tween 20), the membranes were incubated with the corresponding secondary antibody for 1–2 h at room temperature. The bands were visualized using chemiluminescence (Rockford, USA). The expression levels were normalized to β-actin.

Statistical analysis

The data is presented as means ± standard error (SE) and analyzed using SPSS v. 13.0 software (SPSS Inc., Chicago, USA). Statistical analysis was carried out with one-way analysis of variance (ANOVA). A p-value ≤0.05 was considered to be statistically significant.

Results

Determination of cerebral infarct volume in rats pretreated with isoflurane

The TTC staining analysis showed that isoflurane preconditioning significantly reduced the infarct volumes of both the cortical ($129.9 \pm 7.3 \text{ mm}^3$ vs $109.2 \pm 5.9 \text{ mm}^3$; $p < 0.05$; Fig. 1A) and subcortical ($59.2 \pm 5.1 \text{ mm}^3$ vs $41.6 \pm 5.9 \text{ mm}^3$; $p < 0.05$; Fig. 1A) brain areas.

Determination of cerebral infarct volume in SHR rats pretreated with isoflurane

In the SHR group, TTC staining analysis revealed that isoflurane preconditioning significantly reduced the infarct volumes of the subcortical brain areas ($62.9 \pm 5.3 \text{ mm}^3$ vs $43.1 \pm 5.6 \text{ mm}^3$; $p < 0.05$; Fig. 1B) but not the cortical brain areas ($131.8 \pm 7.2 \text{ mm}^3$ vs $129.9 \pm 6.1 \text{ mm}^3$; Fig. 1B).

SPK1/2 expression in cortical and subcortical brain areas of Wistar and SHR rats pretreated with isoflurane

Before isoflurane preconditioning, the SPK1 and SPK2 expression levels in both the cortical and subcortical brain areas of the Wistar rats and the SHR rats did not significantly differ from those of the control group (Fig. 2,3). After isoflurane preconditioning, the SPK1 expression levels were not altered in either the cortical or subcortical brain areas of the Wistar and SHR rats (Fig. 2). However, SPK2 expression levels increased in the cortical and subcortical brain areas of the Wistar rats ($p < 0.05$; Fig. 3A,C). In the SHR rats, isoflurane preconditioning clearly increased SPK2 expression in the subcortical brain areas ($p < 0.05$; Fig. 3), but not in the cortical region.

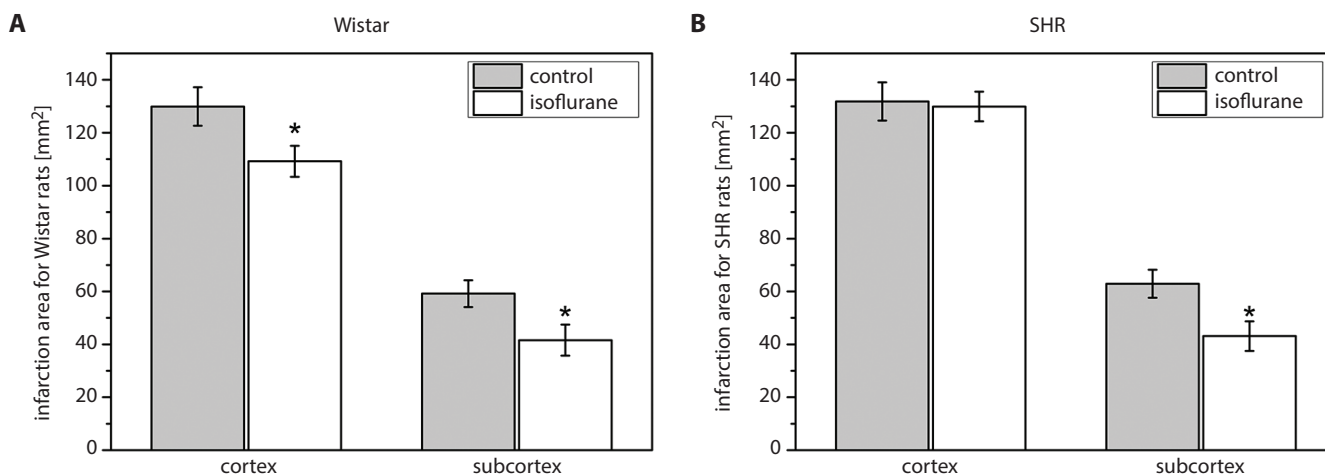


Fig. 1. A. Effects of isoflurane preconditioning on infarct volume of Wistar rats after cerebral hypoxia/ischemia. Both the infarct volume of brain cortical areas and subcortical areas were significantly reduced after isoflurane preconditioning (* $p < 0.05$). B. Effects of isoflurane preconditioning on infarct volume of SHR rats after cerebral hypoxia/ischemia. Only the infarct volume of brain subcortical areas was significantly reduced after isoflurane preconditioning (* $p < 0.05$)

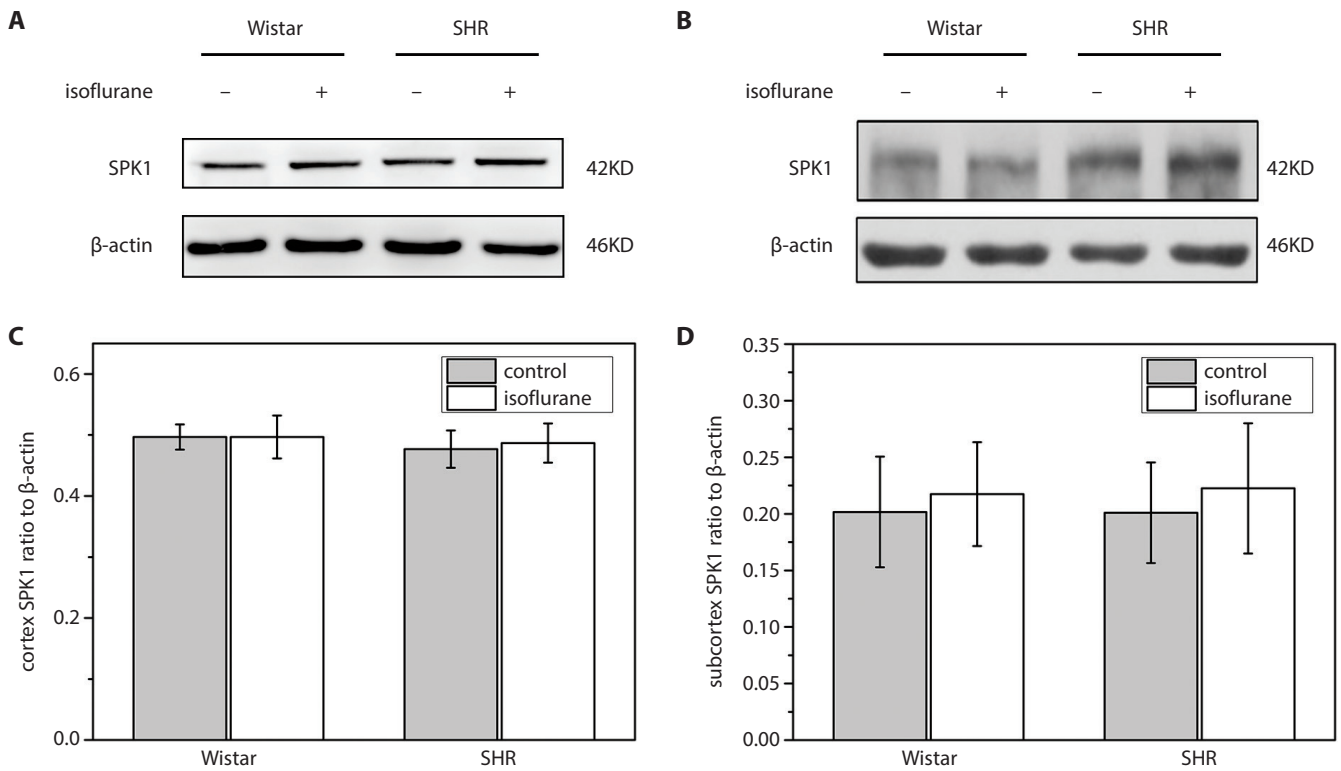


Fig. 2. A and C. Effects of isoflurane preconditioning on SPK1 expression in cerebral cortical areas: isoflurane preconditioning had no effect on SPK1 expression in the cortical brain areas of either Wistar rats or SHR rats. B and D. Effects of isoflurane preconditioning on SPK1 expression in sub-cerebral cortical areas: isoflurane preconditioning had no effect on SPK1 expression in subcortical brain areas of either Wistar rats or SHR rats

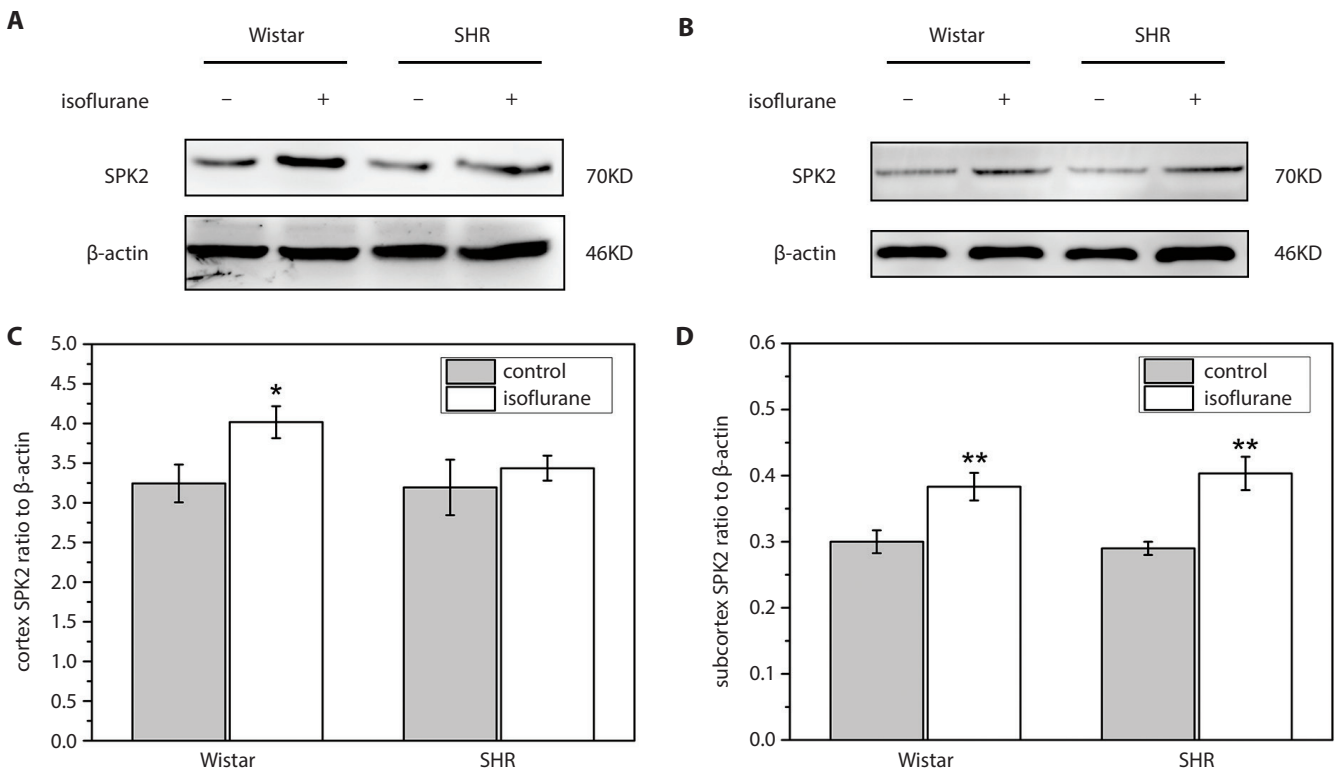


Fig. 3. A and C. Effects of isoflurane preconditioning on SPK2 expression in cerebral cortical areas: isoflurane preconditioning significantly increased SPK2 expression in cortical brain areas in Wistar rats but not in SHR rats (* $p < 0.05$). B and D. Effects of isoflurane preconditioning on SPK2 expression in sub-cerebral cortical areas: isoflurane preconditioning significantly increased SPK2 expression in subcortical brain areas in Wistar rats and SHR rats (* $p < 0.05$)

Discussion

Cerebral preconditioning has a neuroprotective effect, to a certain extent, and it particularly enhances tolerance to cerebral hypoxia-/ischemia-induced injury. A recent study has suggested that the neuroprotective role of isoflurane preconditioning may be mediated by the upregulation of SPK.⁹ Our study demonstrated that, after cerebral hypoxia-/ischemia-induced injury, isoflurane preconditioning reduced the infarct volumes of cortical and subcortical brain areas, which was associated with the upregulation of SPK2. However, isoflurane preconditioning of SHR rats had a neuroprotective effect on the cortical brain, but not on the subcortical brain areas. In addition, the protective effects of isoflurane on brain damage tissue caused by hypoxia-/ischemia-induced injury could be mainly associated with upregulated SPK2. However, in hypertension, the connection between SPK2 and isoflurane in the brain cortex might be weaker.

The SPK1 and SPK2 are the 2 isoforms of SPK. Their amino acid sequences are 80% homologous and differ only in the central domain and the amino terminal. They differ in their cellular distribution, subcellular localization, and enzymatic characteristics. The SPK1 is mainly distributed in the renal proximal tubules and cardiocytes, while SPK2 is primarily expressed in the brain tissue.¹² Consistent with a previous study, SPK1 was detected in both the cortical and subcortical brain areas of Wistar rats, and its expression was not altered after isoflurane preconditioning.⁹ In SHR rats, SPK1 expression in cortical and subcortical brain areas did not differ from that in Wistar rats before and after isoflurane preconditioning. This data suggests that SPK1 might not be related to the hypertension and neuroprotective effects induced by isoflurane preconditioning. A recent study has indicated that cerebral microvascular SPK2 may play an important role in the protective effects induced by cerebral preconditioning with hypoxia.^{9,13} In addition, upregulated expression of SPK2 in cortical brain areas was shown to be associated with the neuroprotective role of isoflurane preconditioning.⁹ Our study demonstrated that isoflurane preconditioning enhanced the SPK2 expression levels in both the cortical and subcortical brain areas, which was closely related to the neuroprotective effects induced by isoflurane preconditioning. However, a neuroprotective effect was only induced in the subcortical brain areas in SHR rats, which was related to the upregulation of SPK2, which suggests that isoflurane preconditioning mainly protects the subcortical brain areas from cerebral hypoxia-/ischemia-induced injury – probably through the upregulation of SPK2.

Numerous studies have demonstrated that SPK can be activated by various stimuli, such as activation of G-protein-coupled receptors^{14,15} and tyrosine kinase receptors.^{16,17} The SPK can also mediate phosphorylation and proliferation targeting on cell membranes.¹⁸ These studies suggest that the change in activity or expression of SPK may be the common signal involved in the neuroprotective role










induced by cytokines and drugs. Moreover, SPK-related sphingomyelin metabolites could regulate hypoxia-induced factor (HIF) and other signaling pathways. Combined with previous studies, our data suggests that SPK2 could be one of the signals involved in the neuroprotective effect induced by cerebral preconditioning. Song et al.¹⁹ have found that SPK2 could play its role through interacting with Bcl-2. In our study, prior to isoflurane preconditioning, SPK2 expression (in the cortical and subcortical brain areas) in SHR rats did not differ from that in Wistar rats, suggesting that SPK2 may not be involved in hypertension and its pathophysiological changes. However, isoflurane preconditioning attenuated the neuroprotective effect in the cerebral cortex without SPK2 changes, suggesting that the cerebral SPK2-related signaling pathways (supposedly Bcl-2) are altered in hypertension. Bcl-2 is closely related to pregnancy hypertension, with a downregulated expression of Bcl-2.²⁰ We assume there is also a special relationship between Bcl-2 and hypoxic/ischemic brain damage with hypertension.

Furthermore, our study provides experimental support for the treatment of patients with hypertension using cerebral preconditioning with isoflurane. It is worth mentioning that fingolimod (FTY720), an analogue of sphingosine, is applied in the treatment of multiple sclerosis; after phosphorylation by SPK, particularly SPK2, fingolimod can be transformed into its active state and further activate 4 S1P receptors to exhibit its therapeutic action.²¹ The present study suggests that decreased expression of SPK2 in a hypertension-related cerebral cortex could lead to altered efficacy of fingolimod in patients with multiple sclerosis and hypertension. This data provides an experimental basis for evaluating the pharmacodynamics of fingolimod or for designing novel SPK2-related drugs.

Conclusions

The present study demonstrates that isoflurane preconditioning reduces the infarct volume not only in MCA-occluded Wistar rats, but also in SHR rats with MCA occlusion. More importantly, the protective effects against hypoxia/ischemic damage gained from isoflurane preconditioning were associated with an upregulated expression of cerebral SPK2. In hypertension patients, we propose that the brain protection effects induced by isoflurane preconditioning would be somewhat impaired after an ischemic injury.

ORCID iDs

Jun Ge  <https://orcid.org/0000-0002-3823-5409>
Keyu Kong  <https://orcid.org/0000-0002-5839-6074>
Xiaoqiang Cheng  <https://orcid.org/0000-0002-6853-9083>
Tianyi Wu  <https://orcid.org/0000-0002-5549-6272>
Dingge Liu  <https://orcid.org/0000-0001-7936-3127>
Lingling Peng  <https://orcid.org/0000-0002-6711-6695>
Zhijia Shen  <https://orcid.org/0000-0003-4535-6767>
Guoyuan Lu  <https://orcid.org/0000-0003-0389-3935>
Yanping Shen  <https://orcid.org/0000-0002-4546-850X>

References

1. Dirnagl U, Becker K, Meisel A. Preconditioning and tolerance against cerebral ischaemia: From experimental strategies to clinical use. *Lancet Neurol.* 2009;8(4):398–412.
2. Gidday, JM. Cerebral preconditioning and ischaemic tolerance. *Nat Rev Neurosci.* 2006;7(6):437–448.
3. Zheng, S, Zuo Z. Isoflurane preconditioning induces neuroprotection against ischemia via activation of P38 mitogen-activated protein kinases. *Mol Pharmacol.* 2004;65(5):1172–1180.
4. Harada J, Foley M, Michael M, Waeber C. Sphingosine-1-phosphate induces proliferation and morphological changes of neural progenitor cells. *J Neurochem.* 2004;88(4):1026–1039.
5. Zhou Y, Lekic T, Fathali N, et al. Isoflurane posttreatment reduces neonatal hypoxic-ischemic brain injury in rats by the sphingosine-1-phosphate/phosphatidylinositol-3-kinase/Akt pathway. *Stroke.* 2010;41(7):1521–1527.
6. Altray O, Yu H, Sherchan P, et al. Isoflurane delays the development of early brain injury after subarachnoid hemorrhage through sphingosine-related pathway activation in mice. *Crit Care Med.* 2012;40(6):1908–1913.
7. Yu H, Suzuki H, Takumi S, Rolland W, Zhang JH. Activation of sphingosine 1-phosphate receptor-1 by FTY720 is neuroprotective after ischemic stroke in rats. *Stroke.* 2010;41(2):368–374.
8. Wei Y, Yemisci M, Kim HH, et al. Fingolimod provides long-term protection in rodent models of cerebral ischemia. *Ann Neurol.* 2011;69(1):119–129.
9. Ming YL, Ying W, Tao Q, Wang Y, Smith C, Waeber C. Sphingosine kinase 2 mediates cerebral preconditioning and protects the mouse brain against ischemic injury. *Stroke.* 2012;43(1):199–204.
10. Izumi Y, Roussel S, Pinard E, Seylaz J. Reduction of infarct volume by magnesium after middle cerebral artery occlusion in rats. *J Cereb Blood Flow Metab.* 1991;11(6):1025–1030.
11. O'Donnell ME, Lien T, Lam T, Liu X, Anderson SE. Bumetanide inhibition of the blood-brain barrier Na-K-Cl cotransporter reduces edema formation in the rat middle cerebral artery occlusion model of stroke. *J Cereb Blood Flow Metab.* 2004;24(9):1046–1056.
12. Bryan L, Kordula T, Spiegel S, Milstein S. Regulation and functions of sphingosine kinases in the brain. *Biochim Biophys Acta.* 2008;1781(9):459–466.
13. Wacker BK, Park TS, Gidday JM. Hypoxic preconditioning-induced cerebral ischemic tolerance: Role of microvascular sphingosine kinase 2. *Stroke.* 2009;40(10):3342–3348.
14. Graler MH, Goetzl EJ. The immunosuppressant FTY720 downregulates sphingosine 1-phosphate G-protein-coupled receptors. *FASEB J.* 2004;18(3):551–553.
15. Kluk MJ, Hla T. Signaling of sphingosine-1-phosphate via the S1P/EDG-family of G-protein-coupled receptors. *Biochim Biophys Acta.* 2002;1582(1–3):72–80.
16. Wang FH, Nobes C, Hall A, Spiegel S. Sphingosine 1-phosphate stimulates rho-mediated tyrosine phosphorylation of focal adhesion kinase and paxillin in Swiss 3T3 fibroblasts. *Biochem J.* 1997;324(Pt 2):481–488.
17. Yogi A, Glauca EC, Anna BA, et al. Sphingosine-1-phosphate-induced inflammation involves receptor tyrosine kinase transactivation in vascular cells: Upregulation in hypertension. *Hypertension.* 2011;57(4):809–818.
18. Grey A, Xu X, Hill B, et al. Osteoblastic cells express phospholipid receptors and phosphatases and proliferate in response to sphingosine-1-phosphate. *Calcif Tissue Int.* 2004;74(6):542–550.
19. Song DD, Zhang TT, Chen JL, et al. Sphingosine kinase 2 activates autophagy and protects neurons against ischemic injury through interaction with Bcl-2 via its putative BH3 domain. *Cell Death Dis.* 2017;8(7):e2912.
20. Varol F, Uzunoglu R, Erbas H, Süt N, Sayın C. VEGFR-1, Bcl-2, and HO-1 ratios in pregnant women with hypertension. *Clin Appl Thromb Hemost.* 2015;21(3):285–288.
21. Hla T, Brinkmann V. Sphingosine 1-phosphate (S1P): Physiology and the effects of S1P receptor modulation. *Neurology.* 2011;76(8 Suppl 3):S3–S8.

Application of 3D-FS-SPGR imaging combined synovial fluid GG CX detection in the evaluation of knee osteoarthritis

Lvlin Yang^B, Dongsheng Niu^A, Zhigang Bai^F, Jun Ma^D, Xichun Sun^C, Yuqi Liang^C, Jie Zhang^A

Department of Orthopedics, Autonomous Region People's Hospital of Ningxia Medical University, China

A – research concept and design; B – collection and/or assembly of data; C – data analysis and interpretation; D – writing the article; E – critical revision of the article; F – final approval of the article

Advances in Clinical and Experimental Medicine, ISSN 1899–5276 (print), ISSN 2451–2680 (online)

Adv Clin Exp Med. 2020;29(6):701–706

Address for correspondence

Lvlin Yang
E-mail: gufwcbqkp4wdzuvq@sina.com

Funding sources

The study was funded by the Ningxia Natural Science Foundation (grant No. NZ17203).

Conflict of interest

None declared

Received on October 15, 2018
Reviewed on November 12, 2018
Accepted on April 30, 2020

Published online on July 1, 2020

Abstract

Background. Osteoarthritis represents a kind of chronic and degenerative joint disease characterized by articular cartilage injury and osteoproliferation. Osteoarthritis especially poses a serious threat to the elderly patients. At present, the diagnosis of osteoarthritis mainly consists of clinical examination, X-ray examination, magnetic resonance imaging (MRI), and arthroscopy. However, limitations and misdiagnosis are found within the single method.

Objectives. This article intends to investigate the feasibility of assessing the condition of knee osteoarthritis through quantitative analysis of cartilage using nuclear magnetic resonance 3D fast-spin spoiled gradient-recalled echo (NMR 3D-FS-SPGR) imaging and γ -glutamic acid carboxylase (GGCX) detection in synovial fluid.

Material and methods. A total of 60 patients with primary knee osteoarthritis were enrolled. All the patients were staged and received 3D-FS-SPGR sequence MRI scan for grading based on scan results and cartilage injury. Cartilage tissues were collected for immunohistochemistry (IHC). The GG CX in cartilage was detected using western blotting to analyze the correlation with arthritis.

Results. The condition of articular cartilage injury in arthritis patients was clearly observed using 3D-FS-SPGR sequence. The expression of GG CX was decreased in 46 patients ($p < 0.05$). The expression of GG CX in synovial fluid was significantly reduced following upstaging ($p < 0.05$). The sensitivity measured using combined 3D-FS-SPGR imaging and synovial fluid GG CX detection for the evaluation of arthritis condition was significantly higher than that of the single detection method ($p < 0.05$).

Conclusions. Our data showed that the sensitivity of combined detection was obviously higher than single detection for the evaluation of arthritis. The 3D-FS-SPGR combined with synovial fluid GG CX detection could be treated as a promising strategy for arthritis evaluation.

Key words: arthritis, MRI, 3D-FS-SPGR sequence, synovial fluid, GG CX

Cite as

Yang L, Niu D, Bai Z, et al. Application of 3D-FS-SPGR imaging combined synovial fluid GG CX detection in the evaluation of knee osteoarthritis. *Adv Clin Exp Med.* 2020;29(6):701–706. doi:10.17219/acem/121522

DOI

10.17219/acem/121522

Copyright

© 2020 by Wrocław Medical University
This is an article distributed under the terms of the Creative Commons Attribution 3.0 Unported (CC BY 3.0) (<https://creativecommons.org/licenses/by/3.0/>)

Introduction

Osteoarthritis, as a chronic and degenerative joint disease, leads to articular cartilage damage and osteo-proliferation. It dramatically impairs mobility in the elderly patients.¹ Periodic evaluation and continuous monitoring of patients with arthritis are helpful and critical in the long-term management of the disease.² Although it is possible to diagnose osteoarthritis with a clinical examination, X-ray examination, magnetic resonance imaging (MRI), and arthroscopy, there are still limitations and misdiagnoses which call for further improvement in the methods of diagnosis.³

Magnetic resonance imaging employs nuclear magnetic resonance (NMR) phenomena of human protons in the magnetic field to collect MR signal for diagnosis using spatial coding technology.⁴ Magnetic resonance imaging examination is considered as non-radiation, non-invasive and multi-faceted scanning, and characterized by high soft tissue resolution. It is advantageous in pre-treatment diagnosis and routine observation over other examination methods.⁵ Therefore, MRI is currently recognized as the best way to check the pathological changes of the knee. The sensitivity of MRI sequences in the diagnosis of knee joint cartilage lesions has been widely reported. For instance, it has been found that the sensitivity and specificity of 3D fast-spin spoiled gradient-recalled echo (NMR 3D-FS-SPGR) for lesions were 75–85% and 97%, respectively.⁶ In addition, previous evidence also revealed that the sensitivity of 3D-FS-SPGR sequence in cartilage lesions was 97%, and the specificity was 95% in 1.5T magnetic resonance.⁷

A recent study indicated that γ -glutamic acid carboxylase (GGCX) reduced carboxylated matrix γ -carboxylglutamate (Gla) protein level in the cartilage of patients with osteoarthritis compared to that in the normal control group.⁸ In addition, it was demonstrated that GGCX concentration in articular cartilage of patients with osteoarthritis was also lower than that of normal cartilage tissue, and gradually declined as the joint injury aggravated.⁹ Thus, GGCX is proposed to serve to some extent as an indicator for the progression of the disease in patients with arthritis. This study intends to evaluate the value of NMR-3D-FS-SPGR imaging and GGCX detection in synovial fluid in assessing the condition of knee osteoarthritis.

Patients and methods

Main reagents and instruments

Magnetic resonance imaging scan was performed with GeSIGNA 3.0T MRI system (GE Healthcare, Little Chalfont, UK). Immunohistochemistry and western blot antibodies were purchased from Wuhan Mitaka Biotechnology Co., Ltd (Wuhan, China). 3,3'-diaminobenzidine (DAB) was

bought from Wuhan Boster Biological Engineering Co., Ltd. (Wuhan, China). Other reagents involved in this study were obtained from Sinopharm Chemical Reagent Co., Ltd. (Shanghai, China).

Study participants

A total of 60 osteoarthritis patients treated between October 2016 and October 2017 in General Hospital of Ningxia Hui Autonomous Region People's Hospital (Yinchuan, China) were enrolled, including 34 males and 26 females, with mean age of 61.7 ± 5.1 years (range: 57–68 years). Another 20 healthy adults with corresponding age and gender were selected as the control group. The patients presented with repeated knee pain within the past month. X-ray (standing or weight-bearing position) showed joint space narrowing, sclerosis and/or cystic degeneration, and joint osteophyte formation. Synovial fluid (examined at least 2 times) was clear and thick red, with white blood cells (WBC) <2000 cells/mL. Moreover, morning stiffness was shorter than 30 min. Bone friction sound was found during activity. All patients underwent MRI examination after admission and the synovial fluid was taken 1 week later for GGCX detection. The study was reviewed and approved by Ethics Committee of General Hospital of Ningxia Hui Autonomous Region People's Hospital and all patients participating in the study signed an informed consent.

Classification criteria for articular cartilage injury

Knee osteoarthritis was divided into 4 stages according to Kellgren–Lawrence criteria:

Stage 1: in slight discomfort in the joint after activity; joint pain and swelling after increased activity; no evidence of significant cartilage damage on X-ray and computed tomography (CT) examination.

Stage 2: significant pain after activity and reduction after rest; X-ray showed slight change; only CT showed mild cartilage damage; isotope examination exhibited condensation in damaged joint.

Stage 3 (advanced): further osteochondral damage, resulting in joint deformity and loss of function; X-ray showed joint space narrowing, cystic lesions around the joints and articular mobile corpus.

Stage 4 (late): bone hyperplasia and cartilage exfoliation leading to complete loss of function; significant joint deformity; X-ray showed joint space narrowing, severe hyperplasia, coarse joint, and even bone collapse.¹⁰

Magnetic resonance imaging diagnostic grading was based on arthroscopic classifications. Grade 0 represents normal articular cartilage; grade I represents poorly defined cartilage structure or low focal signal within the cartilage; grade II represents mild or moderate irregularity in a cartilage surface profile, and the extent of cartilage

defect is smaller than 50%; grade III represents a severely irregular cartilage surface profile with more than 50% of cartilage defects; grade IV represents full-thickness cartilage defects and subchondral bone exposure.¹¹

Inspection method

The knees of all subjects were examined taking into account the femoral medial and lateral condyles, the tibia medial and lateral platform, the intercondylar femoral condyle, the trochlear articular surface, and patella articulation surface. The MRI scan was performed with a Gesigna 3.0T MRI system using a 3D-FS-SPGR sequence. The main parameters were the following: repetition time (TR) – 13 ms, echo time (TE) – 3.3 ms, thickness – 1.8 mm, interval – 0.9 mm, field of view (FOV) – 18 × 16 cm, numbers of excitations (NEX) – 2, matrix – 288 × 256 ppx, scan time – 348 s. A total of 2 mL of right knee synovial fluid was drawn with local anesthesia of the lower extremity within 1 week after MRI scan. The synovial fluid was transferred to a centrifuge tube and centrifuged at 4,000 g for 10 min at 4°C. The supernatant was stored at –80°C for GGCX detection.

Immunohistochemistry

Articular cartilage samples were obtained from surgery and fixed in formalin. The paraffin-embedded sections were sectioned at a thickness of 3 µm. The paraffin sections were then dewaxed, hydrated and treated with 3% H₂O₂ to block the endogenous peroxidase activity. After being washed with water, the sections were soaked in 0.01 M phosphate-buffered solution (PBS; pH 7.4) for 5 min. Next, the sections were blocked in 5–10% normal goat serum at room temperature for 10 min for blocking. Then, rabbit anti-human GGCX-specific primary antibody working solution was added to the sections (1:1,000) at 37°C for 2 h. After being washed 3 times, the sections were incubated in biotin labeled anti-rabbit secondary antibody working solution (1:200) at 37°C for 10–30 min. Next, horseradish enzyme-labeled streptavidin working solution was added to the sections at 37°C for 10–30 min. Finally, the sections were developed with DAB for 10 min and counterstained with hematoxylin for 2 min. After dehydration and hyalinization, the sections were observed under a microscope. Results

evaluation showed that GGCX was expressed in the cytoplasm. The cells were considered positive if the brown particles appeared in the cytoplasm. The positive cell ratio over 40% was treated as GGCX high expression.

Western blot

The synovial fluid samples were lysed with pre-cooled cell lysate and total protein was extracted. Then, the protein was separated using sodium dodecyl sulfate polyacrylamide gel electrophoresis (SDS-PAGE) and transferred to polyvinylidene fluoride (PVDF) membrane at 70 V for 3 h. Next, the membrane was blocked in 5% skim milk at 37°C for 1 h and incubated in rabbit anti-human GGCX antibody (1:1,000) at 4°C overnight. After being washed with phosphate-buffered solution Tween 20 (PBST), the membrane was incubated in horseradish peroxidase (HRP)-labeled mouse anti-rabbit IgG secondary antibody (1:200) at room temperature for 1 h. Finally, the membrane was developed in DAB for 10 min and the image was analyzed using a gel imaging analysis system (Bio-Rad, Hercules, USA).

Statistical analysis

All data analyses were performed on SPSS v. 20.0 software (IBM Corp., Armonk, USA). The qualitative data was compared using rank sum test. The enumeration data was presented as rate or percentage and compared using χ^2 test. The measurement data were presented as $\bar{x} \pm s$ and compared using t-test or one-way analysis of variance (ANOVA) with Student–Newman–Keuls (SNK) post hoc test. P-value <0.05 was considered statistical significance.

Results

3D-FS-SPGR imaging

Knee joint damage using 3D-FS-SPGR imaging was analyzed in all the arthritic patients. The results are shown in Fig. 1. The normal articular cartilage signal was uniform and consistent without cartilage swelling. The edge was clear and smooth with no cartilage defects. 3D-FS-SPGR detection demonstrated less uniform articular cartilage signal in grade I patients. The area with increasing local



Fig. 1. 3D-FS-SPGR imaging of osteoarthritis patients: A) healthy volunteer; B) grade I; C) grade II; D) grade III; E) grade IV

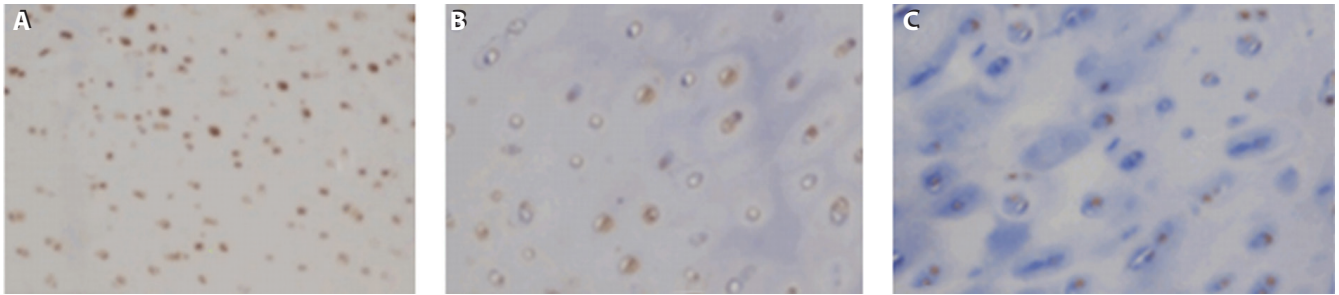


Fig. 2. GGCX expression detected using immunohistochemistry ($\times 100$). A and B. Cartilage tissue with normal GGCX expression. C. Cartilage tissue with low GGCX expression

signal could be found with no articular cartilage defect. In grade II patients, a less uniform articular cartilage signal with local thinner cartilage was observed. The defect did not reach 50% of the full thickness. Grade III patients were characterized by severe fibrosis in the anterolateral cartilage with thinner and non-uniform cartilage. The cartilage defects were more than 50% of the full-thickness, and no subchondral bone was found. In grade IV patients, the whole cartilage of the femur and tibia was lost, and the subchondral bone was exposed. High signal synovial fluid was observed within the cavity, which can be distinguished from cartilage signal.

Expression of GGCX detected with immunohistochemistry

The expression of GGCX in articular cartilage specimens was examined with immunohistochemistry. As shown in Fig. 2, significantly lower GGCX expressions in articular cartilage were presented in 46 patients compared to that of 20 healthy volunteers ($p < 0.01$).

Expression of GGCX in synovial fluid

The expression of GGCX in synovial fluid was tested with western blot (Fig. 3). β -actin was selected as a loading control to calculate the relative amount of GGCX (Fig. 4). Compared with healthy volunteers, we found that the overall GGCX levels in knee articular cartilage of 39 osteoarthritis patients were significantly reduced ($p < 0.01$). Moreover, GGCX expression in synovial fluid was significantly decreased following upstaging (Fig. 5).

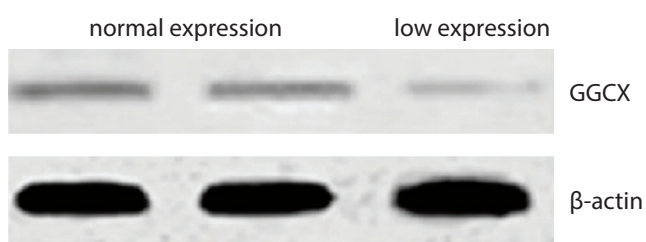


Fig. 3. GGCX expression in synovial fluid detected with western blot

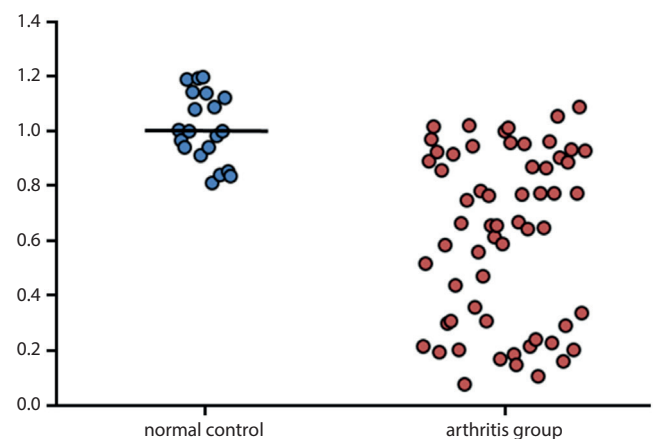


Fig. 4. GGCX expression in synovial fluid from different osteoarthritis patients

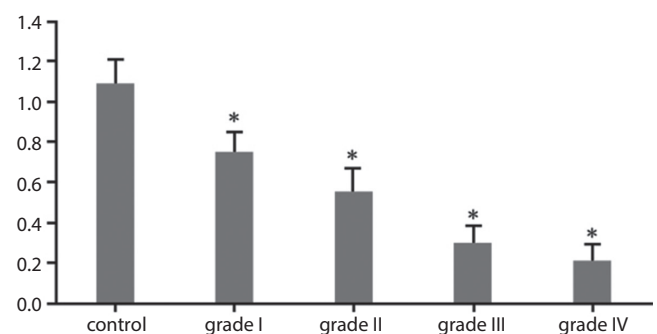


Fig. 5. GGCX expression in synovial fluid of patients with different osteoarthritis degree; * $p < 0.05$ compared with control

The relationship of MRI examination and GGCX expression with osteoarthritis grading

The relationship between MRI examination, GGCX expression and osteoarthritis grading of all patients was listed in Table 1. The sensitivity of the 3D-FS-SPGR imaging combined synovial fluid GGCX detection for the evaluation of arthritis condition was significantly higher, nearly 100%, whereas the specificity was lower than that of the single detection method ($p < 0.05$).

Table 1. The relationship of MRI examination and GGCX expression with osteoarthritis grading

Detection item	OA group (n = 60)	Non-OA group (n = 20)	Sensitivity [%]	Specificity [%]
3D-FS-SPGR detection	53	1	88.3	95.0
GGCX detection	36	4	60.0	80.0
3D-FS-SPGR or GGCX detection	58	5	95.0	75.0
3D-FS-SPGR and GGCX detection	41	0	68.3	100.0

Discussion

Arthroscopy is used to examine osteoarthritis and evaluate cartilage injury.¹² However, arthroscopy still presents drawbacks as a method for detection on the cartilage surface of the articular cavity. Its application is unable to cover the inspection of deep cartilage damage.¹² Magnetic resonance imaging is currently considered the favorable method to check knee lesions. Conventional MRI sequences show the sensitivity of cartilage morphological changes. However, they normally function when the cartilage is damaged to some extent. Routine sequences neither exhibit the hierarchical representation of the cartilage nor explain the exact composition of the cartilage and the specific cause of cartilage damage.¹³ This study thus aims to evaluate the progression of arthritis through 3D-FS-SPGR sequence imaging in MRI and synovial fluid GGCX detection.

Knee cartilage contains water, type II collagen and proteoglycan polymer,¹⁴ which can be divided into 4 layers from inside to outside: calcified layer, radioactive layer, transition layer, and tangential layer.¹⁵ The working principle of MRI is to generate different signal changes to the structure in cartilage matrix through different magnetic fields. Magnetic resonance imaging can accurately reflect the degree of pathophysiology of articular cartilage development. Rubenstein et al. found that the spin-echo (SE) sequence and the 3D-FS-SPGR sequence presented the normal articular cartilage as 3 layers, including the top phase as the tangential layer, the transition layer and the upper part of the radioactive layer; the middle layer as major of the radioactive layer; and the deep layer as the lower part of the radioactive layer.¹⁶ Combined with arthroscopic classification of cartilage injury, the damage occurred in the cartilage tangential and transitional layer in grade I–II degeneration (mild cartilage damage). On the other hand, the lesion reaches the radioactive layer at the stage of the moderate and severe cartilage injury.¹⁷ In the present study, we found that articular cartilage damage and degree can be clearly demonstrated using 3D-FS-SPGR sequence imaging.

The development of osteoarthritis is closely related to the formation of calcium microcrystals, including calcium phosphate (BCP) microcrystals and calcium pyrophosphate dihydrate (CPPD) crystals. Matrix Gla protein

(MGP) is not only expressed in articular cartilage, but also shows a close relationship with cartilage calcification and calcium microcrystal formation.¹⁸ Uncarboxylated MGP (ucMGP) content was significantly increased in the serum and synovial fluid of arthritis patients. The MGP contains 5 vitamin K-dependent amino acid GGCX (Gla) residues, while Gla shows high affinity to calcium and hydroxyapatite, but can only be activated through GGCX carboxylation.¹⁹ It has been demonstrated that GGCX expression in primary osteoarthritis cartilage was significantly lower than in normal cartilage and gradually decreased according to the degree of aggravation. The GGCX levels in synovial fluid of the primary knee osteoarthritis group were significantly lower than in the control group, which is consistent with our data.²⁰ In addition, it was also found that the accuracy of the knee MRI 3D-FS-SPGR sequence in assessing cartilage lesions was 95.0%.²¹ Previous findings indicated that MRI imaging, 3D-FS-SPGR sequence can accurately reflect the changes of articular cartilage morphology and thickness, and thus can accurately evaluate the degree of articular cartilage degeneration.²² In this study, the sensitivity of the combination of 3D-FS-SPGR and synovial fluid GGCX detection reached even 96.67%, which was significantly higher than the sensitivity of a single measurement. However, limitations in our study still exist. The investigation regarding the mechanism ought to be further performed in order to formulate a broader understanding of the diagnosis and therapy of osteoarthritis.

Conclusions

Our data demonstrated that the sensitivity of combined detection was significantly improved compared with single detection for the evaluation of arthritis. This strategy may provide practical basis for the prevention and treatment of arthritis.

References

1. Bijlsma JW, Berenbaum F, Lafeber FP. Osteoarthritis: An update with relevance for clinical practice. *Lancet*. 2011;377(9783):2115–2126.
2. McAlindon TE, Bannuru RR, Sullivan MC, et al. Response to Letter to the Editor entitled "Comments on OARSI guidelines for the non-surgical management of knee osteoarthritis". *Osteoarthr Cartil*. 2014; 22(6):890–891.
3. Loeser RF, Goldring SR, Scanzello CR, Goldring MB. Osteoarthritis: A disease of the joint as an organ. *Arthritis Rheum*. 2012;64(6):1697–1707.

4. Giedd JN, Rapoport JL. Structural MRI of pediatric brain development: What have we learned and where are we going? *Neuron*. 2010; 67(5):728–734.
5. Levman J, MacDonald P, Lim AR, Forgeron C, Takahashi E. A pediatric structural MRI analysis of healthy brain development from newborns to young adults. *Hum Brain Mapp*. 2017;38(12):5931–5942.
6. Li X, Benjamin Ma C, Link TM, et al. In vivo T(1rho) and T(2) mapping of articular cartilage in osteoarthritis of the knee using 3 T MRI. *Osteoarthr Cartil*. 2007;15(7):789–797.
7. Lee JB, Cha JG, Lee MH, Lee YK, Lee EH, Jeon CH. Usefulness of IDEAL T2-weighted FSE and SPGR imaging in reducing metallic artifacts in the postoperative ankles with metallic hardware. *Skeletal Radiol*. 2013;42(2):239–247.
8. Cavaco S, Viegas CS, Rafael MS, et al. Gla-rich protein is involved in the cross-talk between calcification and inflammation in osteoarthritis. *Cell Mol Life Sci*. 2016;73(5):1051–1065.
9. Rafael MS, Cavaco S, Viegas CS, et al. Insights into the association of Gla-rich protein and osteoarthritis, novel splice variants and gamma-carboxylation status. *Mol Nutr Food Res*. 2014;58(8):1636–1646.
10. Schiphof D, Boers M, Bierma-Zeinstra SM. Differences in descriptions of Kellgren and Lawrence grades of knee osteoarthritis. *Ann Rheum Dis*. 2008;67(7):1034–1036.
11. Azuma T, Nakai R, Takizawa O, Tsutsumi S. In vivo structural analysis of articular cartilage using diffusion tensor magnetic resonance imaging. *Magn Reson Imaging*. 2009;27(9):1242–1248.
12. Goldring MB, Goldring SR. Articular cartilage and subchondral bone in the pathogenesis of osteoarthritis. *Ann N Y Acad Sci*. 2010;1192: 230–237.
13. Hunter DJ, Arden N, Conaghan PG, et al. Definition of osteoarthritis on MRI: Results of a Delphi exercise. *Osteoarthr Cartil*. 2011;19(8): 963–969.
14. Potter HG, Jain SK, Ma Y, Black BR, Fung S, Lyman S. Cartilage injury after acute, isolated anterior cruciate ligament tear: Immediate and longitudinal effect with clinical/MRI follow-up. *Am J Sports Med*. 2012; 40(2):276–285.
15. Mosher TJ, Liu Y, Torok CM. Functional cartilage MRI T2 mapping: Evaluating the effect of age and training on knee cartilage response to running. *Osteoarthr Cartil*. 2010;18(3):358–364.
16. Li X, Yu C, Wu H, et al. Prospective comparison of 3D FIESTA versus fat-suppressed 3D SPGR MRI in evaluating knee cartilage lesions. *Clin Radiol*. 2009;64(10):1000–1008.
17. Souza RB, Stehling C, Wyman BT, et al. The effects of acute loading on T1rho and T2 relaxation times of tibiofemoral articular cartilage. *Osteoarthr Cartil*. 2010;18(12):1557–1563.
18. Ea HK, Nguyen C, Bazin D, et al. Articular cartilage calcification in osteoarthritis: Insights into crystal-induced stress. *Arthritis Rheum*. 2011;63(1):10–18.
19. Cranenburg EC, Brandenburg VM, Vermeer C, et al. Uncarboxylated matrix Gla protein (ucMGP) is associated with coronary artery calcification in haemodialysis patients. *Thromb Haemost*. 2009;101(2): 359–366.
20. De Vilder EY, Debacker J, Vanakker OM. GGCC-associated phenotypes: An overview in search of genotype-phenotype correlations. *Int J Mol Sci*. 2017;18(2):240.
21. Yoshioka H, Alley M, Steines D, et al. Imaging of the articular cartilage in osteoarthritis of the knee joint: 3D spatial-spectral spoiled gradient-echo vs fat-suppressed 3D spoiled gradient-echo MR imaging. *J Magn Reson Imaging*. 2003;18(1):66–71.
22. Wenger A, Englund M, Wirth W, Hudelmaier M, Kwok K, Eckstein F; OAI Investigators. Relationship of 3D meniscal morphology and position with knee pain in subjects with knee osteoarthritis: A pilot study. *Eur Radiol*. 2012;22(1):211–220.
23. Fan MP, Si M, Li BJ, et al. Cell therapy of a knee osteoarthritis rat model using precartilaginous stem cells. *Eur Rev Med Pharmacol Sci*. 2018;22(7):2119–2125.

Streptococcus agalactiae and *Chlamydia trachomatis* detection in women without symptoms of infection

Magdalena Frej-Mądrzak^{1,A–D,F}, Agnieszka Jama-Kmiecik^{1,E}, Jolanta Sarowska^{1,E},
Dorota Teryks-Wołyniec^{1,A–C}, Anna Grybos^{2,A,B,F}, Marian Grybos^{3,B}, Irena Choroszy-Król^{1,A}

¹ Department of Basic Sciences, Faculty of Health Sciences, Wrocław Medical University, Poland

² Department of Gynaecology and Obstetrics, Faculty of Health Sciences, Wrocław Medical University, Poland

³ Faculty of Medical Sciences, Public Higher Medical Professional School in Opole, Poland

A – research concept and design; B – collection and/or assembly of data; C – data analysis and interpretation;
D – writing the article; E – critical revision of the article; F – final approval of the article

Advances in Clinical and Experimental Medicine, ISSN 1899–5276 (print), ISSN 2451–2680 (online)

Adv Clin Exp Med. 2020;29(6):707–713

Address for correspondence

Magdalena Frej-Mądrzak
E-mail: magdalena.frej-madrzak@umed.wroc.pl

Funding sources

This study was generously supported by grant No. E090.18.021 from the Wrocław Medical University, Poland.

Conflict of interest

None declared

Received on August 28, 2019
Reviewed on September 7, 2019
Accepted on May 14, 2020

Published online on June 26, 2020

Cite as

Frej-Mądrzak M, Jama-Kmiecik A, Sarowska J, et al. *Streptococcus agalactiae* and *Chlamydia trachomatis* detection in women without symptoms of infection. *Adv Clin Exp Med.* 2020;29(6):707–713. doi:10.17219/acem/122397

DOI

10.17219/acem/122397

Copyright

© 2020 by Wrocław Medical University
This is an article distributed under the terms of the Creative Commons Attribution 3.0 Unported (CC BY 3.0) (<https://creativecommons.org/licenses/by/3.0/>)

Abstract

Background. *Chlamydia trachomatis* (*C. trachomatis*) and *Streptococcus agalactiae* (GBS) may be present in the female cervical canal without any symptoms of infection. Chronic chlamydial infections lead to many serious complications and perinatal infections, while the presence of GBS is a reservoir for infections of newborns or invasive streptococcal infection in adults.

Objectives. To examine healthy women for *C. trachomatis* without symptoms from the reproductive system, assess the frequency of asymptomatic infections, detect GBS in the cervical canal, demonstrate differences in drug susceptibility, and determine the serotype of *S. agalactiae* strains and correlations among the ones present in the cervical canal.

Material and methods. A total of 315 cervical swabs were collected for genetic and microbiological analysis for the presence of *C. trachomatis* and *S. agalactiae*. Latex and diffusion-disk methods were used to determine the serotype and susceptibility of streptococci.

Results. Ten out of 315 women (3.2%) were *C. trachomatis*-positive. Using traditional methods of microscopy, culture and serology, 42 strains (13.3% of the subjects) obtained from patients were identified as *S. agalactiae* and further analyzed. The most common serotypes identified were II (18/42, 42.9%), V (11/42, 26.2%) and III (10/42, 23.8%). The less common serotypes found were VII (2/10, 4.8%), and Ib (1/10, 2.4%); no Ia, IV or VII serotypes were found. All the strains were susceptible to penicillin, while 71.4% of them were susceptible to erythromycin and 81.0% were susceptible to clindamycin. Seven isolates (16.7%) were concomitantly resistant to erythromycin and clindamycin.

Conclusions. *Chlamydia trachomatis* was confirmed in 3.2% of the respondents, and GBS was found in 13.3%, despite a lack of symptoms of infection. The incidence of *C. trachomatis* infections and GBS colonization in Poland is similar to those in other European countries.

Key words: *Chlamydia trachomatis*, *Streptococcus agalactiae*, cervical infection

Introduction

Streptococcus agalactiae or Group B *Streptococcus* (GBS) is a Gram-positive β hemolytic coccus in the *Streptococcus* genus. *Streptococcus agalactiae* most commonly colonizes the lower gastrointestinal tract, anus and the vaginal environment. Epidemiological data indicates that GBS is found in the vaginal tract of 10–30% of healthy women who usually do not show any symptoms of inflammation.^{1–3} In non-pregnant women and in men, GBS is becoming an increasingly common cause of invasive diseases, especially in the elderly, in immunocompromised patients or in those with other (particularly chronic) diseases. The combination of bacterial and host factors determines the course of infection.^{1–3} *Streptococcus agalactiae* causes infection of the skin and subcutaneous tissue, urinary tract, lungs, and endocardium; it also causes group B streptococcal meningitis, which is an important but uncommon manifestation of invasive GBS disease in adults, accounting for up to 4% of all cases of bacterial meningitis in adults. Most cases of GBS meningitis occur in postpartum women, the elderly or adults with serious underlying diseases.⁴ Symptoms of the disease are generally abrupt, and bacteremia occurs in about 80% of cases. A distant focus of infection, such as the endometrium or endocarditis, is often identified. The case–mortality rate is high (27–34%) and closely related to the presence of underlying conditions other than pregnancy. A small but significant proportion of survivors (7%) suffer from permanent hearing loss.⁵ *Streptococcus agalactiae* is particularly dangerous for pregnant women, in whom it multiplies intensively in the vaginal environment during pregnancy and poses a real risk to both the mother and the fetus.⁶ Cervical infections in pregnant women are associated with gynecological-obstetrical complications: miscarriage, premature childbirth, fetal membrane rupture, or pelvic inflammatory disease (PID).⁷

Infants can be infected through aspiration of infected amniotic fluid or during childbirth.^{2,6} Group B *Streptococcus* is associated with invasive disease in newborns. Newborn infections are classified as early when the disease develops in the 1st week of life and manifests as sepsis and pneumonia (so-called early-onset GBS). Late-onset GBS is diagnosed if symptoms appear after the 7th day of life, last until the 3rd month and resemble meningitis. In pregnant women or immediately postpartum, GBS are responsible for inflammation of the urinary tract, fetal membrane and endometrium, for sepsis, and rarely for meningitis.²

Chlamydia trachomatis and *S. agalactiae* may be present in the female cervical canal without any symptoms of infection. Chronic chlamydial infections lead to many serious complications in women and perinatal infections, while the presence of GBS is a reservoir for infections of newborns or invasive streptococcal infection in adults. *Chlamydia trachomatis* is a bacterium with 3 biotypes responsible for different infections. The 1st one causes

pneumonia in mice; the 2nd one, lymphogranuloma venereum (LGV; serotypes L1–L3), is responsible for LGV; and the 3rd one (serotypes A–C) leads to trachoma or urogenital infections, conjunctivitis in adults and children, and pediatric pneumonia (serotypes D–K). *Chlamydia trachomatis* (especially D–K serotypes) is the most common infection worldwide.⁸

Transmission of *C. trachomatis* usually takes place through direct mucous membrane contact (vagina, anus) with an infected person during sexual intercourse or oral sex, or immediately after birth through mother's infected cervical canal. The risk of transmission during a single act of vaginal intercourse is estimated to be 10%, and about 55% for people who have had at least 2 sexual partners in the last 6 months. Partners of people with *C. trachomatis* infections are very likely to be infected, so it is important to notify and treat them. Despite literature reports on spontaneous clearance of *C. trachomatis*, it is recommended that appropriate tests be performed in symptomatic and asymptomatic sexually active individuals, and after pathogen identification, to treat infected individuals and their sexual partners from the previous 6 months.

Due to its affinity for the female columnar epithelium, *C. trachomatis* infects the cervix, urethra and rectum, which leads to cervicitis, and inflammation of the fallopian tubes and pelvic organs. The complications may include infertility, peritoneal tissue inflammation (which occurs throughout the continuity of tissues), the Fitz-Hugh–Curtis syndrome (PID with peritoneal tissue inflammation) and conjunctivitis, most often as an autoinfection. In women, inflammation of the rectum may occur through direct infection and/or PID complications.

In Europe, detected and registered *C. trachomatis* infections mainly affect heterosexual women (51%) and men (35%); perinatal infections amount to <1%, and the remaining infections appear in homosexual men (10%) or are unspecified.⁹ However, these values are underestimated due to the small number of reports on such infections. Only 1,628 cases out of over 2 million in Europe were registered in Poland in 2013–2017.⁹

The developmental lifecycle of *C. trachomatis* is intracellular and lasts up to 72 h, during which the bacterium occurs as an elementary body (EB), i.e., an infectious form of the bacteria incapable of division, and as a reticular body (RB), which multiplies in a host. Under unfavorable conditions, the bacteria can pass into persistent forms unable to transform into EB, which blocks the cycle and leads to the formation of large atypical forms. Factors that induce the formation of persistent forms in vitro include β -lactam antibiotics, e.g., penicillin, which block RB division and prevent further transformation into EBs. Exposure to β -lactam antibiotics results in the accumulation of large aberrant RBs, so-called penicillin forms.¹⁰ Moreover, the formation of persistent forms of bacteria is influenced by nutritional factors such as decreased access to basic amino acids and ions, e.g., lowered exogenous

tryptophan or iron levels, and immunological factors – pro-inflammatory cytokines and interferon γ (IFN γ). The interferon blocks RB replication – such large aberrant forms of *Chlamydia* can be observed in cells with IFN γ under in vitro conditions.¹¹ Chronic and persistent infections are more likely to cause complications.

In 70–95% of women, chlamydial infections are asymptomatic. If symptoms do occur, they usually develop 10–14 days after sexual contact and most frequently include mucosal cervicitis, later purulent, cervical bleeding, friability, edema, and ulcers.¹² Furthermore, *C. trachomatis* infection is accompanied by dysuria, vaginal discharge, post-coital and intermenstrual bleeding, and poorly differentiated abdominal pain or lower abdominal pain. In women, asymptomatic or untreated chlamydial infection can lead to complications such as PID (including endometritis, salpingitis, parametritis, tubo-ovarian abscess, or peritonitis), chronic pelvic pain, infertility, ectopic pregnancy, or fetal membrane rupture. Symptoms suggesting PID include tenderness and pain in the abdomen and lower abdomen – usually bilateral – tenderness and pain during gynecological examinations, acute dyspareunia, abnormal bleeding, as well as abnormal discharge from the vagina or cervix as a result of cervicitis, endometritis or bacterial vaginosis. Moreover, women may develop sexually acquired reactive arthritis (SARA) (<1%).¹³ Adult inclusion conjunctivitis is most commonly associated with urogenital infections (autoinfection) with clinical presentation that includes tearing, conjunctival congestion, photophobia, moderately swollen eyelids, and the presence of mucus. This conjunctivitis does not lead to blindness, although complications such as corneal pannus or ulcer have been observed.¹⁴

The Polish Gynecological Society recommends annual *C. trachomatis* screening to pregnant and non-pregnant women ≤ 25 years (especially before a planned pregnancy). Screening in pregnant women should be performed in the 1st and 3rd trimester of pregnancy (during the first visit). Non-pregnant women older than 25 years should be examined at least once a year – in particular women who engaged in high-risk sexual behavior before a planned pregnancy. Pregnant women >25 years should be examined in the 1st trimester (recommended during their first visit), and in the 3rd trimester only if at risk.¹⁵ According to the European Guideline on the Management of *C. trachomatis* Infections, the indication for laboratory tests for *C. trachomatis* is the presence of risk factor(s) and/or other sexually transmitted infections (STIs), i.e., age <25 years, new sexual contact in the last year or more than 1 partner in the last year.¹³ Laboratory tests are recommended for men aged <40 years with symptoms of acute epididymo-orchitis and/or risk factors for STI, and for women with cervical or vaginal discharge with risk factors for STI, acute pain and/or PID symptoms. In both sexes, testing should be performed in all cases of rectal inflammation/colitis due to the risk of STIs and conjunctivitis; and in neonates,

in cases of purulent conjunctivitis or atypical interstitial pneumonia. A separate group of patients referred for laboratory testing are those diagnosed with other STIs or having sexual contacts with STI or PID individuals, after pregnancy termination, or following any intrauterine interventions or manipulations.¹⁶

The aims of this study was to examine healthy women for *C. trachomatis* without symptoms from the reproductive system, to assess the frequency of asymptomatic infections, to detect GBS in the cervical canal, to demonstrate differences in drug susceptibility, and to determine the serotype of *S. agalactiae* strains and correlations among the bacterial strains present in the cervical canal.

Material and methods

All the procedures involving human participants were performed in accordance with the ethical standards of Wroclaw Medical University (Poland) and with the 1964 Helsinki declaration and its later amendments. The study protocol was accepted by the Ethics Committee of Wroclaw Medical University.

Cervical specimens were collected by gynecologists during prophylactic examinations. Swabs were taken from 315 women aged 18–32 years without previous genital symptoms from chlamydial or streptococcal infections. The mean age of the patients was 24.86 ± 3.15 years. Information on the number of partners in the previous year and the frequency of intercourse per week was collected from the patients during interviews. The women declared an average of 1.14 sexual partners in the previous 24 months and 2.05 sexual contacts per week. For chlamydia testing, we used a commercial DNA isolation kit and a *C. trachomatis* PCR kit (both from GeneProof a.s., Brno, Czech Republic) which allow simultaneous detection of a conservative region encoding 16S rRNA and a conservative region of a cryptic DNA plasmid, including deletion mutation in the cryptic plasmid (the Swedish variant). To detect GBS, specimens were tested using standard culturing methods. The cultures obtained were used to isolate small grey smooth colonies with β -hemolysis. The identification process included Gram-staining, and microscopic assessment of bacterial cells and colony purity. The Lancefield serological grouping was performed using a commercial streptococcal grouping kit (Oxoid Ltd., Basingstoke, UK). The culture properties of the collected *S. agalactiae* strains were tested using Columbia agar with 5% sheep blood (Graso Biotech, Starogard Gdański, Poland) and selected media: either CHROMagar Strep B (Graso Biotech) or Granada agar/Columbia CNA +5% sheep blood, (bioMérieux, Warszawa, Poland). *Streptococcus agalactiae* strains were identified and tested for their susceptibility to antibiotics (benzylpenicillin 1 IU, erythromycin 15 μ g, clindamycin 2 μ g; medium: Mueller-Hinton fastidious agar (MH-F); inoculum: 0.5 McFarland; incubation conditions: 5% CO₂, 36°C, 18 \pm 2 h). This

methodology was recommended by the European Committee on Antimicrobial Susceptibility Testing (EUCAST). The isolates were serotyped using the Immulex™ StrepB kit (SSI Diagnostica, Hillerød, Denmark) for serotypes Ia, Ib, II, III, IV, V, VI, and VII.¹⁷

Results

Out of the 315 women involved in the study, 10 (3.2%) were *C. trachomatis*-positive. Using traditional methods of microscopy, culture and serology, 42 strains obtained from patients (13.3% of the subjects) were identified as *S. agalactiae* and further analyzed. The most common serotypes identified were II (in 18 out of the 42, or 42.9%), V (11/42, 26.2%) and III (10/42, 23.8%). The less common serotypes found were VII (2/42, 4.8%) and Ib (1/42, 2.4%), with no Ia, IV or VII serotypes found. All the strains were susceptible to benzylpenicillin. The distribution of resistance-phenotypes among the GBS serotypes isolated from women without symptoms of infection is presented in Table 1.

Table 1. Distribution of resistance phenotypes among GBS serotypes isolated from women without symptoms of infection

Serotype, n	Resistant (%)
Ib (1)	E (100)
II (18)	E (22.2), DA (22.2)
III (10)	E (10.0), DA (10.0)
V (11)	E (54.5), DA (27.3)
VII (2)	E (0), DA (0)

Resistance phenotype: E – erythromycin; DA – clindamycin.

Statistical analysis

We found no correlation between positive results for *C. trachomatis* and GBS; the value of the χ^2 test with the Yates's correction is $\chi^2(1) = 0.248$, $p = 0.875$. This result confirms the significance value of the asymptotic odds ratio (OR) ($p = 0.75$) indicating that there is no relationship between the variables. Among the patients with positive results for *C. trachomatis*, 10% were also positive for GBS. In the GBS-positive study group, 2.4% were also positive for *C. trachomatis*.

Discussion

Infections caused by GBS are commonly detected in the vagina. In our study, *Streptococcus* were isolated in smears from the cervical canal. The GBS colonization was confirmed in 42 patients (13.3%) and isolates were identified as *S. agalactiae*. The GBS colonization is transient in nature, and little is known about the host and bacterial

factors controlling GBS persistence. Patras et al. used human cervical and vaginal epithelial cells in the mouse model of GBS vaginal colonization to characterize key host factors responsible for GBS colonization.³ The authors identified GBS strains that persisted for more than a month in the murine vagina, while other strains were more easily cleared. Moreover, they demonstrated that the persistent strain more readily invades cervical cells compared to vaginal cells, suggesting that GBS may potentially use the cervix as a reservoir to establish long-term colonization. The authors noted that compared to serotype Ia, serotype III had increased adherence to vaginal cells, which confirms the previously noted increased vaginal epithelial adherence of serotype III strains over serotype Ia strains. Furthermore, they demonstrated that serotype V invades and/or survives within the cervical epithelium more readily than other serotypes, which may be beneficial in niche establishment and long-term cervical-vaginal persistence.³

Similar results were obtained by Sadeh et al. in a study involving non-pregnant women. They obtained 70 isolates from 413 patients (16.9%). The most numerous group were serotypes III (50%), II (27.1%) and V (12.9%).¹⁸

Newborns most commonly contact GBS from the mother's genital tract. The GBS is detected in the vagina and rectum of 10–30% of pregnant women.³ Based on their capsular polysaccharides, GBS isolates can be divided into 9 different serotypes. However, the distribution of serotypes varies according to geographic location. In the present study, the most common serotypes found in 315 women were II (18/42, 42.9%), V (11/42, 26.2%) and III (10/42, 23.8%). Less common serotypes included VII (2/42, 4.8%) and Ib (1/42, 2.4%), whereas serotypes Ia, IV and VII were not found at all. Persson et al. reported that the serotype distribution of colonizing strains is similar to the distribution of invasive strains, but 2 studies have shown that the proportion of serotype III strains is higher among invasive strains than among colonizing strains.¹ This indicates that serotype III strains may be more virulent than strains of other serotypes, which could be related to a failure to obtain an adequate serum antibody response to serotype III during colonization.

There are some unexplained geographical differences between the serotype distributions of colonizing GBS strains. The most striking is the high prevalence of serotypes VI and VIII in pregnant Japanese women, whereas these strains seem currently absent or rare in Europe and North America.⁸ Serotypes Ia, Ib, II, and III prevail in many parts of the world, but serotype V is the most frequently isolated in many countries.¹⁹

Clinical manifestations of GBS infection in adults are numerous and quite varied. Since Group B streptococci can colonize skin and mucosal surfaces and may be isolated from infected sites along with other virulent organisms, their role in pathogenesis has often been questioned. However, studies of invasive GBS infection in which microorganisms are isolated from normally sterile sites, such

as blood or cerebrospinal fluid (CSF), provide direct evidence that Group B streptococci are the etiologic agents in many clinical syndromes.¹³ Types Ia, III and V are currently the most frequently isolated serotypes from adult patients in nearly equal proportions.¹³ We found a prevalence of serotypes II, V and III, the presence of which in the cervix may act as a reservoir for invasive diseases, even if they escalate over time or in combination with another underlying disease. Special attention should be paid to serotype III GBS, which is considered extremely virulent. Tazi et al. examined GBS strains isolated from adults with invasive infections in France and found that such infections are more frequent among people aged ≥ 65 years of age, as described in other European and US surveys, with serotypes Ia, III and V accounting for 72% of all examined strains.²⁰

In 2009, Brzychczy-Włoch et al. reported a different distribution of serotypes in pregnant women colonized by GBS: Those authors found that serotype III was predominant (35%), followed by serotypes Ia (20%), V (17%) and II (15%). They demonstrated that pregnancy hormones and changes in the reproductive system significantly affect GBS colonization and the distribution of predominant serotypes in pregnant women.²¹ Wolny-Kołodka examined 250 *S. agalactiae* strains isolated from female reproductive tracts and found that the predominant serotypes were III (54%) and V (12%), followed by the Ia serotype (17%), which was not found in our study.²² Epidemiological data from European countries demonstrate that Ia, II, III, and V are the most frequently isolated serotypes in European countries.^{1,6,7,21} Except for Ia, all these serotypes were confirmed in our study.

In our study, 71.4% of the strains were susceptible to erythromycin, 81.0% were susceptible to clindamycin, and the others (19.0%) were clindamycin-resistant. We found 7 strains (16.7%) that were simultaneously resistant to erythromycin and clindamycin. Garland et al. reported that in many countries, erythromycin resistance ranges from about 3% in Japan and Australia to 54% in the USA.²³

Out of the 7 strains simultaneously resistant to erythromycin and clindamycin in our study, we found 4 strains with serotype II and 3 strains with serotype V. Strain with serotypes Ib was resistant to erythromycin. Jannati et al. conducted research in Iran to determine the serotype distribution and antibiotic resistance of 56 GBS strains.¹⁹ Their results showed that all the isolates were susceptible to penicillin. Only 3 isolates (5.3%) were intermediate to erythromycin (serotypes II, V and 1 unidentified); the remaining isolates were susceptible to erythromycin. Only 2 isolates (3.5%) were resistant to clindamycin (serotypes II and III); 2 (3.5%) were intermediate; the rest were susceptible to clindamycin.¹⁹ Therefore, in our study and in the Iranian study, serotypes V, II and III were resistant to both erythromycin and clindamycin. Tazi et al. reported that erythromycin resistance has increased since 2007, reaching 35.24% in 2010; in their study, erythromycin resistance was prevalent in serotype V.²⁰

Because women who suffer from *C. trachomatis* infection may have no clinical symptoms, periodic or prophylactic health examinations can help detect and confirm chlamydial infection. In our study, PCR tests showed that 3.2% of the participants were *Chlamydia*-positive. According to the literature, in Europe, the level of *C. trachomatis* infections among women ranges between 3% and 5.3%,^{13,16} which is consistent with the results of our research. It is also estimated that 70–95% of infected women do not experience any symptoms in the genital system, which leads to uncontrolled spread of this microorganism.^{13,16} Undiagnosed and untreated patients are potential reservoirs of this bacterium.¹¹ Detecting *C. trachomatis* infection before or during early pregnancy helps to avoid complications related to premature rupture of membranes, preterm birth and neonatal infections.^{13,16} In Germany, Dudareva-Vizule et al. analyzed the results for *C. trachomatis* obtained between 2008 and 2014, and found that 3.9% of the women were infected with this microorganism.²⁴ In the age group < 25 years, 26.9% of the women underwent screening tests. The highest percentages of positive results were found in women aged 15–19 years (5%) and 20–24 years (4.9%). Most of the women who underwent the tests were pregnant (41.9%); these were preventive check-ups.²⁴

In 2008–2013, Bianchi et al. used a nested polymerase chain reaction (PCR) assay to detect *C. trachomatis* cryptic plasmid in cervical smears from women who had not reported any clinical symptoms of *C. trachomatis* infection.²⁵ The authors detected *C. trachomatis* infection in 4.4% of the participants, with the highest percentage of infection recorded in women aged 20–21 years (5.5%) and the lowest in women aged 22–23 years (3.5%). The differences between infection rates in different age groups were not significant.²⁵ The frequency of detecting chlamydial infections depends on the region and diagnostic methods. Genetic PCR tests are the reference method, but due to their limitations, immunofluorescence or enzyme-linked immunosorbent assay (ELISA) assays are more often used.⁹ Arsić et al. obtained a significantly higher percentage of positive results in the Balkans than the published data by other authors indicated.²⁶ In 1 center, *C. trachomatis* ELISA assays were positive in 7.1% of the patients (i.e., 100/1400); in Skopje, where direct fluorescent antibody (DFA) tests were used, *Chlamydia* antigens were detected in 6.8% of the women (120/718).²⁶ In our own earlier study (2012–2013), we examined investigated the presence of *C. trachomatis* in cervical swabs among women aged 18–30 using direct immunofluorescence (DIF) and reported that 4/109 patients (3.7%) were *Chlamydia*-positive,¹⁴ which is very close to our current results obtained with PCR.

Chlamydia-positive sexual partners are at high risk of transmitting this pathogen through sexual contact. Therefore, both sexual partners should be examined for infection and treated at the same time. Berntsson et al. examined 99 women with partners who had tested positive





for *C. trachomatis*.¹² Using genetic methods, they obtained positive *C. trachomatis* results in 53 out of 99 women (53.5%). Among the women infected with *C. trachomatis*, 50% did not declare any clinical symptoms, while the remaining 50% reported dysuria or vaginal discharge.¹²

Our study found no correlation between the presence of *C. trachomatis* and GBS colonization of the cervical canal. The coexistence of both microorganisms was found in only 1 patient. Neither Friedek et al. nor Honig et al. found this correlation, but they examined *C. trachomatis* in cervical swabs and streptococci in vaginal swabs.^{27,28}

Conclusions

Early diagnosis, awareness of the need to look for deeply advanced infection and adequate antimicrobial therapy are essential elements of effective treatment for GBS infection. The high morbidity and mortality of invasive GBS infections has made the development of a multivalent conjugate polysaccharide vaccine a major focus for research. Awareness of the distribution of and changes in GBS serotypes in different populations is important. Continued surveillance of invasive GBS disease in adults and genetic characterization of the isolated strains are essential, as they may impact the use of antibiotics and vaccine design. In our study, the distribution of GBS serotypes was similar to results from other European countries and confirms the geographical variability of occurrence. Further research is needed to confirm the risk factors for GBS infection. Penicillin is used for GBS prophylaxis, and erythromycin and clindamycin remain suitable alternatives for women with β -lactam antibiotic allergies. Unfortunately, the number of strains resistant to macrolides and lincosamides is growing, so it is necessary to monitor the sensitivity of isolates of GBS. In our study, the incidence of *C. trachomatis* infections and GBS colonization is similar to other European countries. We found no positive correlation between the presence of GBS and *C. trachomatis* in the cervical canal. We did not find any correlation between the presence of *C. trachomatis* and the number of sexual partners or sexual contacts, because the percentage of positive results was too low.

ORCID iDs

Magdalena Frej-Mądrzak  <https://orcid.org/0000-0002-8138-2586>
 Agnieszka Jama-Kmieciak  <https://orcid.org/0000-0001-6514-8629>
 Jolanta Sarowska  <https://orcid.org/0000-0001-9710-2721>
 Dorota Teryks-Wołyniec  <https://orcid.org/0000-0003-0488-3579>
 Anna Gryboś  <https://orcid.org/0000-0002-7456-4373>
 Marian Gryboś  <https://orcid.org/0000-0003-0216-8088>
 Irena Choroszy-Król  <https://orcid.org/0000-0002-5006-4059>

References

- Persson E, Berg S, Trollfors B, et al. Serotypes and clinical manifestations of invasive Group B streptococcal infections in western Sweden 1998–2001. *Clin Microbiol Infect.* 2004;10:791–796. doi:10.1111/j.1469-0691.2004.00931.x
- Shabayek S, Spellerberg B. Group B streptococcal colonization, molecular characteristics, and epidemiology. *Front Microbiol.* 2018;9:437. doi:10.3389/fmicb.2018.00437
- Patras KA, Rösler B, Thoman ML, Doran KS. Characterization of host immunity during persistent vaginal colonization by Group B *Streptococcus*. *Mucosal Immunol.* 2015;8(6):1339–1348. doi:10.1038/mi.2015.23
- Lyhs U, Kulkas L, Katholm J, et al. *Streptococcus agalactiae* serotype IV in humans and cattle, Northern Europe. *Emerg Infect Dis.* 2016;22(12):2097–2103. <https://dx.doi.org/10.3201/eid2212.151447>
- Farley MM. Group B streptococcal disease in nonpregnant adults. *Clin Infect Dis.* 2001;33:556–561.
- Wolny K, Gołda-Matuszak E. *Streptococcus agalactiae* (GBS): The characteristic of isolated strains from productive women's vagina. *Med Dośw Mikrobiol.* 2010;62:141–151.
- Kierzkowska M, Majewska A, Kądzilska J, et al. Evaluation of bacterial flora found in the cervix of pregnant women. *Perinatologia, Neonatologia i Ginekologia.* 2012;5(1):26–29.
- Meyer T. Diagnostic procedures to detect *Chlamydia trachomatis* infections. *Microorganisms.* 2016;4(3):25. doi:10.3390/microorganisms4030025
- European Centre for Disease Prevention and Control. *Chlamydia infection*. In: *ECDCA Annual Epidemiological Report for 2017*. Stockholm, Sweden: ECDC; 2019
- Storey C, Chopra I. Affinities of β -lactams for penicillin binding proteins of *Chlamydia trachomatis* and their antichlamydial activities. *Antimicrob Agents Chemother.* 2001;45(1):303–305. doi:10.1128/AAC.45.1.303-305.2001
- Frej-Mądrzak M, Gryboś A, Gryboś M, et al. PCR diagnostics of *Chlamydia trachomatis* in asymptomatic infection by women. *Ginekolog Pol.* 2018;89(3):115–119. doi:10.5603/GP.a2018.0020
- Berntsson M, Tunbäck P. Clinical and microscopic signs of cervicitis and urethritis: Correlation with *Chlamydia trachomatis* infection in female STI patients. *Acta Derm Venereol.* 2013;93:230–233. doi:10.2340/00015555-1536
- Lanjouw E, Ouburg S, de Vries HJ, Stary A, Radcliffe K, Unemo M. 2015 European guideline on the management of *Chlamydia trachomatis* infections. *Int J STD AIDS.* 2016;27(5):333–348. doi:10.1177/0956462415618837
- Frej-Mądrzak M, Teryks-Wołyniec D, Jama-Kmieciak A, Sarowska J, Gościński G, Choroszy-Król I. *Chlamydia trachomatis* infections of the genitourinary tract and conjunctiva in adults and children in 2012–2013. *Fam Med Primary Care Rev.* 2014;16(3):225–227.
- Polish Gynecological Society recommendations regarding *Chlamydia trachomatis* infections in obstetrics and gynecology. *Ginekolog Pol.* 2007;78:574–575.
- European Centre for Disease Prevention and Control. Guidance on *Chlamydia* control in Europe – 2015. Stockholm, Sweden: ECDC; 2016. doi:10.2900/667703
- The European Committee on Antimicrobial Susceptibility Testing. Breakpoint tables for interpretation of MICs and zone diameters. Version 9.0, 2019. <http://www.eucast.org>.
- Sadeh M, Firouzi R, Derakhshandeh A, Khalili MB, Kong F, Kudinha T. Molecular characterization of *Streptococcus agalactiae* isolates from pregnant and non-pregnant women at Yazd University Hospital, Iran. *Jundishapur J Microbiol.* 2016;9(2):e30412. doi:10.5812/jjm.30412
- Jannati E, Roshani M, Arzanlou M, Habibzadeh S, Rahimi G, Shapuri R. Capsular serotype and antibiotic resistance of group B streptococci isolated from pregnant women in Ardabil, Iran. *Iran J Microbiol.* 2012;4(3):130–135.
- Tazi A, Morand PC, Reglier-Poupet H, et al. Invasive group B streptococcal infections in adults, France (2007–2010). *Clin Microbiol Infect.* 2011;17(10):1587–1589. doi:10.1111/j.1469-0691.2011.03628.x
- Brzychczy-Włoch M, Gosiewski T, Bodażewska M, Pabian W, Bulanda M, Heczko PB. Analysis of serotypes distribution of Group B streptococci origin from pregnant carriage using multiplex PCR [in Polish]. *Med Dośw Mikrobiol.* 2009;61(4):293–299.
- Wolny-Koładka K. Evaluation of ITS-PCR and PCR MP techniques for *Streptococcus agalactiae* genetic differentiation [in Polish]. *Med Dośw Mikrobiol.* 2014;66(3–4):149–160.
- Garland SM, Cottrill E, Markowski L, et al. Antimicrobial resistance in Group B streptococcus: The Australian experience. *J Med Microbiol.* 2011;60(Pt 2):230–235. doi:10.1099/jmm.0.022616-0

24. Dudareva-Vizule S, Haar K, Sailer A, et al; *Chlamydia trachomatis* Laboratory Sentinel Team. Establishment of a voluntary electronic *Chlamydia trachomatis* laboratory surveillance system in Germany, 2008 to 2014. *Euro Surveill.* 2017;22(6):30459.
25. Bianchi S, Frati ER, Canuti M, et al. Molecular epidemiology and genotyping of *Chlamydia trachomatis* infection in a cohort of young asymptomatic sexually active women (18–25 years) in Milan, Italy. *J Prev Med Hyg.* 2016;57(3):E128–E134.
26. Arsić D, Milovanović DR, Ferati AB, et al. Monitoring of *Chlamydia trachomatis* genitourinary infection in women: Analytical comparative study using public health records from two Balkan countries. *Cent Eur J Public Health.* 2016;24(1):16–21. doi:10.21101/cejph.a4088
27. Friedek D, Ekiel A, Romanik M, et al. Co-occurrence of urogenital mycoplasmas and Group B streptococci with chlamydial cervicitis. *Pol J Microbiol.* 2005;54(3):253–255.
28. Honig E, Mouton JW, van der Meijden WI. The epidemiology of vaginal colonisation with Group B streptococci in a sexually transmitted disease clinic. *Eur J Obstet Gynecol Reprod Biol.* 2002;105(2):177–180.

Detecting tumor-infiltrating Forkhead box P3-positive T cells in the prognosis of lung adenocarcinoma: Possible role of clustering tumor interleukin-12 subunit alpha and transforming growth factor beta 1 expression

Hiroyasu Matsuoka^{1,A–F}, Hirochika Matsubara^{1,D–F}, Aya Sugimura^{1,C,F}, Tsuyoshi Uchida^{1,C,F}, Tamo Kunimitsu^{1,C,F}, Tomofumi Ichihara^{1,C,F}, Yuichiro Oonuki^{2,C,F}, Yoshihiro Miyauchi^{2,C,F}, Tetsuo Kondo^{3,A,C}, Hiroyuki Nakajima^{1,A,C,F}

¹ Department of Surgery, Faculty of Medicine, University of Yamanashi, Chuo, Japan

² Department of Thoracic Surgery, National Hospital Organization Disaster Medical Center, Tachikawa, Tokyo, Japan

³ Department of Pathology, Faculty of Medicine, University of Yamanashi, Chuo, Japan

A – research concept and design; B – collection and/or assembly of data; C – data analysis and interpretation;

D – writing the article; E – critical revision of the article; F – final approval of the article

Advances in Clinical and Experimental Medicine, ISSN 1899–5276 (print), ISSN 2451–2680 (online)

Adv Clin Exp Med. 2020;29(6):715–725

Address for correspondence

Hiroyasu Matsuoka

E-mail: aphyosemion@hotmail.co.jp

Funding sources

None declared

Conflict of interest

None declared

Acknowledgements

We would like to thank Professor Atsuhito Nakao and Dr. Hiroki Ishii for their valuable advice regarding the assessment of Tregs.

We would like to thank Ms. Wakaba Iha, Dr. Kazuyoshi Hirayama and Dr. Shota Tanaka for their advice regarding experimental technique. We would like to thank Editage (www.editage.jp) for editorial support in the form of medical writing.

Received on February 25, 2019

Reviewed on September 6, 2019

Accepted on May 1, 2020

Published online on June 30, 2020

Cite as

Matsuoka H, Matsubara H, Sugimura A, et al. Detecting tumor-infiltrating Forkhead box P3-positive T cells in the prognosis of lung adenocarcinoma: Possible role of clustering tumor interleukin-12 subunit alpha and transforming growth factor beta 1 expression. *Adv Clin Exp Med.* 2020;29(6):715–725. doi:10.17219/acem/121922

DOI

10.17219/acem/121922

Copyright

© 2020 by Wrocław Medical University

This is an article distributed under the terms of the Creative Commons Attribution 3.0 Unported (CC BY 3.0) (<https://creativecommons.org/licenses/by/3.0/>)

Abstract

Background. While regulatory T cells (Tregs) are a poor prognostic factor for lung cancer, they may be detected as Forkhead box P3+ (FOXP3+) and cluster of differentiation (–CD) 4+ T cells by classifying FOXP3+CD4+ T cells into different subpopulations of CD4 cells.

Objectives. To classify clusters of tumor-infiltrating Tregs in lung adenocarcinoma based on the mRNA expression levels of interleukin-12 subunit alpha (*IL12A*) and transforming growth factor beta 1 (*TGFB1*) in tumor specimens.

Material and methods. Seventy-nine patients with lung adenocarcinoma were evaluated in this study. Clinical data were obtained from the patients' medical records, while tumor tissue samples were preserved as formalin-fixed paraffin-embedded (FFPE) tissue specimens. Immunohistochemical staining for CD4, CD8 and FOXP3 was performed and stained cell counts were obtained under 5 high-power fields. cDNA was synthesized from total RNA extracted from FFPE tissue specimens and amplified with Taqman probes for *FOXP3*, *IL12A*, *TGFB1*, and the glyceraldehyde-3-phosphate dehydrogenase gene.

Results. Two clusters were identified: *IL12A*low*TGFB1*low (Cluster 1: n = 44) and *IL12A*high*TGFB1*high (Cluster 2: n = 39). Although no significant difference in the FOXP3+ cell/CD4+ cell ratio was observed between the 2 clusters (p = 0.921), the high FOXP3+/CD4+ cell ratio group showed a significantly poorer relapse-free survival rate than the low FOXP3+/CD4+ cell ratio group in Cluster 1 (p = 0.031).

Conclusions. Although the results revealed no direct association between Tregs and prognosis according to each subtype, these results suggest that if a lung cancer specimen contains low levels of *IL12A* and *TGFB1*, the FOXP3+/CD4+ cell ratio is useful for predicting the prognosis of lung cancer.

Key words: adenocarcinoma, prognosis, T-lymphocytes, regulatory

Introduction

Tumor-infiltrating Forkhead box P3+ (FOXP3+) and regulatory T cells (Tregs) are poor prognostic factors for many types of malignant tumors,¹ including lung cancer.^{2–8} Recently, FOXP3+ and cluster of differentiation (CD) 4+ T cells in peripheral blood lymphocytes were classified into 3 subpopulations based on the expression levels of *FOXP3* and *CD45RA*: subpopulation I, *FOXP3^{low}CD45RA+*; subpopulation II, *FOXP3^{high}CD45RA-*; and subpopulation III, *FOXP3^{low}CD45RA-*. Subpopulation II, known as effector Tregs, exhibits suppressive activity and increased numbers of these cells are found among tumor-infiltrating lymphocytes compared to peripheral blood lymphocytes.^{9,10} In colorectal cancer (CRC), tumor infiltration, predominantly by *FOXP3^{high}/CD4+* Tregs, is strongly associated with the prognosis of malignant tumors.¹¹ In biomedical laboratories, flow cytometry is used to identify Tregs due to the difficulty in assessing effector Tregs using only formalin-fixed, paraffin-embedded (FFPE) tissues.

Saito et al. described a classification system based on mRNA expression of interleukin-12 subunit alpha (*IL12A*) and transforming growth factor beta 1 (*TGFBI*) in CRC specimens to distinguish subpopulations of (non-Treg) poor cases from Fr-III rich cases.¹¹ They classified CRC into 2 groups using this method and performed a survival analysis based on the *FOXP3* mRNA expression level in the same specimens. The current study used the same approach to evaluate lung adenocarcinoma (LAC) using only FFPE tissue. As tumor cells frequently express *FOXP3* in lung cancer, this method revealed *FOXP3* mRNA expression in lung cancer specimens, as well as the number of tumor-infiltrating Tregs.^{3,7,12–14} In flow cytometry, Tregs are assessed as a fraction using the ratio of each Fr Treg/CD4+ mononuclear cell count.¹¹ Thus, the *FOXP3+/CD4+* ratio in FFPE tissue specimens was also assessed using immunohistochemical analysis.

Lung adenocarcinoma contains several histological subpopulations that include lepidic, acinar, papillary, solid, mucinous, and micropapillary subpopulations.¹⁵ Cell density of lepidic LAC is lower than that of other subpopulations. Consequently, the stained cell counts of lepidic subpopulations tend to be lower than that of other subpopulations. Adenocarcinomas in situ and minimally invasive adenocarcinomas have been associated with positive prognoses,¹⁶ which may be partly due to the generally lower numbers of FOXP3+ cells and tumor cells in these subpopulations, compared with others. However, this feature alone does not enable adequate assessment of the relationship between cell counts and prognosis. Furthermore, *FOXP3* may appear in lung tumor cells, suggesting that the number of tumor-infiltrating Tregs is not adequately reflected by *FOXP3* levels in tumor tissue.

Against such a background, the objective of this study was to classify clusters of tumor-infiltrating Tregs

in LAC based on the mRNA expression levels of *IL12A* and *TGFBI*. This study was conducted to determine whether the FOXP3+/CD4+ cell ratio is a better estimator of the number of tumor-infiltrating Tregs in a tissue sample, and whether FOXP3+-rich regions are better for evaluating stained cell counts without being affected by the biased association with histological subpopulations.

Material and methods

Patients and samples

Seventy-nine patients with LAC who underwent pulmonary resection and regional lymph node dissection at University of Yamanashi hospital, between 2004 and 2011 were included in this study. Patients were excluded if they had other malignancies 5 years before or 2 years after LAC, complications related to autoimmune disease, had undergone treatment with non-radical excision, or had been treated using adjuvant chemotherapy. Clinical and pathological data was obtained from the patients' medical records at the hospital. Pathological data were re-evaluated according to the 8th edition of the Tumor-Node-Metastasis Classification for lung cancer.¹⁷

Ethical considerations

Tumor tissue samples were obtained during pulmonary resection and preserved as FFPE tissue specimens. All participants provided informed written consent prior to pulmonary resection. The study was approved by the Ethics Committee of University of Yamanashi. The research was conducted in accordance with the 2013 Declaration of Helsinki.

Immunohistochemical staining

The FFPE tissue blocks were sliced into 3 µm-thick tissue sections using a sliding microtome (Yamato Kohki Industrial Co., Ltd., Asaka, Japan). Following deparaffinization in xylene and dehydration using increasing concentrations of alcohol, sections were pretreated by heat-mediated antigen retrieval in a 95°C water bath with Target Retrieval Solution (DAKO, Glostrup, Denmark) at pH 6.0 for 30 min (CD4), pH 9.0 for 30 min (CD8) and pH 9.0 for 40 min (FOXP3). Prior to the application of CD8 and FOXP3 antibodies, endogenous peroxidase activity was inhibited by incubating the samples in 3.0% hydrogen peroxidase for 15 min at 37°C. For CD4, endogenous peroxidase activity was inhibited following primary antibody incubation using the same method. After protein blocking with Blocking I (Nacalai Tesque, Kyoto, Japan) for 15 min at 37°C, sections were incubated for an additional 2 h at 37°C with anti-CD4 (rabbit monoclonal, dilution 1:100; ab133616), anti-CD8 (mouse monoclonal, dilution 1:50; ab17147) and

anti-FOXP3 (mouse monoclonal, dilution 1:100; ab20034) antibodies (Abcam, Cambridge, UK). After being washed 3 times with phosphate-buffered saline (PBS), sections were incubated for 30 min at 37°C with secondary antibodies: Histofine Max-PO(M) (horseradish peroxidase (HRP)-conjugated anti-mouse immunoglobulin polyclonal) and Histofine Max-PO(R) (HRP-conjugated anti-rabbit immunoglobulin polyclonal; Nichirei Biosciences, Inc., Tokyo, Japan). A 3,3'-diaminobenzidine peroxidase stain kit (Nacalai Tesque) was used as the chromogen. Sections were counterstained using hematoxylin. Positive and negative staining controls for CD4/8 and FOXP3 were prepared using lymph node and tonsil sections, respectively. Staining of the positive control was performed as described above. The negative control was stained using PBS rather than with primary antibodies.

Evaluation of immunohistochemical staining

For CD4 and FOXP3, continuous sections were stained and counted. FOXP3+-rich regions in the tumor stroma were selected for counting CD4+ and FOXP3+ cell numbers. CD8+-rich regions in the tumor stroma were selected for counting CD8+ cell numbers. Each count was based on 5 fields from high-powered digital images ($\times 400$ magnification). The average cell count was used for statistical analysis. FOXP3+ tumors were defined as $>20\%$ staining of tumor cells in a section as previously described.³

Quantitative real-time polymerase chain reaction

Total RNA was extracted from FFPE tumor specimens using an Ambion™ MagMAX™ FFPE Total Nucleic Acid Isolation Kit (Invitrogen, Carlsbad, USA). Next, cDNA was synthesized from 0.5 μg of total RNA using a SuperScript III Reverse Transcriptase Kit with random primers (Invitrogen) and amplified via 10.0 μM each of Taqman probe (*FOXP3*, *IL12A*, *TGFBI*, and glyceraldehyde-3-phosphate dehydrogenase (*GAPDH*); Applied Biosystems, Foster City, USA) and 10.0 μL of Taqman Gene Expression Master Mix (Life Technologies, Carlsbad, USA) according to the manufacturer's instructions. Relative mRNA expression was evaluated after normalization to *GAPDH* expression.

Tumor cell content analysis

Tissue sections continuous to FFPE tumor specimens used to extract RNA were stained with hematoxylin and eosin (H&E) and analyzed using ImageJ software (National Institutes of Health, Bethesda, USA; <http://rsb.info.nih.gov/ij/>). Analysis was based on 5 fields of view randomly chosen within the limits of RNA extraction in high-powered digital images ($\times 400$ magnification). The margins

of the tumor cells were marked and the enclosed area was calculated as the area of the tumor cells. Total cell area was calculated by excluding any cell-free areas from the overall area of each image. The tumor content ratio was determined by the tumor cell area divided by the total cell area.

Statistical analyses

Categorical variables were compared using Fisher's exact tests and continuous variables were compared using non-parametric Mann–Whitney U tests or Kruskal–Wallis one-way analysis of variance (ANOVA) and post hoc Tukey's tests. All statistical analyses were conducted using SPSS v. 24.0 software (IBM Corp., Armonk, USA). Statistical significance was set at $p < 0.05$. The cut-off value for experimental data was defined using Youden's index (J) as follows; $J = \text{sensitivity} + \text{specificity} - 1$, for variables with $p < 0.05$ (recurrence: "yes" vs "no"). Remaining continuous variables were divided by the median value. Survival curves were estimated using the Kaplan–Meier method and compared using the log-rank test. Cox proportional hazards models were used for univariate and multivariate analyses. Relapse-free survival was used as a dependent variable. Independent variables were selected from categorical variables that were significant according to univariate analysis ($p < 0.05$).

Results

Patient characteristics

A total of 79 LAC patients were included in this study. The mean age was 67.2 years (range: 32–88 years) and 38.0% (30/79) were males. Nineteen percent (15/79) of these patients were relapsed LAC cases. The mean total tumor size was 2.48 cm (range: 0.6–8.0 cm), and 81% (64/79) of patients were at the pathological stage of 0–1. Histological subtypes of the tumors were lepidic in 30/79 cases, acinar in 17/79, papillary in 16/79, solid in 9/79, and mucinous in 7/79. Fifty-four percent (43/79) of tumor samples were positive for FOXP3 staining.

Immunohistochemical staining analysis

In the positive controls, the cytoplasm of lymphocytes in lymph node tissue specimens was stained with CD4 and CD8 antibodies, whereas nuclei were stained with FOXP3 antibodies. For positive controls, cells displaying nuclear FOXP3 staining were confirmed as lymphocytes using CD4/CD8 antibodies, while cells displaying cytoplasmic FOXP3 staining were confirmed as non-lymphocytes. In negative controls, it was confirmed that tonsil tissue specimens were not stained by secondary antibodies in the absence of primary antibodies.

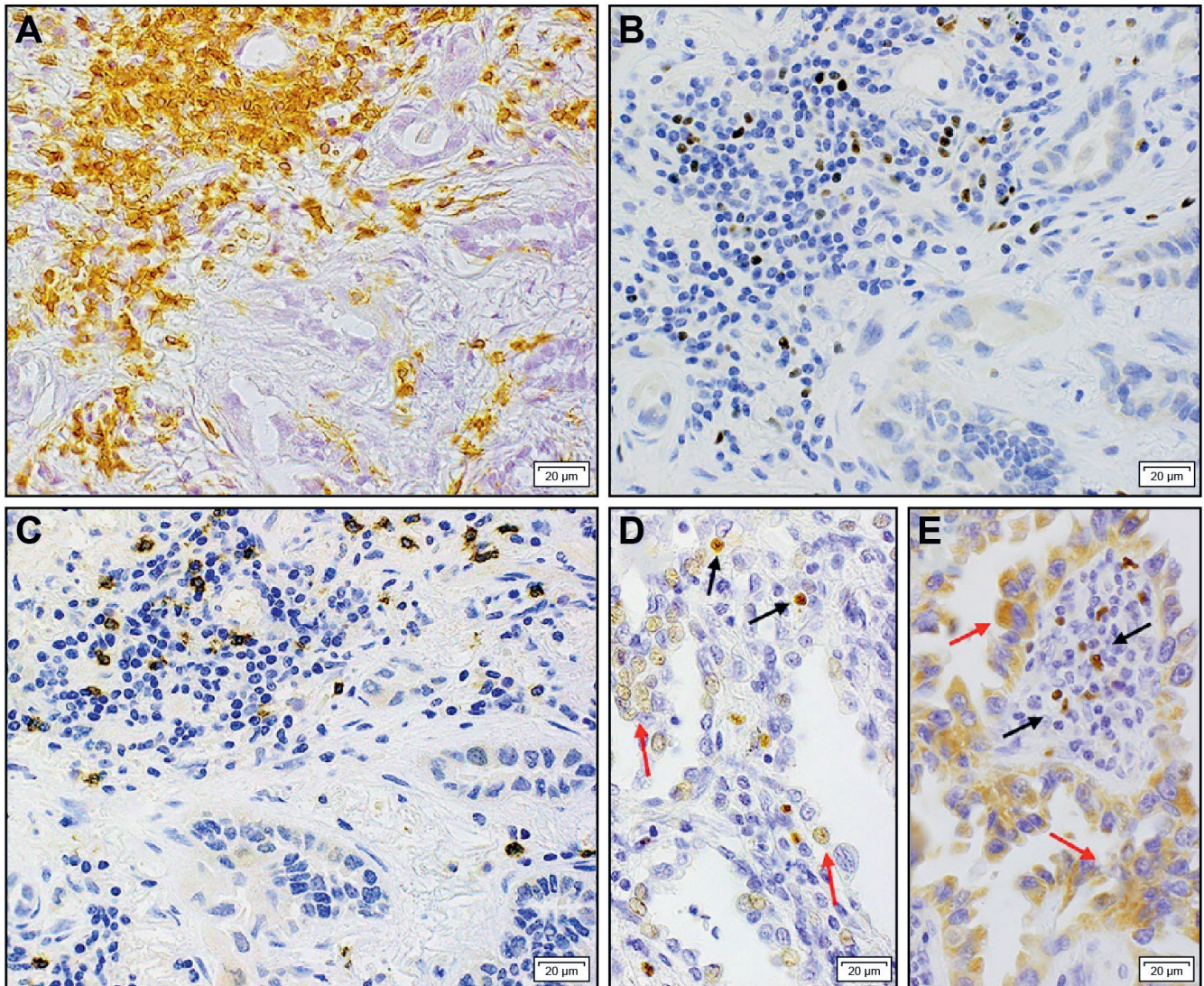


Fig. 1. Forkhead box P3 (FOXP3) antibody staining of lung cancer tissues. A. Staining of lymphocyte cytoplasm for CD4. B. Staining of nuclei for FOXP3. C. Staining of cytoplasm for CD8. D. FOXP3 staining was observed in nuclei of tumor cells (red arrow) and nuclei of lymphocytes (black arrow). E. FOXP3 staining was observed in the cytoplasm of tumor cells (red arrow) and nuclei of lymphocytes (black arrow). The red arrows indicate stained cancer nuclei (D) and cytoplasm (E). The black arrows indicate stained lymphocytes. All images were acquired using tumor tissues

Forty-three LAC samples (54.4%) were positively stained with FOXP3 antibodies (Fig. 1A–E). In these samples, FOXP3 was mainly concentrated in areas rich in CD4+ and/or CD8+ cells and was localized to the nuclei of lymphocytes, as well as to either the nuclei or cytoplasm of non-lymphocytic tumor cells (Fig. 1D,E). The mean FOXP3+ cell count in tumor samples from relapsed patients ($n = 15$) was significantly higher than that in samples from non-relapsed patients ($n = 64$) at 63 cells compared to 37 cells, respectively ($p = 0.018$). There were more CD4+ cells than FOXP3+ cells in all LAC samples, and therefore FOXP3+/CD4+ cell count ratios ranged between 0.05 and 0.48. The mean FOXP3+/CD4+ cell count ratio was significantly higher in relapsed than in non-relapsed patients (0.23 vs 0.16, respectively; $p = 0.012$). FOXP3+/CD8+ cell count ratios varied between samples, within a range between 0.04 and 1.94.

mRNA expression and clustering analysis

The median relative mRNA expression levels of *FOXP3*, *IL12A* and *TGFBI* in lung tumor specimens were set to 1.0. The mRNA expression level ranges were 0.10–5.12, 0.07–5.58 and 0.14–3.36, respectively. Two clusters were identified by unsupervised hierarchical clustering analysis based on *IL12A* and *TGFBI* expression levels. A heatmap was generated, where red indicated high levels of mRNA expression and blue indicated low levels of mRNA expression for each gene of interest. Most Cluster 1 analyses exhibited low levels of *IL12A* and *TGFBI* expression, while Cluster 2 analyses exhibited high mRNA expression levels of *IL12A* and *TGFBI* (Fig. 2).

Although lung tumor *FOXP3* expression was significantly higher in Cluster 2 than in Cluster 1 ($p < 0.001$), for *FOXP3*+ cases compared with *FOXP3*– cases ($p < 0.05$)

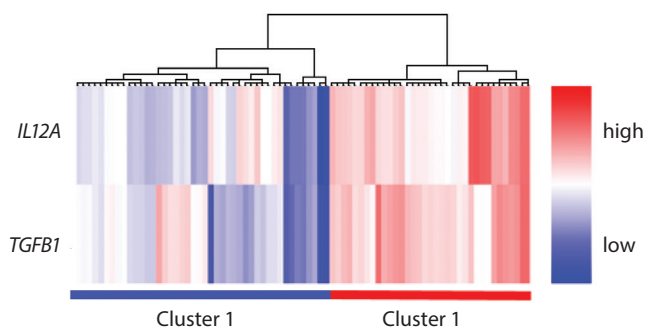


Fig. 2. Expression levels of interleukin-12 subunit alpha (*IL12A*) and transforming growth factor beta 1 (*TGFB1*) in Cluster 2. Heatmap images were created using RNA expression to *GAPDH* expression ratios (mean value of 3 samples was used in the analysis). Logarithmic transformation was used to determine the normal distributions of RR values, which were standardized using Z-scores. “0” is shown in white and $\pm 2SD$ is shown in red and blue, respectively

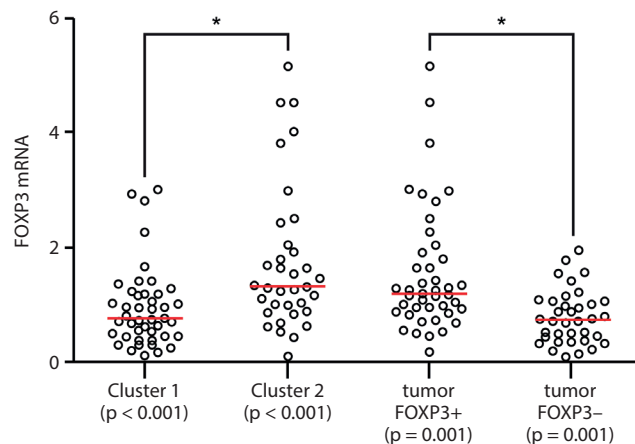


Fig. 3. *FOXP3* expression levels in clusters, FOXP3+, and FOXP3– cases. *IL12A*^{low}*TGFB1*^{low} (Cluster 1: n = 44); *IL12A*^{high}*TGFB1*^{high} (Cluster 2: n = 39)

FOXP3 – Forkhead box P3.

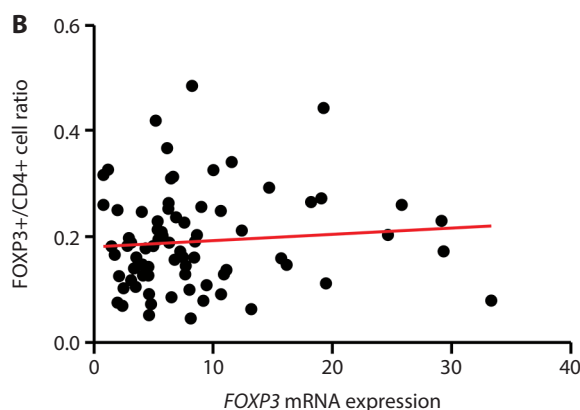
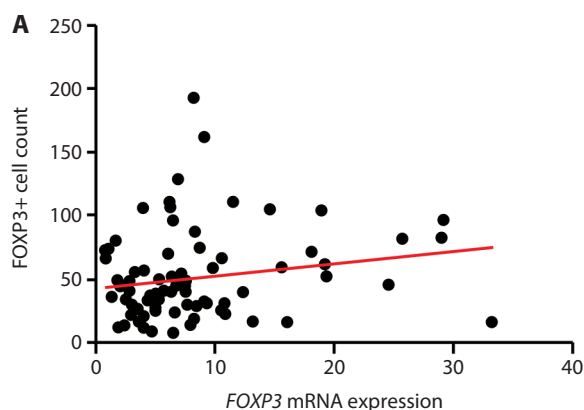


Fig. 4. Correlation analysis for *FOXP3* mRNA expression. Correlation between *FOXP3* mRNA expression and *FOXP3*+ cell counts (A) or *FOXP3*+/*CD4*+ cell ratio (B) in lung tumor tissues was not significant

(Fig. 3), Spearman’s rank-order correlation indicated that *FOXP3* mRNA expression was unrelated to *FOXP3*+ cell counts (correlation coefficients: 0.171, $p = 0.131$; Fig. 4A) or the *FOXP3*+/*CD4*+ cell ratio (correlation coefficients: 0.0819, $p = 0.472$; Fig. 4B). Survival curves for all groups are shown (Fig. 5). Cluster 1 showed a higher survival rate compared to Cluster 2, when clusters of all cases were compared.

Association between clinicopathological characteristics and experimental data

The *FOXP3*+ cell counts and *FOXP3*+/*CD4*+ cell ratios were significantly higher in lung tumor samples from relapsed cases than from non-relapsed cases ($p = 0.018$ and $p = 0.012$, respectively), and expression level of each mRNA was significantly lower in the relapsed groups than in the non-relapsed group ($p < 0.01$) (Table 1).

Clusters 1 and 2 comprised 44 and 35 patients, respectively. Cluster 1 patients showed unfavorable pathological characteristics, such as large tumor diameter, lymph node metastasis and vascular invasion, compared with

Cluster 2 patients. Although Cluster 1 patients showed a significantly higher risk of recurrence than Cluster 2 patients ($p = 0.039$), no significant differences in *FOXP3*+ cell counts or *FOXP3*+/*CD4*+ cell ratios were observed between the 2 clusters. Cluster 1 comprised 14 relapsed patients and 30 non-relapsed patients. *FOXP3*+ cell counts and *FOXP3*+/*CD4*+ and *FOXP3*+/*CD8*+ cell ratios were significantly higher in lung tumor samples from relapsed cases than in those from non-relapsed cases of Cluster 1. *FOXP3* mRNA expression was significantly lower in samples from relapsed cases than in non-relapsed cases (Table 2).

Association between the tumor cell content and other experimental data

The mean tumor content ratio was 0.373 (range: 0.088–79.4). When samples were divided into 3 evenly sized groups according to tumor cell content ratio, no significant differences in cell counts or mRNA expression levels were observed. However, the amount of mRNA extracted from the low tumor content ratio group was significantly less than in the high tumor content ratio group (Table 3).

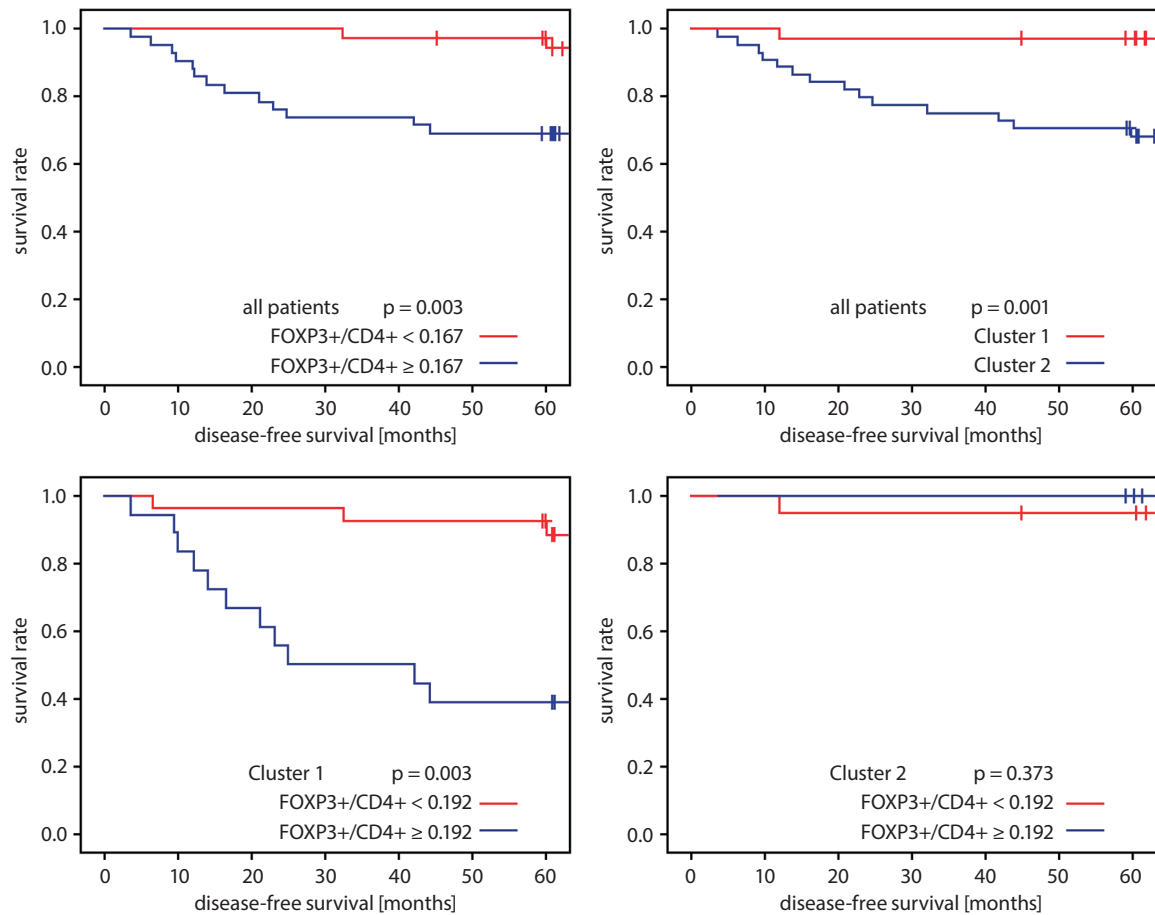


Fig. 5. Survival curves for all groups. The upper left panel shows the FOXP3+/CD4+ ratio of lung tumor tissue samples for all cases. The upper right panel shows the comparison between clusters of all cases. The bottom left panel shows the FOXP3+/CD4+ ratio of Cluster 1. The bottom right panel shows the comparison of FOXP3+/CD4+ ratio of Cluster 2

FOXP3 – Forkhead box P3; CD – cluster of differentiation. Survival curves were estimated using the Kaplan–Meier method and compared using the log-rank test.

Univariate and multivariate analysis of risk factors affecting relapse-free survival rate

Univariate analysis of all cases revealed older age (>73 years), larger total tumor size (>2.9 cm), larger invasion size (>2.4 cm), advanced T/N factor, advanced pathological stage, pleural invasion, advanced tumor grade, lymphatic invasion, vessel invasion, solid adenocarcinoma, higher tumor FOXP3+/CD4+ cell ratio, FOXP3– tumor, lower tumor *FOXP3*, as well as *IL12A*, and *TGFB1* mRNA expression levels and larger tumor cell content ratio (>0.55) as poor prognostic factors for relapse-free survival. In Cluster 1 patients, univariate analysis revealed that larger total tumor size (>3.5 cm), larger invasion size (>2.4 cm), advanced N factor, advanced pathological stage, lymphatic invasion, vessel invasion, higher tumor FOXP3+/CD4 cell ratio (>0.192), higher tumor FOXP3+/CD8+ cell ratio (>0.400), as well as lower tumor *FOXP3* and *TGFB1* mRNA expression levels were poor prognostic factors affecting relapse-free survival (Table 4).

In multivariate analysis of all cases, advanced N factor, advanced pathological stage, and vessel invasion, were confirmed as independent prognostic factors for relapse-free survival. In Cluster 1 patients, multivariate analysis confirmed larger total tumor size (>3.5 cm), advanced N factor, vessel invasion, and higher tumor *FOXP3*+/*CD4*+ cell ratio (>0.192) as independent prognostic factors for relapse-free survival (Table 5).

Discussion

Tregs play a key immunosuppressive role in malignant tumors.^{18–20} High tumor-infiltrating Tregs and peripheral blood Treg counts are poor prognostic factors for lung cancer.^{2–8} Treg fractions have been described previously. Flow cytometry is required to distinguish between fractions. In CRC, Saito et al. reported that FOXP3+ non-Tregs in tumor samples were associated with inflammation and that their development depended on the secretion of *IL12A* and *TGFB1* from tumor cells or tumor-associated cells.¹¹

Table 1. Comparison of *FOXP3*, *IL12A* and *TGFB1* mRNA expression levels and patient characteristics

Characteristics	Mean relative mRNA ^a expression level (range)					
	<i>FOXP3</i>	p-value ^b	<i>IL12A</i>	p-value ^b	<i>TGFB1</i>	p-value ^b
Age [years] <73 (n = 29) ≥73 (n = 50)	6.76 (0.68, 29.14) 4.88 (0.70, 33.18)	0.32	0.25 (0.05, 1.15) 0.15 (0.01, 0.88)	<0.001	0.89 (0.12, 2.57) 0.53 (0.11, 2.53)	0.04
Sex male (n = 30) female (n = 49)	4.91 (0.68, 29.01) 7.45 (1.06, 33.18)	0.03	0.19 (0.02, 1.15) 0.23 (0.01, 1.01)	0.45	0.72 (0.11, 2.57) 0.88 (0.11, 2.46)	0.29
Emphysema yes (n = 13) no (n = 66)	4.59 (2.43, 18.90) 6.76 (0.68, 33.18)	0.47	0.14 (0.04, 0.42) 0.23 (0.01, 1.15)	0.03	0.53 (0.15, 1.16) 0.88 (0.11, 2.57)	0.05
Tumor factor Tis,1 (n = 57) T2–4 (n = 32)	7.12 (0.68, 33.18) 4.16 (0.70, 18.90)	0.03	0.24 (0.01, 1.15) 0.13 (0.02, 0.35)	0	0.94 (0.11, 2.57) 0.47 (0.11, 1.41)	<0.001
Nodal factor N0 (n = 70) N1,2 (n = 9)	6.97 (0.68, 33.18) 2.95 (1.82, 9.82)	0.01	0.23 (0.02, 1.15) 0.09 (0.01, 0.22)	0	0.85 (0.11, 2.57) 0.45 (0.11, 1.01)	0.01
Pathological stage stage 0, I (n = 64) stage II, III (n = 15)	6.97 (0.68, 33.18) 3.52 (0.70, 18.90)	0.03	0.24 (0.01, 1.15) 0.12 (0.02, 0.31)	0	0.92 (0.11, 2.57) 0.45 (0.11, 1.01)	0
pl factor pl0 (n = 69) pl1–3 (n = 10)	6.83 (0.68, 33.18) 3.12 (1.06, 14.52)	0.01	0.23 (0.01, 1.15) 0.15 (0.05, 0.35)	0.13	0.87 (0.11, 2.57) 0.45 (0.22, 1.05)	0.02
Lymphatic invasion negative (n = 61) positive (n = 18)	6.83 (0.68, 33.18) 5.32 (0.70, 14.52)	0.14	0.24 (0.05, 1.15) 0.13 (0.01, 0.31)	0	0.94 (0.12, 2.57) 0.37 (0.11, 1.01)	<0.001
Vessel invasion negative (n = 62) positive (n = 17)	6.76 (0.68, 33.18) 4.46 (0.70, 15.57)	0.1	0.24 (0.04, 1.15) 0.13 (0.01, 0.35)	0	0.93 (0.12, 2.57) 0.45 (0.11, 1.21)	<0.001
Grade G1 (n = 37) G2,3 (n = 42)	7.47 (0.68, 33.18) 5.81 (0.70, 19.29)	0.04	0.27 (0.07, 1.15) 0.17 (0.01, 0.88)	0	1.05 (0.29, 2.57) 0.50 (0.11, 2.53)	<0.001
Histological subtype lepidic (n = 30) mucinous (n = 7) acinar (n = 17) papillary (n = 16) solid (n = 9)	8.17 (0.68, 33.18) 5.28 (1.28, 10.55) 5.61 (1.06, 19.29) 6.54 (2.43, 15.57) 2.95 (0.70, 9.82)	0.01	0.28 (0.07, 1.15) 0.18 (0.09, 1.01) 0.20 (0.05, 0.88) 0.18 (0.05, 0.43) 0.08 (0.01, 0.49)	0.01	1.11 (0.29, 2.57) 0.76 (0.45, 1.50) 0.69 (0.22, 2.53) 0.52 (0.12, 1.21) 0.33 (0.11, 1.55)	<0.001
Tumor FOXP3 staining negative (n = 36) positive (n = 43)	4.38 (0.68, 29.01) 7.67 (1.06, 33.18)	0	0.20 (0.02, 1.15) 0.23 (0.01, 1.01)	0.57	0.73 (0.11, 1.96) 0.90 (0.11, 2.57)	0.22

FOXP3 – Forkhead box P3; *IL12A* – interleukin-12 subunit alpha; *TGFB1* – transforming growth factor beta 1; G – grade. ^amRNA level relative to *GAPDH*; ^bmean expression levels for each mRNA type was compared between patient characteristic subgroups. Categorical variables were compared using Fisher’s exact tests and continuous variables were compared using nonparametric Mann–Whitney U tests or Kruskal–Wallis one-way ANOVA and post hoc Tukey tests.

Particularly, *TGFB1* influences metastasis through epithelial-to-mesenchymal transition by transactivating epidermal growth factor signaling.²¹

Cluster analysis performed as previously described¹¹ revealed 2 clusters of tumor samples. Cluster 1 was characterized by *IL12A*^{low}*TGFB1*^{low} and Cluster 2 by *IL12A*^{high}*TGFB1*^{high}.¹¹ Although no significant differences in FOXP3+ cell counts or FOXP3+/CD4+ cell ratios were observed between these 2 clusters, Cluster 1 patients showed a significantly higher risk for recurrence than Cluster 2 patients. Moreover, among Cluster 1 patients, the high FOXP3+/CD4+ cell ratio group was associated with a significantly poorer relapse-free survival rate than that of the low

FOXP3+/CD4+ cell ratio group. Although there was no direct association between Tregs and prognosis according to each subtype, clustering based on tumor *IL12A* and *TGFB1* mRNA expression may be useful to exclude cases in which Tregs are not associated with disease prognosis.

The findings indicate that this method may be useful for excluding groups without immune escape by Tregs, thereby increasing the accuracy of analysis. Secondly, using Treg evaluation as a marker for treatment adaptation and effective prediction will likely enhance case exclusion accuracy and enable administration of treatments targeting Tregs (such as CTLA-4 inhibitors) in clinical practice.

FOXP3 staining of tumor cells has been reported

Table 2. Comparison of clinical and experimental characteristics among relapsed and non-relapsed and Cluster 1 and 2 patients (n = 79) with lung adenocarcinoma

Characteristics	All patients					
	non-relapsed	relapsed	p-value	Cluster 1	Cluster 2	p-value
Number of patients	64	15		44	35	
Age [years] (range)	67 (32–78)	74 (36–88)	0.024	73 (32–88)	65 (48–83)	0.039
Gender (%)						
male	21 (32.8)	9 (60.0)	0.075	20 (45.5)	10 (28.6)	0.163
female	43 (67.2)	6 (40.0)		24 (54.5)	25 (71.4)	
Emphysema (%)						
yes	8 (12.5)	5 (33.3)	0.114	12 (27.3)	1 (2.9)	0.005
no	56 (87.5)	10 (66.7)		32 (72.7)	34 (97.1)	
total size [cm] (range)	2.0 (0.6–5.5)	3.8 (1.2–8.0)	<0.001	2.5 (1.2–8.0)	1.8 (0.6–3.8)	<0.001
invasion size [cm] (range)	1.2 (0–5.4)	3.0 (0.8–8.0)	<0.001	2.4 (0.1–8.0)	0.6 (0.0–3.8)	<0.001
Tumor factor (%)						
Tis,1	52 (81.2)	5 (33.3)	0.001	25 (56.8)	32 (91.4)	0.001
T2–4	12 (18.8)	10 (66.7)		19 (43.2)	3 (8.6)	
Nodal factor (%)						
N0	63 (98.4)	7 (46.7)	<0.001	36 (81.8)	34 (97.1)	0.039
N1,2	1 (1.6)	8 (53.3)		8 (18.2)	1 (2.9)	
Pathological stage (%)						
stage 0, I	60 (93.8)	4 (26.7)	<0.001	30 (68.2)	34 (97.1)	0.001
stage II, III	4 (6.2)	11 (73.3)		14 (31.8)	1 (2.9)	
pl factor (%)						
pI0	60 (93.8)	9 (60.0)	0.002	35 (79.5)	34 (97.1)	0.037
pI1–3	4 (6.2)	6 (40.0)		9 (20.5)	1 (2.9)	
Lymphatic invasion (%)						
negative	56 (87.5)	5 (33.3)	<0.001	27 (61.4)	34 (97.1)	<0.001
positive	8 (12.5)	10 (66.7)		17 (38.6)	1 (2.9)	
Vessel invasion (%)						
negative	56 (87.5)	6 (40.0)	<0.001	30 (68.2)	32 (91.4)	0.014
positive	8 (12.5)	9 (60.0)		14 (31.8)	3 (8.6)	
Grade (%)						
G1	36 (56.2)	1 (6.7)	<0.001	11 (25.0)	26 (74.3)	<0.001
G2,3	28 (43.8)	14 (93.3)		33 (75.0)	9 (25.7)	
Histological subtype (%)						
lepidic	29 (45.3)	1 (6.7)	0.001	8 (18.2)	22 (62.9)	<0.001
mucinous	6 (9.4)	1 (6.7)		3 (6.8)	4 (11.4)	
acinar	15 (23.4)	2 (13.3)		12 (27.3)	5 (14.3)	
papillary	10 (15.6)	6 (40.0)		14 (31.8)	2 (5.7)	
solid	4 (6.2)	5 (33.3)		7 (15.9)	2 (5.7)	
Tumor FOXP3 staining (%)						
negative	25 (39.1)	11 (73.3)	0.022	22 (50.0)	14 (40.0)	0.496
positive	39 (60.9)	4 (26.7)		22 (50.0)	21 (60.0)	
Cell count						
CD4+ (range)	236 (64–636)	256 (127–556)	0.626	246 (106–636)	236 (64–556)	0.782
CD8+ (range)	142 (66–418)	194 (67–284)	0.127	169 (67–418)	129 (66–276)	0.009
FOXP3+ (range)	37 (8–193)	63 (9–111)	0.018	44 (9–163)	40 (8–193)	0.594
Cell count ratio						
CD4+/CD8+ (range)	1.57 (0.35–7.60)	1.50 (0.57–5.35)	0.565	1.49 (0.47–7.60)	1.92 (0.35–4.18)	0.129
FOXP3+/CD4+ (range)	0.16 (0.05–0.48)	0.23 (0.07–0.44)	0.012	0.17 (0.05–0.44)	0.19 (0.05–0.48)	0.921
FOXP3+/CD8+ (range)	0.23 (0.07–1.94)	0.40 (0.04–1.57)	0.127	0.23 (0.04–1.94)	0.3 (0.08–1.20)	0.319
mRNA expression levels						
<i>IL12A</i> (range)	1.18 (0.07–5.58)	0.62 (0.09–1.39)	0.006	0.64 (0.07–1.67)	1.57 (0.86–5.58)	<0.001
<i>TGFβ1</i> (range)	1.16 (0.14–3.36)	0.58 (0.14–1.37)	0.001	0.65 (0.14–1.96)	1.52 (0.92–3.36)	<0.001
<i>FOXP3</i> (range)	1.12 (0.10–5.12)	0.54 (0.11–2.24)	<0.001	0.74 (0.11–2.98)	1.29 (0.10–5.12)	<0.001
Cluster (%)						
Cluster 1	30 (46.9)	14 (93.3)	0.001			
Cluster 2	34 (53.1)	1 (6.7)				

(+) – positive; CD – cluster of differentiation; *FOXP3* – Forkhead box P3; *IL12A* – interleukin-12 subunit alpha; mRNA – messenger RNA; pl – pleural invasion; *TGFβ1* – transforming growth factor beta 1; G – grade.

Table 3. Characteristics of tumor samples by tumor cell content (high >46%, intermediate 27–46%, low <27%)

Parameter	All patients			p-value
	high (n = 27)	intermediate (n = 26)	low (n = 26)	
Patients per cluster (%)				
Cluster 1	16 (59.3)	16 (16.5)	12 (46.2)	0.482
Cluster 2	11 (40.7)	10 (38.5)	14 (53.8)	
Cell count				
CD4+ (range)	237 (91–481)	247 (64–597)	242 (106–636)	0.942
CD8+ (range)	156 (67–418)	152 (66–331)	136 (83–336)	0.566
FOXP3+ (range)	40 (8–193)	43 (9–104)	42 (14–163)	0.79
mRNA expression levels				
FOXP3 (range)	1.00 (0.11–5.12)	0.88 (0.10–4.48)	1.22 (0.45–4.50)	0.183
IL12A (range)	0.92 (0.07–4.91)	0.97 (0.18–5.58)	1.19 (0.25–4.74)	0.272
TGFB1 (range)	0.96 (0.14–2.36)	1.00 (0.16–2.32)	1.25 (0.31–3.36)	0.438
Extracted mRNA [µl/mL]	66.9 (13.5–284)	43.4 (8.7–174.0)	36.8 (11.6–94.7)	0.006

(+) – positive; CD – cluster of differentiation; FOXP3 – Forkhead box P3; IL12A – interleukin-12 subunit alpha; TGFB1 – transforming growth factor beta 1.

Table 4. Univariate analysis of clinical and experimental characteristics influencing the relapse-free survival of all patients (n = 79) and Cluster 1 patients (n = 44) with lung adenocarcinoma

Characteristics	All patients			Cluster 1 patients		
	hazard ratio	95% CI	p-value	hazard ratio	95% CI	p-value
Age; elder	5.677	1.805–17.86	0.003	1.913	0.600–6.102	0.273
Gender; male	2.578	0.917–7.248	0.073	2.347	0.785–7.018	0.127
Emphysema; Yes	2.707	0.924–7.931	0.07	1.49	0.499–4.454	0.475
Total tumor size; large	13.49	4.559–39.95	<0.001	3.861	1.133–9.466	0.012
Invasion size; large	8.532	2.711–26.85	<0.001	5.418	1.867–15.72	0.002
Tumor factor; 2–4	6.665	2.272–19.55	<0.001	2.899	0.970–8.662	0.057
Nodal factor; 1–2	21.97	7.599–63.51	<0.001	17.89	3.447–30.26	<0.001
p-stage; II–III	20.29	6.363–64.67	<0.001	8.728	2.309–23.90	<0.001
Pleural invasion (+)	6.542	2.316–18.48	<0.001	2.716	0.908–8.123	0.074
Lymphatic invasion (+)	8.932	3.037–26.27	<0.001	4.608	1.438–14.76	0.01
Vessel invasion (+)	7.182	2.546–20.26	<0.001	3.591	1.242–10.38	0.018
G; 2–3	14.9	1.959–113.4	0.009	5.373	0.702–41.12	0.105
Subtype; solid	5.279	1.796–15.52	0.002	2.684	0.839–8.583	0.096
CD4+ cell; high	1.173	0.425–3.234	0.758	1.054	0.369–3.006	0.922
CD8+ cell; high	2.009	0.687–5.878	0.203	1.322	0.458–3.811	0.606
FOXP3+ cell; high	3.11	0.989–9.775	0.052	2.947	0.922–9.421	0.068
CD4+/CD8+; low	1.173	0.417–3.175	0.758	1.039	0.364–2.963	0.943
FOXP3+/CD4+; high	4.188	1.332–13.17	0.014	7.691	2.129–27.78	0.002
FOXP3+/CD8+; high	3.099	0.986–9.742	0.053	4.745	1.625–13.86	0.004
Tumor FOXP3; (+)	0.2593	0.083–0.815	0.021	0.315	0.099–1.007	0.051
FOXP3 expression; low	4.329	1.567–11.96	0.005	3.213	1.072–9.626	0.037
IL12A expression; low	10.81	2.438–47.96	0.002	1.411	0.489–4.067	0.524
TGFB1 expression; low	9.257	2.607–32.87	<0.001	3.276	1.025–10.47	0.045
Tumor cell content ratio; low	0.2037	0.072–0.575	0.003	0.280	0.067–1.175	0.08

(+) – positive; CD – cluster of differentiation; FOXP3 – Forkhead box P3; G – grade; IL12A – interleukin-12 subunit alpha; p – pathological; TGFB1 – transforming growth factor beta 1; 95% CI – 95% confidence interval.

Table 5. Multivariate analysis of risk factors for relapse-free survival rate among all patients (n = 79) and among Cluster 1 patients (n = 44) with lung adenocarcinoma

Characteristics	Hazard ratio	95% CI	p-value
All patients			
nodal factor; 1–2	5.219	1.576–17.29	0.007
p-stage; II–III	11.37	3.101–41.71	<0.001
vessel invasion (+)	4.817	1.603–14.48	0.005
Cluster 1 patients			
total tumor size; large	3.88	1.223–12.31	0.021
nodal factor; 1–2	7.683	2.317–22.17	<0.001
vessel invasion (+)	3.945	1.005–8.889	0.022
FOXP3+/CD4+; high	4.461	1.530–21.80	0.031

(+) – positive; CD – cluster of differentiation; FOXP3 – Forkhead box P3; p – pathological; 95% CI – 95% confidence interval.

in various types of malignancies, including breast, gastric and lung cancer.^{3,7,12–14,22,23} In gastric cancer, tumor FOXP3+ staining has been reported as a favorable prognostic factor.²⁴ However, tumor FOXP3+ expression was reported as a poor prognostic factor for oral and oropharyngeal squamous cell carcinomas.²⁵ In breast cancer, the effect of tumor FOXP3+ staining reportedly differs according to location, with nuclear expression associated with a favorable prognosis and cytoplasmic expression associated with a poor prognosis.²³ One study suggested that, in lung cancer, tumor FOXP3+ staining was not a prognostic factor,³ while another study reported that high tumor FOXP3 expression was associated with a favorable prognosis.⁷ The current study did not observe a correlation between lung tumor FOXP3+ staining and FOXP3 expression. Additionally, both FOXP3+ staining as well as high FOXP3 expression in lung tumor samples were associated with a favorable prognosis.

Highly specific information can be elicited by examining the FOXP3+/CD4+ ratios and subpopulations from *IL12A* and *TGFBI*, as well as by considering non-Tregs and excluding groups that are unrelated to prognosis.

This study had some limitations. First, FOXP3 mRNA was derived from both tumor cells and other cells in the tumor microenvironment. Multivariate analysis did not reveal a significant difference in relapse-free survival. It cannot be conclusively stated that tumor FOXP3 expression is a poor prognostic factor. However, the effect of tumor FOXP3 expression on assessing tumor-infiltrating Tregs was not negligible, as indicated by mRNA expression of FOXP3 in tumor specimens. Thus, when assessing FOXP3+ T cells the use of tumor FOXP3 mRNA expression should be avoided in tumors that frequently express FOXP3. Second, although there were no significant differences in mRNA expression of FOXP3, *IL12A* and *TGFBI* between the 3 groups when divided according to the tumor cell content, higher tumor cell content ratio was related



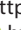







to recurrence in univariate analysis, and the higher tumor cell content group tended to have lower mRNA expression of *IL12A* and *TGFBI*. Therefore, tumor cell content ratio can be a confounding factor of mRNA expression analysis when sampling tumor cells and interstitial tissue together.

This is the first study to apply cluster classification of *IL12A* and *TGFBI* to lung cancer. In addition, we demonstrated the possibility of selecting non-Tregs without the need for flow cytometry analysis.

Conclusions

This study suggests that assessing tumor-infiltrating Tregs in lung cancer from FFPE tissues may be useful in evaluating FOXP3+/CD4+ cell ratios and classifying tumors according to *IL12A* and *TGFBI* mRNA expression levels. However, care should be taken, as tumor cells frequently express FOXP3. Further studies are needed to clarify this diagnostic confounder.

ORCID iDs

Hiroyasu Matsuoka  <https://orcid.org/0000-0002-7850-5258>
 Hirochika Matsubara  <https://orcid.org/0000-0001-7622-4957>
 Aya Sugimura  <https://orcid.org/0000-0002-9241-6948>
 Tsuyoshi Uchida  <https://orcid.org/0000-0002-5462-6565>
 Tamo Kunimitsu  <https://orcid.org/0000-0001-7557-4891>
 Tomofumi Ichihara  <https://orcid.org/0000-0002-5072-8425>
 Yuichiro Oonuki  <https://orcid.org/0000-0002-4448-1403>
 Yoshihiro Miyauchi  <https://orcid.org/0000-0003-2010-1434>
 Tetsuo Kondo  <https://orcid.org/0000-0003-2268-0302>
 Hiroyuki Nakajima  <https://orcid.org/0000-0003-1555-4033>

References

- Shang B, Liu Y, Jiang SJ, Liu Y. Prognostic value of tumor-infiltrating FoxP3+ regulatory T cells in cancers: A systematic review and meta-analysis. *Sci Rep.* 2015;5:15179.
- Shimizu K, Nakata M, Hirami Y, Yukawa T, Maeda A, Tanemoto K. Tumor-infiltrating Foxp3+ regulatory T cells are correlated with cyclooxygenase-2 expression and are associated with recurrence in resected non-small cell lung cancer. *J Thorac Oncol.* 2010;5(5):585–590.
- Tao H, Mimura Y, Aoe K, et al. Prognostic potential of FOXP3 expression in non-small cell lung cancer cells combined with tumor-infiltrating regulatory T cells. *Lung Cancer.* 2012;75(1):95–101.
- Hasegawa T, Suzuki H, Yamaura T, et al. Prognostic value of peripheral and local forkhead box P3+ regulatory T cells in patients with non-small-cell lung cancer. *Mol Clin Oncol.* 2014;2(5):685–694.
- O’Callaghan DS, Rexhepaj E, Gately K, et al. Tumour islet Foxp3+ T-cell infiltration predicts poor outcome in nonsmall cell lung cancer. *Eur Respir J.* 2015;46(6):1762–1772.
- Jackute J, Zemaitis M, Pranys D, et al. The prognostic influence of tumor infiltrating Foxp3(+)CD4(+), CD4(+) and CD8(+) T cells in resected non-small cell lung cancer. *J Inflamm (Lond).* 2015;12:63.
- Usó M, Jantus-Lewintre E, Bremnes RM, et al. Analysis of the immune microenvironment in resected non-small cell lung cancer: The prognostic value of different T lymphocyte markers. *Oncotarget.* 2016;7(33):52849–52861.
- Kinoshita T, Muramatsu R, Fujita T, et al. Prognostic value of tumor-infiltrating lymphocytes differs depending on histological type and smoking habit in completely resected non-small-cell lung cancer. *Ann Oncol.* 2016;27(11):2117–2123.
- Miyara M, Yoshioka Y, Kitoh A, et al. Functional delineation and differentiation dynamics of human CD4+ T cells expressing the FoxP3 transcription factor. *Immunity.* 2009;30(6):899–911.

10. Sugiyama D, Nishikawa H, Maeda Y, et al. Anti-CCR4 mAb selectively depletes effector-type FoxP3+CD4+ regulatory T cells, evoking anti-tumor immune responses in humans. *Proc Natl Acad Sci U S A*. 2013; 110(44):17945–17950.
11. Saito T, Nishikawa H, Wada H, et al. Two FOXP3(+)/CD4(+) T cell subpopulations distinctly control the prognosis of colorectal cancers. *Nat Med*. 2016;22(6):679–684.
12. Karanikas V, Speletas M, Zamanakou M, et al. Foxp3 expression in human cancer cells. *J Transl Med*. 2008;6:19.
13. Dimitrakopoulos FI, Papadaki H, Antonacopoulou AG, et al. Association of FOXP3 expression with non-small cell lung cancer. *Anticancer Res*. 2011;31(5):1677–1683.
14. Li Y, Li D, Yang W, Fu H, Liu Y, Li Y. Overexpression of the transcription factor FOXP3 in lung adenocarcinoma sustains malignant character by promoting G1/S transition gene CCND1. *Tumour Biol*. 2016;37(6): 7395–7404.
15. Travis WD, Brambilla E, Noguchi M, et al. International Association for the Study of Lung Cancer/American Thoracic Society/European Respiratory Society International Multidisciplinary Classification of Lung Adenocarcinoma. *J Thorac Oncol*. 2011;6(2):244–285.
16. Borczuk AC. Prognostic considerations of the new World Health Organization classification of lung adenocarcinoma. *Eur Respir Rev*. 2016; 25(142):364–371.
17. Goldstraw P, Chansky K, Crowley J, et al; International Association for the Study of Lung Cancer Staging and Prognostic Factors Committee, Advisory Boards, and Participating Institutions; International Association for the Study of Lung Cancer Staging and Prognostic Factors Committee Advisory Boards and Participating Institutions. The IASLC Lung Cancer Staging Project: Proposals for revision of the TNM stage groupings in the forthcoming (Eighth) Edition of the TNM Classification for Lung Cancer. *J Thorac Oncol*. 2016;11(1):39–51.
18. Sakaguchi S. Naturally arising Foxp3-expressing CD25+CD4+ regulatory T cells in immunological tolerance to self and non-self. *Nat Immunol*. 2005;6(4):345–352.
19. Zou W. Regulatory T cells, tumor immunity and immunotherapy. *Nat Rev Immunol*. 2006;6(4):295–307.
20. Nishikawa H, Sakaguchi S. Regulatory T cells in cancer immunotherapy. *Curr Opin Immunol*. 2014;27:1–7.
21. Li L, Qi L, Liang Z, et al. Transforming growth factor- β 1 induces EMT by the transactivation of epidermal growth factor signaling through HA/CD44 in lung and breast cancer cells. *Int J Mol Med*. 2015;36(1): 113–122.
22. Martin F, Ladoire S, Mignot G, Apetoh L, Ghiringhelli F. Human FOXP3 and cancer. *Oncogene*. 2010;29(29):4121–4129.
23. Takenaka M, Seki N, Toh U, et al. FOXP3 expression in tumor cells and tumor-infiltrating lymphocytes is associated with breast cancer prognosis. *Mol Clin Oncol*. 2013;1(4):625–632.
24. Ma GF, Miao Q, Liu YM, et al. High FoxP3 expression in tumour cells predicts better survival in gastric cancer and its role in tumour micro-environment. *Br J Cancer*. 2014;110(6):1552–1560.
25. Weller P, Bankfalvi A, Gu X, et al. The role of tumour FOXP3 as prognostic marker in different subtypes of head and neck cancer. *Eur J Cancer*. 2014;50(7):1291–1300.

Relationship between serum potassium level and survival outcome in out-of-hospital cardiac arrest using CAPTURES database of Korea: Does hypokalemia have good neurological outcomes in out-of-hospital cardiac arrest?

Dong Sun Choi^{1,A–D,F}, Sang Do Shin^{1,A,C,E,F}, Young Sun Ro^{2,B,C,E,F}, Kyung Won Lee^{3,D–F}

¹ Department of Emergency Medicine, Seoul National University Hospital, South Korea

² Biomedical Research Institute, Seoul National University Hospital, South Korea

³ Department of Emergency Medicine, Kyung Hee University Hospital at Gangdong, South Korea

A – research concept and design; B – collection and/or assembly of data; C – data analysis and interpretation;

D – writing the article; E – critical revision of the article; F – final approval of the article

Advances in Clinical and Experimental Medicine, ISSN 1899–5276 (print), ISSN 2451–2680 (online)

Adv Clin Exp Med. 2020;29(6):727–734

Address for correspondence

Kyung Won Lee

E-mail: emkwlee@gmail.com

Funding sources

None declared

Conflict of interest

None declared

Received on December 10, 2017

Reviewed on June 12, 2018

Accepted on May 8, 2020

Published online on July 1, 2020

Cite as

Choi DS, Shin SD, Ro YS, Lee KW. Relationship between serum potassium level and survival outcome in out-of-hospital cardiac arrest using CAPTURES database of Korea: Does hypokalemia have good neurological outcomes in out-of-hospital cardiac arrest? *Adv Clin Exp Med.* 2020;29(6):727–734. doi:10.17219/acem/122178

DOI

10.17219/acem/122178

Copyright

© 2020 by Wrocław Medical University

This is an article distributed under the terms of the

Creative Commons Attribution 3.0 Unported (CC BY 3.0)

(<https://creativecommons.org/licenses/by/3.0/>)

Abstract

Background. Sudden cardiac arrest is a major cause of death worldwide. Serum potassium level is an initial laboratory test that serves as part of an electrolyte panel easily obtainable by most emergency departments (EDs).

Objectives. To evaluate the relationship between serum potassium level and the survival outcome for out-of-hospital cardiac arrest (OHCA) patients.

Material and methods. We used the Cardiac Arrest Pursuit Trial with Unique Registration and Epidemiological Surveillance (CAPTURES) database, which made up the OHCA cohort of 27 EDs in Korea from January to December 2014. The inclusion criteria were all OHCA patients in the cohort who had received cardiopulmonary resuscitation (CPR) in the hospital. The patients were excluded if they were transferred from another hospital, had a pre-hospital return of spontaneous circulation (ROSC), or if the potassium level and clinical outcome data were missing or not captured. The main parameter was serum potassium level on ED arrival. According to the serum potassium level, the patients were divided into a hypokalemia group ($K^+ < 3.5$ mEq/L), a normokalemia group ($K^+ = 3.5–5.4$ mEq/L) and a hyperkalemia group ($K^+ \geq 5.5$ mEq/L). The primary outcome was neurologically favorable survival discharge.

Results. Among the 1,616 patients in the CAPTURES cohort, 913 patients were included in the analysis, of whom 46 patients (5.9%) were assigned to the hypokalemia group, 370 patients (40.5%) were assigned to the normokalemia group and 497 patients (54.4%) were assigned to the hyperkalemia group. The hypokalemia group has a significantly higher percentage of good neurological outcomes (26.1%). There was a significant positive correlation with neurologically favorable survival (odds ratio (OR) = 4.45; 95% confidence interval (95% CI) = 1.67–11.91) and a significant positive correlation with survival discharge (OR = 2.25; 95% CI = 1.05–4.82).

Conclusions. In OHCA patients, serum potassium level measured in the hospital showed a significant association with survival outcome. Hypokalemia had a significant association with good neurological outcome and survival discharge.

Key words: potassium, hypokalemia, resuscitation, sudden cardiac death, hyperkalemia

Introduction

Sudden cardiac arrest is a major cause of death worldwide. In addition, the most frequent cause of out-of-hospital cardiac arrest (OHCA) is ischemic heart disease. In the USA, 38 people suffer from OHCA every hour.^{1,2} Over the last few decades, the continuous efforts of the emergency medical services (EMS) and improvements in the “chain of survival” have increased the survival outcome.³ However, the survival rate of OHCA varies markedly and the neurologically favorable survival rate remains low.¹

Early and accurate prediction of the outcome of OHCA can help physicians improve therapeutic efforts in patients who have very good chances of surviving. Predictors of good survival outcome in OHCA patients include initial cardiac rhythm, witnesses to the event, bystander administration of cardiopulmonary resuscitation (CPR), and early defibrillation.^{4–7} After achieving the return of spontaneous circulation (ROSC), physicians can use clinical examination, electroencephalography (EEG) findings, evoked potentials, imaging tests, and brain-specific biomarkers – including neuron-specific enolase (NSE) and S100B – to predict the outcome in post-arrest patients.^{8–10} However, these biomarkers and tools are difficult to access in emergency departments (EDs) immediately after the patients arrive.

Serum potassium level is an initial laboratory test that, as part of an electrolyte panel, can be determined easily at most EDs. Potassium is a major component of internal cellular electrolytes in the body. The electrical difference between internal and external electrolytes is the membrane potential. Therefore, serum potassium level affects membrane potential and myocardial cell conduction. In cardiac arrest, the serum potassium level may influence myocardial function. Hyperkalemia decreases myocardial cell conduction velocity, and it can lead to fatal bradyarrhythmia and cardioplegia. Several observation studies show that hyperkalemia can be associated with poor survival outcome.^{11,12} Hypokalemia increases conduction velocity. In patients with acute myocardial infarction (AMI), several observation studies show that hypokalemia is associated with arrhythmia and increased mortality.^{13,14} Due to these effects, serum potassium level can be an early predictor of survival outcomes.

We conducted this study to evaluate serum potassium level as a predictor of OHCA. We hypothesized that the OHCA patients with normokalemia have better survival outcomes than those with hypokalemia or hyperkalemia.

Material and methods

Study design and data source

This retrospective observational study made use of the Cardiac Arrest Pursuit Trial with Unique Registration and Epidemiologic Surveillance (CAPTURES)

database in Korea. The CAPTURES project was conducted from January to December 2014 on OHCA patients who visited 27 EDs (9 level 1 EDs and 18 level 2 EDs).

The purpose of the CAPTURES project was to identify the risk factors for OHCA and to investigate the prognostic factors. All OHCA patients who visited the participating EDs were included in the CAPTURES project if they received prehospital CPR via EMS and their cardiogenic cardiac arrest was verified by an emergency physician. This study excluded terminal-stage patients, hospice patients, pregnant patients, patients without legal guardians who could provide patient information, homeless patients, and patients with “do not resuscitate” orders. Patients with cardiac arrest caused by apparent trauma, drowning, addiction, burns, or choking were also excluded from the study.

The CAPTURES registry collected information on these patients, such as their socioeconomic status, health, previous medical history, physical or mental stress, Utstein-style prehospital and hospital stage report, hematological examination results, and short-term and long-term results. Emergency physicians of the participating hospitals conducted face-to-face interviews with the patients or the patients' families. The study coordinators obtained the first hematological examination results after the patients' arrival at the ED and cardiac examination results from the medical record, and they collected six-month and twelve-month results of the patients via telephone if the patients survived and were discharged. All data was stored in a server using EpiData v. 3.1 (www.epidata.dk). The collected data was reviewed monthly by a quality management committee, consisting of emergency physicians, preventative medicine physicians and cardiologists of hospitals they had attended, where feedback on the collected data coding was given to the coordinators.¹⁵

Setting and study subjects

Emergency medical services in Korea form a single-tier, government-based system which provides a basic-to-intermediate level of ambulance service in 16 provincial headquarters of the national fire department and serves a population of about 50 million people.^{15,16} The ambulance personnel cannot declare death at the scene or terminate CPR unless there is a ROSC. Therefore, all patients with OHCA are transported to the ED.¹⁷ All EDs in Korea are designated as level 1, 2 or 3 by the government in which the level designation is based on human resources, intensive care units (ICUs), instruments, and equipment available at each ED. Level 1 (n = 19) and level 2 (n = 110) EDs have more resources and better facilities for emergency care and they must be staffed by emergency physicians 24 h a day. All EDs are subject to an annual evaluation by a governmental audit committee. The patients eligible for this study (older than 18 years of age) were all EMS-treated OHCA patients with presumed cardiac etiology who were transported to participating EDs from January

to December 2014. The patients who achieved prehospital ROSC, who were transferred from another hospital or whose initial serum potassium levels were not recorded were excluded from the study.

Patients who arrived at the ER received CPR based on the recommendation of the 2010 American Heart Association (AHA) guideline of advanced cardiovascular life support.¹⁸ Laboratory tests, including arterial blood gas analysis, were routinely performed on arrival.

Measurements

The primary outcome was neurologically favorable survival at hospital discharge, defined a priori as a Glasgow-Pittsburgh Cerebral Performance Category (CPC) of 1 or 2.¹⁹ The CPC was estimated based on a medical record review. The secondary outcome was survival hospital discharge.

Variables

The main parameter was serum potassium level on arrival to the ED. The patients were divided into groups according to their serum potassium levels: a hypokalemia group ($K^+ < 3.5$ mEq/L), a normokalemia group ($K^+ = 3.5$ – 5.4 mEq/L) and a hyperkalemia group ($K^+ \geq 5.5$ mEq/L). We collected the initial laboratory test results from the ED (serum levels of sodium, chloride, creatinine, and blood urea nitrogen (BUN), and arterial blood gas analysis (ABGA) of pH, partial pressure of carbon dioxide ($PaCO_2$), partial pressure of oxygen (PaO_2), and oxygen saturation (SaO_2)). Patients with a creatinine level higher than 1.5 were defined as renally impaired patients. Severe metabolic acidosis was defined as an arterial serum pH level of less than 7.2.

We collected the Utstein-defined covariates, which include gender, age, presence of a witness, bystander CPR, initial electrocardiography (ECG) rhythm, prehospital defibrillation, arrest location, time elapsed from call to ambulance arrival at the scene (EMS response time), time elapsed from arrival at the scene to departure (EMS on-scene time), time elapsed from departure to arrival at the ED (EMS transport time), and level of the ED (level 1 or 2). The time at which the cardiac arrest occurred or the time estimated by an emergency medical technician (EMT) was recorded. In addition, the cardiac arrest to ED arrival time was calculated as the interval from when the cardiac arrest occurred to the hospital arrival time. Previous medical history of diabetes mellitus (DM) and hypertension and treatment method (pharmacotherapy or non-pharmacotherapy) was collected using a survey.¹⁵

Statistical analysis

We compared the patient demographics and arrest characteristics among the hypokalemia, normokalemia and hyperkalemia groups using χ^2 test for the categorical variable

and the Kruskal–Wallis test for the continuous variable. We performed post hoc analysis to compare groups, using χ^2 test with Bonferroni correction for the categorical variable and Dunn's test for the continuous variable. A univariate logistic regression analysis was conducted in order to estimate the association between potassium level and survival outcome. In order to test the collinearity problem, the condition index was applied.

Serum pH had a large effect on the survival outcome. When the serum pH level was included, the condition index was determined to be over 30. Therefore, we divided the serum pH level into severe metabolic acidosis ($pH < 7.2$) and non-severe metabolic acidosis ($pH \geq 7.2$). Hypoxia was defined as a SaO_2 level lower than 90%. Multivariate logistic regression analysis was conducted in order to calculate the adjusted odd ratios (ORs) and 95% confidence intervals (95% CIs) after adjusting for potential confounding variables, including age, gender, primary ECG type, etiology of arrest, presence of a witness, bystander CPR, arrest to ED arrival time, prehospital defibrillation, hypoxia, severe metabolic acidosis, DM, and hypertension. Fully conditional specification (FCS) method was applied for imputing missing values of the arrest to ED arrival time ($n = 59$), DM ($n = 82$), hypertension ($n = 79$), severe acidosis ($n = 37$), and hypoxia ($n = 141$). The analysis was performed using SAS software v. 9.4 for Windows (SAS Institute, Cary, USA).

Results

During the study period, there were 1,616 EMS-treated OHCA patients in the CAPTURES database. We excluded 703 patients according to the study criteria and analyzed the remaining 913 patients (Fig. 1). In the total study group, the median potassium level was 5.7 mEq/L (interquartile range (IQR) = 4.5–7.1). Among the 913 patients, 46 (5.0%) were assigned to the hypokalemia group, 370 patients (40.5%) were assigned to the normokalemia group and 497 (54.4%) were assigned to the hyperkalemia group (Fig. 1). The demographics and arrest characteristics of this study population are summarized in Table 1. The neurologically favorable survival rates were 4.5% in the total study population, 26.1% in the hypokalemia group, 5.7% in the normokalemia group, and 1.6% in the hyperkalemia group (Table 1). There were no patients with neurologically favorable survival at discharge when the serum potassium level was higher than 7.0 mEq/L.

Table 2 shows the initial laboratory test results of each group. The hyperkalemia group had a significantly higher creatinine level than that of the other groups ($p < 0.05$). The median creatinine level was 1.5 mg/dL (IQR = 1.1–2.63 mg/dL) in the hyperkalemia group, 1.26 mg/dL (IQR = 1.03–1.53 mg/dL) in the normokalemia group and 1.23 mg/dL (IQR = 0.98–1.58 mg/dL) in the hypokalemia group. The hyperkalemia group has a significantly lower

Table 1. Demographics of out-of-hospital cardiac arrest patients according to initial serum potassium level

Variables	Total		Hypokalemia		Normokalemia		Hyperkalemia		p-value
	N	%	N	%	N	%	N	%	
Total	913		46		370		497		
Age [years]									0.0001 ^{b,c}
18–64	372	40.7	27	58.7	173	46.8	172	34.6	
65–74	209	22.9	10	21.7	84	22.7	115	23.1	
75+	332	36.4	9	19.6	113	30.5	210	42.3	
median	69	55–78	58.5	46–73	66	53–76	72	57–79	0.0085 ^{e,f}
Gender									0.0429 ^{a,b}
male	621	68.0	39	84.8	247	66.8	335	67.4	
Underlying HTN									0.6212
HTN without medication	54	5.9	4	8.7	17	4.6	33	6.6	
HTN with medication	315	34.5	16	34.8	126	34.1	173	34.8	
Underlying DM									0.0013 ^c
yes	222	24.3	13	28.3	68	18.4	141	28.4	
Prehospital shockable rhythm									<0.0001 ^{b,c}
yes	189	20.7	22	47.8	121	32.7	46	9.3	
Witnessed arrest									0.0007 ^c
yes	590	64.6	34	73.9	262	70.8	294	59.2	
Bystander CPR									0.1819
yes	379	41.5	23	50.0	162	43.8	194	39.0	
Public location									0.0182 ^c
yes	230	25.2	15	32.6	108	29.2	107	21.5	
EMS defibrillation									<0.0001 ^{b,c}
yes	214	23.4	21	45.7	127	34.3	66	13.3	
Response time interval									0.1555
missing	6	0.7	2	4.3	3	0.8	1	0.2	
0–4 min	75	8.2	3	6.5	30	8.1	42	8.5	
4–8 min	484	53.0	28	60.9	206	55.7	250	50.3	
8–12 min	249	27.3	10	21.7	104	28.1	135	27.2	
12–16 min	58	6.4	2	4.3	16	4.3	40	8.0	
>16 min	41	4.5	1	2.2	11	3.0	29	5.8	
median (IQR)	6	5–9	6	5–8	6	5–9	6	5–10	0.1304
Scene time interval									0.3653
missing	17	1.9	3	6.5	7	1.9	7	1.4	
0–4 min	144	15.8	5	10.9	62	16.8	77	15.5	
4–8 min	337	36.9	15	32.6	127	34.3	195	39.2	
8–12 min	281	30.8	13	28.3	115	31.1	153	30.8	
12–16 min	73	8.0	4	8.7	29	7.8	40	8.0	
>16 min	61	6.7	6	13.0	30	8.1	25	5.0	
median (IQR)	7	5–10	8	5–10	7	4–11	7	5–10	0.6652
Transport time interval									0.5640
missing	15	1.6	1	2.2	7	1.9	7	1.4	
0–4 min	59	6.5	3	6.5	25	6.8	31	6.2	
4–8 min	304	33.3	19	41.3	133	35.9	152	30.6	
8–12 min	269	29.5	12	26.1	100	27.0	157	31.6	
12–16 min	123	13.5	3	6.5	48	13.0	72	14.5	
>16 min	143	15.7	8	17.4	57	15.4	78	15.7	
median (IQR)	123	6–14	3	5–11	48	5.5–13	72	6–14	0.1304
Arrest to ED arrival time									0.0065 ^c
missing	59	6.5	2	4.3	15	4.1	42	8.5	
0–15 min	89	9.7	4	8.7	48	13.0	37	7.4	
15–30 min	405	44.4	26	56.5	176	47.6	203	40.8	
>30 min	360	39.4	14	30.4	131	35.4	215	43.3	
median (IQR)	27	21–36	25	20–33	26	20–33	28	21.5–40	0.0009
ED level									0.5917
level 1	400	43.8	17	37.0	166	44.9	217	43.7	
level 2	513	56.2	29	63.0	204	55.1	280	56.3	
Survival outcome									<0.0001 ^{a,b,c}
ROSC	412	45.1	35	76.1	185	50.0	192	38.6	
survival discharge	88	9.6	15	32.6	53	14.3	20	4.0	<0.0001 ^{a,b,c}
good neurological outcome	41	4.5	12	26.1	21	5.7	8	1.6	<0.0001 ^{a,b,c}

^ap-values significant after Bonferroni correction (<0.0167) between hypokalemia and normokalemia groups; ^bp-values significant after Bonferroni correction (<0.0167) between hypokalemia and hyperkalemia groups; ^cp-values significant after Bonferroni correction (<0.0167) between normokalemia and hyperkalemia groups; ^dsignificant difference in Dunn's test ($\alpha = 0.05$) between hypokalemia and normokalemia groups; ^esignificant difference in Dunn's test ($\alpha = 0.05$) between hypokalemia and hyperkalemia groups; ^fsignificant difference in Dunn's test ($\alpha = 0.05$) between normokalemia and hyperkalemia groups. HTN – hypertension; DM – diabetes mellitus; IQR – interquartile range; CPR – cardiopulmonary resuscitation; EMS – emergency medical services; ED – emergency department; ROSC – return of spontaneous circulation.

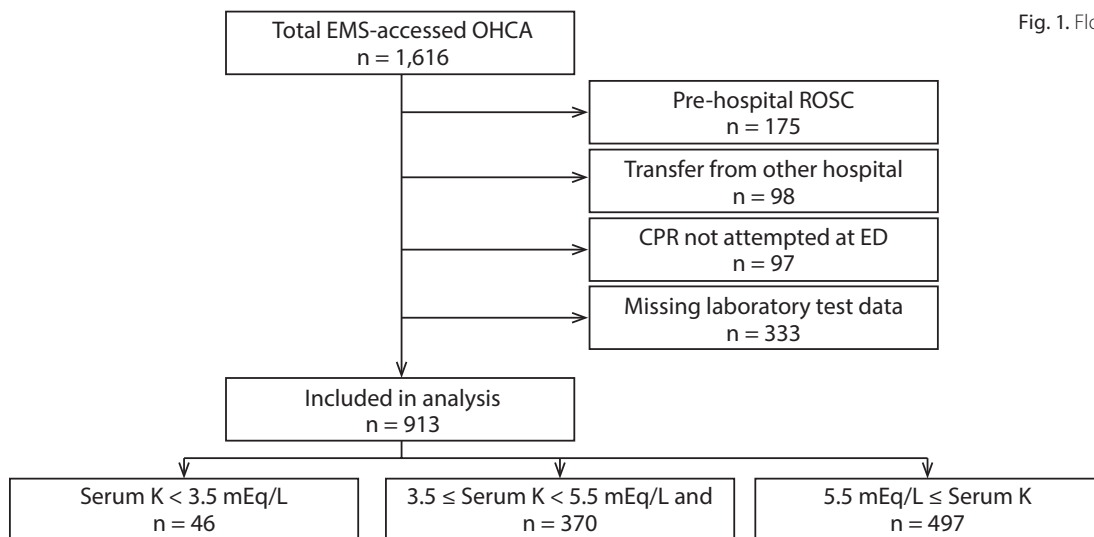


Fig. 1. Flow chart of patient inclusion

Table 2. Biochemical parameters of out-of-hospital cardiac arrest patients according to initial serum potassium level

Parameter	Total median (IQR)	Hypokalemia median (IQR)	Normokalemia median (IQR)	Hyperkalemia median (IQR)	p-value
Na [mmol/L]	140 (136–144)	140.8 (138–145)	141 (138–144.4)	139 (134–143)	<0.0001 ^a
Cl [mmol/L]	103 (99–106)	104 (99–108)	103.4 (100.6–107)	102 (97–106)	0.0004 ^a
BUN [mg/dL]	19 (14.2–30)	15 (12.1–20.5)	17 (13–22.3)	23 (16–45.35)	<0.0001 ^{ab}
Cr [mg/dL]	1.38 (1.09–1.9)	1.23 (0.98–1.58)	1.26 (1.03–1.53)	1.5 (1.1–2.63)	<0.0001 ^{ab}
pH	6.97 (6.85–7.09)	7.07 (6.98–7.23)	7.02 (6.9–7.12)	6.92 (6.81–7.03)	<0.0001 ^{abc}
PaCO ₂ [mm Hg]	73 (53–92)	53.1 (33–77)	73 (55–87.7)	74 (53–16.0)	<0.0001 ^{ac}
PaO ₂ [mm Hg]	33.8 (16–67)	65 (28–92)	29.1 (14–69)	35.5 (17–61.8)	0.0044 ^{ab}
SaO ₂ [%]	38.6 (12.25–81.4)	77 (30.4–95)	33.1 (11.3–81.7)	39.4 (12.4–76.6)	0.0011 ^{ab}
HCO ₃ [mEq/L]	16.65 (12.4–21.4)	16.1 (12–21.7)	18 (13.9–22.2)	16 (11.7–20.3)	<0.0001 ^{abc}

^asignificant difference in Dunn’s test (α = 0.05) between hypokalemia and normokalemia groups; ^bsignificant difference in Dunn’s test (α = 0.05) between hypokalemia and hyperkalemia groups; ^c significant difference in Dunn’s test (α = 0.05) between normokalemia and hyperkalemia groups. IQR – interquartile range; Cr – creatinine; BUN – blood urea nitrogen; PaCO₂ – partial pressure of carbon dioxide; PaO₂ – partial pressure of oxygen; SaO₂ – oxygen saturation.

pH than the other groups (p < 0.05). The median pH level is 6.92 mg/dL (IQR = 6.81–7.03) in the hyperkalemia group, 7.02 mg/dL (IQR = 6.9–7.12) in the normokalemia group and 7.07 mg/dL (IQR = 6.98–7.23) in the hypokalemia group. The hypokalemia group had a significantly lower PaCO₂ level than the other groups (p < 0.05).

The relationship between serum potassium level and survival outcome is shown in Table 3. After adjusting the covariates, hypokalemia had a significantly positive correlation with neurologically favorable survival (OR = 4.45; 95% CI = 1.67–11.91; p = 0.0012) and survival discharge (OR = 2.25; 95% CI = 1.05–4.82; p = 0.0011). Furthermore, the hyperkalemia group had no statistically significant correlation with neurologically favorable survival (OR = 0.79; 95% CI = 0.31–2.02; p = 0.0414), but a significantly negative association with survival discharge (OR = 0.40; 95% CI = 0.22–0.72; p < 0.0001). Table 4 presents the result of the logistic regression analysis of variables according to initial serum potassium level on survival outcomes.

Discussion

We conducted an observational study using a multi-center, prospective-collected database to evaluate initial serum potassium level as a predictor of OHCA. This study demonstrated that hypokalemia at ED arrival is associated with good neurological outcome and survival discharge in OHCA patients. Moreover, hyperkalemia at ED arrival is associated with poor survival discharge in OHCA patients. Therefore, the initial serum potassium level is likely to be used as a prediction marker of survival outcome in patients with OHCA.

This study demonstrated an increasing tendency of median age of the OHCA patients as potassium level increased, and that the rate of prehospital shockable rhythm inversely decreased as potassium level increased. Therefore, this study identified that the cardiac arrest in the hypokalemia group had higher rates of ventricular tachycardia (VT) or ventricular fibrillation (VF) arrest, which suddenly occurred at a younger age, and the cardiac arrest in the hyperkalemia

Table 3. Effect of initial serum potassium level on survival outcomes

Parameter	Total	Outcome		Unadjusted			Adjusted*		
	n	n	%	OR	95% CI	p-value	OR	95% CI	p-value
Primary outcome: neurologically favorable survival									
total	913	41	4.5	–	–	–	–	–	–
hypokalemia	46	12	26.1	5.87	(2.66–12.95)	<0.001	4.45	(1.67–11.91)	0.0012
normokalemia	370	21	5.7	1	–	–	1	–	–
hyperkalemia	497	8	1.6	0.27	(0.12–0.62)	<0.001	0.79	(0.31–2.02)	0.0414
Secondary outcome: survival to discharge									
total	913	88	9.6	–	–	–	–	–	–
hypokalemia	46	15	32.6	2.89	(1.46–5.72)	<0.001	2.25	(1.05–4.82)	0.0011
normokalemia	370	53	14.3	1	–	–	1	–	–
hyperkalemia	497	20	4.0	0.25	(0.15–0.43)	<0.001	0.40	(0.22–0.72)	<0.0001

* adjusted to age, gender, hypertension, diabetes mellitus, initial shockable rhythm, EMS defibrillation, arrest location, bystander CPR, arrest to arrival time, severe acidosis, renal insufficiency, and hypoxia. OR – odds ratio; 95% CI – 95% confidence interval.

group had higher rates of non-shockable rhythm including pulseless electrical activity (PEA) and asystole, which occurred at an older age. This suggests that hypokalemia might have relatively caused VF at a young age, which is a possibility of causality of hypokalemia among young patients. This study also showed that the serum creatinine level gradually increased as the potassium level increased; therefore, we are able to assume that chronic kidney disease (CKD) as an underlying disease was also more prevalent in the hyperkalemia group. However, there was no significant difference in hypertension prevalence among the groups, and DM was more prevalent in patients with hypokalemia and hyperkalemia than in normokalemia. Based on these results, the elderly patients may have a higher rate of underlying diseases, including CKD, which can cause hyperkalemia. On the other hand, the occurrence of cardiac arrest in a private setting among the elderly might be susceptible to the development of hyperkalemia due to the relatively late discovery and treatment, as compared to the occurrence of cardiac arrest in a public setting among younger people, and the reduced prehospital shockable rhythm.

Hyperkalemia resulting from poor perfusion during cardiac arrest could be associated with poor survival outcome. Metabolic acidosis is commonly observed due to generalized poor-perfusion-induced lactic acidosis. Furthermore, hyperkalemia can be caused by extracellular shift during acidosis. In our study, the response time, scene time and transport time did not differ significantly among the 3 groups. However, the total arrest-to-ED-arrival time was significantly longer in the hyperkalemia group, while the hypokalemia group had a lower rate of witnessed cardiac arrest and a lower rate of such event occurring in a public location than the other groups. These conditions were associated with prolonged cardiac arrest time. Furthermore, the median ED arrival time in patients with cardiac arrest due to VF or VT among the hyperkalemia group was 32 min, which was 6 min longer than

that of the patients with cardiac arrest due to VF or VT (26 min) among the normokalemia group. However, there was no statistical significance ($p = 0.06$). This finding may be due to the longer prehospital time causing hyperkalemia, which could result in a different prognosis – even when the shockable rhythms were similar.

Hyperkalemia could result from underlying medical conditions, such as CKD, acute kidney injury or bleeding, or from medications, such as digoxin and potassium-sparing antihypertensive drugs.²⁰ In our study, the hyperkalemia group had more elderly patients, a higher rate of DM and a higher median serum creatinine level. Previous studies showed a similar association with comorbidity and hyperkalemia in OHCA patients.^{21,22} As a result of the comorbidity and decreased physiological reserve in the elderly, the hyperkalemia group could have a negative association with survival outcome.

Hyperkalemia is known to cause conduction delay in the myocardium and fetal bradyarrhythmia.²³ This could cause hyperkalemia to interrupt the electrical disturbance of the myocardium during a resuscitation effort²⁴; thus, hyperkalemia could be associated with poor survival outcome. In addition, the correction of hyperkalemia may improve the survival outcome of the OHCA patients.

In our study, the hypokalemia group was associated with better neurological outcomes than the normokalemia group or the hyperkalemia group. As shown in Table 1, the hypokalemia group was relatively young and had higher rates of prehospital shockable rhythm, bystander CPR and public location, as well as a shorter time from the arrest to arrival at the ED. These factors are known to be good prognostic factors in prehospital cardiac arrest; therefore, the better results of the hypokalemia group might be due to them.^{25,26}

In the study population, the hypokalemia group had a more shockable rhythm. Among the 12 patients with good neurological outcome in the hypokalemia group,

11 of them had a shockable rhythm. Previous studies show that hypokalemia is associated with an increased risk of arrhythmia in patients with cardiovascular disease (CVD).^{27,28} Therefore, the etiology of cardiac arrest due to hypokalemia was VT or VF, which was more reversible than the other causes of cardiac arrest. In addition, sudden cardiac arrest due to VT or VF is more likely to occur in a public setting in the patients' everyday life,²⁹ which could result in a higher likelihood of receiving CPR from a bystander and a shorter arrest to ED time. Therefore, hypokalemia could be associated with survival outcome.

Limitations

This study was insufficient in the application of serum potassium level as a predictor of survival outcome in a pre-hospital setting because the patients with a successful prehospital ROSC, which is associated with good neurological outcome in a prehospital setting, were excluded. In addition, the serum potassium level at the time of the cardiac arrest may differ from the serum potassium level at ED arrival.

This study had several limitations. Firstly, this was an observational study, not a randomized controlled study. In order to adjust for the potential confounders, we used a multivariate logistic regression model including potential confounders. Secondly, the initial serum potassium level was not blinded, and data on whether hyperkalemia or hypokalemia was corrected therapeutically was not collected. The correction of the potassium level could influence the survival outcome of OHCA patients. Thirdly, the CAPTURES registry did not record data on history of CKD or a specific list of the current medical history, such as whether the patient has taken hypokalemia-inducing or hyperkalemia-inducing antihypertensive drugs. These drugs, whether the hypertension is hypokalemia-induced or not, are known to affect the serum potassium level and survival outcome of OHCA patients.²⁴ In order to adjust for CKD history, we defined renal insufficiency as a serum creatinine level of more than 1.5 mg/dL. We also adjusted for history of hypertension with whether the patient was using a hypertensive drug or not. Finally, although a previous history of CVD in the course of previous medical history is an important prognostic factor, this registry did not include CVD history but only a CKD history, such as DM and hypertension. Therefore, the analysis of such information was not possible.

Conclusions

In OHCA patients, the initial serum potassium level had a significant association with survival outcome. This study showed that hypokalemia had a significant association with good neurological outcome and survival discharge, while hyperkalemia had a negative correlation

with survival discharge. These findings suggest that initial serum potassium level is associated with the etiology and result of cardiac arrest. Thus, initial serum potassium level can be used as a prediction marker of survival outcome in patients with OHCA.

References

- Berdowski J, Berg RA, Tijssen JG, Koster RW. Global incidences of out-of-hospital cardiac arrest and survival rates: Systematic review of 67 prospective studies. *Resuscitation*. 2010;81(11):1479–1487.
- Mozaffarian D, Benjamin EJ, Go AS, et al; American Heart Association Statistics Committee; Stroke Statistics Subcommittee. Heart disease and stroke statistics – 2015 update: A report from the American Heart Association. *Circulation*. 2015;131(4):e29–e322.
- Iwami T, Nichol G, Hiraide A, et al. Continuous improvements in “Chain of Survival” increased survival after out-of-hospital cardiac arrests: A large-scale population-based study. *Circulation*. 2009;119(5):728–734.
- Ahn KO, Do Shin S, Suh GJ, et al. Epidemiology and outcomes from non-traumatic out-of-hospital cardiac arrest in Korea: A nationwide observational study. *Resuscitation*. 2010;81(8):974–981.
- Eisenberg MS, Cummins RO, Larsen MP. Numerators, denominators, and survival rates: Reporting survival from out-of-hospital cardiac arrest. *Am J Emerg Med*. 1991;9(6):544–546.
- Pepe PE, Levine RL, Fromm RE Jr, Curka PA, Clark PS, Zachariah BS. Cardiac arrest presenting with rhythms other than ventricular fibrillation: Contribution of resuscitative efforts toward total survivorship. *Crit Care Med*. 1993;21(12):1838–1843.
- Weston CF, Wilson RJ, Jones SD. Predicting survival from out-of-hospital cardiac arrest: A multivariate analysis. *Resuscitation*. 1997;34(1):27–34.
- Böttiger BW, Möbes S, Glätzer R, et al. Astroglial protein S-100 is an early and sensitive marker of hypoxic brain damage and outcome after cardiac arrest in humans. *Circulation*. 2001;103(22):2694–2698.
- Fogel W, Krieger D, Veith M, et al. Serum neuron-specific enolase as early predictor of outcome after cardiac arrest. *Crit Care Med*. 1997;25(7):1133–1138.
- Callaway CW, Donnino MW, Fink EL, et al. Part 8: Post-Cardiac Arrest Care 2015 American Heart Association Guidelines Update for Cardiopulmonary Resuscitation and Emergency Cardiovascular Care. *Circulation*. 2015;132(18 Suppl 2):S465–S482.
- Cohen JG, Boue Y, Boussat B, et al. Serum potassium concentration predicts brain hypoxia on computed tomography after avalanche-induced cardiac arrest. *Am J Emerg Med*. 2016;34(5):856–860.
- Su Y-J, Lai Y-C. Optimal parameters for return of spontaneous circulation in resuscitating out-of-hospital cardiac arrest patients. *Int J Gerontol*. 2009;3(2):96–100.
- Choi JS, Kim YA, Kim HY, et al. Relation of serum potassium level to long-term outcomes in patients with acute myocardial infarction. *Am J Cardiol*. 2014;113(8):1285–1290.
- Patel RB, Tannenbaum S, Viana-Tejedoro A, et al. Serum potassium levels, cardiac arrhythmias, and mortality following non-ST-elevation myocardial infarction or unstable angina: Insights from MERLIN-TIMI 36. *Eur Heart J Acute Cardiovasc Care*. 2017;6(1):18–25.
- Ro YS, Shin SD, Song KJ, et al; Cardiac Arrest Pursuit Trial with Unique Registry and Epidemiologic Surveillance (CAPTURES) investigators. Risk of diabetes mellitus on incidence of out-of-hospital cardiac arrests: A case-control study. *PLoS One*. 2016;11(4):e0154245.
- Ro YS, Shin SD, Song KJ, et al. Interaction effects between hypothermia and diabetes mellitus on survival outcomes after out-of-hospital cardiac arrest. *Resuscitation*. 2015;90:35–41.
- Kim MJ, Ro YS, Shin SD, et al. Association of emergent and elective percutaneous coronary intervention with neurological outcome and survival after out-of-hospital cardiac arrest in patients with and without a history of heart disease. *Resuscitation*. 2015;97:115–121.
- Neumar RW, Otto CW, Link MS, et al. Part 8: Adult advanced cardiovascular life support. *Circulation*. 2010;122(18 Suppl 3):S729–S767.
- Jacobs I, Nadkarni V, Bahr J, et al; International Liaison Committee on Resuscitation; American Heart Association; European Resuscitation Council; Australian Resuscitation Council; New Zealand Resuscitation Council; Heart and Stroke Foundation of Canada; InterAmerican Heart Foundation; Resuscitation Councils of Southern Africa;

- ILCOR Task Force on Cardiac Arrest and Cardiopulmonary Resuscitation Outcomes. Cardiac arrest and cardiopulmonary resuscitation outcome reports: Update and simplification of the Utstein templates for resuscitation registries. A statement for healthcare professionals from a task force of the international liaison committee on resuscitation (American Heart Association, European Resuscitation Council, Australian Resuscitation Council, New Zealand Resuscitation Council, Heart and Stroke Foundation of Canada, InterAmerican Heart Foundation, Resuscitation Council of Southern Africa). *Resuscitation*. 2004;63(3):233–249.
20. An JN, Lee JP, Jeon HJ, et al. Severe hyperkalemia requiring hospitalization: Predictors of mortality. *Crit Care*. 2012;16(6):R225.
 21. Lin C-H, Tu Y-F, Chiang W-C, Wu S-Y, Chang Y-H, Chi C-H. Electrolyte abnormalities and laboratory findings in patients with out-of-hospital cardiac arrest who have kidney disease. *Am J Emerg Med*. 2013;31(3):487–493.
 22. Wissenberg M, Folke F, Hansen CM, et al. Survival after out-of-hospital cardiac arrest in relation to age and early identification of patients with minimal chance of long-term survival. *Circulation*. 2015;131(18):1536–1545.
 23. Ettinger PO, Regan TJ, Oldewurtel HA, Khan MI. Ventricular conduction delay and asystole during systemic hyperkalemia. *Am J Cardiol*. 1974;33(7):876–886.
 24. Niemann JT, Cairns CB. Hyperkalemia and ionized hypocalcemia during cardiac arrest and resuscitation: Possible culprits for postcounter-shock arrhythmias? *Ann Emerg Med*. 1999;34(1):1–7.
 25. Swor RA, Jackson RE, Tintinalli JE, Pirallo RG. Does advanced age matter in outcomes after out-of-hospital cardiac arrest in community-dwelling adults? *Academic Emerg Med*. 2000;7(7):762–768.
 26. Sasson C, Rogers MA, Dahl J, Kellerman RL. Predictors of survival from out-of-hospital cardiac arrest: A systematic review and meta-analysis. *Circ Cardiovasc Qual Outcomes*. 2010;3(1):63–81.
 27. Kjeldsen K. Hypokalemia and sudden cardiac death. *Exp Clin Cardiol*. 2010;15(4):e96–e99.
 28. Alharbi FF, Souverein PC, de Groot MCH, et al. The impact of serum potassium-influencing antihypertensive drugs on the risk of out-of-hospital cardiac arrest: A case-control study. *Br J Clin Pharmacol*. 2017;83(11):2541–2548.
 29. Litwin PE, Eisenberg MS, Hallstrom AP, Cummins RO. The location of collapse and its effect on survival from cardiac arrest. *Ann Emerg Med*. 1987;16(7):787–791.

Oral cancer: The first symptoms and reasons for delaying correct diagnosis and appropriate treatment

Monika Rutkowska^{1,A–F}, Sylwia Hnitecka^{2,A–F}, Marek Nahajowski^{3,A–F}, Marzena Dominiak^{4,E,F}, Hanna Gerber^{5,B,E,F}

¹ Clinical Department of Maxillofacial Surgery, 4th Military Clinical Hospital, Wrocław, Poland

² Dental Clinic, 4th Military Clinical Hospital, Wrocław, Poland

³ Private dental practice, Wrocław, Poland

⁴ Department of Oral Surgery, Wrocław Medical University, Poland

⁵ Department of Maxillofacial Surgery, Wrocław Medical University Hospital, Poland

A – research concept and design; B – collection and/or assembly of data; C – data analysis and interpretation;

D – writing the article; E – critical revision of the article; F – final approval of the article

Advances in Clinical and Experimental Medicine, ISSN 1899–5276 (print), ISSN 2451–2680 (online)

Adv Clin Exp Med. 2020;29(6):735–743

Address for correspondence

Sylwia Hnitecka

E-mail: sylwia.hnitecka@gmail.com

Funding sources

None declared

Conflict of interest

None declared

Received on May 5, 2019

Reviewed on September 12, 2019

Accepted on January 21, 2020

Published online on June 29, 2020

Cite as

Rutkowska M, Hnitecka S, Nahajowski M, Dominiak M, Gerber H. Oral cancer: The first symptoms and reasons for delaying correct diagnosis and appropriate treatment.

Adv Clin Exp Med. 2020;29(6):735–743.

doi:10.17219/acem/116753

DOI

10.17219/acem/116753

Copyright

© 2020 by Wrocław Medical University

This is an article distributed under the terms of the Creative Commons Attribution 3.0 Unported (CC BY 3.0)

(<https://creativecommons.org/licenses/by/3.0/>)

Abstract

Background. The first symptoms of oral cancer are nonspecific. They raise suspicions of other, less serious conditions. Treatment of oral cancer is challenging, and the time of its detection and the implementation of appropriate therapy affect the prognosis.

Objectives. To identify predisposing factors, symptoms, time of, and reasons for delays in the diagnosis and appropriate treatment of oral cancer.

Material and methods. This retrospective analysis includes patients who were hospitalized with a diagnosis of carcinoma at the Clinical Department of Maxillofacial Surgery at the 4th Military Clinical Hospital and Polyclinic in Wrocław, Poland, between 2008 and 2018, and at the Department of Maxillofacial Surgery at Wrocław Medical University Hospital between 2010 and 2018. The analysis took into account the data obtained from the patients' medical records.

Results. This study comprised 305 patients (112 female; 36.7% and 193 male; 63.3%). The most frequent diagnosis was squamous cell carcinoma (N = 294; 96.4%). The floor of the mouth was the most frequent primary site (N = 103; 33.8%), followed by the anterior 2/3 of the tongue (N = 94; 30.8%) and lower gingiva (N = 43; 14.1%). A significant percentage were reported at an advanced stage (73.5% in stages III and IV combined). The reasons for the late-stage diagnoses depended on the patients (40.6%), the doctors (24.9%) or both (10.8%). Only 47.5% of patients reported because of the initial symptom noticed. Nearly half of the patients reported after 3–6 months of observing symptoms, usually to a general practitioner (GP; 35.7%) or a dentist (31.8%).

Conclusions. The oncological awareness of patients and healthcare professionals is an essential issue. Doctors often recommend inappropriate treatment, sometimes without monitoring its effectiveness. Dentists should consider cancer in the differentiation of clinical manifestations of other oral disorders.

Key words: oral diseases, head and neck cancer, oral cancer

Introduction

Oral cancer is a significant public health problem, causing many deaths. According to the GLOBOCAN 2018 project, coordinated by the International Agency for Research on Cancer (IARC) of the World Health Organization, the estimated incidence of lip and oral cancer is 354,864 (2%), and its estimated mortality is 177,384 (1.9%).¹ Over 90% of cancers in the head and neck region are head and neck squamous cell carcinomas (HNSCC).² Oral cancer affects men more often, but the male-to-female ratio is decreasing. The risk of developing this disease is higher after the age of 45.³ The five-year survival rate correlates with tumor advancement: The rate is about 80% for stage I cancer, and only around 20% for patients with stages III or IV.⁴ A significant percentage of patients report with cancer at an advanced stage, which often qualifies the patient for only palliative treatment. At the moment of diagnosis, regional metastases are present in about 40% of cases, and distant metastases in about 6%, despite the accessibility of the oral cavity to examination even without specific diagnostic instruments.^{5,6}

This has given rise to investigations of the causes of these significant diagnostic and therapeutic delays. Oncological awareness in society is crucial; it is the subject of many pro-health campaigns, aimed at drawing attention to the need for early cancer detection. This issue is not common in the literature – such state of affair emphasizes the need to pay more attention to this problem because early diagnosis of oral malignancy at an early stage may reduce death, morbidity and disfigurement from this disease.⁷

Insufficient oncological awareness and ignorance of the potential etiology (cancer) of symptoms are the most relevant aspects concerning the patients. Despite noticing a lesion, patients downplay it as long as it does not interfere with their functionality to a significant extent. Often patients report to the doctor only when pain occurs or, worse, or when they have difficulty in eating or speaking.^{8,9}

The level of doctors' awareness also may require improvement.^{10,11} Most of the time, like patients, they do not associate the presented symptoms with neoplastic etiology. Poor diagnoses and a consequent lack of or correct initial therapy (i.e., long-term, ineffective antibiotic therapy or other pharmacotherapy, periodontal, surgical or endodontic treatment, prosthetic correction) result in significant delays in the appropriate treatment process. Such incorrect treatment may make patients' condition even worse.^{8,11} Besides dangerous delays and failures to continue further diagnosis, the recommended monitoring of the effectiveness of the initial treatment is often lacking.

Oral cancer influences the quality of life of patients because it impairs the efficiency of eating and speech. The esthetics of the oral region is also an important aspect. When the tumor is in an advanced stage, it results in the need for extensive surgery, which has a negative influence on both functionality and esthetics.^{6,11}

The aim of the study was to determine the first symptoms of oral cancer, the reasons that prompt patients to self-report to doctors and the reasons for delays in the appropriate diagnosis and treatment, depending on both healthcare professionals and patients. The 2nd aim was to draw attention to the need to increase the level of oncological awareness in society at large and among healthcare professionals in particular.

Material and methods

The research material comprised patients hospitalized between 2008 and 2018 at the Clinical Department of Maxillofacial Surgery of the 4th Military Clinical Hospital and Polyclinic in Wrocław (Poland), and between 2010 and 2018 at the Department of Maxillofacial Surgery of Wrocław Medical University Hospital.

The analysis included patients with a pathological diagnosis of carcinoma and with tumors within the oral cavity. The analysis excluded patients with a pathological diagnosis other than carcinoma, patients hospitalized because of tumor recurrence or with a primary location other than the oral cavity (metastatic tumor), and patients with any missing data.

This retrospective analysis comprised data from the patients' medical records and pathological results. The data referred to the patients (their age at the time of diagnosis, concomitant systemic diseases, previous oncological therapy, malignancies in the family, addictions); the tumor (the pathological diagnosis, primary site, clinical tumor/node/metastasis (TNM) staging and advancement (I–IV), macroscopic appearance); the diagnostic process and type of therapy before the patient's admission to the hospital (the time that passed from the first noticed symptom to the patient reporting to the ward, the nature of the first symptom, the sign that prompted the patient to self-report to a healthcare provider, the specialty of the first healthcare professional consulted, the first therapy (or other medical activity) implemented, the number of doctors consulted before admission to the ward); and the reasons for delays in implementing the appropriate diagnostic and therapeutic procedures, categorized as reasons that depended on the patients, those that depended on the doctors, or both.

The statistical analysis was carried out using STATISTICA v. 12 software (StatSoft, Inc., Tulsa, USA). The Kolmogorov–Smirnov and Shapiro–Wilk tests were used to check the compatibility of empirical distributions of quantitative traits with the theoretical normal distribution. The non-parametric Mann–Whitney U test verified the significance of differences in the values of average features with distributions different from normal or with heterogeneous variances in 2 independent groups. Pearson's χ^2 test or Spearman's rank correlation coefficient verified the independence of 2 qualitative variables.

Results

Age, sex, addictions, systemic disorders, and past oncological therapy

The analysis included 305 patients (112 female (F, 36.7%) and 193 male (M, 63.3%)). The mean age of the group was 60.7 ± 10.3 years (range: 22–87 years); 14 patients (10 M, 4 F) were under 45 years of age. The women were older than the men by an average of 4.7 years, which was statistically significant ($p < 0.001$). A predominance of males was found at a ratio of 1.7:1.

Among the patients, 248 (81.3%) admitted smoking currently or in the past, 255 (83.6%) reported drinking alcohol, 221 (72.5%) consumed alcohol occasionally, and 34 (11.1%) reported significant alcohol abuse. In 32 cases (10.5%), smoking and significant alcohol abuse coexisted. The men used stimulants more often than women ($p < 0.001$).

We found that 176 of the patients (57.7%) suffered from concomitant systemic diseases such as cardiovascular diseases, diabetes, hypo/hyperthyroidism, or rheumatic diseases. Systemic diseases were more frequent in the older patients (over 60 years of age) than in those under 45 (77.4% vs 39.6%, $p < 0.001$), while older people were less likely to use stimulants (86.3% vs 94.3%, $p = 0.017$).

Investigating the patients' oncological history, we found that 32 of them (10.5%) had undergone other oncological therapy in the past. There were malignancies in family members in 46 cases (15%) (Table 1).

Pathological results, location, clinical stage

The floor of the mouth was the most frequent location ($N = 103$; 33.8%), followed by the anterior 2/3 of the tongue ($N = 94$; 30.8%) and lower gingiva ($N = 43$; 14.1%). The significant advancement of the tumor in 33 cases made it impossible to determine the primary site within the oral cavity. As for the pathological diagnosis, cases of squamous cell carcinoma were dominant ($N = 294$; 96.4%), although there were also patients with a diagnosis of adenoid cystic

Table 1. Characteristics of the cases analyzed

Clinical feature	Value	
Mean age	60.7	
Range	22–87	
Age <45	N = 14	
Age >45	N = 291	
Sex ratio M:F	1.7:1	
Addictions	N	%
Smoking	248	81.3
Drinking alcohol	255	83.6
Diseases	N	%
Concomitant systemic diseases (e.g., cardiovascular disease, diabetes, hypo-/hyperthyroidism, rheumatic diseases)	176	57.7
Oncological history	N	%
Previous oncological treatment	32	10.5
Incidence of cancer in the family	46	15.0
Primary cancer site	N	%
Floor of the mouth	103	33.8
Tongue – anterior 2/3	94	30.8
Lower gingiva	43	14.1
Impossible to determine the primary site	33	10.8
Upper gingiva	13	4.3
Buccal mucosa	11	3.6
Hard palate	8	2.6

N – number of patients; M – male; F – female.

carcinoma ($N = 5$; 1.6%), adenocarcinoma ($N = 4$; 1.3%), lymphoepithelial carcinoma ($N = 1$; 0.3%), and mucoepithelioid carcinoma ($N = 1$; 0.3%). Table 1 shows the distribution of the primary tumor locations.

At the time of the patients' admission to the ward, 81 of them (26.5%) were in the early stages of advancement (I: $N = 26$, II: $N = 55$) and 224 (73.5%) in late stages (III: $N = 64$, IV: $N = 160$). Nodal metastases ($N > 0$) existed in 193 cases (63.3%), while distant metastases (M1) existed in 7 patients (2.3%) (Table 2).

Table 2. Tumor stages, sex and age distribution of the population, time (counted in months) that passed between noticing the first symptom and the patient reported to the ward, and the number of doctors consulted

Variable	Tumor stage				
	I	II	III	IV	
Sex	male, N (% of male)	15 (7.8)	21 (10.9)	41 (21.2)	116 (60.1)
	female, N (% of female)	11 (9.8)	34 (30.4)	23 (20.5)	44 (39.3)
Age	<45 years, N (% of patients <45 years)	1 (7.1)	2 (14.35)	5 (35.7)	6 (42.85)
	45–69 years, N (% of patients 45–69 years)	19 (8.1)	43 (18.3)	46 (19.6)	127 (54)
	≥ 70 , N (% of patients ≥ 70 years)	6 (10.7)	10 (17.9)	13 (23.2)	27 (48.2)
Time [months], average	7.5 ± 9.7	9.1 ± 24.2	6.1 ± 6.0	7.25 ± 11.7	
Number of doctors, average	1.6 ± 0.9	1.5 ± 1	1.75 ± 1.2	1.4 ± 0.85	

N – number of patients.

Total delay time

The time (in months) that had passed from noticing the first symptom until the patient reported to the Department of Maxillofacial Surgery was on average 7.4 ± 13.9 months (min: 2 weeks, max: about 15 years). The time is given approximately because patients could not determine it accurately. There was no significant correlation between gender and delay time ($p > 0.05$) or between tumor advancement and delay time ($p > 0.05$) (Fig. 1). There was no correlation between tumor advancement (stage and metastases) and the presence of any factor delaying correct diagnosis and appropriate therapy ($p > 0.05$) (Table 3), nor between tumor advancement and the time of patient's initial consultation with a doctor (i.e., when the patient reported to a doctor because of the first noticed symptom) ($p > 0.05$).

In some cases, the patient consulted a number of specialists. In this study, the patients most often consulted

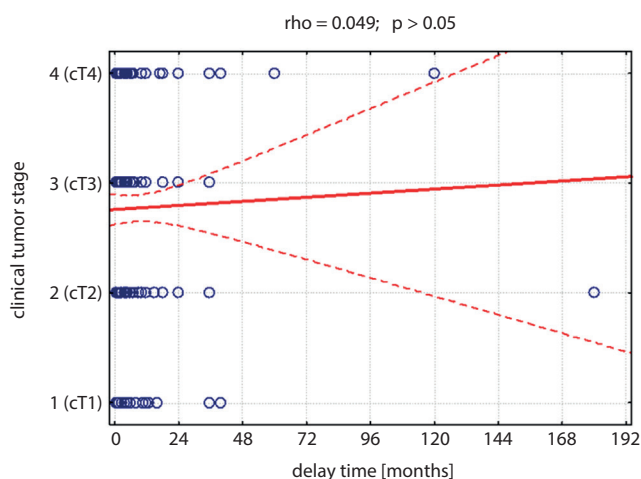


Fig. 1. Correlation diagram between the delay time and the stage of the tumor, with the value of Spearman's rank correlation coefficient (ρ)

Table 3. The influence of delays in appropriate treatment on tumor advancement

Tumor advancement	Delay in appropriate treatment		Test result p-value
	no N = 148	yes N = 157	
cT1	20 (13.5%)	21 (13.4%)	0.572
cT2	42 (28.4%)	49 (31.2%)	
cT3	39 (26.4%)	31 (19.8%)	
cT4	47 (31.8%)	56 (35.7%)	
Metastasis	Delay in appropriate treatment		Test result p-value
	no N = 148	yes N = 157	
M1	5 (3.4%)	2 (1.3%)	0.271
Mx	143 (96.6%)		

N – number of patients; cT – clinical stage of tumor advancement.

1 healthcare professional (N = 132; 43.2%) and slightly less often 2 (N = 88; 28.8%; min: 0 (patients who reported directly to the ward); max: 5; average: 1.5 ± 1 ; Table 2). There was no significant correlation between the tumor stage and the number of doctors consulted ($p > 0.05$), but there was a weak positive correlation between the delay time and the number of doctors consulted before admission to the ward ($p < 0.05$).

Symptoms and other pathological lesions

Ulceration was most frequent clinical appearance of a typical neoplastic lesion (N = 176; 57.7%), followed by induration (N = 135; 44.3%) and rupture (N = 43; 14.1%). The lesion often manifested with symptoms of inflammation and bloody or purulent discharge. Sometimes it had even necrotic parts. Accompanying symptoms depended on the severity of the tumor; a significant correlation was found between increasing tumor advancement and an increasing number of accompanying symptoms ($p < 0.001$) (Fig. 2). Lockjaw was present in 9 cases (3%), impaired tongue movement in 38 (12.5%) and paresthesia of the mandibular nerve (V_3) in 14 (4.6%). No significant correlation between the duration of the disease or location of the tumor and the number of additional symptoms was found ($p > 0.05$). There were also other pathological mucosal lesions within the oral cavity in 25 cases (8.2%), including leukoplakia, dysplastic lesions, papillary or red hypertrophic lesions, lichen planus, or prosthetic stomatitis. A significant oral hygiene deficit was observed in 60 patients (19.7%). A few patients (N = 6; 2%) were suffering from mental disorders caused by their disease, while 21 (6.9%) arrived at the ward in a state of cachexia. Palliative therapy was the only treatment option for 5 patients (1.6%) because of the significant advancement of their cancer.

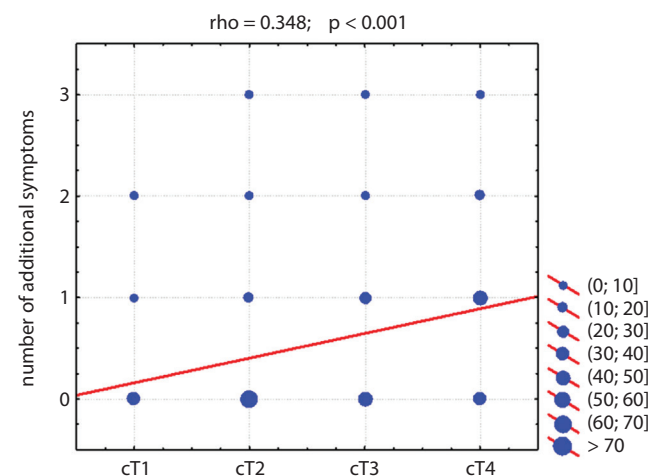


Fig. 2. Correlation diagram between tumor progression and the number of accompanying symptoms, with the value of Spearman's rank correlation coefficient (ρ)

First consultations, reasons and first noticed symptoms

The medical specialists to whom patients most often reported with their first noticed symptoms were established on the basis of interviews. General practitioners (GPs) were the first healthcare professional consulted most frequently (N = 109; 35.7%), with dentists slightly less often (N = 97; 31.8%) (Table 4).

The first symptoms that the patients noticed were also determined. Most often they observed an undefined lesion (N = 90; 29.5%), ulceration (N= 46; 15.1%) or induration (N = 40; 13.1%) (Table 5). The first symptom noticed by the patient (or sometimes incidentally detected by a doctor) prompted a visit to a doctor in only 47.5% of the cases, but there was no significant correlation between patients' early consultation with a doctor

Table 4. Specialist first visited

Type of specialist	N	%
General practitioner	109	35.7
Dentist	97	31.8
Directly to the maxillofacial department	48	15.7
Laryngologist	45	14.8
Oncologist	4	1.3
Dermatologist	1	0.3
Endocrinologist	1	0.3

N – number of patients.

and tumor advancement ($p > 0.05$). Often, patients sought medical help only at the time of the appearance of further symptoms or worsening of existing symptoms (Table 5).

Table 5. The nature of the first symptom noticed and of the symptom that prompted the patient to report to a doctor

First noticed symptom	N	%	Symptom that prompted the patient to report to the doctor	N	%
Lesion	90	29.5	first noticed symptom	145	47.5
Ulceration	46	15.1	enlargement of the lesion	51	16.7
Tumor	40	13.1	pain (appearance after time)	38	12.5
Pain (tumor area)	21	6.9	intensification of symptoms that had been present for some time	22	7.2
Dysphagia	17	5.6	accidental detection	17	5.6
Wound/rupture	13	4.3	lack of healing/improvement after initial treatment implemented	13	4.3
Unnoticed	13	4.3	check-up for another reason	10	3.3
Sore throat	12	3.9	burning feeling	5	1.6
White/grey spot	11	3.6	pain when swallowing	5	1.6
Pain/burning/numbness	8	2.6	difficult speech	4	1.3
Discomfort	6	2	tumor	4	1.3
Tooth pain	6	2	tumor decay	3	1
Hoarseness	6	2	ulceration	2	0.7
Prosthesis mismatch	5	1.6	suppuration	2	0.7
Neck lump	4	1.3	sudden mismatch of prosthesis	2	0.7
Ulceration under a prosthesis	4	1.3	edema	1	0.3
Protuberance	4	1.3	limitation of tongue mobility	1	0.3
Face or neck pain	4	1.3	neck lump	1	0.3
No healing of post-extraction socket	4	1.3	ear pain	1	0.3
Edema	4	1.3	trismus	1	0.3
Infiltration	3	1			
Excrescence	3	1			
Speech disorders	2	0.7			
Cough	2	0.7			
Pain under prosthesis	2	0.7			
Gingival bleeding	2	0.7			
Ear pain	2	0.7			
Feeling an obstacle in the throat	1	0.3			
Loss of smell	1	0.3			
Dry mouth	1	0.3			

N – number of patients.

Focusing on the dental aspect (and counting only people who first consulted a dentist), it was found that patients reported to the dentist because of the first symptom noticed (N = 52; 51.5%), which was most often ulceration (N = 12; 23%), induration (N = 8; 15.4%), an undefined lesion (N = 7; 13.5%), pain (N = 5; 9.6%), or a white or grey spot (N = 5; 9.6%). Other causes that prompted patients to report to a dentist were enlargement of a lesion, a lack of healing or improvement after initial treatment, the onset of pain, intensification of existing symptoms, and in individual cases suppuration, prosthesis mismatch, dysphagia, impaired tongue movement, and a burning sensation in the mouth.

It is noteworthy that in 9 cases (8.9%), patients noticed nothing disturbing and detection (by the healthcare professional) was accidental. Lesions were detected in 3 patients (3%) during a medical visit for a different reason (in 2 patients during oncological monitoring for another cancer and in 1 during a visit to an endocrinologist).

Reasons for delay

This study also includes the most common reasons for delays in the implementation of appropriate treatment. In 125 cases (41%), the patient caused the delay; in 76 cases (25%) the healthcare professionals were the cause; and in 32

Table 6. Patients' reasons for delaying

Patients' reasons for delaying	N	%
No reason	148	48.5
Minor symptoms/not significantly impeding functionality	110	36.1
Home remedies – ointments, pills, rinses, herbs, self-extraction	19	6.2
Did not apply for treatment/monitoring	14	4.6
Linking symptoms to dentition/denture problem	10	3.3
The patient did not notice → accidental detection	9	3

N – number of patients.

cases (10.5%) causes of delay lay on both sides. In 72 patients (23.6%), there was no definitive delaying cause.

Regarding the patients, the most common reason for a delay was that the symptoms of the disease were minor (N = 110; 36.1%) and did not impair their functionality (Table 6). The reason for delays independent of the patient was usually the initial treatment recommended by the doctors (N = 108; 35.4%) who sometimes carried it out for a long time, often without monitoring its effectiveness (Tables 7 and 8). Maxillofacial surgeons were less likely than GPs to refer patients to another doctor; and dentists took bioptic samples more often than GPs (Fig. 3).

Table 7. Initial responses by specialization

Initial medical action	General practitioner [%]	Laryngologist [%]	Dentist [%]	Dermatologist [%]	Oncologist [%]	Endocrinologist [%]	Oromaxillofacial surgeon [%]
Referral to the ward/other doctor (N = 137; 44.9%)	43.8	12.4	39.4	–	2.9	0.7	0.7
Bioptic sample taking (N = 74; 24.3%)	1.4	23	13.5	–	–	–	62.1
Antibiotics (N = 29; 9.5%)	72.4	6.9	20.7	–	–	–	–
Gels, ointments, creams (N = 23; 7.5%)	47.8	4.3	47.8	–	–	–	–
Other pharmacotherapy (N = 18; 5.9%)	72.2	22.2	5.6	–	–	–	–
Extractions (N = 8; 2.6%)	–	–	100	–	–	–	–
Antifungal treatment (N = 7; 2.3%)	28.6	28.6	42.9	–	–	–	–
Mouth rinses (N = 6; 2%)	66.7	–	33.3	–	–	–	–
Endodontic treatment (N = 4; 1.3%)	–	–	100	–	–	–	–
Curettage (N = 3; 1%)	–	–	100	–	–	–	–
Other ad hoc treatment (N = 3; 1%)	–	33.3	66.6	–	–	–	–
Painkillers (N = 2; 0.7%)	50	50	–	–	–	–	–
Prosthetic corrections (N = 2; 0.7%)	–	–	100	–	–	–	–
Periodontology treatment (N = 2; 0.7%)	–	–	100	–	–	–	–
Sore throat pills (N = 1; 0.3%)	100	–	–	–	–	–	–
Laser removal of lesion (N = 1; 0.3%)	–	–	100	–	–	–	–

N – number of patients.

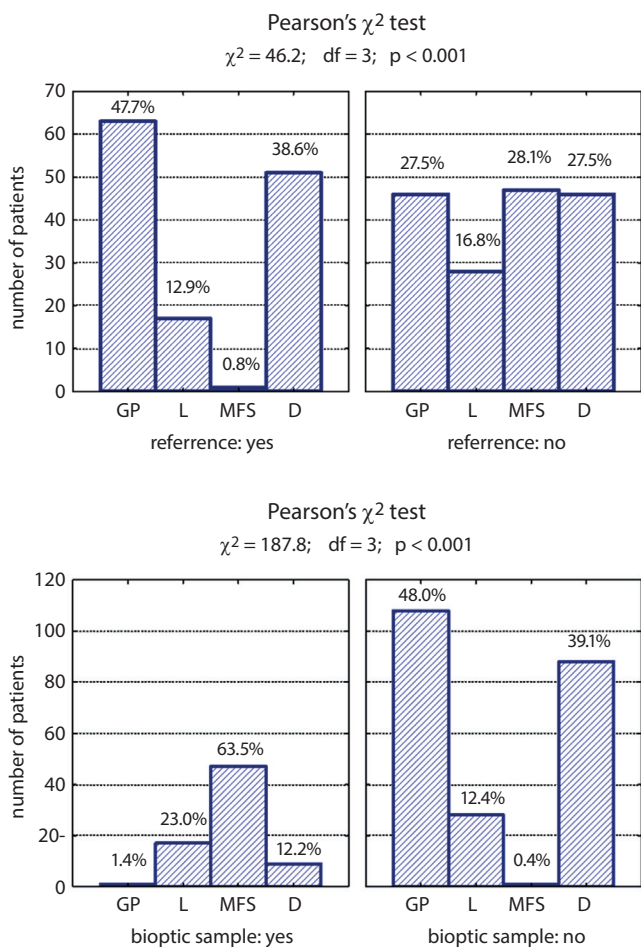


Fig. 3. The number of patients grouped according to primary care and the type of first treatment implemented (referral and bioptic sample retrieval) and the results of the test of independence

GP – general practitioner; L – laryngologist; MFS – maxillofacial surgeon; D – dentist.

Analyzing the individual delays caused by healthcare providers, the most common cause was antibiotic therapy (N = 33; 10.8%), often repeated and prolonged, ointments and mouth rinses (N = 27; 8.9%) or other pharmacotherapy (N = 24; 7.9%) aimed at treating suspected other diseases, such as pharyngitis or aphthous stomatitis, often without monitoring the effectiveness of the treatment. An additional difficulty that increased the possibility of misdiagnosis regarding the oral cavity were symptoms of comorbid inflammation present along with cancer. Other noteworthy problems were incorrect bioptic sample retrieval, long waiting time for appointments or examinations, and above all a lack of oncological awareness on the doctors' part, leading to downplaying the disease and not undertaking further treatment, not retrieving a bioptic sample or even not referring the patient to another specialist (Table 7).

There was no correlation between the type of specialist first visited by the patient and the delay cause ($p > 0.05$), but when analyzing the role of dentists, it was relatively common to implement dental treatment without determining

Table 8. Professionals' reasons for delay

Professionals' reasons for delay	N	%
No reason	197	64.6
Antibiotics	33	10.8
Gels, ointments, rinses – treatment of aphta, ulcers	27	8.9
Other pharmacotherapy	24	7.9
Surgical procedures – extractions/resections	10	3.3
Antifungal treatment	7	2.3
Incorrect taking of the bioptic sample → incorrect result/wrong sending of the sample/result not corresponding to the clinical state	7	2.3
Incorrect diagnosis and no further treatment, referral, sample taking	7	2.3
Numerous examinations that extended the diagnosis	6	2
Periodontology treatment	4	1.3
Long wait for visits	3	1
Prosthesis correction or removal	3	1
Long wait for histopathology result	1	0.3
Photodynamic therapy	1	0.3
Repeated patient referral	1	0.3

N – number of patients.

the real cause of the discomfort. A disturbing fact were the frequently lengthy delays between getting a pathological result from a bioptic sample and implementing appropriate therapy. Often, the time was as long as 2–4 months.

Discussion

The percentage of patients in the early (I–II: 26.5%) and late (III–IV: 73.5%) stages of advancement in the group of patients analyzed are comparable to data from other studies, in which patients at advanced stages accounted for 71.4% of all cases.¹¹ On the other hand, in another analysis, the group of patients in the early stages dominated, with 68% at stages I–II.⁶

The number of doctors consulted by the patient influences the time that passes before the implementation of appropriate treatment. There was a weak positive correlation between the delay time and the number of doctors consulted before a patient's admission to the ward ($p < 0.05$). This confirms that numerous medical consultations extend the total time before the start of appropriate therapy. Patients most often visited healthcare professionals once (43.2%) or twice (28.8%) before they underwent appropriate treatment. This is relatively lower than reported in other studies, where about 60% of patients visited doctors 3–4 times before obtaining a final diagnosis.¹¹ Moreover, prolonged waiting times negatively affect patient's quality of life, which is connected with psychological distress.¹² In our study, a dentist was often the first healthcare professional consulted for oral cancer

(31.8%), which is comparable to Wang et al., who reported that a dentist was one of the specialists in 35% of the cases.⁶ It is important that sometimes the symptoms that patients report to the dentist, like toothache or discomfort related to a denture, raise suspicions of other potentially trivial ailments, common in dental practice, and may lead to misdiagnosis. The real cause should always be established before any treatment, not forgetting about the possibility of cancer.

Many studies categorize the reasons for delays into those dependent on the patients and those dependent on healthcare professionals. This study considers the entire delay time, from the moment of noticing the first symptom until the patients' admission to the Department of Maxillofacial Surgery. The average was 7.4 ± 13.9 months (slightly over 200 days), which is similar to a study by Peacock et al., where the overall mean delay was 203.8 days. Those authors concluded this delay is unacceptable.¹³ Some authors count the time of delay separately for the patients and specialists, and they emphasize that there is no consensus about a time point beyond which a diagnosis could be considered delayed.¹⁴ The definition of professional delay is the period from the patient's first consultation with a healthcare professional up to the final pathological diagnosis. One of the reasons for professional delay is inadequate clinical examination, but also nonspecific clinical symptoms, a low index of suspicion, a lack of familiarity and experience with the disease, and comorbidity.⁷ In a study by Esmaelbeigi et al.,¹¹ the total time was 140 days. As many as 45 days depended on the patient and 86 days on the doctors. Others emphasize the patients' delays, considering them to be the main delaying component, because the duration was over 3 months in 48% of cases.⁶ In our study, the patients caused delays in 41% of the cases, the doctors in 40.55% and both in 10.5%. Sometimes, however, even 80% of reasons for delay are attributed to patients due to the fact that despite noticing a disturbing lesion, 30% of patients wait over 3 months until they see a doctor.¹⁰

Public awareness of oral cancer seems alarmingly low, as Warnakulasuriya et al. reported.¹⁵ Patients are unaware of the etiology of their symptoms and often downplay the first signs even when they are long-lasting. In 1 study, only 13% of the patients thought their symptoms were caused by a potentially serious reason, while 50% of them believed it would get better by itself.¹⁶ The reason is usually that the early symptoms do not affect functionality to a large extent. Patients also often undertake independent home treatment, even without consulting a doctor. Patients who took traditional herbal medication before seeking professional help had significant delays in the diagnosis of cancer.¹⁶ Earlier detection is possible in cases where the patient is concerned about severe symptoms such as painful ulceration or bleeding.⁸

Previously existing symptoms – sore throat, cough or hoarseness because of addictions – may also mask

the appearance of the first symptoms of head and neck cancer in patients abusing tobacco and alcohol.⁹ Unfortunately, doctors often prescribe medications (especially painkillers) to reduce symptoms they perceive as minor. Sometimes they carry out dental treatment that is also only symptomatic. When it comes to dentists, it is noteworthy that a loss of teeth by the patient increases the risk of delay by as much as 4 times. Prior conservative, surgical or periodontal treatment significantly prolongs delays and contributes to the deterioration of the existing condition. The risk of professional delay in such cases increases over 7 times.¹¹ The symptoms that patients report to their primary care doctors are often suggestive of viral infection or tonsillitis, such as a sore throat or enlarged lymph nodes of the neck. This prompts the doctor to prescribe antibiotic therapy instead of looking for the real cause.⁸ This confirms that health professionals' oncological awareness is important, even though the patients' role in delaying the implementation of appropriate treatment is significant.

In the present study, the most frequently reported symptom was an undetermined lesion (23.3%), as Goy et al. also reported.⁹ In contrast, ulceration is the most frequent clinical observation (53.9%), which has been confirmed by data from other authors.¹⁶ Two critical signs present in almost all cancers are induration and fixation. Oral squamous cell carcinomas (OSCCs) present either as a red or white patch, an endophytic ulcerative lesion, or a more exophytic mass with rolled margins, central ulceration and tissue friability.⁷ Lesions of this type should immediately be subjected to further verification.

Reducing the duration of delays is essential, although there was no significant relationship between delay and tumor advancement in our study. Other authors emphasize that patients diagnosed with a certain delay have a 3 times greater risk of a diagnosis of cancer at a more advanced stage than patients diagnosed without delay.¹¹ Long-term survival also depends on tumor advancement. During a long-term analysis, 51.3% of the late-stage patients died, as opposed to 28.1% at an early stage.⁶ Some say, however, that the tumor advancement at diagnosis is mainly determined by the rate of its growth, and with rapid growth this time is shorter and the advancement is higher; and vice versa with slowly growing tumors.^{4,6,17} That sometimes explains a lack of relationship between delay and advancement,¹⁷ just as in our study, where there was no such correlation or dependence between the time and the number of additional symptoms related to a tumor. Tumors of the head and neck region are characterized by relatively rapid proliferation, so the period of early detection is shorter.⁴ With considerable advancement and because of many intensified symptoms, there is a lower risk of missing the tumor and the delay time is shorter.¹⁷ The stronger link between delay and tumor advancement in oral cancer compared to throat cancer reported by some authors is probably because throat cancer metastasizes at earlier stages.¹⁴

Both our analysis and conclusions from the literature draw attention to the level of oncological awareness, as the most common “professional” causes of delay include neglecting to consider cancer in the differential diagnosis and prescribing other treatment.¹¹ It is also necessary to pay attention to pre-cancerous lesions and their continuous monitoring.^{6,14} In our study, the location of the tumor has no significant relationship with the possibility of observing symptoms, which underlines the crucial role of accurate diagnosis by the first healthcare professional consulted. Differential diagnoses including cancer should also be performed among younger patients (under 45 years of age), because a common cause of overlooking cancer is a lack of suspicion because of a patient’s young age.¹⁴

Due to the fact that the only source of data was the patients’ anamnesis, there was a risk of unreliable results. However, our results are similar to the data found in other studies, as has been shown above. Another prospective study specifically considering monitoring treatment effectiveness could be performed in the future to further explore the problem.

Conclusions

The present study confirms the need to improve the level of oncological awareness in society, especially among healthcare professionals (GPs and dentists). Mandatory educational programs for doctors (as well as for medical students), focused primarily on in-depth interviews and clinical examinations, would help reduce the delay and shorten the diagnostic process. It is also essential to inform patients about maxillofacial oncology (attention to first symptoms, self-monitoring), especially those in high-risk groups, both during dental visits and social campaigns. Early detection of cancer may contribute to implementing appropriate treatment at low stages of advancement. Less invasive surgery is undoubtedly associated with a quicker, less demanding convalescence and a higher quality of life after surgery. Because of the necessity to exclude a relatively large group of patients due to the lack of all the required data for the study, it is necessary to create a full medical interview scheme, taking into account all the necessary data for further research.

ORCID iDs

Monika Rutkowska  <https://orcid.org/0000-0003-0243-7751>
 Sylwia Hnitecka  <https://orcid.org/0000-0002-1171-9817>
 Marek Nahajowski  <https://orcid.org/0000-0003-4679-5649>
 Marzena Dominiak  <https://orcid.org/0000-0001-8943-0549>
 Hanna Gerber  <https://orcid.org/0000-0002-0954-3955>

References

- World Health Organization. Global Health Observatory. Geneva, Switzerland: World Health Organization; 2018. who.int/gho/database/en/. Accessed June 21, 2018.
- Lingen MW, Kalmar JR, Karrison T, Speight PM. Critical evaluation of diagnostic aids for the detection of oral cancer. *Oral Oncol.* 2008;44(1):10–22.
- Chang TS, Chang CM, Ho HC, et al. Impact of young age on the prognosis for oral cancer: A population-based study in Taiwan. *PLoS One.* 2013;8(9):75855.
- van der Waal I. Are we able to reduce the mortality and morbidity of oral cancer: Some considerations. *Med Oral Patol Oral Cir Bucal.* 2013;18(1):33–37.
- Carvalho AL, Nishimoto IN, Califano JA, Kowalski LP. Trends in incidence and prognosis for head and neck cancer in the United States: A site-specific analysis of the SEER database. *Int J Cancer.* 2005;114(5):806–816.
- Wang KH, Song BH, Gilde JE, et al. Diagnostic pathway of oral cavity cancer in an integrated health care system. *Perm J.* 2018;22:17–152.
- Baykul T, Yilmaz HH, Aydin U, Aydin MA, Aksoy M, Yildirim D. Early diagnosis of oral cancer. *J Int Med Res.* 2010;38(3):737–749.
- Pitchers M, Martin C. Delay in referral of oropharyngeal squamous cell carcinoma to secondary care correlates with a more advanced stage at presentation, and is associated with poorer survival. *Br J Cancer.* 2006;94(7):955–958.
- Goy J, Hall SF, Feldman-Stewart D, Groome PA. Diagnostic delay and disease stage in head and neck cancer: A systematic review. *Laryngoscope.* 2009;119(5):889–898.
- McGurk M, Scott SE. The reality of identifying early oral cancer in the general dental practice. *Br Dent J.* 2010;208(8):347–351.
- Esmaelbeigi F, Hadji M, Harirchi I, Omranipour R, vand Rajabpour M, Zendehdel K. Factors affecting professional delay in diagnosis and treatment of oral cancer in Iran. *Arch Iran Med.* 2014;17(4):253–257.
- Gigliotti J, Madathil S, Makhoul N. Delays in oral cavity cancer. *Int J Oral Maxillofac Surg.* 2019;48(9):1131–1137.
- Peacock ZS, Pogrel MA, Schmidt BL. Exploring the reasons for delay in treatment of oral cancer. *J Am Dent Assoc.* 2008;139(10):1346–1352.
- Gómez I, Seoane J, Varela-Centelles P, Diz P, Takkouche B. Is diagnostic delay related to advanced-stage oral cancer? A meta-analysis. *Eur J Oral Sci.* 2009;117(5):541–546.
- Warnakulasuriya KA, Harris CK, Scarrott DM, et al. An alarming lack of public awareness towards oral cancer. *Br Dent J.* 1999;187(6):319–322.
- Güneri P, Epstein JB. Late stage diagnosis of oral cancer: Components and possible solutions. *Oral Oncol.* 2014;50(12):1131–1136.
- Seoane-Romero JM, Vázquez-Mahía I, Seoane J, Varela-Centelles P, Tomás I, López-Cedrún J-L. Factors related to late stage diagnosis of oral squamous cell carcinoma. *Med Oral Patol Oral Cir Bucal.* 2012;17(1):35–40.

Current management of pediatric appendicitis: A Central European survey

Vojtech Dotlacil^{1,A–D,F}, Barbora Frybova^{1,B,E}, Natalie Polívka^{1,B}, Daniel Kardos^{2,B,D,E}, Peter Vajda^{2,D,E}, Krystian Toczewski^{3,B,C}, Rebeka Pechanová^{4,B,C}, Jozef Babala^{4,D,E}, Michal Rygl^{1,C–F}, Dariusz Patkowski^{3,D,E}

¹ Department of Pediatric Surgery, Second Faculty of Medicine, Charles University and Motol University Hospital, Prague, Czech Republic

² Department of Pediatrics, Surgical Division, University of Pecs, Hungary

³ Department of Pediatric Surgery and Urology, Wrocław Medical University, Poland

⁴ Department of Pediatric Surgery, Comenius University in Bratislava, National Institute of Children's Diseases, Slovakia

A – research concept and design; B – collection and/or assembly of data; C – data analysis and interpretation;

D – writing the article; E – critical revision of the article; F – final approval of the article

Advances in Clinical and Experimental Medicine, ISSN 1899–5276 (print), ISSN 2451–2680 (online)

Adv Clin Exp Med. 2020;29(6):745–750

Address for correspondence

Vojtech Dotlacil

E-mail: vojtech.dotlacil@fnmotol.cz

Funding sources

None declared

Conflict of interest

None declared

Acknowledgements

The authors are grateful to all departments that participated in the study. Without their help, this work would not have been possible.

Received on December 19, 2019

Reviewed on January 27, 2020

Accepted on May 8, 2020

Published online on June 30, 2020

Cite as

Dotlacil V, Frybova B, Polívka N, et al. Current management of pediatric appendicitis: A Central European survey. *Adv Clin Exp Med.* 2020;29(6):745–750. doi:10.17219/acem/122176

DOI

10.17219/acem/122176

Copyright

© 2020 by Wrocław Medical University

This is an article distributed under the terms of the Creative Commons Attribution 3.0 Unported (CC BY 3.0)

(<https://creativecommons.org/licenses/by/3.0/>)

Abstract

Background. Appendicitis is one of the most common diagnoses in pediatric populations. Although new recommendations for the treatment of pediatric appendicitis were published, management varies among different institutions.

Objectives. To determine current practices in 4 (n = 4) representative pediatric surgical departments in Central Europe.

Material and methods. One department from each of the 4 countries was surveyed using an online questionnaire. Questions focused on preoperative, operative and postoperative practices in 2018, particularly those related to antibiotic (ATB) therapy and laparoscopy.

Results. A total of 519 appendectomies were performed, among which 413 (79.6%) were laparoscopic appendectomies (LAs), with a conversion rate of 5.1%. Appendectomy, as an elective procedure, was performed in 43 (8.3%) patients. One-quarter (129 patients) had complex appendicitis and 72.3% of these were operated laparoscopically. In 3 departments, ATB prophylaxis was administered, based on the decisions of the operating surgeon. One department used standard ATB prophylaxis (metronidazole). Whenever phlegmonous appendicitis was detected, ATB were administered therapeutically in 2 departments. Two other departments administered ATB based on surgeon decision. The choice of ATB was not standardized. If complex appendicitis was detected, all sites administered ATB therapeutically. The type of ATB treatment was standardized in complex cases in 2 departments. Thirty-four complications (6.6%) at surgical sites were recorded – 4.1% (16/390) after uncomplicated and 14% (18/129) after complex appendicitis. Thirty-two occurred after acute surgeries and 26 of these followed laparoscopic procedures. Postoperatively, intra-abdominal abscesses occurred in 3.5% of laparoscopic and in 2.9% of open appendectomy (OA) cases.

Conclusions. This questionnaire study showed that treatment outcomes for appendicitis in children in Central Europe are comparable with data reported in the literature. Laparoscopic appendectomy is the predominant surgical method, but there is a little consensus for ATB treatment in the management of appendicitis at our 4 pediatric surgical departments.

Key words: pediatric surgery, antibiotics, laparoscopy, appendectomy, postoperative complications

Introduction

Appendicitis is one of the most common acute surgical diagnoses in children, with appendectomy being the most commonly performed emergency operation.^{1,2} Inflammation of the vermiform appendix ranges from simple irritation to perforation with diffuse peritonitis. Therapy includes a combination of surgical and antibiotic (ATB) treatment. The traditional approach to appendectomy is the open surgical approach – open appendectomy (OA), first described by McBurney in 1894.³ Laparoscopic appendectomy (LA) was initially controversial (the first LA was performed in 1983 by Professor Kurt Semm), but recently LA has emerged as standard care in pediatric patients with acute appendicitis. Antibiotics are crucial for the treatment of complex appendicitis, and prophylactically before appendectomies.⁴ Their correct indication is important in reducing unjustified use, optimizing hospitalization stays and maximizing savings while maintaining safe levels of healthcare.⁵ According to evidence-based medicine (EBM), new recommendations have been published for the treatment of pediatric appendicitis in surgical terms and ATB therapy.⁶ This pilot study aimed to determine the current practices in 4 representative pediatric surgical departments in Central Europe.

Material and methods

A multicenter retrospective questionnaire was addressed to pediatric departments in the Czech Republic, Hungary, Poland, and Slovakia, using an online survey (SurveyMonkey Inc., San Mateo, USA). The questionnaire (Fig. 1) consisted of 10 questions focusing on the type and number of appendicitis operations, surgical approaches, ATB prophylaxes and therapies, and the number of postoperative complications at surgical site infections (SSIs) in 2018. Data was collected anonymously.

Results

All 4 departments completed the questionnaire. In 2018, 519 appendectomies were performed in participating departments. All departments performed both OA and LA (Fig. 2). Four hundred and thirteen patients (79.6%) had LA, with conversion in 21 (5.1%) patients. Appendectomy as an elective procedure (during surgery for recurrent abdominal pain) was performed in 43 (8.3%) patients. Three-quarters of patients (390) had uncomplicated appendicitis (chronic, catarrhal or inflamed but grossly intact, nongangrenous, nonsuppurative appendix with no associated abscess or peritonitis). The remaining patients (129) had complex appendicitis (gangrene, perforation or peri-appendicular abscess/mass) (Fig. 3).

Thirty-five (OA; 27.1%) patients were operated by open surgery and 94 (LA; 72.9%) were operated laparoscopically. One department used standard preoperative ATB treatment (metronidazole), immediately started when the decision to perform an appendectomy was made. At the remaining departments, ATBs were administered according to decisions made by the consultant surgeon. Antibiotics were therapeutically administered in 2 departments, whenever phlegmonous appendicitis was detected. Two other departments administered ATB based on decisions made by the operating surgeon. The choice of ATB was not standardized. If complex appendicitis was determined, all departments administered ATB therapeutically, 2 according to their protocols. Overall, the SSI rate was 6.6% (34/519). Almost all infections occurred after acute surgeries (94%, 32/34). After surgery for uncomplicated appendicitis, the complication rate was 4.1% (16/390), and 14% after complex appendicitis (18/129). In terms of acute complications, 7% (26/373) occurred after LA and 5.8% (6/103) after OA. In a subgroup of organ-specific complications, abscesses after acute LA were observed in 3.5% (13/373) of patients and 2.9% (3/103) of patients after acute OA.

Discussion

Over the last 2 decades, studies on pediatric appendicitis have been increasing with a focus on the laparoscopic approach, as well as the correct ATB policy for the most effective treatment and reduction of postoperative morbidity.⁷ In our questionnaire study, we focused on the current state of treatment of acute appendicitis in 4 representative pediatric surgical departments in Central Europe.

Laparoscopy

The data showed that equipment for LA was available in all departments and that laparoscopy had become the method of choice for almost 80% (413) of patients at the participating departments. The conversion rate was 5.1%. One-quarter of all patients had complex appendicitis (gangrene, perforation or peri-appendicular abscess/mass) and even in these cases, 72.3% were operated on laparoscopically.

Our results are comparable with the 2017 EUPSA questionnaire, according to which most pediatric surgeons selected a laparoscopic approach (89% of simplex appendicitis cases and 81% of perforated ones).⁸ The results of this comparison are even more interesting in terms of the money spent on healthcare, as most studies on the use of laparoscopy in appendectomy come from Western Europe or the USA, where more money goes to healthcare. In 2017, according to Eurostat, health spending per capita was about €2,773 in the European Union. In this study, in participating countries, this expenditure was almost €1,000

- 1) Number of all classic appendectomies performed in 2018
 1. For acute appendicitis
 2. For planned appendectomy (appendectomy performed during surgical exploration of abdominal cavity due to recurrent abdominal pain)
- 2) Number of all laparoscopic appendectomies performed in 2018
 1. For acute appendicitis
 2. For planned appendectomy (appendectomy performed during surgical exploration of abdominal cavity due to recurrent abdominal pain)
- 3) Number of complicated appendicitis in 2018 (gangrenous, perforated) – according to the perioperative finding – write the absolute number performed for the 1st laparoscopic, for the 2nd classical
- 4) Number of conversions from laparoscopic to classic appendectomy in 2018
- 5) Do you use antibiotic (ATB) prophylaxis before appendectomy (antibiotic prophylaxis = preoperative administration of one ATB dose 0–60 min before surgery)?
 1. Yes, in all cases
 2. Yes, but only in laparoscopic acute appendectomy
 3. Yes, but only in classic acute appendectomy
 4. Yes, but only in laparoscopic planned appendectomy
 5. Yes, but only in the classic planned appendectomy
 6. According to the decision of the surgeon
 7. No, we do not use ATB prophylaxis
- 6) Type of ATB prophylaxis (if you use multiple combinations, choose them)
 1. Amoxicillinum/acidum clavulanicum
 2. Amoxicillinum/acidum clavulanicum + gentamicin
 3. Amoxicillinum/acidum clavulanicum + metronidazole
 4. Amoxicillinum/acidum clavulanicum + gentamicin + metronidazole
 5. Piperacillinum/tazobactamum
 6. Other type or combination of ATB – please list
- 7) Do you use ATB postoperatively in the case of phlegmonous appendicitis?
 1. Yes
 2. No
 3. According to the surgeon
 4. If yes, what (please list and specify dosing schedule)
- 8) Do you use ATB postoperatively in case of gangrenous appendicitis?
 1. Yes
 2. No
 3. According to the surgeon
 4. If yes, what (please list and specify dosing schedule)
- 9) Do you use ATB postoperatively in case of perforated (peritonitis, abscess) appendicitis?
 1. Yes
 2. No
 3. According to the surgeon
 4. If yes, what (please list and specify dosing schedule protocol)
 - Duration
 - Way of administration
- 10) Number of postoperative complications up to the 30th postoperative day – SSI (surface, deep, organ specific – according to CDC – Centers for Disease Control and Prevention)
 1. LAA (laparoscopic acute appendectomies)
 - Surface/Deep/Organ-specific
 2. LPA (laparoscopic planned appendectomies)
 - Surface/Deep/Organ-specific
 3. CAA (classic acute appendectomies)
 - Surface/Deep/Organ-specific
 4. CPA (classic planned appendectomies)
 - Surface/Deep/Organ-specific

Fig. 1. Management of appendicitis in 2018 – survey

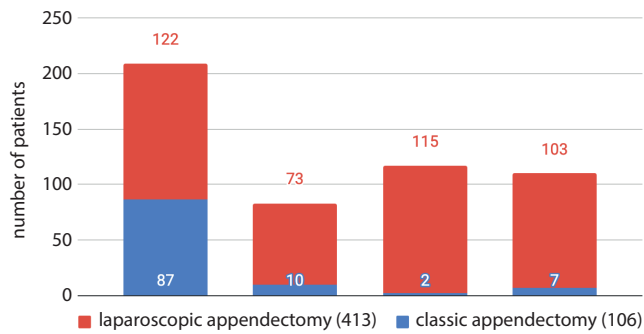


Fig. 2. The number of laparoscopic and classic appendectomies performed at participating departments (n = 4)

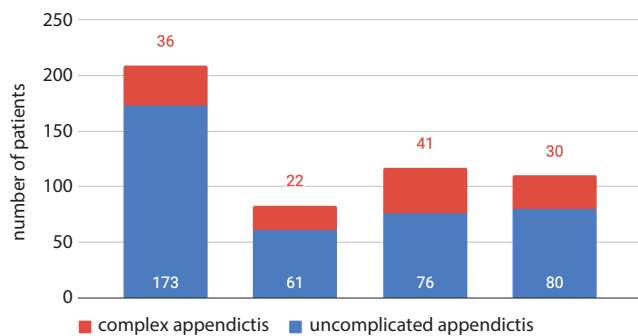


Fig. 3. The number of complex and uncomplicated appendicitis performed at participating departments (n = 4)

lower (the Czech Republic: €1873, Hungary: €1473, Poland: €1409, and Slovakia: €1625).⁹

Laparoscopic appendectomy in children has been used for over 25 years – its first use was described in 1992 by Ure et al.¹⁰ According to recent studies and meta-analyses, LA in children shortens the length of hospitalization, and reduces the risk of wound infections and postoperative pain.^{11–13} Furthermore, favorable cosmetic results after LA have also been demonstrated in children.¹⁴

Antibiotic prophylaxis and treatment

Antibiotics are effective both prophylactically before an appendectomy to reduce postoperative complications, and in the treatment of complex appendicitis, either following surgery, or as a first choice in the treatment of periappendicular mass or abscess.

Our results showed that ATB prophylaxis was a standard part of treatment in only 1 department, where metronidazole was started preoperatively. The other departments administered ATB according to decisions made by the surgeon. Antibiotic was administered in 2 of the departments whenever a perioperative finding of phlegmonous appendicitis was determined, whereas, in the other 2, the decision was left to the surgeon. When complex appendicitis was found, ATBs were always administered; in 2 departments according to standard protocols, but the ATB type varied in each department. Some departments still chose a triple ATB combination in case of perforation (Fig. 4).

The use of any drugs, including ATBs, can in extreme cases lead to prescription errors. Excessive indications or inappropriate duration of administration can prolong treatment, hospitalization, cause of complications, increase ATB resistance, and in general, increase the overall cost of treatment.¹⁵ In 2010, based on a systems review, the American Pediatric Surgery Association's recommendations on prophylaxis and treatment of acute appendicitis were published.¹⁶ According to this publication, ATB prophylaxis is always recommended before appendectomy, and when uncomplicated appendicitis is found, ATB therapy is not continued (the number of postoperative complications has not decreased with continued ATB administration). In cases of complex appendicitis, the use of broad-spectrum ATBs is always recommended. They should be used either as a monotherapy or in combination with other ATBs (e.g., piperacillin/tazobactam + metronidazole). Previous, standard ATB triple combinations

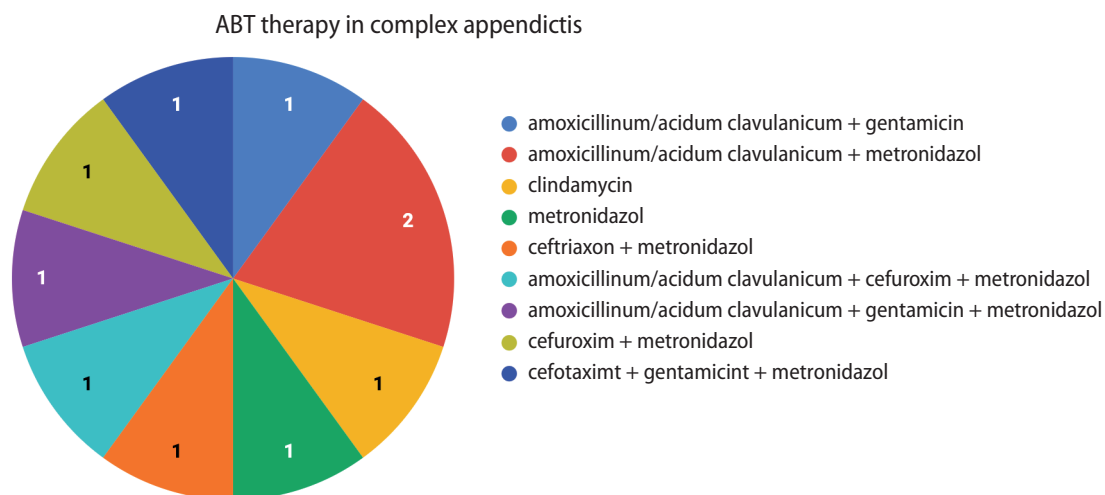


Fig. 4. Wide variation in the use of ATB across departments for complex appendicitis

against Gram-positive, Gram-negative and anaerobic bacteria are no longer recommended.^{17,18}

For phlegmonous appendicitis, all departments in certain cases (2 always, 2 decided by the surgeon) continued with ATB as therapy and did not follow current EBM recommendations. In complex appendicitis cases, according to current EBM recommendations, 100% of departments always indicated ATB, but ATB choices and combinations differed greatly. However, inconsistencies in using ATB as a treatment in these departments may reflect a lack of implementation of recent recommendations, and also they may be partly based on their recommendations and on local microbiological findings and recommendations of ATB centers.

Based on our surgical data and literature recommendations, 2 centers developed a uniform ATB prophylaxis and therapy scheme during 2018.

Complications





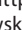





Overall, there were 34 (6.6%) complications; 4.1% after uncomplicated appendicitis and 14% after complex appendicitis, and almost all occurred after acute surgeries. Approximately 7% (26/373) of complications after acute surgeries were noted following laparoscopic procedures, and 5.9% (6/103) were noted following an open procedure. The incidence of intra-abdominal abscesses was 3.5% (13/373) after acute LAs and 2.9% (3/103) after acute OAs.

In 2017 a meta-analysis of randomized controlled trials with 3,642 patients (1810 LA and 1832 OA) reported 9.5% postoperative complications after LA, and 14.8% after OA, and concluded no significant differences between the 2 groups (OR = 0.74, 95% CI = 0.34–1.59, $p = 0.44$).¹⁹ In an extensive literature review from 2012, Markar et al. describing 107,624 patients, laparoscopic approaches did not increase the risk of postoperative complications, and in a sub-analysis of patients undergoing LA for complex appendicitis, the risk of postoperative complications was significantly lower.²⁰ In a 2012 retrospective study in 1,205 patients after appendectomy, investigating the development of postoperative complications and intra-abdominal abscesses in relation to surgical techniques, comparisons were made for uncomplicated and complex appendicitis, with the conclusion that the type of surgical approach did not affect the development of intra-abdominal abscesses (LA, 3.9%(19/491) vs OA, 3.9% (28/714); $p = 1.0$).²¹ Some surgeons chose the open approach for complex appendicitis because of the greater risk of complications following LA, but this remains unconfirmed in these studies. Some studies have shown the contrary; LA led to a significantly lower number of readmissions (1.3% vs 12.3%; $p = 0.006$) and reoperations (4% vs 17.2%; $p = 0.006$), and significantly lower numbers of postoperative wound complications (0% vs 11.5 %; $p = 0.001$).²² Similar conclusion were reached in the study by Chang et al. who reported that the risk of wound infection was significantly higher in the OA group (12.6% vs 4%; $p = 0.032$).²³

Conclusions

This questionnaire study showed that our results of appendicitis treatment in children in Central Europe are comparable with the literature. Laparoscopic appendectomy is the predominant surgical method; however, there appears to be little consensus on ATB treatment for the management of appendicitis at surveyed pediatric surgical departments in Central Europe.

ORCID iDs

Vojtech Dotlacil  <https://orcid.org/0000-0002-7291-7323>
 Barbora Frybova  <https://orcid.org/0000-0001-5744-9747>
 Natalie Polivka  <https://orcid.org/0000-0001-7413-5600>
 Daniel Kardos  <https://orcid.org/0000-0003-4863-1445>
 Peter Vajda  <https://orcid.org/0000-0002-4835-6458>
 Krystian Teczewski  <https://orcid.org/0000-0003-4336-2151>
 Rebeka Pečanová  <https://orcid.org/0000-0002-8310-9436>
 Jozef Babala  <https://orcid.org/0000-0003-1073-9733>
 Michal Rygl  <https://orcid.org/0000-0002-4804-039X>
 Dariusz Patkowski  <https://orcid.org/0000-0002-4583-5517>

References

1. Wan MJ, Murray K, Ungar WJ, et al. Acute appendicitis in young children: Cost-effectiveness of US versus CT in diagnosis. A Markov decision analytic model. *Radiology*. 2009;250(2):378–386. doi:10.1148/radiol.2502080100
2. Buckius MT, McGrath B, Monk J, et al. Changing epidemiology of acute appendicitis in the United States: Study period 1993–2008. *J Surg Res*. 2012;175(2):185–190. doi:10.1016/j.jss.2011.07.017
3. McBurney C. The incision made in the abdominal wall in cases of appendicitis, with a description of new method of operating. *Ann Surg*. 1894;20:38–43. doi:10.1097/00000658-189407000-00004
4. Shawyer AC, Hatchell AC, Pemberton J, et al. Compliance with published recommendations for postoperative antibiotic management of children with appendicitis: A chart audit. *J Pediatr Surg*. 2015;50(5):783–785. doi:10.1016/j.jpedsurg.2015.02.040
5. Fraser JD, Aguayo P, Leys CM, et al. A complete course of intravenous antibiotics vs a combination of intravenous and oral antibiotics for perforated appendicitis in children: A prospective, randomized trial. *J Pediatr Surg*. 2010;45(6):1198–1202. doi:10.1016/j.jpedsurg.2010.02.090
6. Lee SL, Islam S, Cassidy LD, et al. Antibiotics and appendicitis in the pediatric population: An American pediatric surgical association outcomes and clinical trials committee systematic review. *J Pediatr Surg*. 2010;45(11):2181–2185. doi:10.1016/j.jpedsurg.2010.06.038
7. Andersen BR, Kallehave FL, Andersen HK. Antibiotics versus placebo for prevention of postoperative infection after appendectomy. *Cochrane Database Syst Rev*. doi:10.1002/14651858.CD001439.pub2
8. Zani A, Hall N, Rahman A, et al. European Paediatric Surgeons' Association Survey on the management of pediatric appendicitis. *Eur J Pediatr Surg*. 2019;29(01):53–61. doi:10.1055/s-0038-1668139
9. OECD/EU (2018), Health at a Glance: Europe 2018: State of Health in the EU Cycle, OECD Publishing, Paris. https://doi.org/10.1787/health_glance_eur-2018-en
10. Ure BM, Spangenberg W, Hebebrand D, et al. Laparoscopic surgery in children and adolescents with suspected appendicitis: Results of medical technology assessment. *Eur J Pediatr Surg*. 1992;2(6):336–340.
11. Masoomi H, Mills S, Dolich MO, et al. Comparison of outcomes of laparoscopic versus open appendectomy in children: Data from the Nationwide Inpatient Sample (NIS), 2006–2008. *World J Surg*. 2012;36(3):573–578.
12. Jaschinski T, Mosch ChG, Eikermann M, et al. Laparoscopic versus open surgery for suspected appendicitis. *Cochrane Database Syst Rev*. doi:10.1002/14651858.CD001546.pub4
13. Esposito C, Calvo AI, Castagnetti M, et al. Open versus laparoscopic appendectomy in the pediatric population: A literature review and analysis of complications. *J Laparoendosc Adv Surg Tech A*. 2012;22(8):834–839.

14. Chandler NM, Ghazarian SR, King TM, et al. Cosmetic outcomes following appendectomy in children: A comparison of surgical techniques. *J Laparoendosc Adv Surg Tech A*. 2014;24(8):584–588.
15. Ameer A, Dhillon S, Peters M, et al. Systematic literature review of hospital medication administration errors in children. *Integr Pharm Res Pract*. doi:10.2147/IPRP.S54998
16. Lee SL, Islam S, Cassidy LD, et al. Antibiotics and appendicitis in the pediatric population: An American Pediatric Surgical Association outcomes and clinical trials committee systematic review. *J Pediatr Surg*. 2010;45(11):2181–2185. doi:10.1016/j.jpedsurg.2010.06.038
17. Peter ST, Shawn D, Kuojen T, et al. Single daily dosing ceftriaxone and metronidazole vs standard triple antibiotic regimen for perforated appendicitis in children: A prospective randomized trial. *J Pediatr Surg*. 2008;43(6):981–985. doi:10.1016/j.jpedsurg.2008.02.018
18. Dreznik Y, Feigin E, Samuk I, et al. Dual versus triple antibiotics regimen in children with perforated acute appendicitis. *Eur J Pediatr Surg*. 2018;28(06):491–494. doi:10.1055/s-0037-1606847
19. Dai L, Shuai J. Laparoscopic versus open appendectomy in adults and children: A meta-analysis of randomized controlled trials. *United European Gastroenterol J*. 2016;5(4):542–553. doi:10.1177/2050640616661931
20. Markar SR, Blackburn S, Cobb R, et al. Laparoscopic versus open appendectomy for complicated and uncomplicated appendicitis in children. *J Gastrointest Surg*. 2012;16(10):1993–2004. doi:10.1007/s11605-012-1962-y
21. Nataraja RM, Teague WJ, Galea J, et al. Comparison of intraabdominal abscess formation after laparoscopic and open appendicectomies in children. *J Pediatr Surg*. 2012;47(2):317–321. doi:10.1016/j.jpedsurg.2011.11.023
22. Vahdad MR, Troebbs RB, Nissen M, et al. Laparoscopic appendectomy for perforated appendicitis in children has complication rates comparable with those of open appendectomy. *J Pediatr Surg*. 2013;48(3):555–561. doi:10.1016/j.jpedsurg.2012.07.066
23. Chang HK, Han SJ, Choi SH, et al. Feasibility of a laparoscopic approach for generalized peritonitis from perforated appendicitis in children. *Yonsei Med J*. 2013;54(6):1478–1483. doi:10.3349/ymj.2013.54.6.14

Organ of hearing and balance in peri- and postmenopausal women. Effects of hormone replacement therapy on hearing and balance in peri- and post-menopausal women: The current state of knowledge

Krystyna Orendorz-Frączkowska^{A–F}, Hanna Temporale^{A–D,F}

Department and Clinic of Otolaryngology Head and Neck Surgery, Wrocław Medical University, Poland

A – research concept and design; B – collection and/or assembly of data; C – data analysis and interpretation; D – writing the article; E – critical revision of the article; F – final approval of the article

Advances in Clinical and Experimental Medicine, ISSN 1899–5276 (print), ISSN 2451–2680 (online)

Adv Clin Exp Med. 2020;29(6):751–755

Address for correspondence

Hanna Temporale

E-mail: hanna.temporale@gmail.com

Funding sources

None declared

Conflict of interest

None declared

Received on August 1, 2019

Reviewed on October 14, 2019

Accepted on May 1, 2020

Published online on June 26, 2020

Abstract

Sensory-neural hearing loss in people over 50 – senile deafness – is currently an increasing problem due to the growing proportion of the elderly people in the population. We can find a number of worldwide publications on hearing loss and dizziness in peri-menopausal women, but the data is inconsistent. Reports describing the influence of sex hormones on the ear and its aging are similarly controversial. This review attempts to summarize the current state of knowledge regarding hearing and balance in women during menopause, based on recent studies in this field. It describes the possible causes of hearing and balance impairment in post-menopausal women other than the mere physiological aging of the ear. The review concludes that impairment of hearing and balance is significantly related to osteoporosis, which results from estrogen deficiency during menopause. It also presents the results of studies on the impact of hormone replacement therapy (HRT) and of particular hormonal components of HRT on hearing and balance. The European population is aging, so accurate knowledge about the effects of HRT on hearing and balance is crucial in the context of improving the quality of life of elderly women through appropriate qualification for hormone substitution therapy. Further detailed and extensive study is necessary to verify the impact of sex hormones on hearing in post-menopausal women, taking into account the type of HRT used, serum hormone levels and the presence or absence of osteoporosis.

Key words: dizziness, imbalance, benign paroxysmal positional vertigo, menopause, hearing loss

Cite as

Orendorz-Frączkowska K, Temporale H. Organ of hearing and balance in peri- and postmenopausal women. Effects of hormone replacement therapy on hearing and balance in peri- and post-menopausal women: The current state of knowledge. *Adv Clin Exp Med.* 2020;29(6):751–755. doi:10.17219/acem/121935

DOI

10.17219/acem/121935

Copyright

© 2020 by Wrocław Medical University

This is an article distributed under the terms of the Creative Commons Attribution 3.0 Unported (CC BY 3.0) (<https://creativecommons.org/licenses/by/3.0/>)

The period of menopause is associated with the occurrence of many disorders related to deficiencies of female sex hormones caused by the physiological loss of ovarian activity. Estrogens play a significant role in the function of many organs and processes.^{1–5} It is currently known that they are also found in the human brain and are involved in central auditory processes.¹

Menopause occurs on average around the age of 50 (between 45 and 55 years of age). The climacteric syndrome and the intensity of its symptoms is commonly evaluated according to the Blatt–Kupperman menopausal index.^{2,8} The syndrome is present in 78–92% of women, according to different sources, mostly affecting working women and substantially impairing their quality of life.² Vasomotor disorders associated with the release of the luteinizing hormone into the bloodstream and the accompanying low estradiol and progesterone levels are considered the underlying mechanism of climacteric symptoms – vasomotor ones in particular.⁶ Disorders of catecholamine metabolism, especially dopamine and norepinephrine, may be responsible for vertigo, postural instability and emotional volatility, because these neurotransmitters affect the hypothalamic–pituitary axis and have a major impact on mood and physical activity.⁷ Psychological mechanisms associated with a woman's personality type and her socioeconomic status have also been shown to be important factors modifying the severity of climacteric symptoms: Women with a strong personalities and high socioeconomic status deal much better with menopausal symptoms, including dizziness.⁷

Hormone replacement therapy (HRT) was first introduced in 1960s with the aim of reducing unpleasant climacteric symptoms and preventing the occurrence of osteoporosis and cardiovascular events associated with the deficiency of female sex hormones.^{3,8,9} It has been used as a monotherapy, by supplementing estrogens (17-estradiol, estriol); in combinations of estrogens with gestagens (progesterone, 17-hydroxyprogesterone, 19-nortestosterone); or by administering tibolone, a synthetic steroid precursor.⁸ Meta-analyses from numerous studies have assessed the risks and benefits of short- and long-term use of HRT, including reductions in the prevalence of osteoporosis or cardiovascular events, and improvements in cognitive functions.^{8,9}

The association of hearing impairment and menopause is not as clear as dizziness and menopause; moreover, hearing loss is not included in the menopausal syndrome. For many years, scientists have not considered reasons for the deterioration of hearing in post-menopausal women other than the physiological aging of the hearing organ. This was due to the fact that in many menopausal women, despite a subjective impression of deteriorating hearing, threshold tone audiometry showed no greater reduction in hearing sensitivity than what was appropriate for their age.¹ However, Trott et al. showed that in menopausal women with a normal hearing threshold, the latencies in auditory brainstem potentials (ABR) are significantly

longer and their hearing in noisy surroundings is significantly worse compared to a control group of menstruating women of a similar age. This, according to the authors, indicates central hearing deficits in women with sex hormone deficiencies who hear worse despite normal results in audiometric tests.¹ On the other hand, in the opinion of other researchers who have reported sensory-neural hearing loss in some post-menopausal women, the loss results from dysfunction of the cochlea associated with osteoporosis.^{5,10–12}

The results of studies on the impact of HRT on hearing are ambiguous. Some authors have shown that HRT has a beneficial effect on women's hearing in comparison with women who do not use it.^{4,12,13} Chen et al. assessed the risk of sudden sensory-neural hearing loss (SSNHL) in 13,112 women aged 45–79 using HRT and in 39,336 women not taking HRT. They reported no significant difference in the number of cases with SSNHL in the group that used HRT compared to the control group. On this basis, they concluded that HRT is not associated with a greater risk of SSNHL than in menopausal women who do not use HRT.¹⁴ The same authors analyzed the occurrence of tinnitus in a group of 13,920 women using HRT and 41,760 women not using HRT. They reported a significantly lower number of tinnitus cases in the group using HRT, concluding that HRT may potentially be beneficial in the prevention of tinnitus in women during menopause.¹⁵ However, this report is in contradiction to the observations by Curhan et al., who found a higher risk of hearing loss in post-menopausal women using HRT, which increased significantly with the length of time it is used.¹³ According to Lee et al., the risk of tinnitus rises with HRT.¹⁶

Some studies have presented the influence of particular hormones that are components of HRT on the functioning of the hearing organ. Guimaraes et al. noted a negative effect of progesterone on inner ear function and the central auditory pathways; they also found that estrogen monotherapy has no protective effect against the aging of the hearing organ.¹⁷ Price et al. described the side effects of combined estrogen-progesterone HRT on women's hearing in the form of a significant reduction of amplitudes in otoacoustic emission tests after 2 months of this therapy.¹⁸ In 2019, Williamson et al. on the one hand confirmed the negative effect of progesterone on evoked auditory brainstem potentials; on the other hand, by analyzing the results of auditory brainstem response (ABR) and gaps-in-noise (GIN) tests, they hypothesized that progesterone has a protective effect on the central auditory processing mechanisms.¹⁹ In addition, by observing the expression of IGF-1R and FoxO3 genes, they pointed to the positive effect of estrogens on delaying cochlear aging at the cellular level.¹⁹

As a result of the fact that some post-menopausal women are diagnosed with both peripheral and central hearing loss, questions about the pathomechanism

of this phenomenon arise.^{4,5,11,12,20–22} Due to the known association between bone demineralization and estrogen deficiency, osteoporosis has been considered as a potential cause. Progressive changes in the bone structure can potentially lead to the degeneration of the ossicles with decreases in their mass and reductions in the density of the bony cochlear capsule. Changes in the bone structure may also cause disturbances in sound transmission to the cochlea.^{10,11,21–23} Mendy et al. examined more than 8,000 women over 40 years of age and found a significant relationship between the severity of osteoporosis and the occurrence of sensory-neural hearing loss.²² These results have been confirmed by other authors.^{5,10,11,16,20–22,24} Kim et al. analyzed hearing test results in 68,241 people over 50 years of age with osteoporosis, and they showed an additional high risk of SSNHL in women with osteoporosis, significantly higher than in the control group of individuals not burdened with osteoporosis.²⁰

Table 1 summarizes the latest reports showing the results of hearing tests in peri-menopausal women. These works are mainly focused on evaluating hearing impairment and tinnitus risk factors such as osteoporosis and HRT.

Although dizziness is one of the most common symptoms occurring during the climacteric period, its pathomechanisms are not well understood. Rzewnicki et al. showed vestibular dysfunction of mainly a central character

(sporadically peripheral) in post-menopausal women who did not use HRT.²⁵ Similar results were previously reported by Orendorz-Frączkowska et al.² In addition, posturographic studies have shown worse central coordination in the area of the vestibular system, especially after excluding visual control in menopausal women additionally reporting dizziness. In the control group of women using HRT, the postural control parameters were significantly better than in the group that did not use it.² Mendy et al. also registered balance impairment in posturographic tests of a group of 8,863 women over 40 years of age. It appeared predominantly in women over 65 years and was significantly associated with decreases in bone mineral density (BMD).²² The latest research by Berk et al. confirmed these observations. In their opinion, not only osteoporosis but also balance impairment causing an increasing incidence of falls is an important risk factor for bone fractures at this age.⁵

Benign paroxysmal positional vertigo (BPPV) is one of the causes of dizziness during menopause. Dizziness associated with BPPV increases with age regardless of gender; however, it occurs significantly more often in women during menopause. That is why investigators are interested in researching the causes of the increased prevalence of BPPV in women in this period.^{26–30} So far, Owada et al. are the only researches to report BPPV in a similarly high percentage of women with dizziness and climacteric

Table 1. Organ of hearing and balance in peri- and postmenopausal women – current reports

Authors	Published	Aim of the study	Conclusion
Kahveci et al. [10]	<i>Clin Otolaryngol.</i> 2014	Correlation between osteoporosis and hearing impairment	Osteoporosis is associated with an increased risk of sensory-neural hearing loss with cochlear dysfunction.
Mendy et al. [22]	<i>Ann Epidemiol.</i> 2014	Correlation between osteoporosis and hearing and balance impairment	Osteoporosis can cause hearing and balance impairment in elderly women.
Kim et al. [20]	<i>Auris Nasus Larynx.</i> 2016	Correlation between osteoporosis and hearing impairment	Osteoporosis can cause hearing impairment.
Jung et al. [23]	<i>Clin Exp Otorhinolaryngol.</i> 2016	Correlation between osteoporosis and hearing after menopausal period	Osteoporosis can cause hearing impairment.
Upala et al. [24]	<i>Braz J Otorhinolaryngol.</i> 2017	Correlation between osteoporosis and hearing impairment – meta-analysis	Osteoporosis is one of the risk factors of hearing impairment.
Kshithi et al. [11]	<i>Am J Otolaryngol.</i> 2018	Hearing impairment in post-menopausal women in correlation with osteoporosis	Osteoporosis is associated with an increased risk of sensory-neural hearing loss with cochlear dysfunction.
Lee et al. [16]	<i>BMJ Open.</i> 2018	Correlation between severity of osteoporosis and hearing impairment	The risk of hearing impairment increases with the severity of osteoporosis.
Chen et al. [15]	<i>Oncotarget.</i> 2018	Risk of tinnitus in women using HRT	HRT gives the potential benefit of preventing tinnitus.
Trott et al. [1]	<i>J Am Acad Audiol.</i> 2019	Sex hormones and hearing. Central auditory processing in women	Central auditory processing impairment can occur in post-menopausal women with normal hearing.
Chen et al. [14]	<i>Menopause.</i> 2019	Risk of sudden sensory-neural hearing loss in correlation with HRT	There was no increase in the risk of sudden sensory-neural hearing loss when using HRT.
Williamson et al. [19]	<i>Aging Cell.</i> 2019	Correlation between HRT and hearing impairment	Neuroprotective effect of HRT in auditory brainstem evoked potentials.
Yoo et al. [21]	<i>Braz J Otorhinolaryngol.</i> 2019	Correlation between osteoporosis and hearing impairment	Significantly worse hearing thresholds in the presence of osteoporosis.

HRT – hormone replacement therapy.

symptoms (56.2%) as in an age-matched group with dizziness but without menopausal symptoms (52.9%).³¹

To investigate the correlation between dizziness and menopause, Yang et al. experimentally induced menopause in mice by performing bilateral ovariectomies; they noted significant balance behavioral deficits in those animals, showing that estrogen deficiency compromises otoconia maintenance and anchoring by reducing the expression of the otoconial component/anchoring proteins.³² Perhaps this could explain the increase in the prevalence of BPPV in women after the cessation of ovarian activity. A number of reports show a correlation between lower BMD and a higher risk of BPPV.^{5,22,26–30} Studies by Zhai et al. and Zhang et al. have proven that by improving BMD, the use of HRT significantly reduces the incidence of BPPV in women compared to the control group of women not using HRT (17.6% vs 61.5%).^{26,27} These researchers believe that HRT may be worth considering as a preventive treatment in recurrent BPPV in post-menopausal women.^{26,27,30}

Owada et al. have found that women aged 40–59 with climacteric symptoms and dizziness suffer from Meniere's disease (17.8%) significantly more often than women of the same age presenting only dizziness (9.7%). The authors perceived psychological factors as the reason for this difference.³¹ The substantial contribution of psychological factors to the pathomechanism of vertigo has been presented by Terauchi et al., who noted anxiety disorders in 35.7% of their study group of women with dizziness during menopause, indicating that anxiety treatment may reduce dizziness.⁷

Owada and Suzuki investigated the relationship between the presence of vasomotor symptoms and the occurrence of non-systemic recurrent dizziness during menopause.⁶ Women without vasomotor symptoms during the two-month observation presented a significantly higher frequency of recurrences of dizziness than women who had these symptoms, which would suggest a lack of connection between them. However, after the women with menopausal symptoms began using HRT, the dizziness disappeared much faster than in women who did not use HRT.⁶

Due to the aging of European society, it is important to prevent and solve problems of the older population. Hearing loss, tinnitus and dizziness have a significantly strong impact on the patients' quality of life, including their family and professional relationships. Reliable knowledge about hearing and balance disorders in post-menopausal women offers a physician the chance to prevent or at least considerably delay these dysfunctions by adjusting HRT or osteoporosis treatment. At the same time, it is important to eliminate the negative impact of HRT on the functioning of the organ of hearing and balance. These data may provide the basis to specify new indications and contraindications for the use of HRT in the future or to determine the need for audiological monitoring in peri-menopausal women. In addition, evidence of the negative impact

of HRT on hearing and balance should complement the list of side effects of HRT, along with the risks of breast cancer, venous thromboembolism or dementia, so that doctors and patients can make informed decisions about replacement therapy, bearing in mind the risk of hearing impairment. This is especially important for women with hearing impairment diagnosed before hormonal treatment.

Here is a summary of the current state of knowledge regarding hearing and balance in women during menopause, based on a review of current research in this field:

1. Both peripheral and central hearing deteriorate in the peri-menopausal period.

2. Vertigo and dizziness are very common, and their causes are complex. One of the most common causes of dizziness during menopause is BPPV, but Meniere's disease is also more prevalent than in a comparable age group without menopausal symptoms.


3. Impairment of hearing and balance are significantly related to osteoporosis (decreased BMD), which results from the deficiency of estrogen during menopause.


4. Psychogenic factors such as anxiety and depression play an important role in the severity of dizziness.

5. Researchers' assessments of the impact of HRT on hearing organ functionality, including tinnitus as well as vertigo and dizziness, are varied. Some authors point out improvements in hearing and reductions in balance disorders during its use; others suggest the possibility of HRT causing damage to these senses.

ORCID iDs

Krystyna Orendorz-Frączkowska

 <https://orcid.org/0000-0002-9257-5156>

Hanna Temporale  <https://orcid.org/0000-0001-7054-5098>

References

1. Trott S, Cline T, Weihing J, Beshear D, Bush M, Shinn J. Hormones and hearing: Central auditory processing in women. *J Am Acad Audiol.* 2019;30(6):493–501.
2. Orendorz-Frączkowska K, Pośpiech L, Gawron W, Jędrzejuk D. Zawroty głowy u kobiet w okresie menopauzy. *Otolaryngol Pol.* 2004;58(2): 359–364.
3. Greene J. HRT has an uncertainty problem. Does compounding make it worse? *Manag Care.* 2019;28(2):32–35.
4. Hederstierna C, Hultcrantz M, Collins A. Hearing in women at menopause: Prevalence of hearing loss, audiometric configuration and relation to hormone replacement therapy. *Acta Otolaryngol.* 2017; 127(2):149–155.
5. Berk E, Koca TT, Guzelsov SS, Nacitarhan V, Demirel A. Evaluation of the relationship between osteoporosis, balance, fall risk and audiological parameters. *Clin Rheumatol.* 2019;38(11):3261–3268. doi:10.1007/s10067-019-04655-6
6. Owada S, Suzuki M. The relationship between vasomotor symptoms and menopause-associated dizziness. *Acta Otolaryngol.* 2014;134(2): 146–150. doi:10.3109/00016489.2013.841991
7. Terauchi M, Odai T, Hirose A, et al. Dizziness in peri- and post-menopausal women is associated with anxiety: A cross-sectional study. *BioPsychSocial Med.* 2018;12(1). doi:10.1186/s13030-018-0140-1
8. Lobo RA. Hormone-replacement therapy: Current thinking. *Nat Rev Endocrinol.* 2017;13(4):220–231.
9. Marjoribanks J, Farquhar C, Roberts H, Lethaby A, Lee J. Long-term hormone therapy for peri-menopausal and post-menopausal women. *Cochrane Database Syst Rev.* 2017;1(1):CD004143. doi:10.1002/1465185. CD004143.pub5

10. Kahveci OK, Demirdal US, Yucedag F, Cerci U. Patients with osteoporosis have higher incidence of sensory-neural hearing loss. *Clin Otolaryngol*. 2014;39(3):145–149.
11. Kshithi K, Vijendra Shenoy S, Panduranga Kamath M, et al. Audiological profiling in post-menopausal women with osteoporosis. *Am J Otolaryngol*. 2018;39(3):271–276.
12. Kosus N, Kosus A, Turhan N, Kurtaran H. Hearing levels in menopausal women and the effect of tibolone on audiological functions. *J Obstet Gynaecol*. 2012;32(3):294–297.
13. Curhan SG, Eliassen AH, Eavey RD, Wang M, Lin BM, Curhan GC. Menopause and post-menopausal hormone therapy and risk of hearing loss. *Menopause*. 2017;24(9):1049–1056. doi:10.1097/GME.0000000000000878
14. Chen PJ, Chung CH, Chien WC, Chen HC. Hormone therapy is not associated with the risk of sudden sensory-neural hearing loss in post-menopausal women: A 10-year nationwide population-based study. *Menopause*. 2019;26(8):892–898. doi:10.1097/GME.0000000000001323
15. Chen HC, Chung CH, Chen VCF, Wang YC, Chien WC. Hormone replacement therapy decreases the risk of tinnitus in menopausal women: A nationwide study. *Oncotarget*. 2018;9(28):19807–19816.
16. Lee SS, Han KD, Joo YH. Association of perceived tinnitus with duration of hormone replacement therapy in Korean post-menopausal women: A cross-sectional study. *BMJ Open*. 2017;7(7):e013736. doi:10.1136/bmjopen-2016-013736
17. Guimaraes P, Fristina S, Mapes F. Progesterone negatively affects hearing in aged women. *Proc Natl Acad Sci U S A*. 2006;103(38):14246–14249.
18. Price K, Zhu X, Guimaraes P. Hormone replacement therapy diminishes hearing in peri-menopausal mice. *Hear Res*. 2019;252(1–2):29–36.
19. Williamson TT, Ding B, Zhu X, Frisina RD. Hormone replacement therapy attenuates hearing loss: Mechanisms involving estrogen and the IGF-1 pathway. *Aging Cell*. 2019;18:e12939. doi:10.1111/acer.12939
20. Kim JY, Lee SB, Lee CH, Kim HM. Hearing loss in post-menopausal women with low bone mineral density. *Auris Nasus Larynx*. 2016;43(2):155–160.
21. Yoo JI, Park KS, Seo SH, Park HW. Osteoporosis and hearing loss: Findings from the Korea National Health and Nutrition Examination Survey 2009–2011. *Braz J Otorhinolaryngol*. 2019;S1808-8694(18)30488-9. doi:10.1016/j.bjorl.2018.12
22. Mendy A, Vieira ER, Albatineh AN, Lowry D, Gasana J. Low bone mineral density is associated with balance and hearing impairment. *Ann Epidemiol*. 2014;24(1):58–62. doi:10.1016/j.annepidem.2013.10.012
23. Jung DJ, Cho HH, Lee KY. Association of bone mineral density with hearing impairment in post-menopausal women in Korea. *Clin Exp Otorhinolaryngol*. 2016;9(4):319–325.
24. Upala S, Rattanawong P, Vutthikraivit W, Sanguankeo A. Significant association between osteoporosis and hearing loss: A systematic review and meta-analysis. *Braz J Otorhinolaryngol*. 2017;83(6):646–652.
25. Rzewnicki I, Knapp P, Kluz-Kowal AB, Kuryliszyn-Moskal A, Terlikowski R. Activity of vestibular organs in menopausal women non-users hormone replacement therapy (HRT). *Otolaryngol Pol*. 2010;64(1):10–14.
26. Zhai XY, Liu B, Zhang YH, et al. Analysis of BPPV in patients with bone mineral density results [in Chinese]. *Lin Chung Er Bi Yan Hou Tou Jing Wai Ke Za Zhi*. 2016;30(23):1865–1869.
27. Zhang YM, Yang ZD, Li WX, Shi C, Yu YF. The relationship between the recurrence of benign paroxysmal positional vertigo and the level of bone mineral as well as estrogen in post-menopausal women [in Chinese]. *Zhonghua Er Bi Yan Hou Tou Jing Wai Ke Za Zhi*. 2017;7;52(12):881–884. doi:10.3760/cma.issn.1673-0860.2017.12.001
28. Gu CY, Han WW, Wu YQ, Fan ZY, Chen CJ, Chen HM. Study on bone metabolism in post-menopausal women with idiopathic benign paroxysmal positional vertigo [in Chinese]. *Zhonghua Er Bi Yan Hou Tou Jing Wai Ke Za Zhi*. 2018;53(2):134–137. doi:10.3760/cma.issn.1673-0860.2018.02.010
29. Choi HG, Lee JK, Kong IG, Lim H, Kim SY. Osteoporosis increase the risk of benign paroxysmal positional vertigo: A nested case-control study using a national sample cohort. *Eur Arch Otorhinolaryngol*. 2019;276(2):335–342. doi:10.1007/s00405-018-5230-y
30. Liu DH, Kuo CH, Wang CT, et al. Age-related increases in benign paroxysmal positional vertigo are reversed in women taking estrogen replacement therapy: A population-based study in Taiwan. *Front Aging Neurosci*. 2017;12:9:404. doi:10.3389/fnagi.2017.00404
31. Owada S, Yamamoto M, Suzuki M, Yoshida T, Nomura T. Clinical evaluation of vertigo in menopausal women [in Japanese]. *Nihon Jibi-inkoka Gakkai Kaiho*. 2012;115(5):534–539.
32. Yang L, Xu Y, Zhang Y, Vijayakumar S, Jones SM, Lundberg YVW. Mechanism underlying the effects of estrogen deficiency on oticonia. *J Assoc Res Otolaryngol*. 2018;19(4):353–362.

Large animals as models of atrial fibrillation

Piotr Frydrychowski^{1,B,D}, Marcin Michałek^{1,B,D}, Agnieszka Sławuta^{2,C-F}, Agnieszka Noszczyk-Nowak^{1,A-F}

¹ Department of Internal Medicine and Clinic of Diseases of Horses, Dogs and Cats, Faculty of Veterinary Medicine, Wrocław University of Environmental and Life Sciences, Poland

² Department of Internal and Occupational Diseases, Hypertension and Clinical Oncology, Wrocław Medical University, Poland

A – research concept and design; B – collection and/or assembly of data; C – data analysis and interpretation;

D – writing the article; E – critical revision of the article; F – final approval of the article

Advances in Clinical and Experimental Medicine, ISSN 1899–5276 (print), ISSN 2451–2680 (online)

Adv Clin Exp Med. 2020;29(6):757–767

Address for correspondence

Agnieszka Sławuta
E-mail: aslawuta@tlen.pl

Funding sources

None declared

Conflict of interest

None declared

Received on September 12, 2019

Reviewed on January 4, 2020

Accepted on May 6, 2020

Published online on June 30, 2020

Abstract

In clinical practice, atrial fibrillation (AF) is the most common cardiac arrhythmia in humans and it may lead to numerous complications, including central nervous system embolism. The electrical activity of the heart in AF is rapid and chaotic, while the atrioventricular conduction leads to irregular ventricular contraction. Consequently, the stroke volume is reduced, which may lead to symptoms of heart failure. Heart failure is one of the causes of AF as well. Numerous in vivo and in vitro models are used to study the pathophysiology of AF. Animal models play a key role in understanding the mechanisms of arrhythmias as well as in developing treatment regimens. The models of AF include large animals (goats, sheep, pigs, dogs) as well as small laboratory animals. This study reviews the large animal models of AF, which enhance our understanding of numerous mechanisms responsible for the development of AF, but we must be aware that the pathomechanism of AF in humans is complex and is affected by numerous factors, including environmental and congenital ones.

Key words: arrhythmia, atrial fibrillation, animal models

Cite as

Frydrychowski P, Michałek M, Sławuta A, Noszczyk-Nowak A.
Large animals as models of atrial fibrillation. *Adv Clin Exp Med.* 2020;29(6):757–767. doi:10.17219/acem/122130

DOI

10.17219/acem/122130

Copyright

© 2020 by Wrocław Medical University

This is an article distributed under the terms of the
Creative Commons Attribution 3.0 Unported (CC BY 3.0)
(<https://creativecommons.org/licenses/by/3.0/>)

Introduction

Atrial fibrillation (AF) is the most frequently diagnosed arrhythmia in humans.^{1,2} It may accompany organic heart disease or occur as a solitary disorder (so-called lone AF), and its nature is multifaceted.

Numerous experimental *in vitro* and *in vivo* animal models were developed to understand the pathophysiology of AF and its effects on the organism. However, many questions regarding the mechanisms of AF remain unanswered. Studies with animal models are particularly useful, as they combine data from tissue and cell samples with those from clinical examinations and responses to treatment. Regardless of the type of AF animal model, it will always differ to some extent to AF in humans.

Animal models of AF include large animals (goats, sheep, pigs, dogs) as well as small laboratory animals.³ The use of mice, rats or rabbits may be highly advantageous, as these species are easily bred and their maintenance cost is low. In addition, study trials can be frequently repeated. Obtaining genetically modified mice, such as the α MyHC-FKBP12 transgenic mouse that spontaneously develops AF, has enabled their use in electrophysiological studies of AF. However, the use of laboratory animals has many limitations. Due to their small size, all the study procedures are difficult to perform and require the use of specialised, often customized and expensive equipment. Their small size also limits the "study field" of the atria and ventricles. Moreover, the size and availability of the tissue samples (such as heart muscle samples) for further analysis is limited. Although the use of transgenic animals has many benefits, it is very expensive. The lifespan of laboratory animals is relatively short. Hence, some changes observed in humans in the course of AF may never be observed in laboratory animals. This may hinder the long-term assessment of AF in transgenic species. In addition, their physiological parameters such as body temperature, respiratory and heart rate are higher than in humans, which makes it difficult to assess compensatory mechanisms and relate the obtained results to humans. For example, the classification of persistent AF in mice ranges from 1 min⁴ or 3 min,⁵ while the same condition is recognised in humans with AF persisting longer than 7 days.

The use of large animal (goats, sheep, pigs, and dogs) models may replace certain laboratory animal models. Surgical procedures are easier to perform on large animals. The body mass as well as the heart mass of pigs are similar to those in humans, so more study samples can be obtained. Large animal models also have limitations, such as higher maintenance costs or longer study periods. However, the abovementioned advantages seem to outweigh the limitations, suggesting that large animals are a good model of human AF.

Goats

Goats were the first animals to be used in studies on AF. In 1995, Wijffels et al. developed a goat model of AF to assess the electrophysiological changes inflicted by long-term AF.⁶ Atrial fibrillation was triggered by pacing the atrium using one-second impulses. After conversion to a sinus rhythm, the pacemaker pulse generator sent impulses to repeat the arrhythmia. This method gave a long-term model of persistent AF, which made it possible to confirm that rapid AF leads to atrial remodeling, affecting the refractory period of the myocardium. Disorders of the refractory period increase the atrial susceptibility to stimuli that induce and maintain AF, meaning that, *de facto*, AF may beget AF.⁶ Both electrical and structural atrial remodeling were assessed often as a cause of AF. By inflicting a complete atrioventricular block in goats, Neuberger et al. confirmed the hypothesis that atrial dilatation elongates episodes of AF by local conduction delays.⁷ In addition, the atrioventricular (AV) block was used to develop a model that allowed associating atrial contractility disorders with atrial enlargement caused by a slow ventricular rhythm, which develops secondary to AV blocks and atrial remodeling associated with AF.⁸ Van der Velden et al. investigated persistent AF and proved that the reconstruction of the Cx40 gap junctions may affect the pathogenesis of persistent AF.⁹ In that study, AF was induced using two-second 50 Hz impulses and maintained from 1 to 16 weeks.⁹ Ausma et al. focused on the influence of remodeling on AF using a goat model.^{10–12} They studied the mutual relations between persistent AF and myocardial structural remodeling. Atrial fibrillation was induced using 50 Hz impulses. Their studies revealed that persistent AF leads to structural changes in atrial myocytes, which may explain the worse myocardial contractility following cardioversion.¹⁰ In addition, it was found that goats with AF suffer from progressive cellular structural remodeling in the atrial myocardium,¹¹ which is a very slow and reversible process, while remodeling of the junction gaps is completely reversible.¹² Atrial structural and electrical changes following an induced AV block were also studied by Neuberger et al. in goats.¹³ After applying burst pacing to trigger AF for 48 h, the degree of atrial remodeling was measured. Then, after complete reversal of electrical remodeling, AV block was obtained and the procedure of burst pacing was repeated. Following their measurements, the authors found that electrical remodeling secondary to AF was present in dilated and non-dilated atria.¹³ Remes et al. performed an interesting study with a vascular shunt by connecting the aorta and the left atrium.¹⁴ The aim of that study was to assess the effect of left atrial overload on the occurrence and maintenance of AF. The results indicated that long-term AF can be a result of chronic atrium overload and occurs

in most animals without a decrease in the atrial effective refractive period (AERP).

Goats seem to be a good model of atrial remodeling in the course of AF. The mortality rate of the animals in the reported studies was low, and AF was induced relatively easily and in a repeatable manner. This model seems particularly useful in studies requiring long-term persistent AF as it can be maintained for periods of up to 20 weeks, and it does not require specialist equipment or additional procedures. Many of the mechanisms described in the studies on goats are similar to AF in humans. Undeniably, this is beneficial as in the study of the pathomechanism and treatment of AF in humans. The limitations of this model include a lower respiratory rate in goats and a maximal physiological heart rate lying within the lower reference range for humans. In addition, goats require species-specific anesthesia. Due to the fact that ruminants have a unique anatomy and physiology, their anesthesia carries a risk of complications.

Sheep

Sheep have also been used in cardiac studies, particularly those concerning atrial remodeling. The remodeling was mainly obtained by rapid atrial pacing, sometimes coupled with experimentally induced hypertension or heart failure.

Rapid atrial pacing for AF induction was used by Anné et al.¹⁵ In addition, Hiss bundle ablation was performed in some of the animals, followed by ventricular pacing at a frequency of 80 bpm and with the administration of quinapril and losartan or a placebo. The results were obtained after a 15-week observation period. The researchers found that there was sufficient atrial electrical remodeling to induce AF. However, structural changes are essential for the occurrence of permanent AF.

Atrial pacing to induce AF was also used in another model, where the structural and functional effects of chronic left atrial dilatation enabled an anastomosis between the aorta and the pulmonary artery.¹⁶ That procedure increased the blood flow in the pulmonary vein leading to a volume overload. The recording and pacing was carried out using quadripolar electrode placed in the right atrium. The study led to the conclusion that even moderate atrial volume overload may cause significant changes in the electrophysiological properties of the atrial muscle. These changes resemble those observed during AF and are likely to increase the susceptibility to AF. In human medicine, these findings may constitute an early clinical intervention aiming at normalizing hemodynamic parameters associated with atrial overload, which may occur in mitral valve disease.¹⁶

A modification of the model of atrial remodeling caused by rapid atrial pacing was proposed by Kistler, who studied electrical and structural changes in the atria of sheep with elevated blood pressure.¹⁷ Hypertension is one of the most

common factors involved in the pathogenesis of AF. The authors administered dexamethasone to pregnant sheep on the 27th day of gestation. After obtaining cardiac access, electrodes were sewn into Bachman's bundle and into the appendages and free walls of both atria. As mentioned previously, AF was induced by rapid atrial pacing. A prolongation of AF and an atrial conduction delay were observed in animals with elevated blood pressure compared with the control group. Due to the fact that changes in the structure of the atria, such as atrial hypertrophy and histological remodeling, were also observed, the authors concluded that slow conduction and an increased inductance of AF were associated with structural changes in atria.¹⁷ Sheep were also used to create a model of heart failure.¹⁸ That was done by rapid ventricular pacing, which caused dilated cardiomyopathy and dilatation of the left atrium. In all the animals, epicardial electrodes were sewn into the free wall of the left atrium and near right ventricular apex and in some animals into the free wall of the right atrium additionally. The leads were connected to a pacemaker eliciting rapid ventricular pacing (190 beats/min). In the course of the study, 42-day long atrial pacing was performed. A significantly higher atrial susceptibility to AF, a significantly larger LA and prolongation of the atrial effective refractory period were observed. The speed of left atrial enlargement was directly proportional to the increase in AF susceptibility.¹⁸

Mandapati et al. proposed another ovine model of heart disease using isolated hearts.¹⁹ Atrial fibrillation was induced by electrodes placed in the left and right atrium. The study enabled exact mapping of the areas of periodic activity during AF. In that model AF was most likely maintained via stable micro re-entrant sources.¹⁹

Despite some limitations of the sheep model, which are similar in goats, such as a lower respiratory rate, the risk of prion infections or some limitations during echocardiography caused by different anatomical topography of the digestive tract, the sheep is considered a good model for research on AF. In addition, a model of hypertension and a model of heart failure, which are often factors influencing AF, were created using this species. Sheep anesthesia, similarly to that in goats, requires special attention in order to minimize perioperative mortality.

Pigs

The use of pigs as a model of AF seems promising, as pigs have a similar body mass, heart size, metabolism, and heart rate as humans. These features allow direct translation of the results obtained in these studies into human medicine. As in the abovedescribed sheep and goat models, the developed swine models used rapid atrial pacing and some required non-standard surgical procedures.

Lee et al. aimed to develop a repeatable and simple swine model of maintaining AF, which would not require

chronic intervention within the atria.²⁰ Therefore, they accessed the heart by sternotomy and AF was induced using 3 maneuvers. The 1st maneuver was manual. If that had not induced AF, a pacing lead placed in the upper part of the right atrium was used for rapid atrial pacing, including burst pace. The 3rd maneuver was the administration of neostigmine, leading to an increased vagal tone with shortening of the atrial refractory period. Following neostigmine administration, the previous 2 maneuvers were repeated. If AF lasted longer than 1 min, it was considered continuous. In 14 of the 21 pigs with AF, AF was maintained without neostigmine. This produced a model of acute AF, which can be easily remodelled, as gives reliable results and does not require earlier preparatory procedures. It may be used in studies on ablation procedures and assessing new technologies in the treatment and prevention of AF.²⁰ Atrial remodeling caused by rapid atrial pacing was also used to compare the rate of changes in animals with hypertension and normotension.²¹ The six-hour rapid pacing at a frequency of 600 bpm was performed by a pacemaker in the free wall of the right atrium. Digoxin was administered in order to slow down the AV conduction. One group of animals received deoxycorticosterone acetate (DOCA) subcutaneous implants and a salt-rich (4%) diet for induction of hypertension. Rapid atrial pacing was commenced 2 weeks after the DOCA implantation. The use of this protocol made AF last longer than 60 min. Noticeable dilatation of the left atrium without heart insufficiency was observed 2 weeks after the pacing. The authors also found that AF in this model accelerated the structural remodeling of the atria and stabilised AF,²¹ which confirms the negative effect of hypertension in patients with simultaneous AF.

Linz performed an interesting study using a swine model in order to confirm the hypothesis that low-level baroreceptor stimulation (LL-BRS) may reduce the inducibility of AF in obstructive sleep apnoea (OSA).²² The animals in that

Table 1. Individual animal models, taking into account the type of induced AF

Model	Types of induction	Species
AF in an isolated heart	atrial pacing	sheep ¹⁹
Acute AF	neostigmine administration, mechanical cardiac stimulation, rapid atrial pacing	pig ²⁰
	rapid atrial pacing	pig ²⁴
Long-term AF	long-term atrial pacing	goat, ⁶ sheep ¹⁸
Persistent AF	remodeling of gap junctions	goat ⁹
Persistent AF	rapid atrial pacing, phenylephrine	dog ³¹
AF resistant to vernakalant	rapid atrial pacing	pig ²³
AF in obstructive sleep apnoea	negative tracheal pressures (ntp), atrial pacing	pig ²²

Table 2. Individual animal models in which induced AF was associated with the structure of the atria and its changes

Model	Types of induction	Species
Structural atrial remodeling	AV block	goat ^{8,13}
	atrial overload	goat, ¹⁴ sheep ¹⁶
	hypertension	sheep, ¹⁷ pig ²¹
	chronic heart failure	sheep, ¹⁸ dog ^{34,35}
	rapid atrial pacing	sheep, ^{15,17} pig, ²¹ dog ^{25,26,34}
Acute atrial damage	acute ischemia	dog ^{32,33}
Foci sensitive to catecholamines in the course of AF	rapid atrial pacing	dog ²⁸
Focal activity in pulmonary veins and atria in persistent AF	rapid atrial pacing	dog ³⁰
Involvement of pulmonary veins and the vein of Marshall in AF	atrial pacing, chronic heart failure	dog ³⁶

study underwent a tracheotomy to obtain negative tracheal pressure (NTP). Following AF induction via atrial pacing, carotid baroreceptor stimulation was performed. The obtained results confirmed that low-level baroreceptor stimulation inhibited the NTP-induced shortening of the atrial refractory period and induction of AF. These results confirm the use of LL-BRS as a novel therapeutic method in the treatment of AF in obstructive sleep apnoea.²² Pigs were also used to study new therapies of drug-resistant AF. Diness et al. created a model of AF to verify whether the SK channel inhibitor, known as AP14145, can effectively terminate AF resistant to vernakalant.²³ To begin with, they received seven-day pacing of the right atrium at a frequency of 420 bpm in order to induce sustained AF. Then, they placed electrodes into both the left atrial appendage and the left ventricle for the purpose of recording and pacing. After persistent AF was confirmed, the pigs received vernakalant as pharmacological cardioversion. If that had proven successful, the animals received repeated seven-day pacing, followed by vernakalant administration. If AF did not convert to sinus rhythm (SR), the animals received AP14145 intravenously.

Rapid atrial pacing aimed at inducing AF was also used by Jones et al. They carried out a study on pigs using CARTO[®] mapping to identify anatomical causes of conduction disturbances triggered by poorly overlapping ablation lines, leading to incomplete pulmonary vein isolation.²⁴ Atrial fibrillation was achieved by rapid atrial pacing. The pulmonary veins were isolated using cryoisolation. The authors found that their results were similar to those in patients with persistent or paroxysmal AF, which indicates that the swine model is a valuable experimental model of AF.²⁴

In pigs, like in other animals, rapid ventricular pacing was used to cause congestive heart failure. However, unlike the aforementioned study on the ovine model,¹⁸ no higher atrial susceptibility to AF or the occurrence of the arrhythmia of was observed.²⁵

The swine model of AF proved easily inducible and useful in studies on novel AF therapies. Rapid atrial pacing, which induced AF, is a simple and repeatable procedure in pigs.

Dogs

Dogs have been frequently used to develop models to better understand AF. The simplicity of surgical procedures in this species is an unquestionable advantage, allowing various studies to use dogs of different weights and sizes. An important factor in favor of canine models is the possibility of studying AF in animals with heart failure or atrial ischemia. In addition, due to the size of dogs, certain devices and equipment are suitable for pediatric electrotherapy. At the same time, dogs have a higher natural heart rate than humans, and this is one of the limitations of the canine model. Still, dogs have turned out to be particularly useful in the study of the parameters and atrial electrophysiological changes that lead to AF or contribute to its maintenance. In addition, dogs were used to determine the mechanism and effect of certain drugs on AF, which increased the putative pool of antiarrhythmic drugs.

The effect of drugs on atrial remodeling and electrophysiology parameters was reported by Shiroshita-Takeshita et al.^{26,27} The authors assessed the effect and mechanisms of simvastatin, vitamin C or vitamin E on a model of AF induced by atrial tachypacing (ATP). An AV block was induced to control the ventricular rhythm.²⁶ In another study, Shiroshita-Takeshita et al. assessed the effect of ibuprofen on the tachycardia-remodeling in dogs.²⁷ The authors used the same model of ATP as in the previously mentioned study but the dogs were administered ibuprofen, cyclosporine A or prednisone.²⁷ Rapid atrial pacing was also used by Gaspo et al.²⁸ In their model, the lead

in the right atrium was connected to a pacemaker placed subcutaneously in the neck area. The pacing frequency was set at 400 bpm and lasted 1, 7 and 42 days, depending on the group. Atrial fibrillation was induced using 2 ms impulses at 10 Hz. If the AF exceeded 45 min, it was considered long-term and was cardioverted. The study indicated that chronic atrial tachycardia not only reduces AERP (atrial effective refractory period), the conduction time and the wavelength, but also increases the capacity of atrial extrasystoles to induce and extend the duration of AF. The study was valuable, as it enabled an assessment of electrophysiological changes crucial for persistent AF.²⁸ Doshi et al. used a canine model to localize catecholamine-sensitive foci in the left atrium and then assessed their activity during AF induced via rapid atrial pacing. That study required in vivo and in vitro assessment. First, some dogs underwent a cardiectomy in order to collect samples for the in vitro and electrophysiological studies, including an infusion of isoproterenol into the coronary artery. In the remaining dogs, a pacing lead in the right atrium was connected to a subcutaneous pacemaker. The animals were monitored periodically for long-term AF, which was recorded in dogs 10, 11 and 41 weeks after lead placement. The authors found that the isoproterenol infusion may induce activity in the ligament of Marshall, and that this activity is higher in dogs with AF induced by tachypacing. It was also observed that rapid activity during the isoproterenol infusion may induce AF in vitro in the left atrium of dogs with long-term AF. This phenomenon is not observed in healthy atria. The results led to the conclusion that heightened sensitivity to isoproterenol following pacing may contribute to the development of AF in the described model.²⁹ The same method of AF induction was used to test the hypothesis that long-term stimulated AF is characterized by the presence of chaotic waves as well

RIGHT ATRIUM Rapid atrial pacing	LEFT ATRIUM Rapid atrial pacing Vascular shunt (aorta and LA; aorta and pulmonary artery) Isoproterenol
BOTH ATRIA Complete atrioventricular block – atrial dilatation elongating episodes of AF Atrial contractility disorders associated with atrial enlargement Persistent AF leading to structural changes Neostigmine Manual maneuver Low level baroreceptor stimulation in obstructive sleep apnea Atrial ischemia (ligating the branch of the right coronary artery) Arrhythmogenic atrial remodeling (angiotensin II)	
VENTRICULAR MYOCARDIUM Dexamethasone-hypertension Deoxycorticosterone acetate and salt rich diet Pacing-induced heart failure	

Fig. 1. The mechanisms of AF in animal models

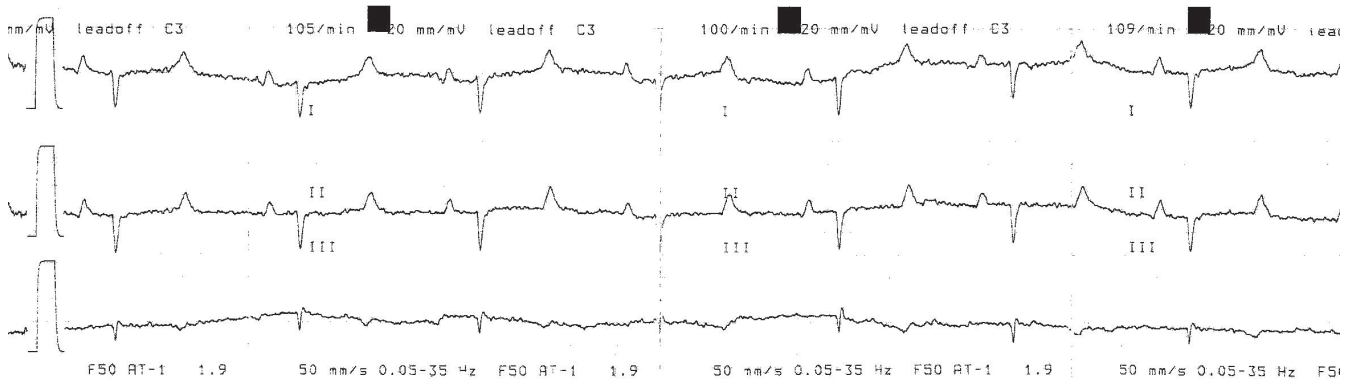


Fig. 2. Sinus rhythm in sheep

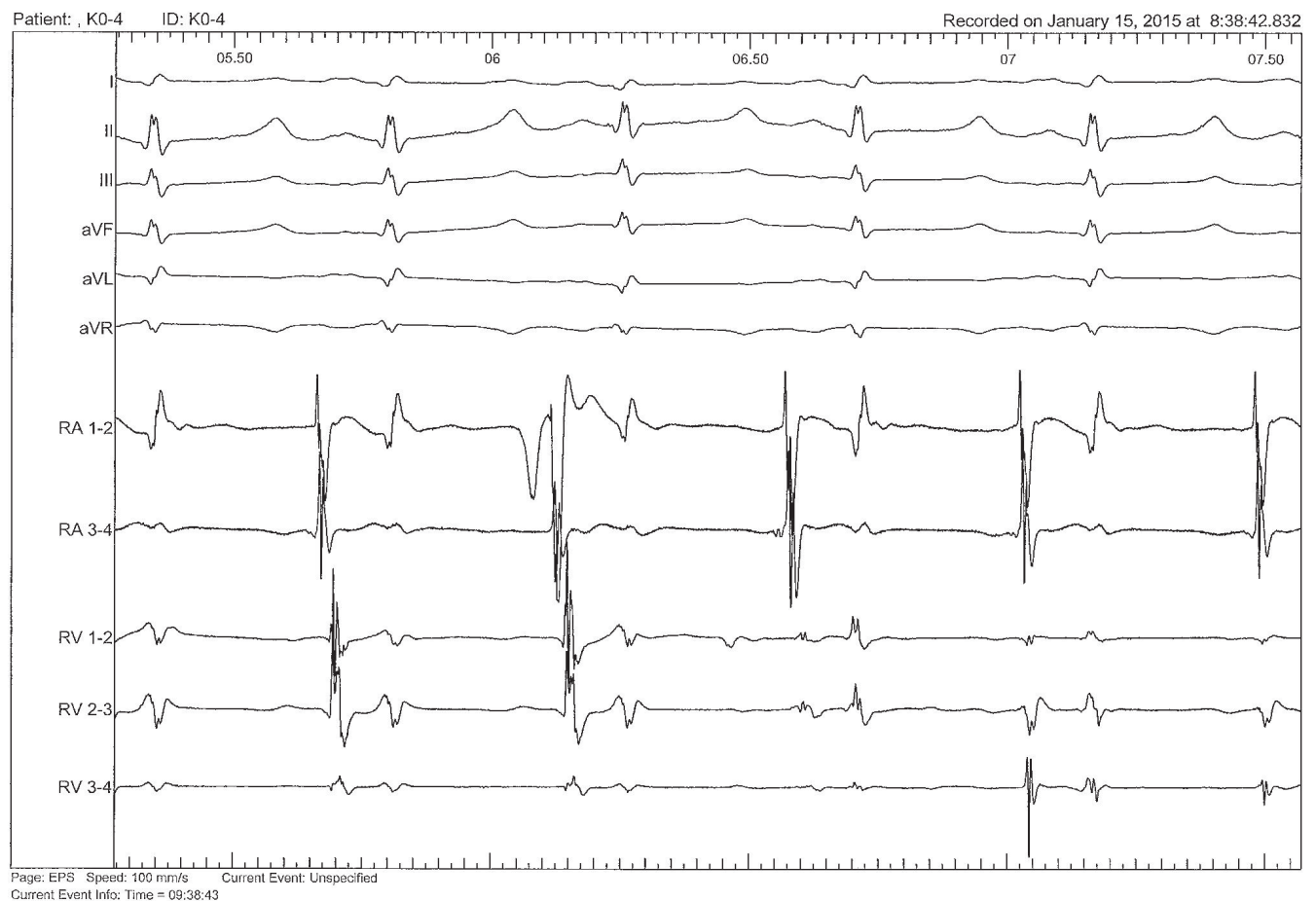


Fig. 3. Sinus rhythm in pig

as organized re-entry waves.³⁰ A bipolar electrode connected with a pacemaker was inserted into the right atrium. After confirming AF, the animals underwent mapping. The study confirmed the presence of chaotic disorganized and organized re-entry waves during persistent AF. In addition, the authors concluded that the ligament of Marshall and the pulmonary veins are the sources of rapid activation in the course of long-term AF induced by chronic stimulation.³⁰ Electrophysiological studies using a model based on rapid pacing were also performed by Zhou et al. to determine the patterns of activity in the pulmonary veins and

atria during AF.³¹ Intermittent rapid pacing was performed using a neurostimulator connected to a screw-in bipolar lead placed in the left atrium appendage in order to induce continuous AF. The pulse generator was programmed to burst with pacing interval of 50 ms for 5 s, followed by a two-second period without pacing. The arrhythmia was considered continuous if it persisted for >48 h after the pacemaker was turned off. This study found that rapid focal activations were present in the pulmonary veins following persistent AF caused by left atrium pacing. Such activation pattern is not present in pulmonary veins during

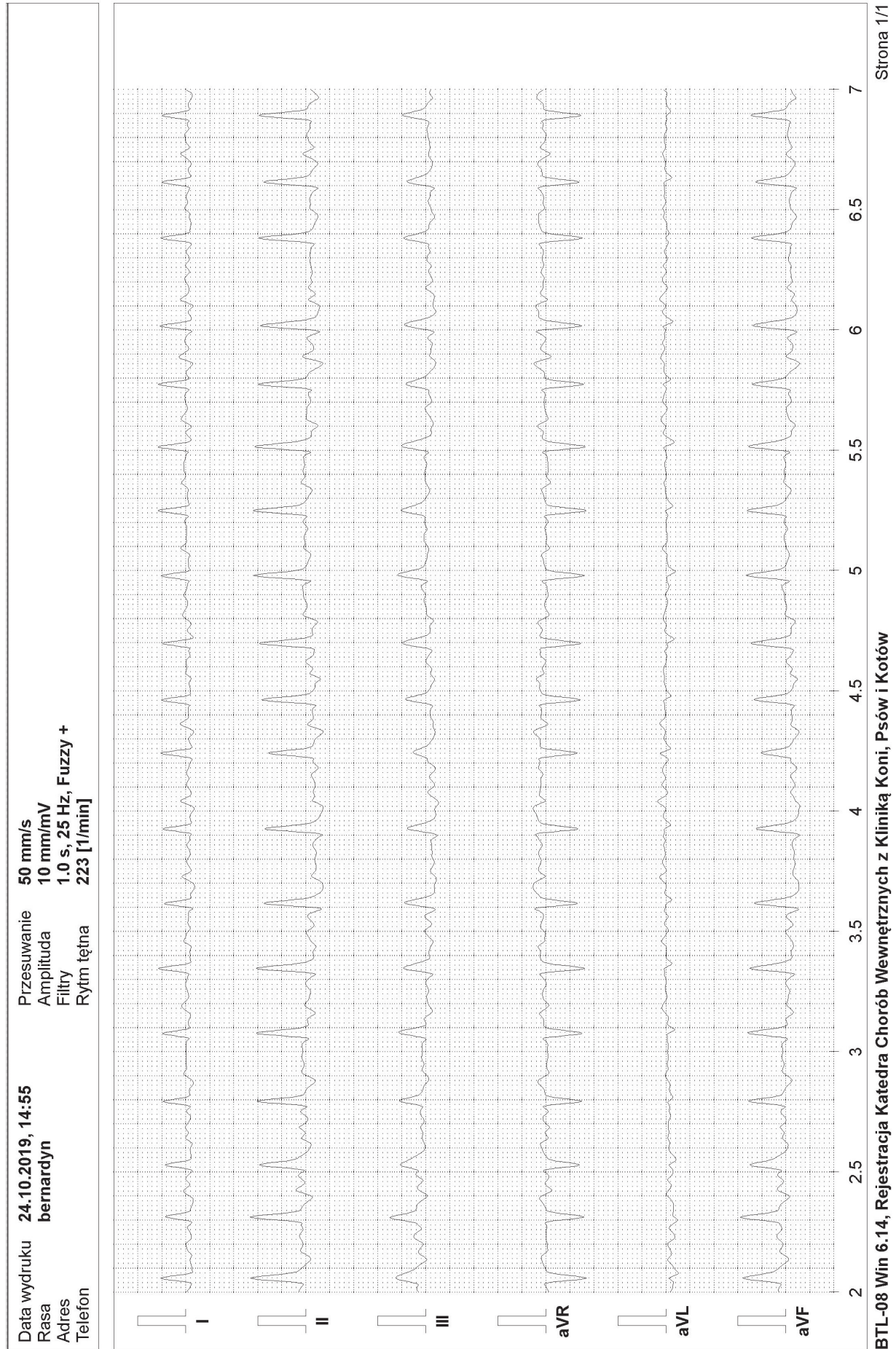
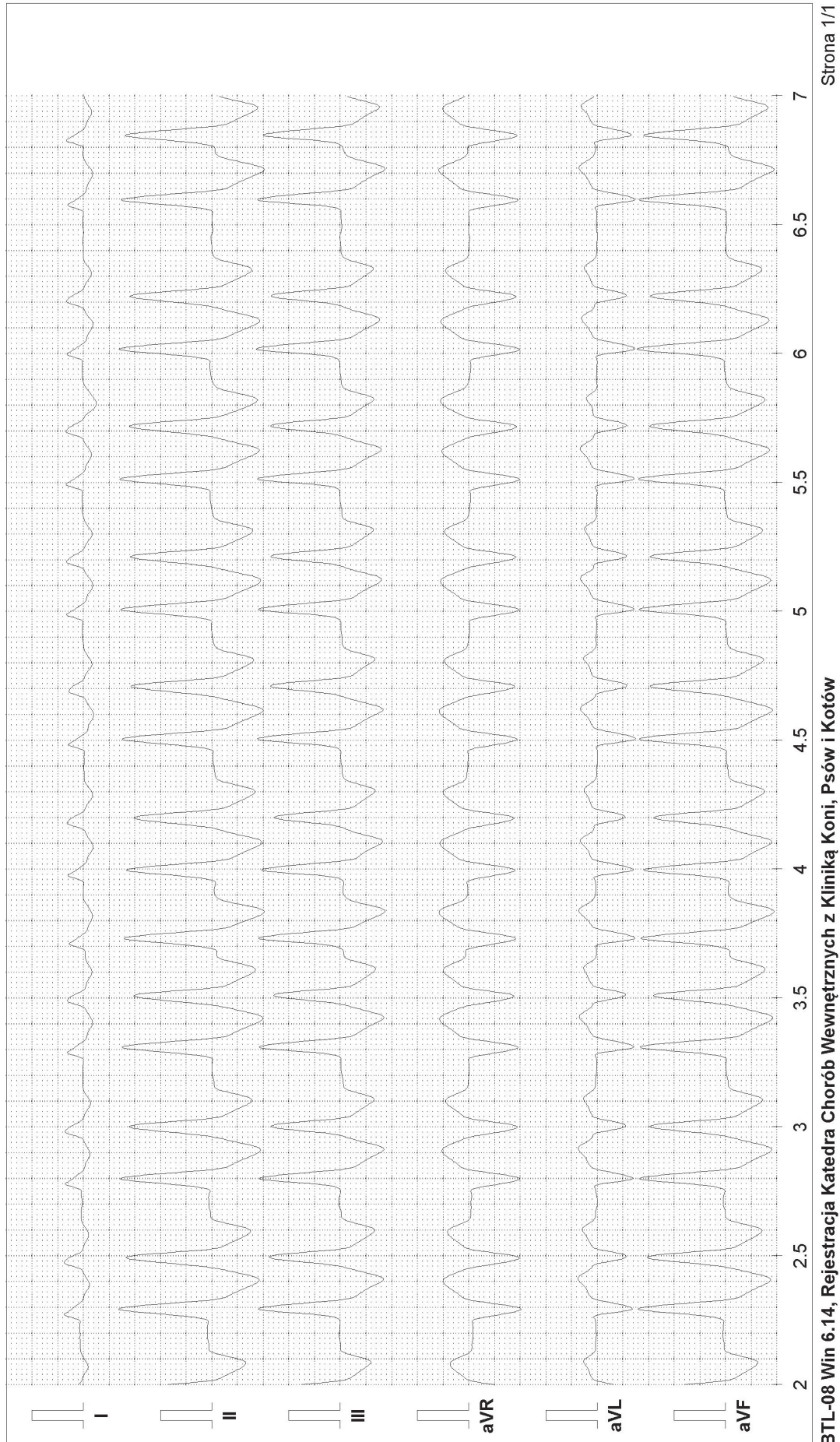


Fig. 4. Atrial fibrillation in dogs

Data wydruku 25.10.2019, 9:46
 Adres
 Telefon
 Rasa

Przesuwanie 50 mm/s
 Amplituda 10 mm/mV
 Filtry 1.0 s, 25 Hz, Fuzzy +
 Rytm tętna 229 [1/min]



BTL-08 Win 6.14, Rejestracja Katedra Chorób Wewnętrznych z Kliniki Koni, Psów i Kotów

Fig. 5. Atrial fibrillation and intraventricular conduction delay in cat

non-persistent AF. The results of that study confirmed the hypothesis that the pulmonary veins and ligament of Marshall are sources of rapid focal activations in a canine model of induced AF.³¹

The maintenance of AF in these studies required rapid pacing for extended periods of time. Therefore, studies on the AF model were carried out in such a way that the AF could be maintained for a sufficiently long time to perform all the necessary tests. Kijawornrat et al. used atrial stimulation with 2 ms waves at a frequency of 40 Hz.³² Some dogs received carbachol and phenylephrine in addition to the stimulation, which was ended after 20 min. The heart rate was then assessed in order to identify and confirm the induction of AF. In half of the tested dogs, the administration of phenylephrine causing an increase in arterial pressure led to the maintenance of AF for a period longer than 40 min.³²

A canine model of ischemia was also developed by Sinno et al.³³ In the study, atrial ischemia was achieved by ligating the branch of the right coronary artery. Atrial fibrillation was induced using 10 Hz impulse from leads placed in the left and right atrium appendage. The authors concluded that atrial ischemia maintains AF through slowing of conduction. The results of that study may be implemented in patients with coronary disease.³³ The results of that study and the described model were used to assess the effect of antiarrhythmic drugs on the electrophysiological consequences of acute atrial ischemia.³⁴ The authors also compared the effect of the drugs on ischemic and vagal AF. The ischemia model was obtained analogously to that in the study by Sinno et al.³³ The dogs were divided into groups including animals without treatment that underwent pacing, paced dogs that received diltiazem, nadolol, flecainide or dofetilide, and dogs with vagal AF. The study showed that that some drugs effectively prevent changes in atrial conduction and AF in acute atrial ischemia but the effects of these drugs on vagal AF were quite different. The obtained results may be of value for studies assessing the variable efficacy of antiarrhythmic drugs in the treatment of AF.³⁴

The assessment of changes leading to cardiac remodeling and the development of AF in congestive heart failure (CHF) is especially important. As is well known, this arrhythmia may lead to the occurrence and progression of heart failure, although heart failure itself is a known risk factor of AF. Therefore, models based on CHF appear to be extremely helpful in studies on the induction and course of AF. Dogs were also used to create this type of model. In their study, Li et al. described the electrophysiological and structural changes in the atria caused by experimentally induced chronic heart failure.³⁵ The authors also wanted to verify whether those changes could facilitate the induction of AF and to compare atrial remodeling in CHF with that caused by rapid atrial pacing. In the dogs, heart failure was induced by rapid ventricular pacing. In another group of dogs, the atria were paced at 400 bpm. Atrial fibrillation was induced by applying

a maximum of 3 consecutive extrastimuli, followed by atrial pacing with impulses at 10 Hz from 1 s to 10 s. Atrial fibrillation was considered persistent if it lasted longer than 30 min and needed to be discontinued by cardioversion. The study found that chronic heart failure favors persistent AF through a mechanism other than chronic atrial tachycardia.³⁵ In another study, Li et al. assessed the involvement of angiotensin II activation and mitogen-activated protein kinases (MAPK) in the induction of AF that promotes structural atrial remodeling.³⁶ Canine models were used to assess changes in atrial angiotensin II and MAPK in chronic heart failure caused by ventricular tachypacing (VTP) and the effects of ACE-I (angiotensin converting enzyme inhibitors) on the atrial angiotensin II, MAPK and the development of AF.³⁶ Ventricular pacing was carried out according to a methodology described by the same author,³⁵ while AF was induced by atrial pacing using 10 Hz impulses. Atrial fibrillation was considered persistent if it lasted longer than 20 min. The study found that ventricular pacing increases the concentration of atrial angiotensin II and MAPK. Enalapril suppressed those substances and was found to reduce the arrhythmogenic atrial remodeling.³⁶ Okuyama et al. used a canine model associated with CHF in order to confirm the hypothesis that proarrhythmic remodeling occurs in the tunica media of the thoracic veins.³⁷ Similar conclusions were reached by Wu et al.³⁰ The dogs underwent ventricular pacing in order to induce chronic heart failure. Then, the device was switched off and atrial tachyarrhythmia (AT) was induced by leads placed in the right atrium or the left atrial appendage. The study showed that some AF episodes in dogs with CHF are characterized by the presence of focal activation in the pulmonary veins and the vein of Marshall (oblique vein of the left atrium), suggesting their role in atrial arrhythmias in chronic heart failure. Pulmonary veins may also play a role in the progression of AT to AF.³⁷

Cats

Cats have also been used as animal models in AF studies. The research focused mainly on supraventricular arrhythmias induced with aconitin; however, only a few studies describing experiments with this substance are available in the literature.^{38–43} Ammar and Kudrin were the first to describe the effects of aconitin administration to the sinus node on the heart rhythm.³⁸ Gendenshtein et al. induced AF by local administration of 0.05% aconitin into the right atrium.³⁹ Byrne and his team, in turn, used a saturated solution of aconitin, which successfully induced AF in 3 out of 5 tested cats.⁴⁰ Winslow also tested the arrhythmogenic effect of aconitin. He conducted his experiment on anesthetized cats in whom arrhythmia was induced by a local application to the middle part of the left atrial appendage of 0.04% aconitin nitrate solution. The administration was performed using a cotton swab moistened

with the aconitin solution in a polyethylene tube.⁴¹ Winslow created a model in which supraventricular arrhythmias, including AF, can be easily induced by topical administration of aconitin. In addition, this model may be useful in antiarrhythmic drugs research. This model proved to be more effective in inducing AF than those tested in previous experiments.^{38–40,42–44} It is worth mentioning that AF may be developed secondary to left atrial enlargement in the natural course of feline hypertrophic cardiomyopathy.

New perspectives in antiarrhythmic therapy in animal models

TWIK-related acid-sensitive K⁺(TASK) channels belong to the two-pore-domain potassium (K2P) channel family. They are relevant for the pathogenesis of many different cardiovascular diseases including AF. TASK-1 channels are promising drug targets for the treatment of AF. The expression and function of those channels is enhanced in atrial cardiomyocytes of patients with chronic AF resulting in action potential duration shortening. The inhibition of TASK-1 in rodents caused prolongation of action potentials. The mechanism previously demonstrated in rodents was successfully elucidated in porcine model by Schmidt et al.⁴⁵ As porcine channel protein is almost identical to human, this model is perfect for the experiments with novel antiarrhythmic target. In recent studies, Schmidt et al. showed that genetic ablation of TASK-1 in porcine model significantly reduced AF burden, which was associated with the reduction of TASK-1 currents and the prolongation of action potential duration.⁴⁶ In search for a perfect animal model for research on the latest antiarrhythmic drugs, Wiedmann et al. studied transgenic mice and concluded that murine, porcine and human TASK-1 channels share many functional similarities.⁴⁷


Conclusions


The above discussion presents animal models used to assess AF. To date, numerous models based on various mechanisms related to this disorder have been created, although none is perfect. The pathomechanism of AF in humans is complex and is affected by numerous factors, including environmental and congenital ones. Even the most advanced animal model of AF is unable to reflect the complexity and diversity of the etiopathogenesis of this arrhythmia. The use of animals as models of AF is flawed to some extent due to the fact that this type of model imitates chosen AF pathophysiological changes. Species differences affect the development and the course of diseases. However, these models enhance our understanding of numerous mechanisms responsible for the development of AF


as well as new therapies to cure this type of arrhythmia. The knowledge and information obtained from the results of the described studies of AF enable a better understanding of the causes and principles of AF, which will hopefully lead to the development of new treatment and preventive methods. All the conclusions drawn from the animal studies of AF need to be analyzed with care, considering differences to the human organism. Studies using mathematical models based on animal models are gaining popularity, as they may enable scientific research without the need to utilize live animals.

ORCID iDs

Piotr Frydrychowski  <https://orcid.org/0000-0001-6688-3051>

Marcin Michałek  <https://orcid.org/0000-0002-3762-1201>

Agnieszka Sławuta  <https://orcid.org/0000-0001-5671-9864>

Agnieszka Noszczyk-Nowak  <https://orcid.org/0000-0001-7899-3936>

References

- Allessie MA, Boyden PA, Camm AJ, et al. Pathophysiology and prevention of atrial fibrillation. *Circulation*. 2001;103(5):769–777.
- Noszczyk-Nowak A, Paśławska U, Zyśko D, Gajek J, Nicpoń J, Hebel M. Migotanie przedsionków u psów. *Medycyna Wet*. 2008;64:686–689.
- Saunders A, Gordon S, Miller M. Canine atrial fibrillation. *Compend Contin Educ Vet*. 2009;31(11):E1–9.
- Ninio DM, Saint DA. Passive pericardial constraint protects against stretch-induced vulnerability to atrial fibrillation in rabbits. *Am J Physiol Heart Circ Physiol*. 2006;291(5):H2547–2549.
- Henry BL, Gabris B, Li Q, et al. Relaxin suppresses atrial fibrillation in aged rats by reversing fibrosis and upregulating Na⁺ channels. *Heart Rhythm*. 2016;13(4):983–991.
- Wijffels MC, Kirchhof CJ, Dorland R, Allessie MA. Atrial fibrillation begets atrial fibrillation: A study in awake chronically instrumented goats. *Circulation*. 1995;92(7):1954–1968.
- Neuberger HR, Schotten U, Verheule S, et al. Development of a substrate of atrial fibrillation during chronic atrioventricular block in the goat. *Circulation*. 2005;111(1):30–37.
- Greiser M, Neuberger HR, Harks E, et al. Distinct contractile and molecular differences between two goat models of atrial dysfunction: AV block-induced atrial dilatation and atrial fibrillation. *J Mol Cell Cardiol*. 2009;46(3):385–394.
- van der Velden HM, Ausma J, Rook MB, et al. Gap junctional remodeling in relation to stabilization of atrial fibrillation in the goat. *Cardiovasc Res*. 2000;46(3):476–486.
- Ausma J, Wijffels M, Thoné F, Wouters L, Allessie M, Borgers M. Structural changes of atrial myocardium due to sustained atrial fibrillation in the goat. *Circulation*. 1997;96(9):3157–3163.
- Ausma J, Litjens N, Lenders MH, et al. Time course of atrial fibrillation-induced cellular structural remodeling in atria of the goat. *J Mol Cell Cardiol*. 2001;33(12):2083–2094.
- Ausma J, van der Velden HM, Lenders MH, et al. Reverse structural and gap-junctional remodeling after prolonged atrial fibrillation in the goat. *Circulation*. 2003;107(15):2051–2058.
- Neuberger HR, Schotten U, Blaauw Y, et al. Chronic atrial dilation, electrical remodeling, and atrial fibrillation in the goat. *J Am Coll Cardiol*. 2006;47(3):644–653.
- Remes J, van Brakel TJ, Bolotin G, et al. Persistent atrial fibrillation in a goat model of chronic left atrial overload. *J Thorac Cardiovasc Surg*. 2008;136(4):1005–1011.
- Anné W, Willems R, Holemans P, et al. Self-terminating AF depends on electrical remodeling while persistent AF depends on additional structural changes in a rapid atrially paced sheep model. *J Mol Cell Cardiol*. 2007;43(2):148–158.
- Deroubaix E, Folliguet T, Rücker-Martin C, et al. Moderate and chronic hemodynamic overload of sheep atria induces reversible cellular electrophysiologic abnormalities and atrial vulnerability. *J Am Coll Cardiol*. 2004;44(9):1918–1926.

17. Kistler PM, Sanders P, Dodic M, et al. Atrial electrical and structural abnormalities in an ovine model of chronic blood pressure elevation after prenatal corticosteroid exposure: Implications for development of atrial fibrillation. *Eur Heart J*. 2006;27(24):3045–3056.
18. Power JM, Beacom GA, Alferness CA, et al. Susceptibility to atrial fibrillation: A study in an ovine model of pacing-induced early heart failure. *J Cardiovasc Electrophysiol*. 1998;9(4):423–435.
19. Mandapati R, Skanes A, Chen J, Berenfeld O, Jalife J. Stable micro-reentrant sources as a mechanism of atrial fibrillation in the isolated sheep heart. *Circulation*. 2000;101(2):194–199.
20. Lee AM, Miller JR, Voeller RK, et al. A simple porcine model of inducible sustained atrial fibrillation. *Innovations (Phila)*. 2016;11(1):76–78.
21. Schwarzl M, Alogna A, Zweiker D, et al. A porcine model of early atrial fibrillation using a custom-built, radio transmission-controlled pacemaker. *J Electrocardiol*. 2016;49(2):124–131.
22. Linz D, Hohl M, Khoshkish S, et al. Low-level but not high-level baroreceptor stimulation inhibits atrial fibrillation in a pig model of sleep apnea. *J Cardiovasc Electrophysiol*. 2016;27(9):1086–1092.
23. Diness JG, Skibsbøye L, Simó-Vicens R, et al. Termination of vernakalant-resistant atrial fibrillation by inhibition of small-conductance Ca(2+)-activated K(+) channels in pigs. *Circ Arrhythm Electrophysiol*. 2017;10(10):e005125.
24. Jones DL, Guiraudon GM, Skanes AC, Guiraudon CM. Anatomical pitfalls during encircling cryoablation of the left atrium for atrial fibrillation therapy in the pig. *J Interv Card Electrophysiol*. 2008;21(3):187–193.
25. Paslawska U, Gajek J, Kiczak L, et al. Development of porcine model of chronic tachycardia-induced cardiomyopathy. *Int J Cardiol*. 2011;153(1):36–41.
26. Shiroshita-Takeshita A, Schram G, Lavoie J, Nattel S. Effect of simvastatin and antioxidant vitamins on atrial fibrillation promotion by atrial-tachycardia remodeling in dogs. *Circulation*. 2004;110(16):2313–2319.
27. Shiroshita-Takeshita A, Brundel BJ, Lavoie J, Nattel S. Prednisone prevents atrial fibrillation promotion by atrial tachycardia remodeling in dogs. *Cardiovasc Res*. 2006;69(4):865–875.
28. Gaspo R, Bosch RF, Talajic M, Nattel S. Functional mechanisms underlying tachycardia-induced sustained atrial fibrillation in a chronic dog model. *Circulation*. 1997;96(11):4027–4035.
29. Doshi RN, Wu TJ, Yashima M, et al. Relation between ligament of Marshall and adrenergic atrial tachyarrhythmia. *Circulation*. 1999;100(8):876–883.
30. Wu TJ, Ong JJ, Chang CM, et al. Pulmonary veins and ligament of Marshall as sources of rapid activations in a canine model of sustained atrial fibrillation. *Circulation*. 2001;103(8):1157–1163.
31. Zhou S, Chang CM, Wu TJ, et al. Nonreentrant focal activations in pulmonary veins in canine model of sustained atrial fibrillation. *Am J Physiol Heart Circ Physiol*. 2002;283(3):H1244–H1252.
32. Kijawornrat A, Roche BM, Hamlin RL. A canine model of sustained atrial fibrillation induced by rapid atrial pacing and phenylephrine. *Comp Med*. 2008;58(5):490–493.
33. Sinno H, Derakhchan K, Libersan D, Merhi Y, Leung TK, Nattel S. Atrial ischemia promotes atrial fibrillation in dogs. *Circulation*. 2003;107(14):1930–1936.
34. Rivard L, Sinno H, Shiroshita-Takeshita A, Schram G, Leung TK, Nattel S. The pharmacological response of ischemia-related atrial fibrillation in dogs: Evidence for substrate-specific efficacy. *Cardiovasc Res*. 2007;74(1):104–113.
35. Li D, Fareh S, Leung TK, Nattel S. Promotion of atrial fibrillation by heart failure in dogs: Atrial remodeling of a different sort. *Circulation*. 1999;100(1):87–95.
36. Li D, Shinagawa K, Pang L, et al. Effects of angiotensin-converting enzyme inhibition on the development of the atrial fibrillation substrate in dogs with ventricular tachypacing-induced congestive heart failure. *Circulation*. 2001;104(21):2608–2614.
37. Okuyama Y, Miyauchi Y, Park AM, et al. High resolution mapping of the pulmonary vein and the vein of Marshall during induced atrial fibrillation and atrial tachycardia in a canine model of pacing-induced congestive heart failure. *J Am Coll Cardiol*. 2003;42(2):348–360.
38. Ammar EM, Kudrin AN. Comparative antiarrhythmic activity of beta-N-hexamethyleneimino-P-butoxypropiofenone, quinidine and novocaine amide in aconitine auricular fibrillation and flutter in cats. *Farmakol Toksikol*. 1969;32(4):415–418.
39. Gendenshtein EI, Kostin IV, Simon IB. Anti-arrhythmic activity of the beta2-adrenoblockader alpheprol. *Biull Eksp Biol Med*. 1976;81(6):694–696.
40. Byrne JE, Gomoll AW, McKinney GR. Antiarrhythmic properties of MJ 9067 in acute animal models. *J Pharmacol Exp Ther*. 1977;200(1):147–154.
41. Winslow E. Hemodynamic and arrhythmogenic effects of aconitine applied to the left atria of anesthetized cats: Effects of amiodarone and atropine. *J Cardiovasc Pharmacol*. 1981;3(1):87–100.
42. Gendenshtein EI, Kostin IV. Antiarrhythmic activity of trimecaine in experimental arrhythmia and its effect on the heart conduction system. *Farmakol Toksikol*. 1976;39(4):426–428.
43. Gendenshtein EI, Kostin V, Volkova ND. Antiarrhythmic activity of adrenergic blockaders with different mechanisms of action. *Kardiologiya*. 1977;17(4):116–120.
44. Kaverina NV, Senova ZP, Vikxliäev Iul, Ul'ianova OV. Antiarrhythmic properties of ethmozine. *Farmakol Toksikol*. 1970;33(6):693–697.
45. Schmidt C, Wiedmann F, Langer C, et al. Cloning, functional characterization, and remodeling of K2P3.1 (TASK-1) potassium channels in a porcine model of atrial fibrillation and heart failure. *Heart Rhythm*. 2014;11(10):1798–1805.
46. Schmidt C, Wiedmann F, Beyersdorf C, et al. Genetic ablation of TASK-1 (tandem of P domains in a weak inward rectifying K(+) Channel-related acid-sensitive K(+) Channel-1) (K(2P)3.1) K(+) channels suppresses atrial fibrillation and prevents electrical remodeling. *Circ Arrhythm Electrophysiol*. 2019;12(9):e007465.
47. Wiedmann F, Schulte JS, Gomes B, et al. Atrial fibrillation and heart failure-associated remodeling of two-pore-domain potassium (K(2P)) channels in murine disease models: Focus on TASK-1. *Basic Res Cardiol*. 2018;113(4):27.

Pruritus in renal transplant recipients: Current state of knowledge

Piotr K. Krajewski^{1,B–D}, Magdalena Krajewska^{2,A,E}, Jacek C. Szepietowski^{1,A,E,F}

¹ Department of Dermatology, Venereology and Allergology, Wrocław Medical University, Poland

² Department of Nephrology and Transplantation Medicine, Wrocław Medical University, Poland

A – research concept and design; B – collection and/or assembly of data; C – data analysis and interpretation; D – writing the article; E – critical revision of the article; F – final approval of the article

Advances in Clinical and Experimental Medicine, ISSN 1899–5276 (print), ISSN 2451–2680 (online)

Adv Clin Exp Med. 2020;29(6):769–772

Address for correspondence

Piotr K. Krajewski

E-mail: pkrajewski@icloud.com

Funding sources

None declared

Conflict of interest

None declared

Received on February 23, 2020

Reviewed on February 29, 2020

Accepted on May 8, 2020

Published online on June 23, 2020

Abstract

Chronic itch (CI) is the most common symptom in dermatology. It is considered a great burden with a large impact on patients' quality of life, interfering with everyday activities. During the course of chronic kidney disease (CKD) many patients develop end-stage renal disease (ESRD)-associated CI (ESRD CI). Its pathogenesis is yet to be fully explained, but multiple mechanisms have been described, including, among others, dysregulation of calcium, phosphorus, parathyroid hormone and vitamin D axis, microinflammation, and accumulation of uremic toxins. The treatment consists of both topical and systemic therapy, but unfortunately it is usually difficult and unsatisfactory. Renal transplantation (KTx) as the best renal replacement therapy improves considerably the patient's life quality and decreases the mortality rate. However, its influence on CI has not been well described. In this review, we presented the available literature on the influence of KTx on ESRD CI and demonstrated the possible ways in which transplanted kidney could help patients suffering from CI.

Key words: kidney transplantation, pruritus, uremia

Cite as

Krajewski PK, Krajewska M, Szepietowski JC. Pruritus in renal transplant recipients: Current state of knowledge. *Adv Clin Exp Med.* 2020;29(6):769–772. doi:10.17219/acem/122174

DOI

10.17219/acem/122174

Copyright

© 2020 by Wrocław Medical University

This is an article distributed under the terms of the Creative Commons Attribution 3.0 Unported (CC BY 3.0) (<https://creativecommons.org/licenses/by/3.0/>)

Introduction

Chronic kidney disease (CKD) is a global health problem affecting 13.4% of the world population (stages 1–5), while 10.6% of people suffer from advanced stage of the disease (stages 3–5).¹ This disease is defined as a chronic (more than 3 months) decrease in renal function or abnormal renal structure. For the diagnosis, at least 1 of the following criteria must be met: glomerular filtration rate (GFR) <60 mL/min/1.73 m², markers of kidney damage (albuminuria, abnormal urine sedimentation rate, tubular disorders), histologic and radiologic abnormalities, or a history of renal transplantation (KTx). It can be classified into one of 5 stages on the basis of GFR.² The loss of kidney function leads to frequent hospitalization, lower quality of life and higher morbidity rate. Chronic kidney disease patients often suffer from higher cardiovascular risk and develop a series of complications such as hyperparathyroidism and bone disorders, anemia, and dyslipidemias.³ Another troublesome symptom for patients with advanced stages of CKD is end-stage renal disease-associated chronic itch (ESRD CI), also known as a uremic itch. It was first described in 1932⁴ and till today remains an important problem for both patients and the doctors; it decreases patients' quality of life and poses a significant therapeutic challenge. Although numerous therapies have been described until now,⁵ there are still patients suffering from persistent itch. Generally, KTx is the most effective treatment for kidney failure. However, there is still very little known about the influence of KTx on the uremic itch. Moreover, our clinical experience suggests that at least some of KTx recipients may complain of chronic itch (CI). Therefore, we decided to conduct a literature review on the topic of itch in the patients after KTx.

Methods

A literature search according to PRISMA guidelines within the Medline and SCOPUS databases was conducted in March 2020 for papers discussing the problem of itch in KTx patients without setting time limits, using the terms 'pruritus' and 'itch' in conjunction with 'kidney transplantation' or 'renal transplantation'. The search was limited to English, Polish, Spanish, and German literature. Articles that did not address the topics were excluded, and the full text of the remaining articles was subsequently reviewed. Finally, 16 articles were analyzed, from which 8 papers were included in the study (Fig. 1).

Results

The recent study by Schricker et al. shows that 12% of the renal transplant recipients (RTR) are diagnosed with CI.⁶ The authors reported that the prevalence of itch in KTx patients is lower than in the hemodialyzed (HD) ones (12% and 35%, respectively). The mean pruritus score assessed with visual analog scale (VAS) was 3.2 points, indicating mild itch. Moreover, there was a moderate correlation ($r = 0.3$; $p = 0.018$) established between the intensity of CI and the transplant function. In the study by Altmeyer et al., 49 patients after KTx were examined and skin biopsies were taken from them.⁷ The authors observed that all the dermatological skin disorders associated with end-stage renal disease (ESRD) (among them xerosis and generalized itch) disappeared completely after the successful transplantation. The histopathologic examination showed a normalization of uremic altered skin, including xerosis.

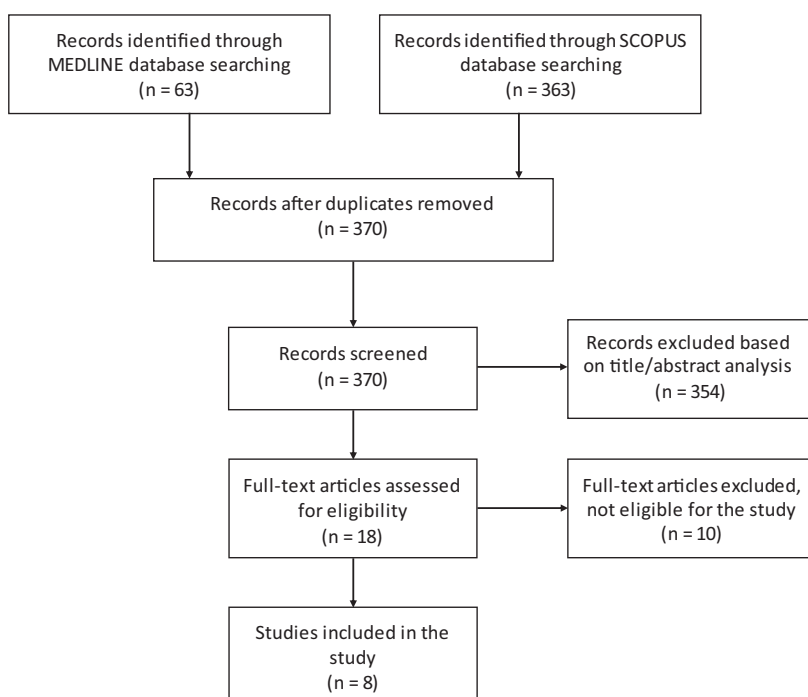


Fig. 1. Literature search procedure

However, the alteration of connective tissue, like actinic elastosis, persisted after the transplantation. Panuccio et al. compared the prevalence of itch and its influence on the quality of life between 133 KTx patients, 29 HD patients and 62 healthy subjects.⁸ There was a significant difference ($p < 0.001$) found in the itch incidence between HD and post-KTx patients (62% and 32%, respectively). Although the prevalence of the pruritus was lower after KTx, it was still higher than in the healthy subjects (32% and 11%, respectively). The authors also emphasized that the itch after KTx was associated with social, emotional and working limitation ($p < 0.05$). Moloney et al. in their study reported that among 173 RTR, 43 people suffered itching (24.9%).⁹ Moreover, in 57% of them, the itch had a large impact on their lives (>10 points in Dermatology Life Quality Index). In the study by Amro et al., the authors analyzed 110 patients who had received a KTx and reported a statistical and clinical decrease in the negative influence on life quality by itching ($p = 0.001$).¹⁰ Also, Avermaete et al. in their report showed a difference in itch prevalence between HD and transplant patients (48–73% vs 2%).¹¹ Furthermore, Tăranu et al. in their study reported a 5.3% prevalence of itchiness; however, the authors associated it with immunotherapy.¹² Yates et al. described a patient with generalized itchiness because of an atypical presentation of chronic scabies infestation.¹³ However, after successful treatment with permethrin, the itch disappeared.

Discussion

End-stage renal disease-associated chronic itch, also known as uremic pruritus or uremic itch, is a common symptom in CKD patients. It affects 35% of patients treated with HD.^{14–16} The sensation is usually localized, but affects whole body in almost $\frac{1}{4}$ of subjects.¹⁷ Patients suffering from uremic itch often report decreased quality of life and poor sleep quality, more frequently develop depression and their relationship satisfaction is significantly lower than in asymptomatic individuals.^{15,18,19} The pathogenesis of ESRDCI has not been fully explained yet and various factors are reported to play an important role in the pathogenesis of pruritus. Among them authors mention high serum levels of parathormone, urea and creatinine, xerosis, microinflammation, dysregulation of opioid receptors, and neuropathy.^{20–24} Due to the complex pathomechanisms and associated comorbidities, the management of uremic itch remains a therapeutic challenge. It is reported that peritoneal dialysis may be beneficial and, if not possible, adjustment of HD parameters (e.g., blood flow) may reduce itchiness.²⁵ The treatment consists of both topical and systemic therapy. At the beginning, mostly moisturizing agents and emollients are used, but the treatment often ends with antidepressants and opioids.⁵

Kidney transplant is the treatment of choice in ESRD. In comparison to HD, KTx significantly improves quality

of life and reduces the risk of mortality.²⁶ Moreover, it has been proven that KTx has a big influence on ESRDCI risk factors. Firstly, the HD, in comparison to properly functioning kidney, does not effectively remove middle-size and protein-bound toxins,²⁷ which could play a role in pruritus pathogenesis.²⁸ Furthermore, during dialysis the interaction of peripheral blood lymphocytes with dialytic membrane increases production and release of pro-inflammatory cytokines,²⁹ which ceases to be a problem after KTx. Authors also mention equilibration of calcium, phosphate, PTH, and vitamin D levels in KTx recipients.³⁰ Furthermore, some authors reported that KTx improves neurological complication of renal failure such as uremic polyneuropathy and autonomic neuropathy.^{31–33} Besides the existence of many reports on KTx influence on the ESRDCI risk factors, there is still very little known about pruritus in KTx recipients.

The available literature focused on this topic is very limited and consists of 7 articles. All of them state that KTx leads to the reduction of itch incidence. In the newest study by Schricker et al., the incidence of CI after KTx was 13% lower than in the HD group.⁶ Moreover, the transplant function was correlated with the intensity of CI. In the study by Altmeyer et al., all patients noticed the total disappearance of uremic itch.⁷ Although the results are promising, the report has its limitations. It was conducted on a small group of patients (49 people) and only generalized pruritus was considered. Panuccio et al. in their study compared the prevalence of itch between RTR, HD patients and healthy subjects.⁸ There was a statistically significant difference between the itch in KTx patients and those treated with HD (32% and 62%, respectively, $p < 0.001$). Furthermore, the retrospectively assessed pre-transplant itch prevalence in RTR was similar to the one found in HD patients. While the post-transplant decrease in uremic itch was noted, the prevalence was still almost 3 times higher than in the general population. Moreover, no statistically significant association with well-known uremic itch risk factors was established. Nevertheless, uremic itch in the KTx patients was strongly associated ($p < 0.05$) with a decrease in the quality of life, suggesting that the symptom is an important psychological burden. In a paper by Amro et al., the authors reported a statistically and clinically significant decrease in the influence of pruritus on the quality of life ($p = 0.001$ and Cohen's $d = 0.8$).¹⁰ The improvement was visible both for patients extremely bothered and moderately bothered by itch. Having this in consideration, one may conclude that KTx may have decreased itch intensity in those subjects. Additionally, Avermaete et al. reported the difference in the incidence of pruritus between RTR and the HD patients.¹¹ Moreover, Tăranu et al. in their study reported that only 5.3% of the patients after KTx had pruritus and suggested that the observed itch was associated with immunosuppressive therapy.¹²

It is important to emphasize that the itch in KTx patients could be of a different origin than the uremic pruritus.

The available reports stated that up to 88% of RTR suffer from infection³⁴ and up to 58.4% can develop drug-related skin manifestation,³⁵ while in some subjects new itchy dermatoses appear (e.g., lichen planus, psoriasis and seborrheic dermatitis).¹¹ Moreover, the possibility of persistent or tertiary hyperparathyroidism exists, which could increase pruritus.³⁶

Conclusions

The literature on uremic itch after KTx is very limited. Although the available reports present the beneficial effect of KTx, there is still more to be discovered. Therefore, future studies on larger populations are crucial to fully evaluate the actual effect of KTx on uremic itch.

ORCID iDs

Piotr Krajewski  <https://orcid.org/0000-0003-4722-8531>

Magdalena Krajewska  <https://orcid.org/0000-0002-2632-2409>

Jacek Szepietowski  <https://orcid.org/0000-0003-0766-6342>

References

- Hill NR, Fatoba ST, Oke JL, et al. Global prevalence of chronic kidney disease: A systematic review and meta-analysis. *PLoS One*. 2016;11(7):e0158765.
- Szczeklik A, Gajewski P. *Interna Szczeklika 2018*. Kraków, Poland: Medycyna Praktyczna; 2018.
- Thomas R, Kalso A, Sedor JR. Chronic kidney disease and its complications. *Prim Care*. 2008;35(2):329–344.vii.
- Chargin L, Keil H. Skin diseases in nonsurgical renal disease. *AMA Arch Derm*. 1932;26(2):314–335.
- Reszke R, Szepietowski JC. End-stage renal disease chronic itch and its management. *Dermatol Clin*. 2018;36(3):277–292.
- Schricker S, Weisshaar E, Kupfer J, Mettang T. Prevalence of pruritus in a single cohort of long-term kidney transplant recipients. *Acta Derm Venereol*. 2020;100(4):adv00066.
- Altmeyer P, Kachel HG, Schafer G, Fassbinder W. Normalization of uremic skin changes following kidney transplantation [in German]. *Hautarzt*. 1986;37(4):217–221.
- Panuccio V, Tripepi R, Bellantoni M, et al. Pruritus and quality of life in renal transplant patients. *Clin Transplant*. 2017;31(3). doi:10.1111/ctr.12893
- Moloney FJ, Keane S, O'Kelly P, Conlon PJ, Murphy GM. The impact of skin disease following renal transplantation on quality of life. *Br J Dermatol*. 2005;153(3):574–578.
- Amro A, Waldum-Grevbo B, von der Lippe N, Brekke FB, Miaskowski C, Os I. Symptom clusters from dialysis to renal transplantation: A five-year longitudinal study. *J Pain Symptom Manage*. 2016;51(3):512–519.
- Avermaete A, Altmeyer P, Bacharach-Buhles M. Skin changes and tumours after renal transplantation. *Nephron*. 2002;91(2):188–194, discussion 194–186.
- Tăranu T, Covic A, Buhaescu I, Taranu T. Drug-induced dermatological pathology in renal transplantation patients [in Romanian]. *Rev Med Chir Soc Med Nat Iasi*. 2005;109(1):36–39.
- Yates JE, Bleyer AJ, Yosipovitch G, Sanguenza OP, Murea M. Enigmatic pruritus in a kidney transplant patient. *Clin Kidney J*. 2013;6(2):194–198.
- Murtagh FE, Addington-Hall JM, Edmonds PM, et al. Symptoms in advanced renal disease: A cross-sectional survey of symptom prevalence in stage 5 chronic kidney disease managed without dialysis. *J Palliat Med*. 2007;10(6):1266–1276.
- Pisoni RL, Wikstrom B, Elder SJ, et al. Pruritus in haemodialysis patients: International results from the Dialysis Outcomes and Practice Patterns Study (DOPPS). *Nephrol Dial Transplant*. 2006;21(12):3495–3505.
- Hayani K, Weiss M, Weisshaar E. Clinical findings and provision of care in haemodialysis patients with chronic itch: New results from the German Epidemiological Haemodialysis Itch Study. *Acta Derm Venereol*. 2016;96(3):361–366.
- Welz-Kubiak K, Reszke R, Szepietowski JC. Pruritus as a sign of systemic disease. *Clin Dermatol*. 2019;37(6):644–656.
- Susel J, Batycka-Baran A, Reich A, Szepietowski JC. Uraemic pruritus markedly affects the quality of life and depressive symptoms in haemodialysis patients with end-stage renal disease. *Acta Derm Venereol*. 2014;94(3):276–281.
- Ibrahim MK, Elshahid AR, El Baz TZ, Elazab RM, Elhoseiny SA, Elsaie ML. Impact of uraemic pruritus on quality of life among end stage renal disease patients on dialysis. *J Clin Diagn Res*. 2016;10(3):WC01–05.
- Kaysen GA. The microinflammatory state in uremia: Causes and potential consequences. *J Am Soc Nephrol*. 2001;12(7):1549–1557.
- Morton CA, Lafferty M, Hau C, Henderson I, Jones M, Lowe JG. Pruritus and skin hydration during dialysis. *Nephrol Dial Transplant*. 1996;11(10):2031–2036.
- Kurban MS, Boueiz A, Kibbi AG. Cutaneous manifestations of chronic kidney disease. *Clin Dermatol*. 2008;26(3):255–264.
- Makhloogh A, Emadi N, Sedighi O, Khademloo M, Bicmohamadi AR. Relationship between serum intact parathyroid hormone and pruritus in hemodialysis patients. *Iran J Kidney Dis*. 2013;7(1):42–46.
- Wikstrom B, Gellert R, Ladefoged SD, et al. Kappa-opioid system in uremic pruritus: Multicenter, randomized, double-blind, placebo-controlled clinical studies. *J Am Soc Nephrol*. 2005;16(12):3742–3747.
- Aliasgharpour M, Zabolypour S, Asadinoghabi A, Haghani H, Lesanpezeski M. The effect of increasing blood flow rate on severity of uremic pruritus in hemodialysis patients: A single clinical trial. *J Natl Med Assoc*. 2018;110(3):270–275.
- Abecassis M, Bartlett ST, Collins AJ, et al. Kidney transplantation as primary therapy for end-stage renal disease: A National Kidney Foundation/Kidney Disease Outcomes Quality Initiative (NKF/KDOQIM) conference. *Clin J Am Soc Nephrol*. 2008;3(2):471–480.
- Wolley MJ, Hutchison CA. Large uremic toxins: An unsolved problem in end-stage kidney disease. *Nephrol Dial Transplant*. 2018;33(Suppl 3):iii6–iii11.
- Cupisti A, Piccoli GB, Gallieni M. Charcoal for the management of pruritus and uremic toxins in patients with chronic kidney disease. *Curr Opin Nephrol Hypertens*. 2020;29(1):71–79.
- Zaza G, Pontrelli P, Pertosa G, et al. Dialysis-related systemic microinflammation is associated with specific genomic patterns. *Nephrol Dial Transplant*. 2008;23(5):1673–1681.
- Bouquegneau A, Salam S, Delanaye P, Eastell R, Khwaja A. Bone disease after kidney transplantation. *Clin J Am Soc Nephrol*. 2016;11(7):1282–1296.
- Bolton CF, Baltzan MA, Baltzan RB. Effects of renal transplantation on uremic neuropathy: A clinical and electrophysiologic study. *N Engl J Med*. 1971;284(21):1170–1175.
- Agarwal A, Anand IS, Sakhuja V, Chugh KS. Effect of dialysis and renal transplantation on autonomic dysfunction in chronic renal failure. *Kidney Int*. 1991;40(3):489–495.
- Whitaker RH, Hamilton D. Effect of transplantation on non-renal effects of renal failure. *Br Med J (Clin Res Ed)*. 1982;284(6311):221–222.
- Oh CC, Lee HY, Tan BK, Assam PN, Kee TYS, Pang SM. Dermatological conditions seen in renal transplant recipients in a Singapore tertiary hospital. *Singapore Med J*. 2018;59(10):519–523.
- Alper S, Kilinc I, Duman S, et al. Skin diseases in Turkish renal transplant recipients. *Int J Dermatol*. 2005;44(11):939–941.
- Yamamoto T, Tominaga Y, Okada M, et al. Characteristics of persistent hyperparathyroidism after renal transplantation. *World J Surg*. 2016;40(3):600–606.